UNIVERSITY OF LONDON THESIS

Degree PhD   Year 2007   Name of Author WILSON, Gary William

COPYRIGHT

This is a thesis accepted for a Higher Degree of the University of London. It is an unpublished typescript and the copyright is held by the author. All persons consulting this thesis must read and abide by the Copyright Declaration below.

COPYRIGHT DECLARATION

I recognise that the copyright of the above-described thesis rests with the author and that no quotation from it or information derived from it may be published without the prior written consent of the author.

LOANS

Theses may not be lent to individuals, but the Senate House Library may lend a copy to approved libraries within the United Kingdom, for consultation solely on the premises of those libraries. Application should be made to: Inter-Library Loans, Senate House Library, Senate House, Malet Street, London WC1E 7HU.

REPRODUCTION

University of London theses may not be reproduced without explicit written permission from the Senate House Library. Enquiries should be addressed to the Theses Section of the Library. Regulations concerning reproduction vary according to the date of acceptance of the thesis and are listed below as guidelines.

A.   Before 1962.   Permission granted only upon the prior written consent of the author. (The Senate House Library will provide addresses where possible).

B.   1962-1974.   In many cases the author has agreed to permit copying upon completion of a Copyright Declaration.

C.   1975-1988.   Most theses may be copied upon completion of a Copyright Declaration.

D.   1989 onwards. Most theses may be copied.

This thesis comes within category D.

☑   This copy has been deposited in the Library of University College London

☐   This copy has been deposited in the Senate House Library,
Senate House, Malet Street, London WC1E 7HU.

Hyperpolarisation-activated ion channels as a target for nitric oxide-cGMP signalling in the rat brain

Gary William Wilson

Thesis submitted in fulfilment of the degree of Doctor of Philosophy, University College London (Wolfson Institute for Biomedical Research).

UMI Number: U592503

UMI

Dissertation Publishing

UMI U592503

ProQuest

I, Gary William Wilson, confirm that the work presented in this thesis is my own. Where information has been derived from other sources, I confirm that this has been indicated in the thesis.

1st October 2007

Abstract

Most of the known physiological effects of nitric oxide (NO) in the brain are mediated by activation of specialised guanylyl cyclase-coupled receptors, leading to a rise in intracellular cGMP. Apart from protein kinase activation little is known about subsequent cGMP signal transduction. In optic nerve axons, hyperpolarisation-activated cyclic nucleotide-gated (HCN) channels, which bind cGMP (and cAMP) directly, appear to be a target. The objective was to test this possibility directly using electrophysiological methods. Studies were initially carried out by recording extracellularly from Schaffer collateral/commissural axons in hippocampal slices, where the NO-cGMP pathway contributes to synaptic plasticity. Pharmacological manipulation of the NO-cGMP pathway failed to affect significantly axonal conduction at 0.2 - 5 Hz, a frequency range in which HCN channels were found to influence conduction reliability. Raising cAMP levels were similarly ineffective suggesting that, unlike in optic nerve, the subunit composition is likely to render the HCN channels relatively cyclic nucleotide-insensitive. Next, I investigated two neuronal types known to express the cyclic nucleotide-sensitive HCN channel subunits (HCN2 and/or HCN4), namely the principal cells of the medial nucleus of the trapezoid body and of the deep cerebellar nuclei. Using whole-cell voltage clamp, I found no reproducible evidence of regulation of HCN channel function by NO, even though exogenous cGMP was effective routinely and the neurones expressed NO-activated guanylyl cyclase, as shown by immunohistochemistry. I then carried out a series of non-invasive sharp electrode current-clamp recordings in deep cerebellar nuclear neurones. Using the characteristic voltage sag as an index of HCN channel operation, exogenous NO was found to modulate the channels reproducibly. Attempts to refine the original whole-cell recording solution to optimise preservation of the NO-cGMP pathway failed to restore NO-sensitivity. Minimising cell dialysis by using the perforated-patch variant of the whole-cell method, however, was successful. The results provide direct evidence that HCN channels are potential downstream mediators of NO-cGMP signaling in the deep cerebellar nuclei and suggest that the importance of this transduction pathway may have been previously overlooked because of unsuitable recording methods.

Acknowledgements

I would like to express my gratitude to John Garthwaite for his guidance, critique and supervision throughout the course of my research. Special thanks also go to Barrie Lancaster for imparting his vast electrophysiological expertise with witticisms as well as Giti Garthwaite for her technical assistance with immunohistochemistry and unrelenting encouragement. Many thanks to the camaraderie of the occupants of 3.1.03 and the ensuing banter over the past three years. I wish to thank everyone in the Neural Signalling group, friends and colleagues in the Cruciform building who have made the experience a fun one. In addition, a nod to Huntley Street, without which this would not have been possible.

I thank the Wellcome Trust for funding me so generously over the last 3 years. I am grateful to Jamie Johnston and Ian Forsythe of the University of Leicester for their help with slicing of the auditory brainstem.

I wish to express thanks to my family for their constant support of my decisions. I also would like to thank my friends and particularly Helene, for always being there when things have not gone quite to plan!

Table of Contents

List of Figures

List of Tables

Abbreviations

AC	adenylyl cyclase
AP	action potential
ATP	adenosine 5'-triphosphate
BSA	bovine serum albumin
aCSF	artificial cerebrospinal fluid
CAP	compound action potential (= FV)
cAMP	adenosine 3'-5'-cyclic monophosphate
cGK (PKG)	cGMP-dependent protein kinase
cGMP	guanosine 3'-5'-cyclic monophosphate
CN	cochlear nucleus
CNBD	cyclic nucleotide binding domain
CNG	cyclic nucleotide gated
cNMP	nucleoside 3'5'-cyclic monophosphate
CNS	central nervous system
DAPI	4',6'-diamidino-2-phenylindole
DCN	deep cerebellar nuclei
DEA/NO	2-(N,N-diethylamino)-diazenolate-2-oxide
DMSO	dimethyl sulphoxide
fEPSP	field excitatory postsynaptic potential
FV	fibre volley (= CAP)
eNOS	endothelial nitric oxide synthase
GTP	guanosine 5'-triphosphate
HCN	hyperpolarisation-activated cyclic nucleotide-modulated
Hz	Hertz
IBMX	3-Isobutyl-1-methylxanthine
L-NNA	N^G-nitro-L-arginine
MNTB	medial nucleus of the trapezoid body
NAB	Normal assay buffer
NMDA	N-methyl-d-aspartate
nNOS	neuronal nitric oxide synthase
NOS	nitric oxide synthase

NO	nitric oxide
$NO_{GC}R$	guanylyl cyclase-coupled nitric oxide receptor (formerly sGC)
ODQ	1-H-[1,2,4]oxadiazolo[4,3-a]quinoxalin-1-one
$ONNO^-$	peroxynitrite
$O_2^{\cdot-}$	superoxide
PAPA/NO	(Z)-1-[N-(3-Ammoniopropyl)-N-(n-propyl)-amino]/NO
PDE	cyclic 3'-5' monophosphate phosphodiesterase
PSD-95	post-synaptic density-95
RD	rebound depolarisation
sGC	souble guanylyl cyclase (= $NO_{GC}R$)
spHCN	sea urchin sperm HCN channels
$V_{1/2}$	voltage to causing half-maximal activation
WCS	Whole-cell solution

Chapter 1 - General introduction

The functional significance of the nitric oxide (NO) - guanosine 3'-5'-cyclic monophosphate (cGMP) -hyperpolarisation-activated channel signalling pathway has not been well documented. NO is an unconventional, freely diffusible neurotransmitter of physiological and pathological importance throughout the brain. The hyperpolarisation-activated channel, which carries a current often referred to as the funny or queer current because of its initially puzzling properties, has been found to be crucial in both the central nervous system (CNS) and cardiovascular system. cGMP is a ubiquitous second messenger that could link these two components to a number of neurophysiological processes. Here, the discovery of these two entities and the general aspects of their signalling in the CNS will be considered. More detailed discussion of specific topics pertaining to each chapter will be discussed therein.

1.1 THE HISTORICAL IDENTIFICATION OF NO

NO was first studied by Joseph Priestly during the 18th century, when it was classified as a colourless, toxic gas. Indeed, on breathing NO, Humphrey Davy spoke of a terrible burning in his tongue, throat and chest (Sprigge 2002). Since being named "molecule of the year" by the journal *Science* in 1992 and earning three scientists the Nobel Prize for Physiology or Medicine in 1998, NO has become one of the most researched molecules.

NO rose to biological fame in the 1980s when it was identified as a diffusible endothelium-derived relaxing factor (EDRF) in a series of seminal experiments in the vascular system. As the name implies, EDRF was released from endothelial cells lining blood vessels to cause relaxation of the underlying smooth muscle, thereby influencing blood flow and blood pressure (Furchgott & Zawadzki 1980; Cocks & Angus 1983). This endothelial-dependent relaxation was thought to be mediated through cGMP and cGMP-dependent phosphorylation (Rapoport & Murad 1983; Rapoport *et al.* 1983). Prior to these studies, nitroglycerin, used clinically for many years for its vasodilatatory properties, and other organic nitrates were proposed to release NO, stimulate a guanylyl cyclase and cause a rise in cGMP (Katsuki *et al.* 1977; Arnold *et al.* 1977). The similarity of the tissue

response to EDRF and nitrovasodilators led Furchgott, Ignarro and Moncada to propose more-or-less simultaneously that EDRF was NO. This was later confirmed when bradykinin was shown to release a substance from endothelial cells with indistinguishable chemical reactivity, stability and biological activity to authentic NO (Palmer *et al.* 1987).

The following year, NO was found to be the substance produced following activation of the N-methyl-D-aspartate (NMDA) class of glutamate receptors on brain neurones to relay signals to neighbouring cells (Garthwaite *et al.* 1988). This potentially explained the earlier finding in the cerebellum that cGMP accumulation did not predominantly occur in the same cells that were stimulated by NMDA, suggesting an intercellular messenger (Garthwaite & Garthwaite 1987). This factor was subsequently demonstrated to share the same properties as EDRF and authentic NO, such as Ca^{2+}-dependent release and smooth muscle relaxation (Garthwaite *et al.* 1989). NO as a neurophysiological messenger was discovered.

Around the same time, a third, unrelated body of research confirmed the link between NO and cellular toxicity. Previously it had been shown that urinary levels of nitrate (NO_3^-) exceeded dietary intake indicative of a synthetic pathway (Green *et al.* 1981). Following an inflammatory stimulus, the synthesis of NO_3^- was increased (Wagner *et al.* 1983), which was later attributed to activated macrophages (Stuehr & Marletta 1985). The dependence of the cytotoxic action of activated macrophages on L-arginine (Hibbs, Jr. *et al.* 1987) led to the confirmation of NO being part of repertoire of defences against foreign organisms (Hibbs, Jr. *et al.* 1988).

These three diverse functions, smooth muscle relaxation, neural communication, and immune defence, remain at the core of NO biology and are subserved largely by the processes outlined in the following sections

1.2 NO PRODUCTION

The physico-chemical properties of NO set it apart from conventional signalling molecules, such as neurotransmitters like glutamate. Firstly, like O_2 and CO_2, NO lacks chemical specialization. It does, however, possess an extra (unpaired)

electron, making it a radical. Whilst some other related radicals are chemically reactive and can cause damage to cells (Keynes *et al.* 2003), NO is relatively stable in physiological concentrations, which are thought to be a nanomolar or less (Garthwaite 2005). Second, also like O_2 and CO_2, NO diffuses very quickly through membranes, obviating the need for a specialized release mechanism and giving it the ability to act on neighbouring cells within milliseconds of its manufacture.

Nitric Oxide Synthases

Following the discovery of NO, it was not long before synthetic machinery for NO was identified, in the form of nitric oxide synthase (NOS) which was found to be highly expressed in brain (Bredt *et al.* 1990; Bredt & Snyder 1990). NOS catalyses the stereoselective conversion of the amino acid L-arginine and molecular oxygen to citrulline and NO. Three distinct genes encode the three mammalian enzymes, known as neuronal (n)NOS, inducible (i)NOS and endothelial (e)NOS. This group of enzymes were first identified in 1989 and subsequently characterised throughout the 90's.

These proteins are homodimers of subunits (figure 1.1), each consisting of an N-terminal oxygenase domain and a C-terminal reductase domain. The former contains binding motifs for haem, tetrahydrobiopterin (BH_4, a cofactor) and the substrate, L-arginine. The reductase domain possesses NADPH, FAD and FMN binding sites. Functionally, electrons are donated by NADPH to the reductase domain and proceed via the FAD and FMN redox carriers to the oxygenase domain, whereupon interaction with the haem iron and BH_4 at the active site catalyses the generation of NO. The two domains are linked by a binding site for calmodulin, through which Ca^{2+}-calmodulin binding facilitates electron flow through the enzyme.

Figure 1.1 Synthesis of NO by NOS: structure and catalytic function.

Proposed arrangement of NOS monomers; the reductase domain oxidises NADPH to NADP+, donating electrons which are transferred *via* the bound flavoproteins, FAD and FMN to the haem moiety in the oxygenase domain of the other monomer. Two oxygenation cycles then occur, the first forming N-hydroxy-L-arginine (NHA) by the N-oxygenation of L-arginine in a reaction which requires tetrahydrobiopterin (BH$_4$). In the second cycle, NHA is converted by oxidative cleavage to NO (Adapted from Alderton *et al.* 2001, and http://www.sgul.ac.uk/depts/immunology/~dash/no/synthesis.htm

The Ca^{2+}-dependence of NO synthesis varies with the NOS isoforms, nNOS and eNOS having a requirement for much higher concentrations than iNOS. The calcium-insensitivity of iNOS is the result of the lack of an auto-inhibitory loop insert of 40-50 amino acids within its FMN-binding subdomain that, in the other two isoforms, acts by destabilizing calmodulin binding at low Ca^{2+} concentrations (Alderton *et al.* 2001). Loss of eNOS activity at low calcium concentrations is circumvented when the protein is phosphorylated, typically by the kinase known as Akt, or protein kinase B (Dimmeler *et al.* 1999). Physiologically, eNOS phosphorylation may be the most important device for maintaining NO output in blood vessels in the brain.

NOS inhibitors

Knowledge of the enzymatic mechanism for NO synthesis led rapidly to the identification of inhibitors, which have become invaluable tools for investigating the

biological roles of NO. First-generation inhibitors were L-arginine derivatives with substituents on the guanidine nitrogen normally used for NO synthesis, compounds such as N^G-monomethyl-L-arginine (Hibbs, Jr. *et al.* 1987) and N^G-nitro-L-arginine (Moore *et al.* 1990). As expected, these inhibitors are simple competitive inhibitors for the L-arginine binding site. They inhibit all NOS isoforms with reasonable potency (K_i in the low micromolar range). Compounds showing good selectivity for nNOS over eNOS are now available such as N^5-(1-Imino-3-butenyl)-L-ornithine (L-VNIO) and [N-(3-aminoethylyl)benzyl]-acetamidine (1400W; Babu & Griffith 1998; Boer *et al.* 2000).

NOS distribution and NO generation in the nervous system

The nNOS isoform is found predominantly in neurones and has a distribution in the brain and spinal cord as wide as that of the major neurotransmitters glutamate and GABA, although the amounts vary from region to region. In some brain areas, such as the cerebellum, nNOS is found in virtually all cells whereas in others, like the striatum and cerebral cortex, it is found in a subpopulation of interneurones comprising only a small percentage of the total neuronal number. Nevertheless even in those regions that are relatively sparsely endowed with nNOS-containing neurones, dense nNOS-containing fibre networks are to be seen ramifying throughout the neuropil, suggesting that the majority of neurons receive NO signals (Vincent & Kimura 1992; Rodrigo *et al.* 1994).

In many of these brain regions, NO formation is coupled to the stimulation of the NMDA-sensitive class of glutamate receptor (NMDA-R), which is found in almost all excitatory synapses. This special relationship is the result of the NMDA-R-associated ion channels having a high permeability to calcium ions and by the compartmentalization of the nNOS and NMDA proteins into a complex at synaptic sites. The scaffold for this complex is post-synaptic density-95 (PSD-95) protein which contains several PDZ domains, the modular protein-protein interaction motifs. The N-terminus of nNOS contains a PDZ domain which interacts with the second PDZ domain on PSD-95 (Brenman *et al.* 1996). PSD-95 also binds the C-terminal PDZ domain of NMDA-Rs (Kornau *et al.* 1995), leading to the assembly of these proteins into a ternary complex (Christopherson *et al.* 1999). This

colocalisation of NMDA-Rs and nNOS appears to be functionally significant as suppression of PSD-95, using anti-sense oligonucleotide techniques, blocks the production of cGMP following NMDA-R activation and Ca^{2+}-influx, but not following activation of other Ca^{2+}-channels or non-specific depolarisation (Sattler *et al.* 1999). Association of nNOS with the membrane and NMDA-Rs thus enables synaptic activation of NO synthesis.

In addition to the functional coupling with NMDA receptors postsynaptically, there are other instances where NO is formed presynaptically. In parts of the brain, nNOS is concentrated strongly in axons such as in the parallel fibres in the cerebellum (Shibuki and Kimura, 1997) and it may perform an analogous "orthograde" transmitter function at these locations.

Although nNOS is the main isoform in the nervous system, emerging evidence suggests that NO from eNOS in the microvasculature can also influence neurons. This represents a conceptual departure from the traditional view of brain function, where signal processing is perceived as being performed by neurones with the support of nearby glial cells. On the other hand, any point in the brain is maximally only about a cell diameter (approximately 25 µm) away from a capillary (Pawlik *et al.* 1981) and the geometry of the capillary network is ideal for distributing a molecule like NO within a tissue volume, just as it is for oxygen. At least *in vitro*, the global NO signal deriving from the endothelium can influence the membrane potential of axons in the optic nerve (Garthwaite 2006), the baroreceptor reflex in the solitary tract nucleus (Paton *et al.* 2002) and the capacity for synaptic plasticity in the hippocampus (Hopper & Garthwaite 2006).

1.3 NO INACTIVATION

NO is a small non-polar molecule that can readily cross cell membranes by diffusion. Therefore a mechanism is required to curtail its spatial and temporal spread. Diffusion alone ensures rapid dissipation of the molecules from small volumes (Wood & Garthwaite 1994). Reaction with oxyhaemoglobin in red blood cells in the vasculature probably plays some role (Liu *et al.* 1998), however a sub-

physiological level concentration of oxyhaemoglobin in *in vitro* brain slices may negate its significance compared to the *in vivo* situation.

Active NO inactivation is more likely to be of importance in shaping the NO concentrations when there are many nearby sites of simultaneous NO synthesis. Brain tissue avidly consumes NO such that its half life at physiological concentrations is estimated to be in the 10 millisecond time scale (Hall & Garthwaite 2006). Chemically, NO can also react with oxygen in solution, but this process (termed autoxidation) is particularly slow, and so may be of minimal physiological importance. NO also reacts very rapidly with lipid peroxyl radicals (Keynes *et al.* 2005), a process likely to be significant in pathological conditions associated with oxidative stress. More recently, a new mechanism, independent of lipid peroxidation, has been identified in brain slices that would be important in shaping NO signals when several sources are active (Hall & Garthwaite 2006; see chapter 6). The molecular identity of this mechanism remains unclear, although much literature points perhaps to unidentified (flavohaemo)proteins. Despite a large volume of research, the means by which the NO signal is actively quenched remains unclear.

1.4 NO SIGNAL TRANSDUCTION

S-Nitrosation

Previously known as S-nitrosylation, this form of chemical modification involves the transfer of the NO moiety to thiol groups (Koppenol 2002). This would therefore be an important route for NO signal transduction as protein function is often affected by covalent modification (Stamler *et al.* 2001). Within the brain, NMDA-Rs have been reported to be modified by S-nitrosation (Stamler *et al.* 2001; Lipton *et al.* 2002). The chemical reactivity of NO is such that it can not simply associate with thiols in a reversible manner; the direct reaction of NO and thiols generates a thiol sulphide, not a nitrosothiol; the stable covalent link between sulphur and nitrogen in a S-nitrosothiol is not particularly susceptible to homolysis except during strong irradiation (Hogg 2002). Therefore some reconciliation of the biological and chemical data is required to consider the physiological significance of S-nitrosation. More recently, the regulation of NMDA-Rs by S-nitrosation has been suggested to

be produced only when high, supra-physiological concentrations of NO are concurrently present with UV light, indicative of artefactual generation of suitable nitrosating species (Hopper *et al.* 2004). The evidence as yet points more towards similarly aberrant generation of the critical nitrosating species, for example by use of high NO concentrations or donors that may not generate authentic NO. Therefore S-nitrosation may become more relevant during pathophysiological situations such as hypoxia (Takahashi *et al.* 2007). As the physiological relevance of NO-mediated S-nitrosation of proteins is unclear, it will not be further considered here.

The NO receptor

The mechanism of signal transduction preceded the identification of NO as a biological messenger. During the 1970s, it was found that NO was a powerful activator of guanylyl cyclase (GC) enzymes, causing the synthesis of cGMP (Kimura *et al.* 1975). This observation provided crucial evidence for the hypothesis that EDRF was NO because the factor was found to cause relaxation through cGMP generation. Because of its location in the soluble fractions in tissue homogenates, the enzyme became known as "soluble" GC. It is now clear that these enzymatic proteins constitute the major physiological receptors for NO having a ligand-binding site and transduction unit (Bellamy & Garthwaite 2002a). I refer to them here as GC-coupled NO receptors ($NO_{GC}Rs$).

The receptors capture and transduce low-level NO signals, even very transient ones. The ligand-binding site is a specialized haem moiety that excludes oxygen (Martin *et al.* 2006), allowing NO to bind without becoming oxidized, in contrast to its reaction with oxyhemoglobin, when NO is converted to nitrate ions. The transduction unit to which the haem is attached are heterodimers of α- and β-subunits and the enzyme exists in two main isoforms. Attachment is via a covalent link between the ferrous centre of the haem binding site and histidine residue 105 of the β-subunit (Wedel *et al.* 1994). The β1 subunit appears to be the common subunit and it is partnered by either α1 or α2. At the mRNA and protein level, both isoforms are found abundantly in brain tissue but have an uneven distribution, some areas or cells showing prominently α1β1 and others, α2β1 (Gibb &

Garthwaite 2001). A special feature of the $a2\beta1$ isoform is that it binds to synaptic scaffold proteins containing PDZ domains (Russwurm *et al.* 2001), which would be convenient for transducing localized NO signals from nNOS, whereas the $a1\beta1$ may have a less localized distribution in neurones. A $\beta2$ subunit, which lacks the initial N-terminal region relative to residues of the β_1 subunit, is present in low quantities at the mRNA level (Gibb & Garthwaite 2001) but there is conflicting evidence as to its functional significance (Gupta *et al.* 1997; Gibb *et al.* 2003) and, to date, there has been no evidence that β_2-protein exists physiologically.
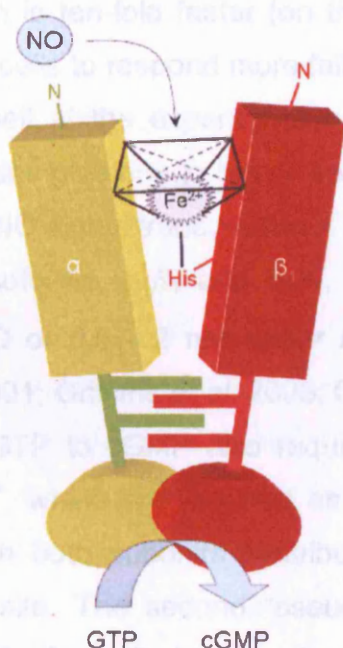
Figure 1.2 Binding of NO activates the guanylyl cyclase-linked NO receptor

The binding of NO to the iron centre binding site in the N-terminal region of the enzyme results in the formation of a 6-coordinated haem. Activation follows cleavage of the proximal His bond leading to a conformational change in the tertiary structure of the protein that, by some means, is conveyed to the catalytic site.

The binding of NO to the vacant coordination site on haem group of the $NO_{GC}R$ (figure 1.2) is extremely rapid, being nearly diffusion-limited (Zhao *et al.* 1999). Initially, a six-coordinate nitrosyl-haem complex is formed but the subsequent snapping of the bond between the haem and a nearby histidine residue results in a five-coordinate species (Bellamy & Garthwaite 2002a). This bond breakage causes a conformational change that presumably propagates to the catalytic domain, accelerating conversion of GTP into cGMP by a thousand-fold or more (Garthwaite 2005).

NO binds very avidly to haem groups possessing vacant coordination sites. Indeed, the capacity of haemoglobin to bind and inactivate NO was well known

(Martin *et al.* 1985a; Martin *et al.* 1985b) long before NO was recognized as a biological messenger, and this property proved to be an important one in assembling the hypothesis that the biological messenger was NO, and in testing that hypothesis. The binding of NO to most haem groups is so tight that it often takes hours or days for it to unbind, a property that would preclude a dynamic signalling role for NO. Although of high affinity (dissociation constant around 1 nM), binding of NO to the purified $NO_{GC}R$-haem is readily reversible (rate of dissociation 0.04 s^{-1}) so that, on removal of NO, the associated cyclase activity switches-off with a half-life of a few seconds (Kharitonov *et al.* 1997). In cells however, the rate of deactivation is ten-fold faster (on the 100-millisecond timescale), which allows the $NO_{GC}R$ in cells to respond more faithfully to brief NO transients than it would do otherwise, albeit at the expense of a lowered NO sensitivity (Garthwaite 2005). These properties give rise to highly sensitive NO detectors within cells for efficient physiological NO signal transduction.

Both isoforms, $\alpha_1\beta_1$ and $\alpha_2\beta_1$, share similar kinetic properties, with EC_{50} values for NO of 0.5 - 2 nM under steady-state conditions in cells (Griffiths & Garthwaite 2001; Griffiths *et al.* 2003; Gibb *et al.* 2003; Wykes & Garthwaite 2004). Catalysis of GTP to cGMP also requires the presence of divalent cations, most probably Mg^{2+}, which are required as substrate co-factors to facilitate binding of GTP. Although both subunits contribute to the catalytic domain there is only a single active site. The second "pseudosymmetric" site, which is thought to be analogous to the forskolin binding site in adenylyl cyclases, may have a regulatory function. ATP is an inhibitor thought to act, in part, by competing with GTP for binding at an allosteric site (Ruiz-Stewart *et al.* 2004), which could be the pseudosymmetric site. Binding of Ca^{2+} to two allosteric sites also results in inhibition of the enzyme (Kazerounian *et al.* 2002). $NO_{GC}R$ can also be inhibited by cGMP-dependent kinase-dependent phosphorylation setting up a negative feedback circuit to impede further formation of cGMP (Murthy 2004).

On stimulation with NO, $NO_{GC}R$ desensitises within seconds in intact cells (Bellamy *et al.* 2000; Wykes *et al.* 2002; Mo *et al.* 2004), unlike purified enzyme, which produces cGMP at a constant rate for prolonged periods of time. The rapid physiological desensitisation highlights the dynamic nature of cellular $NO_{GC}R$

activity, as is also evidenced by the fast activation (within 20 ms) and deactivation (half-time of 200 ms) on addition or removal of NO (Bellamy & Garthwaite 2001b). These properties mean that $NO_{GC}Rs$ can sense NO concentrations of about 0.1 nM or more, convert them into approximately one thousand-fold higher concentration of cGMP within a second, and then cease activity when NO production stops, again within a second. Thus, although many details of their functioning remain to be explained, the $NO_{GC}Rs$ are highly effective proteins for transducing NO signals into greatly amplified levels of cGMP with good temporal fidelity.

There are a number of widely used pharmacological tools for modulating and probing the function of $NO_{GC}R$. The most widely used is a selective, potent (IC_{50} ~20 nM) inhibitor, 1-H-[1,2,4]oxadiazolo[4,3-a]quinoxalin-1-one (ODQ; Garthwaite et al. 1995). Spectroscopic measurements have shown that ODQ causes a characteristic Soret peak shift, indicative of oxidation of the $NO_{GC}R$ haem moiety (Schrammel et al. 1996). This change in redox state is thought to underlie the irreversible, much decreased NO-stimulated activity following ODQ application. At higher concentrations, ODQ becomes non-specific, inhibiting other proteins containing a haem moiety such as cytochrome P-450 (Feelisch et al. 1999). 10 µM ODQ is now the benchmark concentration to inhibit $NO_{GC}R$ and to confirm that an NO-induced effect is mediated by cyclase activation and cGMP generation. Whether or not other NO receptors exist remains to be determined.

The localisation of $NO_{GC}R$ and cGMP signal

The distribution of $NO_{GC}R$ in the rat brain has been mapped using cGMP immunocytochemistry following perfusion of animals with NO donors (see figure 1.3; Southam & Garthwaite 1993). A comparison of the sites of endogenous NO production and of action, namely the distribution of NOS and the $NO_{GC}R$ respectively gave an insight into the workings of the NO-cGMP signalling pathway. Both proteins are functionally expressed in close proximity; there is a complementary relationship suggesting NO is an autocrine and a paracrine agent.

Nitric oxide synthase
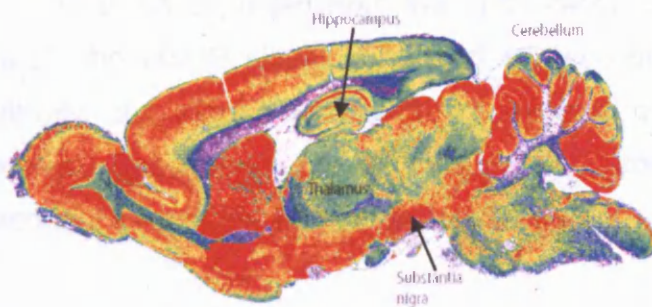
Nitric oxide-evoked cGMP accumulation
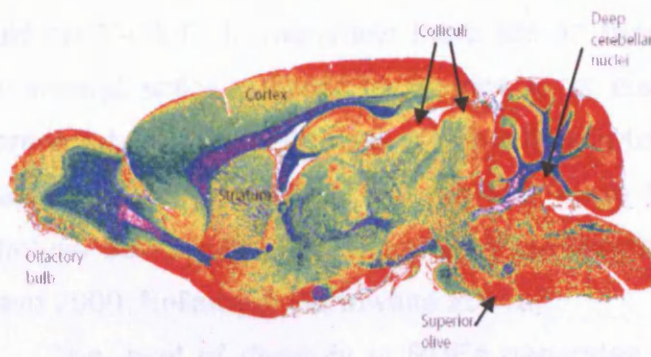
Figure 1.3 Distribution of NOS and cGMP accumulation in parasagittal sections of rat brain

The top panel was prepared using NADPH diaphorase histochemistry, a marker for NOS in the brain while the bottom utilized cGMP immunohistochemistry following perfusion of the NO donor, sodium nitroprusside. The stainings are displayed as heat maps with red being strong and blue being weak. There is a good match between the presence of the enzyme and cGMP production ina number of brain regions such as the colliculi and substantia nigra. Often the locations are complementary rather than identical such as in part of the brainstem. (Adapted from Southam & Garthwaite 1993)

For example, numerous nNOS-like immunoreactive fibres form bouton-like structures onto mesencephalic trigeminal (Mes-V) neurones, while cGMP immunoreactivity is found only in the recipient Mes-V neurones (Pose *et al.* 2003). Likewise, a small number of NOS-positive multipolar neurones radiate throughout neocortical layers 2-6, while NO-stimulated cGMP accumulation is seen in almost all neurones in these layers (Southam & Garthwaite 1993). In the cerebellum, the molecular layer neuropil homogeneously stains for NOS, while the downstream Purkinje cells are devoid of NOS (Vincent & Kimura 1992), but contain $NO_{GC}R$ (Ariano *et al.* 1982). Immunohistochemistry of the CA1 region of the hippocampus revealed a postsynaptic localisation of NOS and presynaptic cyclase (Burette *et al.* 2002). This complementary distribution of the sources and targets of NO supports its role as an intercellular signalling molecule; it can be synthesised presynaptically from axon terminals or from a mesh of fibres radiating throughout the parenchyma,

or postsynaptically in dendrites and spines, permitting signalling in either the anterograde or retrograde directions in different neural circuits.

As to be expected from this large range of different 'set-ups' of NOS and NO$_{GC}$R, the cGMP signal generated at the various locations is quite different. Intuitively, the signal generated will depend on the balance between cGMP formation, dependent upon cyclase activity, and degradation, which is mainly dependent upon phosphodiesterases (PDEs).

PDEs are often homodimeric enzymes that catalyse the hydrolysis of cyclic nucleotides to the corresponding non-cyclised monophosphate, which for cGMP would be 5'-GMP. In mammals there are 11 familes of PDE, encoded by genes with several splice variants giving rise to at least 50 proteins that may exhibit different subcellular localisation or tissue distributions. Of these, PDE 5 and 9 show greater selectivity for cGMP over cAMP, while PDE 1, 2, 3, 4, 10 and 11 will hydrolyse both cyclic nucleotides to a certain degree (Beavo 1995; Soderling & Beavo 2000; Bellamy & Garthwaite 2001a).

The level of diversity in PDEs generates heterogeneity in the amplitude, duration and localisation of cGMP (and therefore NO) signalling throughout the various subcellular domains. For example, in cerebellar astrocytes, the low PDE activity and rapid desensitisation of NO$_{GC}$R following NO application results in a large increase in cGMP and a long-lived plateau (Bellamy *et al.* 2000). Conversely in rat platelets, NO stimulation (EC$_{50}$ = 10 nM) leads to very transient increase in cGMP, peaking after 2-5 s. This profile is caused partly by NO$_{GC}$R desensitisation (half-life of up to 3 s) and partly by PDE5 catalytic activity (Mo *et al.* 2004). However, the lack of information about endogenous NO and cGMP signals is the major deficit in our current understanding of NO signalling within the nervous system and the body as a whole.

1.5 DOWNSTREAM TARGETS FOR cGMP

The effects of NO are mediated, directly and indirectly, by cGMP binding to cGMP-modulated kinases, phosphodiesterases and ion channels:

cGMP-dependent protein kinase

cGMP-dependent protein kinase (cGK) or protein kinase G (PKG) is activated by submicromolar cGMP concentrations (Gamm *et al.* 1995) and phosphorylates serine or threonine residues. There are three types: cGKIα and 1β (splice variants) and cGKII. cGKI is cytosolic enzyme, whereas cGKII is targeted to the membrane by myristoylation of an N-terminal glycine residue (Vaandrager *et al.* 1996).

Activation of cGK appears to involve cGMP binding to the regulatory domain, which contains two allosteric cGMP sites both of which must be occupied for full catalytic activity (Gamm *et al.* 1995); cGMP binding results in a conformational change that relieves the N-terminal autoinhibition of the C-terminal catalytic centre. The N-terminal domain is also important for the homodimerisation of the kinase subunits. Autophosphorylation of this region can also occur, causing a more persistent kinase activity that could outlast the original cGMP signal.

In brain, cGKIα is concentrated in Purkinje cells in the cerebellum and cGKIβ in the hippocampus. cGKI is also found at variable levels throughout the CNS. Similarly, cGKII expression is widespread, being found particularly abundantly in the cerebral cortex, thalamus, olfactory bulb and superior colliculi (El-Husseini *et al.* 1999; de Vente *et al.* 2001; Feil *et al.* 2005). One role of cGKII is in the regulation of circadian rhythm, via effects on gene expression in the suprachiasmatic nucleus (Oster *et al.* 2003).

The known substrates of cGK include G-substrate (Detre *et al.* 1984), G-substrate-like DARPP-32 (Tsou *et al.* 1993), ADP ribosyl cyclase (Galione *et al.* 1993), vasodilator-stimulated phosphoprotein (VASP), inositol triphosphate receptor (IP$_3$R), IP$_3$R-associated cGMP kinase substrate (IRAG), Ca^{2+}-activated K$^+$ channels and RhoA (Hofmann *et al.* 2000). Some of these proteins have been implicated in a number of process involving synaptic plasticity and learning, behaviour and nociception as well as development (Schlossmann *et al.* 2005).

cGMP-regulated PDEs

Of the 11 known families, PDE2, 5, 6, 10 and 11 contain one or two N-terminal GAF domains. These motifs, as well as the catalytic site, can bind cGMP in addition to the enzyme catalytic site, usually one cGMP molecule per monomer. In

the case of PDE 2, which can hydrolyse both cyclic nucleotides, the binding of cGMP to a non-catalytic GAF site activates the enzyme increasing the rate of breakdown of both cAMP and cGMP (Martins *et al.* 1982; Martinez *et al.* 2002). This important modulatory effect again highlights the potential cross-talk between signalling pathways and provides an important means by which cGMP can shape the level of cellular cAMP.

Like PDE2, binding of cGMP to a PDE5 GAF domain increases the rate of hydrolysis (Mullershausen *et al.* 2003) and also permits the enzyme to be phoshorylated by cGKI (Turko *et al.* 1998). Phosphorylation of human PDE5 increases the cGMP-binding affinity of the allosteric domain by approximately tenfold, which in turn further enhances the stimulatory effect of cGMP on hydrolysis (Corbin *et al.* 2000).

cGMP inhibits the effect of PDE 3, yet not by an allosteric mechanism. The catalytic site of PDE 3 only efficiently degrades cAMP, yet has a high affinity for cGMP. Therefore cGMP simply competes with cAMP for the catalytic site (Degerman *et al.* 1997).

These indirect effects of cGMP, by potentiating and diminishing the cAMP signal add another facet to the NO-cGMP pathway.

Cyclic nucleotide-gated (CNG) channels

Another group of known receptors for cGMP are the families of cyclic nucleotide-gated ion channels. CNG channels were first discovered in retinal rod photoreceptors (Kaupp *et al.* 1989) and then in retinal cone cells (Bonigk *et al.* 1993) and olfactory receptor cells (Dhallan *et al.* 1990), but there is now evidence for a more widespread distribution, such as in the hippocampus (Kingston *et al.* 1996) and cerebellum (Kingston *et al.* 1999; Strijbos *et al.* 1999).

Molecular cloning has identified two subfamilies of subunits in vertebrates, namely CNGA(1-4) and CNGB(1,3). CNGA1 is primarily found in rod-type receptors, CNGA3 in cones and CNGA2 and CNGA4 in olfactory receptors. CNGB1 has two important splice variants, B1a and B1b, expressed in rods and olfactory receptors respectively and CNGB3 mainly identified in cones. Heterologous expression of subunits has identified CNGA1-3 as core subunits being capable of forming functional homomeric channels, whereas CNGA4 and

B1,3 do not, and are therefore considered to have a modulatory effect as co-expression with core subunits leads to formation of channels with different ion selectivity, ligand sensitivity and gating properties (Kaupp & Seifert 2002).

CNG channels belong to the superfamily of voltage-gated K^+ channels and therefore are thought to be a tetrameric assembly of subunits arranged around a central pore. Physiologically, rod CNG channels are thought to consist of an assembly of three CNGA1 subunits and one CNGB1 subunit (Weitz et al. 2002), while those in cone photoreceptors seem to contain of two CNGA3 and two CNGB3 subunits (Peng et al. 2004). Like cone receptors, olfactory receptor channels are thought to be composed of two core CNG2A subunits and two regulatory subunits (one CNGA4 and one CNGB1; Zheng & Zagotta 2004).

By hydropathy plotting, each subunit is predicted to consist of 6 transmembrane regions (S1-6) and a pore region located between S5 and S6, which under physiological conditions, carries inward currents of Ca^{2+} and Na^+ ions. Interestingly, despite similar homology to other voltage-sensitive channels in the voltage-sensing S4 domain, CNG channels are virtually voltage-independent. Following the S6 domain, there is an intracellular cyclic nucleotide-binding domain (CNBD), which shares homology with other cyclic nucleotide-binding proteins such as cGK and the E. coli catabolite gene activator protein. The binding of cGMP or cAMP to the CNBD results in the direct opening of the channel (Matulef & Zagotta 2003).

cGMP is the preferred agonist for rod- and cone-type channels whereas olfactory-type channels are relatively non-selective between cyclic nucleotides. It is conceivable that membrane potential and Ca^{2+}-influx could be modulated by NO-cGMP-mediated activation of CNG channels (Biel et al. 1998). For example, NO from nearby amacrine cells could increase cGMP levels to augment CNG channel activity in retinal ganglion cells (Ahmad et al. 1994). Unfortunately, the pharmacology of CNG channels is poorly developed at the moment, making studies of their participation in NO signal transduction difficult. Nevertheless, there is evidence that, in response to activation of the NO-cGMP pathway, the channels can promote neurotransmitter release from cone presynaptic terminals and increase neuronal firing postsynaptically (Savchenko et al. 1997). More recent

work suggests that the NO-stimulated activation of CNG channel and cGK stimulates neuritic sprouting in cones, an important part of structural synaptic plasticity (Zhang *et al.* 2005).

HCN channels

The last target for NO-cGMP pathway is another member of the CNBD-containing family of ion channels (Craven & Zagotta 2005), the hyperpolarisation-activated cyclic nucleotide-modulated (HCN) channels. They exhibit the most unusual property of being activated at more hyperpolarized membrane potentials (typically negative to -50 mV) earning the current carried the title of funny (I_f) or queer (I_q). Within the brain, this current is now known as I_h and is a mixed cation current of both K^+ and Na^+ in a ratio of permeability from 3:1 to 5:1 respectively (Robinson & Siegelbaum 2003). There is some evidence for I_h being carried also by Ca^{2+} ions (Yu *et al.* 2004).

Molecular identification of HCN channels in brain

The channel carrying I_h in the mouse brain was identified initially through its interaction with the SH3 domain of neuronal Src (Santoro *et al.* 1997). A subsequent paper from the same group functionally expressed this candidate gene, known as BCNG-1 (equivalent to HCN1), yielding a current with considerable similarities to native neuronal I_h. In addition they reported the identification of three other partial clones in the mouse brain, named BCNG-2, - 3 and -4 and two human clones (Santoro *et al.* 1998). This was swiftly followed by two back-to-back papers in Nature; the first study identified a hyperpolarisation-activated current in sea urchin sperm (spI_h) carried by spHCN channels, which is directly modulated by cAMP, not by cGMP (Gauss *et al.* 1998); the second identified a family of three mammalian hyperpolarisation-activated currents (HACs) using BLAST analysis for the CNBD of CNG channels (Ludwig *et al.* 1998). HAC-1, -2 and -3 corresponded to BCNG-2, -1 and-4 respectively. HAC4 was then identified by screening a rabbit sinoatrial node (SAN) library (Ishii *et al.* 1999). The cloning of the four mammalian genes, termed HCN1-4 instead of HAC1-4 (Clapham 1998) was then completed and show, on the basis of the amino acid

sequence, they are members of the voltage-gated superfamily and have a structure and proposed topology (figure 1.4) as described for CNG channels.
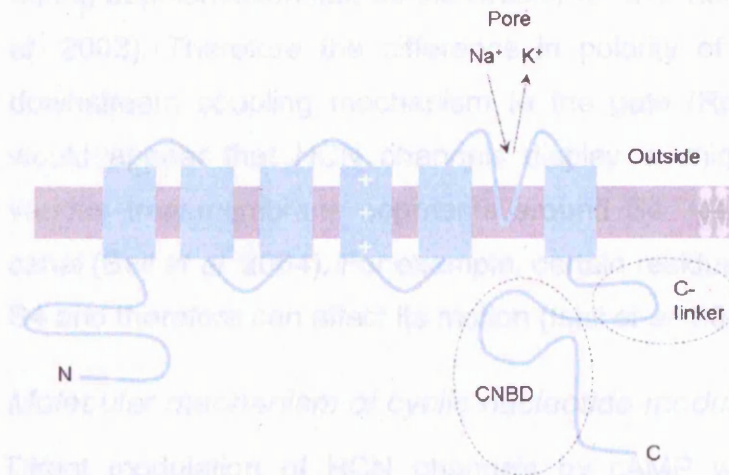
Figure 1.4 The proposed topology and structure for HCN channel subunits

A single subunit is composed of 6 *α*-helical membrane-spanning segments (S1-6), a positively-charged S4 domain, cytoplasmic N- and C- termini, the latter containing a cyclic nucleotide binding domain (CNBD). The putative pore region between S5 and S6 extends into the membrane.

Voltage dependence and kinetics of activation

The currents produced by heterologously-expressed homomeric HCN channels are activated by hyperpolarisation but have quite different steady state voltage-dependence and relative rates of activation. The half-maximal voltages ($V_{1/2}$) for HCN1, 2 and 4 are about -73, -92 and -81 mV respectively (Accili *et al.* 2002) HCN1 has the fastest kinetics (τ < 500 ms), followed by HCN 2 (τ = s) and then HCN4 (Altomare *et al.* 2001).

An integrated allosteric model is compatible with the voltage-gating of HCN channels (as well as modulation by cAMP). This model suggests channel opening is a combination of two processes: the first is the displacement of the four voltage sensors from a reluctant to willing state and secondly, the conformational rearrangement of all subunits from closed to open. Therefore the voltage sensors are gated by voltage alone; whereas the channel closed and open transitions occur allosterically. The faster rate of activation of homomeric HCN1 channels may be explained by the faster activation of the voltage sensor along with a weaker interaction between the subunits in the closed-to-open transition (DiFrancesco 1999; Altomare *et al.* 2001).

Unexpectedly, the voltage-sensing mechanism is conserved among the superfamily of ion channels despite being gated by opposite voltages. The S4 region of HCN and other hyperpolarisation-activated channels moves outward during depolarisation just as the Shaker K^+ channel (Mannikko *et al.* 2002; Sesti *et al.* 2003). Therefore the difference in polarity of activation must lie within the downstream coupling mechanism to the gate (Rosenbaum & Gordon 2004). It would appear that HCN channels display a unique internal re-arrangement in various transmembrane segments around S4, leading to changes in the gating canal (Bell *et al.* 2004). For example, certain residues of S1 face a mobile region of S4 and therefore can affect its motion (Ishii *et al.* 2006).

Molecular mechanism of cyclic nucleotide modulation of HCN channels

Direct modulation of HCN channels by cAMP was first identified by a study involving macropatches from rabbit SAN myocytes (DiFrancesco & Tortora 1991). cAMP causes a depolarising shift in the steady-state activation curve. The efficacy of cAMP has been found to differ between isoforms, with HCN1 being far less responsive (shift of 2-5 mV) than HCN2 and 4 (shift of up to 20 mV; Robinson & Siegelbaum 2003). The construction of truncation mutants showed that the CNBD caused the inhibition of activation of the core transmembrane domain. The difference in modulation by cAMP between HCN1 and HCN2 is due to the different efficacy of CNBD inhibition (Wainger *et al.* 2001). Deletion of the CNBD mimics the effect of cAMP by moving the voltage dependence of HCN gating in a depolarising direction to a similar level seen with cAMP.

A series of chimeric subunit studies subsequently showed that the difference in cAMP efficacy arises due to the conserved 80 amino acid C-linker. This domain has no intrinsic inhibitory influence, yet it is the interaction of the C-linker and the CNBD that accounts for the differences in basal gating and cAMP modulation (Wang *et al.* 2001). Taken together, the basal gating of HCN4 and HCN2 is shifted to more hyperpolarised potentials than HCN1 because of greater tonic inhibition elicited by the appropriate C-linker/CNBD.

The crystal structure of the C-terminal region of HCN2 gives insight into the relationship between the CNBD, C-linker and core transmembrane domains. The CNBD consists of 4 α-helices (A, P, B and C) with a β-roll of 8 β-strands in a jelly

32

roll between the A- and B-helices (Zagotta *et al.* 2003). The binding of cAMP is in the *anti* formation between the β-roll and the C-helix, while cGMP binds in the *syn* configuration which permits a hydrogen bond with a β-roll threonine residue, which thought to explain the structural basis for ligand discrimination in CNG channels (Altenhofen *et al.* 1991). The C-terminal regions of the 4 subunits assemble as tetramers like a pyramid, but the CNBDs do not interact appreciably. Conversely, the C-linkers mediate most of the subunit-subunit contacts; each linker consists of 6 a-helices (A'-F'); A' and B' of one subunit forming an antiparallel helix-turn-helix that interacts with C' and D' of the next subunit. Binding of cAMP or cGMP is thought to change this 'elbow-to-shoulder' arrangement and this conformational change is then translated to pore opening (Zagotta *et al.* 2003).

Binding of cAMP, and probably cGMP, is thought to promote the formation of this four-fold symmetric gating ring from a state in which the subunits interact as two-fold symmetric dimer of dimers. A particular tripeptide sequence near the N-terminal end of the C-linker accounts for the efficacy of ligand gating in CNG channels. Interestingly, the mutation of QEK in HCN1 or 2 to FPN of the cNMP-insensitive CNG4A results in cAMP becoming a negative agonist promoting the disassembly of the tetrameric gating ring on binding (Zhou *et al.* 2004).

HCN channels have been shown to coassemble and form heteromers. For example, a concatenated construct of HCN1 and HCN2 subunits shows modulation by cAMP that is intermediate to homomeric HCN1 and HCN2 channels (Ulens & Tytgat 2001; Chen *et al.* 2001). As a consequence of four distinct subunits, a range of channels with different properties could arise depending on the proportion of different isoforms.

In native and heterologously expressed channel, $I_{h/f}$ was activated, not only by cAMP, but also cGMP with similar efficacy, although with a reduced sensitivity; the channels are about thirty-fold less sensitive to cGMP compared to cAMP as shown by apparent dissociation constants (DiFrancesco & Tortora 1991; Ludwig *et al.* 1998). As such, cAMP is often considered the natural ligand being approximately ten-fold more potent than cGMP (DiFrancesco & Tortora 1991; Ludwig *et al.* 1998; Zagotta *et al.* 2003). However, both nucleotides have also been shown to have similar concentration-effect profiles (Ingram & Williams 1996).

HCN3

HCN3 have only recently been studied through heterologous expression, using lentiviral infection to overcome previous HCN3 expression problems (Mistrik *et al.* 2005). The rate of homomeric channel activation is between that of HCN2 and HCN4, while $V_{1/2}$ is similar to HCN2 (~ -95 mV). Unlike channels formed from the other HCN subunits which all show positive, depolarising shifts in the steady-state activation curves, HCN3 channels display a negative shift (~ -5 mV) in the presence of cAMP or cGMP.

Pharmacological manipulation of I_h

There are a number of organic blockers of HCN channels, the most commonly used being ZD7288. Like a quarternary cation, it has a lipophilic structure and is thought to cross the cell membrane and exert its action from the internal side. Therefore it is relatively slow (10 - 15 min) to take effect. In hippocampal CA1 pyramidal neurones, IC_{50} is ~ 10 μM (Gasparini & DiFrancesco 1997). This is in contrast to low mM Cs^+ that blocks quickly on the external surface (Harris & Constanti 1995).

In CA1 pyramidal cells, the anticonvulsant, lamotrigine, causes a depolarising shift in the steady-state activation curve, translating into a decreased number of action potentials following current injection in the dendrites. This may be due to a decreased R_{in} decreasing excitability; however the reported effects on R_{in} are inconsistent (Poolos *et al.* 2002).

The anaesthetic propofol causes a concentration-dependent hyperpolarising shift in the activation curve and a decrease in conductance of HCN channels in thalamic neurones. This disrupts the regular frequency of δ-oscillations (Ying *et al.* 2006). The inhalation anaesthetic, halothane, also has a similar effect that can be reversed by cAMP. The site of action was localised to the C-terminal region (Chen *et al.* 2005).

Instantaneous current component

HCN channels (sea urchin sperm HCN and HCN2 subunits heterologously expressed) produce an instantaneous current in addition to the slower, time-

34

dependent current (I_h) activated during hyperpolarisation. This instantaneous current is independent of that from the prevailing background current that may arise from constitutive activation of I_h at the holding potential. Unlike I_h, the instantaneous current is insensitive to block by Cs^+ and to mutation in the S4 voltage sensor and is therefore voltage insensitive, earning it the designation of the voltage-independent current (VIC). It appears that this current is carried by a leaky, Cs^+-insensitive state of the channel (Proenza *et al.* 2002). Both it and I_h show similar reversal potentials and are blocked by ZD7288, which blocks the channel pore, suggesting that both currents are carried through the pore. Further work looking at the rates of inhibition by ZD7288 suggests the voltage-independent and I_h are carried by two distinct populations of HCN channel (Proenza & Yellen 2006). The interconversion between both states is not currently understood. In areas that express a large amount of HCN protein, VIC may act as an important background conductance and could presumably contribute to a large leakage current, such as in reticular neurones (Santoro *et al.* 2000).

Further modulation of HCN channels

The comparison of native channel properties and of functionally expressed HCN isoforms and concatenated constructs in HEK 293 cells suggests that native channels are made up of different isoforms in certain combinations, but there may also be unknown factors modulating HCN channels. It seems that, as for NO signalling, there are 'context'-dependent mechanisms at work (Qu *et al.* 2002; Altomare *et al.* 2003). For example, a yeast two-hybrid screen identified an interaction of HCN1, but not 2 or 4, with filamin A, a cytoplasmic scaffold protein which links transmembrane proteins to the actin cytoskeleton. This C-terminal interaction, downstream of the CNBD, doubles the conductance of the channel and causes a hyperpolarising shift in $V_{1/2}$. This is in concert with the clustering of the channel in discrete spots of the plasma membrane (Gravante *et al.* 2004). This clustering may lead to the arrangement of the channels into subcellular complexes to facilitate signalling.

TPR-containing Rab8b-interacting protein (TRIP8b), a protein with no previously ascribed function, has been found to interact specifically with a conserved C-terminal region in all four HCN subunits. Both proteins are also

colocalised in the dendrites of CA1 pyramidal cells, suggesting a physiological function. In heterologous expression, TRIP8b disrupts the trafficking of HCN channels to the plasma membrane causing an accumulation in the cytoplasm, resulting in a reduced I_h density. Infection of CA1 pyramidal cells with TRIP8b also reducs the native current density. This suggests that TRIP8b is involved in regulating channel density in the plasma membrane (Santoro *et al.* 2004).

Many other voltage-gated channels have accessory or β-subunits that modulate the core channel properties. The role of minK-related peptide 1 (MiRP1) was first confirmed by co-expression with HCN1 or 2 in Xenopus oocytes. A member of the KCNE family of 1 transmembrane domain proteins, MiRP1 (or KCNE2) enhanced the amplitude of I_h and increased the maximum conductance. This peptide had no effect on the midpoint of activation yet significantly increased the rate of activation (Yu *et al.* 2001). In heterologous expression in CHO cells, MiRP1 disrupts the ability of homomeric HCN2 channels to move from the leaky to open state, thereby increasing VIC and reducing the time-dependent I_h (Proenza *et al.* 2002). Another study demonstrated an interaction with the HCN4 isoform expressed in CHO cells; MiRP1 increased I_h amplitude, but with slowing of kinetics and a negative shift in $V_{1/2}$ (Decher *et al.* 2003). However, a similar investigation using HEK293 cells showed no effect (Altomare *et al.* 2003). An attempt to resolve this inconsistent set of results from using different isoforms and expression systems was made by Qu *et al.* (2004) by coexpressing HCN2 and MiRP1 in neonatal ventricular myocytes which already express a small hyperpolarisation-activated current. At physiologically relevant voltages, MiRP1 increased the current amplitude, conductance and accelerated the gating kinetics with no effect on the instantaneous component. Therefore it would seem that MiRP1 acts as a β-subunit, although its prevalence in the brain and its role are as yet unknown.

The majority of the reported effects of cGMP and cAMP appear to be though direct binding to the CNBD and independent of activation of PKG and PKA respectively (Pedarzani & Storm 1995; Garthwaite *et al.* 2006), although there are exceptions such as in rat olfactory receptor neurones (Vargas & Lucero 2002). More recently there have been studies elucidating the role of phosphorylation by other kinases on channel function. In DRG and cardiac tissue, general inhibition of

protein tyrosine kinases or specific inhibition of Src-family kinases results in a slowing of the kinetics of activation with little effect on $V_{1/2}$ (Zong *et al.* 2005). In the hippocampus, inhibition of p38 MAPK, but not related kinases, causes a hyperpolarising shift in voltage-dependent activation affecting temporal summation (Poolos *et al.* 2006).

Vitronectin, a component of the extracellular matrix, has been shown to increase the conductance of HCN channels in murine CA1 and CA3 cells, with little effect on the voltage for half-maximal activation; there is also a relative increase in the HCN1 immunoreactivity (Vasilyev & Barish 2004). Vitronectin levels are commonly elevated at injury sites and in activated microglia. This change in I_h may contribute to persistent excitability in some neurological pathologies.

1.6 THE FUNCTIONS OF I_h IN THE BRAIN

I_h is important in setting the membrane potential of CA1 pyramidal neurones (Gasparini & DiFrancesco 1997), thalamic relay neurones (McCormick & Pape 1990a), neocortical layer I interneurones (Wu & Hablitz 2005), basket cells in the dentate gyrus (Aponte *et al.* 2006) and many other cells in the CNS by virtue of the range of activation of the channels near the resting membrane potential. The wide ranging expression of HCN channels within the brain (Notomi & Shigemoto 2004) coupled with their unique properties mean that it is involved in several other important physiological processes:

Rhythmicity

HCN channels interact functionally with T-type Ca^{2+} channels, which carry I_t, to generate rhythmic oscillations in thalamic relay neurones. The activation of I_h depolarises the membrane to threshold for I_t which further depolarises the membrane to spiking threshold. The prolonged depolarisation results in inactivation of T-type channels and the deactivation of HCN channels. This produces a hyperpolarising overshoot and afterhyperpolarisation (AHP) that is essential to remove inactivation of T-type channels and to activate I_h to restart the cycle (McCormick & Pape 1990a). A similar process is thought to function in the inferior olive, where rhythmic spikes are generated by an interaction of I_t and a Ca^{2+}-

activated K^+ current (Bal & McCormick 1997). Therefore I_h is thought to act as a genuine pacemaker, similar to its function in the heart.

In other networks I_h is thought to play a more regulatory role, rather than generating rhythmogenic pacemaker potentials. In the medial septum, an important generator of hippocampal theta rhythm, I_h plays a role in the generation of high (6-9 Hz), but not low (3-5 Hz), frequency theta oscillations. In the motor cortex, blockade of I_h does not suppress the prevailing oscillations; instead it may act to stop stronger long-lasting oscillations (Castro-Alamancos et al. 2007)

Dendritic integration

HCN channels figure prominently in the dendritic mechanisms that control temporal summation of excitatory input. In CA1 pyramidal cells, the HCN channels throughout the soma and dendritic arbour have similar activation and deactivation kinetics, however there is a seven-fold increase in the density of I_h from the soma to the distal dendrites. This means that not only is input resistance (R_{in}) much lower in the distal portions of the neurone, but the shunting action of deactivating HCN channels means the membrane time constant (τ_{mem}) and length constant both are decreased, which in CA1 cells are important to normalise spatially the temporal summation of EPSPs. The deactivating, non-uniform I_h therefore influences the cable properties of the dendrites and in turn shapes the time course of the EPSP as it is propagated to the soma. Without active HCN channels, the output of the soma becomes highly dependent upon the location of the dendritic inputs (Magee 1998; Magee 1999).

In layer V/VI of the frontal cortex, an area concerned with working memory tasks, inwardly-rectifying and leak K^+ currents (I_{Kir} and I_{leak}) are important in sustaining the activity of HCN channels to maintain appropriate temporal summation (Day et al. 2005). The blocking of these K^+ conductances results in depolarisation of the cell membrane, deactivation of HCN channel and enhanced spiking. Therefore a suitable interplay of channels is required for the function of I_h.

In the subiculum, there are bursting and regularly-spiking neurones. The HCN channel conductance in the former is double that of the latter; this doesn't explain the difference in spiking. However, bursting cells show ~ 50 % less summation of excitatory inputs from CA1 pyramidal cells. Computer modelling

suggested that the higher level of I_h in the bursting neurones allows better discrimination of high frequency input arising from gamma oscillations (van Welie *et al.* 2006).

I_h and synaptic facilitation

At the crayfish neuromuscular junction, 5-HT, forskolin and Br-cAMP depolarise the prejunctional axon and increase the excitatory junction potential. This was found to be caused by a direct effect of cAMP on I_h in the afferent nerve. This phenomenon could be mimicked by hyperpolarising the neuronal membrane to give a period of prolonged HCN channel activation. Therefore, simply increasing the amplitude of I_h is sufficient to increase synaptic strength (Beaumont & Zucker 2000). Intense electrical stimulation of the motor nerve results in a long-term facilitation of transmitter release that absolutely requires HCN channel activation during the stimulation and the ensuing ten minutes. During this period, an actin-dependent process called synaptic tagging occurs. This results in subsequent cAMP-induced synaptic enhancement being HCN channel-independent (Zhong & Zucker 2004).

I_h and synaptic plasticity

LTP at the hippocampal mossy fibre synapse is independent of NMDA receptors (Zalutsky & Nicoll 1990) and is thought to be expressed presynaptically involving increased Ca^{2+} and cAMP. A role for I_h in this LTP was deduced by employing the blocker, ZD7288; application of 1-50 µM ZD7288 blocked LTP following tetanisation or bath application of forskolin. Induction of LTP following a tetanus appears to arise from the increase in presynaptic Ca^{2+} which activates a Ca^{2+}-sensitive adenylyl cyclase; there is a rise in the level of cAMP which increases the activation of the I_h, in turn, depolarising the terminal and increasing glutamate release into the synaptic cleft (Mellor *et al.* 2002). The increase in I_h amplitude could be blocked by a PKA-inhibitor, suggesting that not just a direct binding of cAMP to the CNBD accounted for the increase in HCN channel activation.

The results of this study were later questioned because higher concentrations (~ 50 µM) of ZD7288 were found to depress basal synaptic transmission. This depressive effect was also observed with DK-AH269, another organic blocker of I_h. Blockade of HCN channels with Cs^+ did not occlude this

depression, suggesting it is I_h-independent. This effect is not synapse specific being also seen at the hippocampal Schaffer collateral-CA1 pyramidal cell and the cerebellar parallel fibre-Purkinje cell synapses (Chevaleyre & Castillo 2002; Huang & Hsu 2003). An attempt to replicate the initial work found the effect of cAMP to be independent of I_h. The same was found for parallel fibre LTP, which shares common mechanisms with mossy fibre LTP (Chevaleyre & Castillo 2002). However, Huang and Hsu (2003) report that cAMP is involved, and directly modulates HCN channels via the CNBD, independent of the action of PKA.

At hippocampal Schaffer collateral-CA1 synapses, LTD induced by a 15 min train at 1 Hz is blocked by 2 mM Cs^+, suggesting the involvement of I_h in the maintenance of plasticity (Maccaferri *et al.* 1994).

In a Hebbian manner, the pairing of the theta-burst stimulation of Schaffer collateral inputs and postsynaptic firing results in the localised increase in synaptic strength and dendritic excitability. Therefore, at these potentiated sites there is a higher efficiency in the EPSP-action potential coupling, such that presynaptic spikes often generate postsynaptic action potentials more effectively. This strengthening of synaptic transmission is accompanied by a decrease in cellular excitability. This decrease is accompanied by an increase in HCN1 protein and is sensitive to ZD7288 suggesting a role for an increased I_h. The increase in HCN channel conductance results in a decrease in R_{in}, thereby limiting cellular excitability. This may provide a negative feedback mechanism to normalise postsynaptic output and promote network stability (Fan *et al.* 2005). Similarly, *α*-latrotoxin-induced increased synaptic activity results in an increased somatic I_h, which decreases the R_{in} and depolarises the membrane potential. This shifts the output range of the CA1 pyramidal cells, so that a higher level of input is required. In this way, I_h influences the homeostatic scaling of neuronal excitability (van Welie *et al.* 2004).

1.7 THE PHYSIOLOGICAL FUNCTIONS OF NO IN THE NERVOUS SYSTEM

NO has been implicated in numerous behaviours in mammals, including learning and memory formation, cardio-respiratory function, feeding, sleeping, reproductive behaviour, aggression and anxiety. Interestingly, some of these roles appear conserved across many millions of years of evolution. For example, the jellyfish *Aglantha digitale* (phylum Cnidaria) first appeared about half a billion years ago and contains a very primitive nervous system consisting of a nerve net, photoreceptors and mechanosensitive nerve cells. NOS-containing neurones are found in the tentacles and NO plays a key role in swimming behaviour associated with feeding, with cGMP being the effector molecule (Moroz *et al.* 2004). The NO-cGMP pathway is involved in feeding behaviour in molluscs (Korneev *et al.* 2005) and honeybees (Menzel & Muller 1996), where it contributes to the formation of long-lasting associations between scent and food reward. In mammals, NO regulates the passage of food through the intestine (Geiselhoringer *et al.* 2004) and affects feeding behaviour (Morley & Flood 1992; Yamada *et al.* 1997).

The neuronal activity associated with feeding is just one of the numerous physiological functions in the central nervous system (CNS) thought to involve NO. The effect of NO as a messenger between neurones can either be in the short-term or can persist over various timescales.

Acute effects on neuronal function

NO can modulate neuronal function in the short term by effects on excitability. This can manifest as a depolarisation, modulation of the firing rate, or changes in neurotransmitter release.

In the lateral geniculate nucleus of the thalamus, NO and cGMP depolarise the neurones and increase the responses to ionotropic glutamatergic receptor activation by sensory stimulation (Shaw *et al.* 1999). NO augments the spontaneous discharge rate of medial vestibular nucleus neurones probably by direct activation of CNG channels leading to a depolarisation (Podda *et al.* 2004). However, in the hypothalamic paraventricular nucleus (PVN) and the nucleus of

thesolitary tract (NTS), NO depolarises only a subset of neurones through a cGMP-dependent mechanism which involves an increase in conductance (Bains & Ferguson 1997; Wang *et al.* 2006b). The delayed-rectifier K^+ channel in neocortical neurones is enhanced by NO (Han *et al.* 2006).

In the visual cortex, decreases in endogenous NO levels leads to a decrease in the responses to visual stimuli in 38% of cells, an increase in 5 % and no effect in the remaining 57% (Cudeiro *et al.* 1997). In lamina X of the spinal cord, NO and cGMP increases the firing rate of most neurones apart from 2% showing a decrease. This is in contrast to laminae I and II where half were inhibited and only 28% activated. Interestingly, cAMP only caused an excitatory response (Schmid & Pehl 1996; Pehl & Schmid 1997). This disparate range of effects of NO on the neuronal activity highlights that production of cGMP alone does not allow any prediction about an excitatory or inhibitory effect. These differences most likely result from the different downstream targets for the NO-cGMP pathway, although the role of $NO_{GC}R$ was not addressed.

Repetitive stimulation of the hippocampal Schaffer collateral axon at 2 Hz leads to a robust lowering of its activation threshold that lasts in excess of 30 min, an effect that requires NOS (McNaughton *et al.* 1994). Activation of eNOS and production of NO causes depolarisation of optic nerve axons apparently by engaging I_h suggesting that microvascular endothelial cells participate in signal processing in the brain (Garthwaite *et al.* 2006). Such lowering of axonal thresholds would be expected to alter downstream synaptic responses.

In some hypothalamic PVN neurones, the potentiation of a Ca^{2+} conductance by NO could provide a mechanism by which these cells could increase the release of neurotransmitters (Bains & Ferguson 1997). This is the case in rostral ventrolateral medullary neurones where the NO-cGMP-cGK pathway enhances N-type channel Ca^{2+} entry leading to increased glutamate release and an enhancement in synaptic transmission (Huang *et al.* 2003). In the salamander retina, NO and cGMP activate CNG channels clustered at cone terminals and cause an increase in glutamate

release onto the NO-synthesising horizontal cells, setting up a feedback circuit (Savchenko *et al.* 1997). The potentiation of GABA release from NTS neurones by NO involves increasing Ca^{2+} levels by engagement of the stores sensitive to the NAD^+ metabolite, cADPR (Wang *et al.* 2006a). More recent work in the NTS shows that NO potentiates both EPSPs and IPSPs, but the threshold concentration for an increase in EPSP is about ten-fold lower suggesting this difference in sensitivity may underlie the specificity of the effects (Wang *et al.* 2006b).

Long-term modulation of neuronal function

NO and cGMP have frequently been found to participate in synaptic plasticity, which refers to the capability of synapses to adjust their strength enduringly upwards or downwards in response to brief periods of altered input, and which is commonly regarded as a cellular correlate of learning and memory formation (Bliss & Collingridge 1993). Long-term potentiation (LTP) in the hippocampus, cerebral cortex, cerebellum, amygdala, and spinal cord have all been reported to involve the NO-cGMP pathway, as has long-term depression (LTD) in the cerebellum and striatum.

In some cases, NO appears to act as a retrograde trans-synaptic messenger, conveying information about postsynaptic NMDA-R activity to the presynaptic terminal and influencing neurotransmitter release. Theta-burst stimulation of mossy fibre afferents induces LTP at the synapse with granule cells in the cerebellum. This is accompanied by NMDA-R- and NOS-dependent rise in the levels of NO in the granule cell layer and a concomitant rise in the presynaptic mossy fibre terminal, suggesting that NO acts as a retrograde messenger by diffusion (Maffei *et al.* 2003).

Within the hippocampus, there is also evidence consistent with a retrograde messenger role for NO, which is released post-synaptically from CA1 pyramidal cells (Arancio *et al.* 1996). The CA1 region is enriched in the cGMP-dependent kinase (cGK)1 isoform, which is important in the NO-dependent initiation of LTP in this region (Zhuo *et al.* 1994; Arancio *et al.* 2001). However, which kinase substrates are physiologically responsible for these functional changes has not yet been investigated. Hippocampus-specific cGKI knockout mice show normal LTP in

young animals (4-6 weeks), but reduced LTP in older animals (12 weeks); related behaviour tests for hippocampus-dependent learning are unexpectedly normal (Kleppisch *et al.* 2003). Presynaptic LTD of the release of the readily-releasable pool induced by low frequency stimulation also requires NMDA-R activation, the extracellular diffusion of NO and the activation of cGK (Stanton *et al.* 2003). This suggests that there may be a subtle mechanistic switch that dominates the final direction of plasticity. Therefore these conflicting results could be explained by the different extents to which both LTP and LTD are engaged depending on the stimulus protocol used in slices and the training regime employed in behavioural studies.

A further layer to this complexity is that NO appears to act not just as an acute signalling molecule released during LTP induction but has an equally important role outside this phase (Bon & Garthwaite 2003). NO has also been implicated in the later phases of the plasticity through cGMP-dependent alterations in gene expression driven by cGK-dependent phosphorylation of the transcription factor, CREB (Lu *et al.* 1999). More recently, it was found that a prevailing, tonic eNOS-generated low level of NO is required in addition to the activity-induced phasic nNOS-generated burst of NO for LTP induction at Schaffer Collateral-CA1 synapse (Hopper & Garthwaite 2006). However, the precise roles of these two sources of NO remain to be elucidated.

Cerebellar LTD appears to require activation of NMDA-R found presynaptically on parallel fibres (Casado *et al.* 2002). Activation of parallel fibres seemingly results in the release of NO (Shibuki & Kimura 1997), which acts on the postsynaptic spines of the Purkinje cells in an anterograde fashion. Purkinje cells contain a high concentration of cGKI*α* (Lohmann *et al.* 1981; El-Husseini *et al.* 1999) and also express a cGK-target protein, G-substrate, which functions as a protein phosphatase inhibitor (Hall *et al.* 1999; Endo *et al.* 1999). By engaging this cascade in postsynaptic cells, NO contributes to LTD at the parallel fibre-Purkinje cell synapse possibly by causing the declustering of synaptic AMPA receptors (Launey *et al.* 2004). More recently, the source of NO has been disputed implicating the interneurones rather than parallel fibres (Shin & Linden 2005).

Purkinje cell-specific cGK-knockout mice show strongly reduced LTD as expected as well as defects in certain types of motor learning in the cerebellum (Feil *et al.* 2003). Very recently, the NMDA-R-stimulated release of NO was shown to increase Ca^{2+} transients in activated parallel fibres, which is thought to underlie a presynaptic form of LTP at the parallel fibre-Purkinje cell synapse (Qiu & Knopfel 2007).

Clearly there are numerous ways in which NO can modulate the response of a given neurone or network of cells and this will depend on the downstream target components expressed. While the acute actions of NO on neuronal function are seemingly divergent, the ability to change both presynaptic and postsynaptic responses highlights the versatility of NO as a signalling molecule, acting in both anterograde and retrograde directions. This means, however, that its precise function will need to be understood on a more regional context-specific basis.

1.8 THE PHYSIOLOGICAL FUNCTION OF NO-cGMP-HCN CHANNEL PATHWAY

As mentioned before, the interaction of I_h and I_t is important in generating rhythmic oscillations in thalamocortical neurones. Further work identified one of the first reported instances of regulation of I_h by NO. NO and a membrane permeable analogue of cGMP cause a depolarisation of the membrane potential in these relay neurones and decrease R_{in}. Current-voltage relationships suggest a greater effect of NO at hyperpolarised potentials suggesting an effect on I_h. Indeed, NO shifted the voltage for half-maximal activation of the channels by about 5 mV in a depolarised direction. A combination of all these factors decreases the rebound depolarisation because of less de-inactivation of the I_t, thereby decreasing rebound action potentials. Ultimately, NO is able to potently and reversibly block the slow oscillatory activity in spontaneously active neurones (Pape & Mager 1992). Fibres from the cholinergic tegmental neurones contain NOS (Vincent & Kimura 1992) and extend into the thalamus. These neurones are thought to increase in firing rate just prior to the transition from sleep to wakefulness, an effect which would presumably liberate NO into the thalamus. It would therefore appear that the NO-

cGMP-HCN channel pathway could play an important role in the functional control of neuronal networks.

A decade later, a pair of papers from the same group showed an effect of the NO-cGMP pathway on trigeminal motor pool and mesencephalic neurones. In both sets of cells, NO and cGMP reversibly depolarise the membrane potential and reduce the threshold of firing. There is little-to-no change in R_{in}. This is presumably by action of cGMP on I_h noted by observing effects on the voltage 'sag' to hyperpolarising current injections (Abudara et al. 2002; Pose et al. 2003). In this case, the augmentation of HCN channel function is excitatory, a property that may be important in various jaw reflexes and movements.

Earlier work on the trigeminal ganglia suggested that sensitisation of primary afferent neurones by prostaglandin-E_2 involves a depolarising shift in the activation curve for I_h via a direct effect of cAMP (Ingram & Williams 1996). The concentration-effect profiles for Br-cAMP and Br-cGMP are very similar suggesting that cAMP and cGMP may have equal efficacy and potency for causing depolarising shifts in HCN channel voltage dependence, indicating that the NO-cGMP pathway could play a part in nociceptive processing. In the neurones of the substantia gelatinosa, NO enhances I_h indicating a role in central sensitisation through a change in the properties of these important relay neurones (Kim et al. 2005).

In the optic nerve, tonic eNOS-derived NO raised cGMP levels which then cause membrane depolarisation, apparently by directly engaging HCN channels. eNOS appears only to be expressed in the neighbouring endothelial cells, providing a novel mechanism, at least in vitro, by which the microvasculature persistently signal to axons. This prevailing 'tone' is approximately at the midpoint of possible changes in membrane potential, such that the system is well poised to respond to changes in eNOS activity (Garthwaite et al. 2006).

1.9 GENERAL AIMS OF THE STUDY

The functions of the NO-cGMP pathway and HCN channels individually have been studied extensively throughout the brain and the body as a whole. However, there is still little known about how they interact within the CNS. The previous section highlights the precedents for NO and/or cGMP modulating HCN channels in neurones. The ubiquity of NO as an intercellular messenger and the prevalence of HCN channels throughout the brain suggest that I_h is a realistic and plausible target for NO-cGMP signalling. In the following chapters, the NO-cGMP-HCN channel pathway in regions of the hippocampus, cerebellum and brainstem are investigated and discussed. The delicate nature of the NO-cGMP-HCN channel interaction is emphasised in later chapters.

OVERARCHING HYPOTHESIS: The NO-cGMP-HCN channel signalling pathway is present in the brain.

2.1 MATERIALS

Compound	Abbreviation	Source

Chapter 2 - General materials and methods

2.1 MATERIALS

Compound	Abbreviation	Source
Adenosine 5'-triphosphate magnesium salt	ATP	Sigma
4-Aminopyridine	4-AP	Sigma (fluka)
(Z)-1-[N-(3-Ammoniopropyl)-N-(n-propyl)-amino]/NO	PAPA/NO	Alexis
Amphotericin B (solubilised)	-	Sigma
Apamin	-	Alamone
Bovine serum albumin (fraction V)	BSA	Sigma
8-Bromoadenosine 3',5' cyclic monophosphate	8-Br-cAMP	Sigma
8-Bromoguanosine 3',5' cyclic monophosphate	8-Br-cGMP	Sigma
8-(4-chlorophenylthio)-guanosine 3',5'-cyclic monophosphate sodium salt	8-pCPT-cGMP	Sigma
Caesium chloride	Cs^+	Sigma
6-cyano-7-nitroquinoxaline-2,3-dione	CNQX	Tocris
Guanosine 3'-5'-cyclic monophosphate	cGMP	Sigma
Guanosine 5'-triphosphate sodium salt	GTP	Sigma
D(-)-2-amino-5-phosphonopentanoate	D-AP5	Tocris
3,3'-Diaminobenzadine	DAB	Sigma
Diethylamine NONOate: 2-(N,N-Diethylamino)-diazenolate-2-oxide . diethylammonium salt	DEA/NO	Alexis
Dimethyl sulfoxide	DMSO	Sigma
DPX mounting medium	-	VWR
Ethylene glycol-bis(β-aminoethyl ether)-N,N,N',N'-tetraacetic acid	EGTA	Sigma
Forskolin	-	Sigma/Tocris
Gramicidin	-	Sigma
N-2-Hydroxyethylpiperazine-N'-2-ethanesulfonic acid	HEPES	Sigma
3-Isobutyl-1-methylxanthine	IBMX	Sigma
Isoprenaline	IsoP	Sigma
Mayers haemalum	-	Lamb
N^G-nitro-L-arginine	L-NNA	Tocris
Noradrenaline	NorA	Sigma
OCT embedding medium	OCT	Lamb
Picrotoxinin	Ptx	Sigma
1,4-Piperazinediethanesulfonic acid	PIPES	Sigma
Poly-D-lysine	-	Sigma
Potassium Acetate	KAc	Sigma
Potassium Methylsulphate	KMeSO$_4$	City
Proteinase XXIII	-	Sigma
Proteinase inhibitor	-	Sigma
Saclofen	-	Sigma
Soluble guanylyl cyclase (bovine lung)	sGC	Sigma
Sodium hydroxide	NaOH	Sigma
Tetrodotoxin	TTX	Latoxan
Tris(hydroxymethyl)aminomethane hydrochloric acid	Tris	Sigma
Tritiated cyclic guanosine monophosphate	^{3}H-cGMP	Amersham
Triton X-100	-	Sigma
Trizma base	Tris Base	Sigma
Vectastain Elite ABC complex		Vector
4-ethylphenylamino-1,2-dimethyl-6-methylaminopyrimidinium chloride	ZD7288	Tocris

Table 2.1 List of compounds

All standard reagents were obtained from BDH (VWR) unless stated otherwise.

Key

Agar:	Agar Scientific, Stansted, UK.
Alexis:	Axxora Ltd, Nottingham, UK.
Amersham:	Chalfont St.Giles, Bucks, UK.
City:	City Chemical, West Haven, CT, USA.
Lamb:	Raymond A Lamb Ltd, Eastbourne, UK.
Latoxan:	Latoxan Laboratories, Rosans, France.
Sigma:	Sigma-Aldrich Company Ltd, Poole, Dorset, UK.
Tocris:	Tocris Cookson Ltd, Avonmouth, Bristol, UK.
Vector:	Vector Labs Ltd., Peterborough U.K.
VWR:	VWR International, Dorset, UK.

2.2 GENERAL SOLUTIONS

Artificial cerebral spinal fluid (aCSF)

119 mM NaCl, 2.5 mM KCl, 1.3 mM $MgCl_2$, 2.0 mM $CaCl_2$, 1.0 mM $NaH_2PO_4.H_2O$, 26.2 mM $NaHCO_3$, and 11 mM glucose, equilibrated with 95% O_2 - 5% CO_2 (carbogen) give a pH of 7.4 at 30 -32 °C.

Phosphate buffer (PB)

Stock 'A' and 'B' solutions were prepared; 'A' contained 31.2 g / l $NaH_2PO_4.2H_2O$; 'B' contained 35.6 g / l $Na_2HPO_4.2H_2O$. 0.2 M stock PB solution was prepared using 95 ml of 'A', and 405 ml of 'B'. All stock solutions were stored at 4 °C

Tris-buffered saline (TBS)

5.85 g Tris (MW 121.0) was added to 250 ml distilled water; 3.4 ml concentrated HCl was diluted in 200ml water; 250 ml Tris, 192 ml HCl, and 8.77 g NaCl was topped up to 1000 ml.

NO donors

Stock solutions at 100 - 1000 x final concentration were prepared freshly each day in 10 mM NaOH, and kept on ice to prevent decomposition until use. During the course of my experiments, I have used two members of the 1-substituted diazen-1-ium-1,2-diolate ('NONOate') class of compounds that generate authentic NO at reliable rates (Keefer *et al.* 1996), namely DEA/NO and PAPA/NO (table 2.2). I chose these compounds because their relatively short half-lives fit with the timeframe of my experiments.
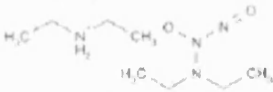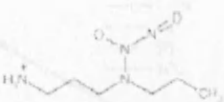
Donor	Structure	Efficiency of NO release (E_{NO}, mol NO/mol donor)	Half-life
DEA/NO		1.5	2 min at 37 °C 16 min at 22-25 °C
PAPA/NO		2	15 min at 37 °C 77 min at 22-25 °C

Table 2.2 The structure and properties of two NONOates (Keefer *et al.* 1996)

In buffer at pH 7.4, the rates of release of NO for all NONOates are thought to be first order, while the primary route of NO breakdown involves an interaction with oxygen in the aqueous solution in a process termed 'autoxidation'. To predict these reactions quantitatively, I have used an established mathematical model (Schmidt *et al.* 1997) and the following notations:

t = time(s)
$c_{NO}(t)$ = concentration of NO at time t (M)
$c_D(t)$ = concentration of donor at time t (M)
c_0 = initial concentration of donor (M)
e_{NO} = mol of NO per mol donor
O_2 = concentration of oxygen (M); 1 mM in aCSF equilibrated with carbogen
k_1 = rate constant for donor decomposition (s^{-1})
k_2 = rate constant for NO oxidation ($M^{-2}s^{-1}$); known to be 13.6×10^6 at 37 °C; values are not available for 30 - 32 °C, so this was used as an estimate

Assuming that the NO donor (D) decays exponentially, the change in NO is given by the difference between formation and the third order process of autoxidation:

$$\frac{d}{dt}c_{NO}(t) = k_1 c_D(t) e_{NO} - k_2 O_2 c_{NO}(t)^2$$

with initial conditions: $c_D(0) = c_0$ and $c_{NO}(0) = 0$

As all the electrophysiological experiments are carried out at 30 - 32 °C, an approximate intermediate half-life, compared to table 2.2, of 8 and 45 min was used for DEA/NO and PAPA/NO respectively to generate NO concentration profiles (figure 2.1).
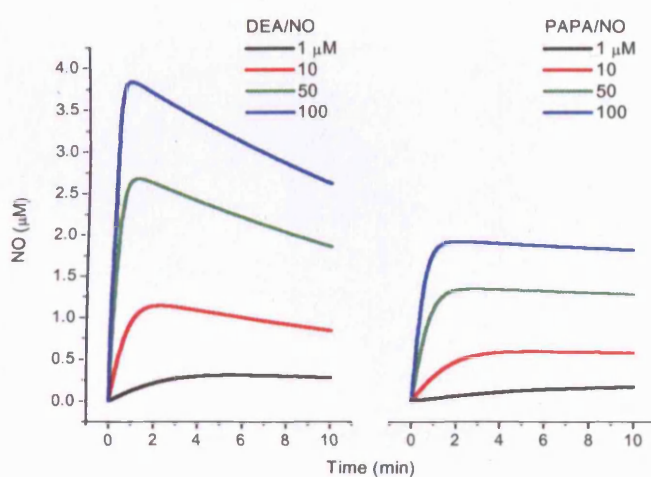
Figure 2.1 The predicted concentration profiles for two NONOates utilised in subsequent electrophysiological experiments

The faster kinetics of DEA/NO means there is a greater release of NO, peaking around the 2nd or 3rd min and then decrease.

The slower kinetics of PAPA/NO results in the level of NO almost reaching a plateau after ~ 1-2 mins.

2.3 STATISTICAL ANALYSIS

Analyses were conducted using Origin 7 (OriginLab Corporation, Northampton, MA) and SPSS for Windows v11.5 (SPSS U.K. Ltd., Woking, U.K.) as appropriate. p values < 0.05 were considered statistically significant. Data are presented as mean value ± standard error of the mean (sem).

Chapter 3 - The NO-cGMP-HCN channel pathway and axonal conduction in the hippocampus

3.1 INTRODUCTION

The importance of the hippocampus in learning and memory has led to a boom in research on their presumed biological correlate, hippocampal synaptic plasticity; during the past two decades a multitude of pre- and postsynaptic alterations that contribute to long-term potentiation (LTP) and depression (LTD) have been identified (Bliss & Collingridge 1993; Malenka & Bear 2004). The NO-cGMP signalling pathway has been suggested to have various roles (chapter 1). I_h is involved in LTP (Mellor *et al.* 2002) and LTD (Maccaferri *et al.* 1994) within this brain region. HCN channels also affect the summation of synaptic inputs, either to allow greater discrimination of high frequency inputs in the subiculum (van Welie *et al.* 2006) or to normalise input spatially in CA1 pyramidal cells (Magee 1998).
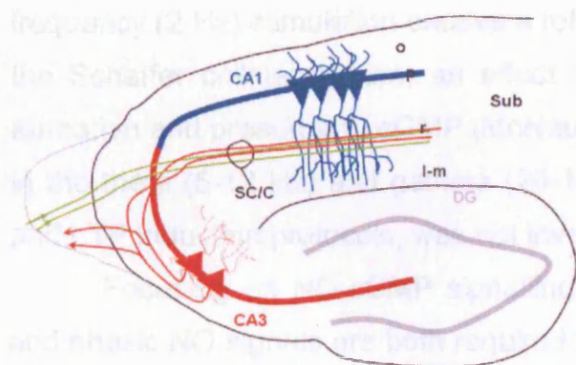
Figure 3.1. The hippocampal formation

The CA3 (red thick line) and CA1 (thick blue line) areas are connected by Schaffer Collateral (thin red line) and commissural (thin green line) axons (SC/C) from ipsilateral and contralateral CA3 pyramidal cells (red triangles) respectively.

o, p, r, l-m indicate the strata oriens, pyramidale, radiatum and lacunosum moleculare respectively; sub = subiculum, DG = dentate gyrus.

The *stratum radiatum* of area CA1 in the hippocampus (figure 3.1) contains mostly unmyelinated axons, which form the Schaffer Collateral/commissural (SC/C) pathway coursing from ipsilateral and contralateral area CA3 pyramidal cells (Johnston & Amaral 2004). These fibres, amongst the thinnest axons in the mammalian CNS (Shepherd & Harris 1998), possess abundant boutons that form *en passant* synaptic contacts with CA1 pyramidal cell apical dendrites. Plasticity at these synapses is typically elicited by activating the presynaptic axons at certain frequencies. The associated changes, if any, in the presynaptic axonal firing properties are not well documented, despite their importance in determining release of neurotransmitter and, hence, the degree of synaptic activation.

In these axons, it is known that I_h is required to maintain the reliability in conduction at relatively low frequencies (1-5 Hz; Soleng et al. 2003), indicating an important link between HCN channel activity and axon function. The modulation of axonal I_h could influence the SC/C fibre activity and ultimately the signal conveyed to the postsynapse.

Both cAMP and cGMP are potential modulators of HCN channels (chapter 1) and both cyclic nucleotides have been extensively implicated in the induction of hippocampal LTP (Pockett et al. 1993; Boulton et al. 1995; Arancio et al. 1996; Arancio et al. 2001; Pineda et al. 2004), but little attention has been given to the possibility that their participation may, at least in part, be explained by an action on axonal HCN channels. There is some evidence for modulation of axonal conduction via cAMP in the cerebellum (Chen & Regehr 1997) but its effect on hippocampal axons does not appear to have been examined. Repetitive low frequency (2 Hz) stimulation causes a robust lowering of the activation threshold of the Schaffer collateral axon, an effect that was dependent on endogenous NO formation and presumably cGMP (McNaughton et al. 1994). The outcome at stimuli in the theta (5-12 Hz) and gamma (20-100 Hz) range, often used in various LTD and LTP induction protocols, was not investigated.

Focusing on NO-cGMP signalling, it was recently demonstrated that tonic and phasic NO signals are both required for hippocampal LTP, particularly where a high frequency stimulus is used to enhance postsynaptic activation. Conversely a low frequency stimulation and postsynaptic pairing protocol is less likely to be affected by NO-dependent effects on presynaptic axon properties. The tonic and phasic NO signals are generated, respectively, by eNOS and nNOS, the former in blood vessels and the latter in neurones (Hopper & Garthwaite 2006). In this respect, it is notable that nerve fibres are prominent sites of cGMP accumulation in response to NO in the hippocampus (van Staveren et al. 2004). In other central axons (optic nerve), endogenous NO, via cGMP, causes a depolarisation apparently by directly engaging HCN channels (Garthwaite et al. 2006), an effect that would be expected to improve the fidelity of conduction (Soleng et al. 2003).

Immunohistochemical localisation of HCN channel subunits in the rat brain reviews a high density of HCN1 and HCN2 within the stratum radiatum of CA1

(Notomi & Shigemoto 2004). Expression of a functional heteromer of murine HCN1 and HCN2 channels, using a concatenated construct, gives rise to channels with a voltage dependence of activation similar to HCN2, whereas sensitivity to cyclic nucleotides was intermediate to both (Ulens & Tytgat 2001). Therefore the h-current in SC/C axons could potentially be regulated by cyclic nucleotides and compounds that affect the levels of cyclic nucleotides, such as NO.

3.2 AIM

This study was carried out to investigate axonal conduction during theta and gamma band stimulation of the SC/C pathway and, in particular, the influence of HCN channel function upon conduction and its possible modulation by NO-cGMP.

HYPOTHESIS: The NO-cGMP-HCN channel signalling pathway is present in the SC/C axons; NO and cGMP modulate axonal function via axonal HCN channels.

3.3 METHODS

Tissue preparation

All procedures were in accordance with regulations the Animals (Scientific Procedures) Act 1986. For extracellular recordings, hippocampal slices were prepared from six to eight week-old male Sprague-Dawley (SD) rats. The animals were killed by stunning followed by cervical dislocation and decapitation. For intracellular recordings, hippocampi were obtained from male or female 16- to 25-day-old SD rats after cervical dislocation and decapitation; younger animals were used as CA3 pyramidal cells at this post-natal age are more amenable to patch-clamping. The brain was rapidly removed and the hippocampus dissected out and placed in cold (4 °C) artificial cerebrospinal fluid (aCSF). Transverse slices, 400 μm thick, were prepared using a McIlwain tissue chopper (for extracellular recordings) or a Vibratome (for intracellular recordings) and maintained in a humidified interface holding chamber containing aCSF at room temperature. After a period of recovery (at least 60 min), one slice was transferred into a submerged chamber and continuously perfused with oxygenated aCSF.

Electrophysiological recordings (at 30 – 32 °C)

Bipolar twisted NiCr-insulated electrodes were placed more towards the fimbrial end of the SC/C pathway relative to the recording electrode; the recording electrode (5-10 MΩ) was filled with aCSF. A stimulus (200 μs duration) at constant voltage is generated using a Digitimer stimulator (Welwyn Garden City, Hertfordshire). The recording and stimulating electrodes were positioned in *stratum radiatum* of area CA1 to elicit an appreciable presynaptic CAP and field excitatory postsynaptic potential (fEPSP; figure 3.2A); the presynaptic action potentials were isolated pharmacologically from postsynaptic activity by bath application of 20 μM CNQX and 50 μM D-AP5 (figure 3.2B). Initially the input-output relationship of stimulus intensity (typically between 1 and 20 V) against CAP amplitude was determined, and the voltage adjusted to about a third of maximum, i.e. a submaximal stimulus. Baseline recordings for about 15 min at 0.2 Hz, controlled by a Master-8 scheduler (Intracel Ltd, Royston, UK) were performed to ensure stability

of the slice. For all extracellular recordings, 'n' refers to the number of individual slices. Test trains consisting of 80 pulses at 5, 30 or 100 Hz, separated by 5 min intervals at 0.2 Hz. All recordings were made at 30 - 32 °C. Signals were amplified with an Axoclamp-2B (Axon Instruments, Foster city, CA), filtered at 5 kHz, digitised at 20 kHz (100 Hz stimulation) or 50 kHz (0.2 Hz and 5 Hz stimulation) and stored on the computer hard disk using pClamp6 (Axon instruments, Foster City, CA). To minimise the stimulus artefact obscuring the triphasic fibre volley, a trace in the presence of 0.5 μM TTX was retrospectively subtracted.

CAP amplitudes were measured from the first positive to the most negative peak; latencies were measured from the start of the stimulus artefact to the most negative peak (figure 3.2B). Test frequency values were normalised relative to the mean of the 5 min baseline stimulation at 0.2 Hz.

L-nitroarginine (L-NNA), Br-cGMP, pCPT-cGMP, forskolin, ZD7288 and CsCl were washed in and out for at least 20 min; the CAP at 0.2 Hz was recorded throughout, and no change observed; Br- and pCPT-cGMP were added to the same slice; all forskolin concentrations were added cumulatively to the same slice. DEA/NO was present for 30 s at 0.2 Hz, prior to switching to 5 Hz. A series of interleaved control experiments were carried out to confirm the long-term stability of the preparation.

Figure 3.2 Field recording of the response to stimulation of SC/C fibres in the *stratum radiatum*

A, Following a stimulus, the presynaptic compound action potential (CAP) and the field excitatory postsynaptic potential (fEPSP), resulting from activation of the fibres and associated synapses in the vicinity of the recording electrode, can be seen. B, In the presence of the excitatory synaptic blockers, CNQX and D-AP5, the presynaptic CAP is isolated (Trace in TTX subtracted retrospectively).

Whole-cell recordings were made from CA3 *stratum pyramidale* without visual identification at 30 - 32 °C; all cells included in the study had a stable resting

membrane potential less than -50 mV. Pipette solutions contained (in mM): 150 $KMeSO_4$, 10 KCl, 10 HEPES, 4 NaCl, 4 MgATP; the pH was adjusted to 7.39 - 7.4 and the osmolarity to 280-290 mOsm / l. Open pipette resistance was 2-4 MΩ. Antidromic activation of the Schaffer collateral was carried out using a supramaximal stimulus. Under voltage clamp conditions, currents were recorded using an Axopatch 1D amplifier and pClamp7 (Axon Instruments, Foster city, CA) in neurones clamped at holding potentials from -60 to -75 mV. Stable access resistances were 30-75 MΩ; 80% compensation of the series resistance was used; voltages were not corrected for liquid junction potentials. The recordings were filtered at 1 kHz and sampled at 2 kHz. I_h amplitudes were obtained by single exponential fits to the charging curve; current amplitude was measured as the difference between the plateau current level at the end of the hyperpolarising step and the point where the fitted line intersected with the capacitative transient. The instantaneous current component was measured as the difference between this point of intersection and the holding current. Cells that showed any conduction failures or little or no I_h (n=5 of 18; arbitrarily < 40 pA) were rejected.

For current clamp, the neuronal membrane potential was held approximately at -62 mV (the apparent average resting membrane potential) and signals were recorded by using an Axoclamp-2B amplifier in bridge mode and pClamp7 (Axon Instruments, Foster City, CA). The bridge balance was constantly monitored throughout the experiment and adjusted appropriately. The voltage signal was filtered at 1 kHz and sampled at 2 kHz, which appeared sufficient to record accurate waveforms. Cells included in the study had an action potential height of at least 60 mV. The afterdepolarisation, immediately following the initial fast repolarisation, was measured as the area under the curve up to 60 ms (as full time of scale at 5 Hz) to the baseline membrane potential.

All analyses were performed offline using Clampfit 8.0 (Axon Instruments, Foster City, CA). Patch longevity was usually a maximum of 30 min, so CsCl (2 mM) was used to block I_h because of the longer wash in times required (10 - 15 minutes) for ZD7288 and other organic blockers.

Statistics

At 5 Hz, a Student's paired t-test was performed on the last stimulus to determine if the control and test situation were different at the end of the train of activity. At 30 and 100 Hz, a repeated measure ANOVA was performed on the entire 80 stimuli, as well as on bins of 10 stimuli to determine when the control and test cases were different during the course of the stimulation.

3.4 RESULTS

The CAP resulting from electrical stimulation of the SC/C pathway was recorded within the CA1 *stratum radiatum* after pharmacological isolation from potentials mediated by ionotropic glutamate receptors. Preliminary experiments indicated that blockade of I_h, with Cs^+ (2 mM) or ZD7288 (10 μM), had no obvious effect on the CAP properties at 0.2 Hz stimulation, so this frequency was adopted as the baseline. Test frequencies of 5, 30 and 100 Hz were chosen for study because they cover the theta and gamma rates of stimulation typically used in LTD and LTP induction protocols.

100 and 30 Hz stimulation

Following an action potential, a brief supernormal period of reduced firing threshold and increased conduction velocity has been observed in many different axons (Gardner-Medwin 1971; Wigstrom & Gustafsson 1981). In accordance with these findings, after two successive stimuli of equal intensity there was a decrease in the latency of the second volley with no significant effect on the amplitude (figure 3.3A), implying that the same numbers of fibres was being activated. Stimulation with 80 pulses at 100 Hz (figure 3.3B) resulted in an initial increase in peak amplitude followed by a decrease (figure 3.4A), the changes in volley latency reciprocating this trend (fig. 3.4C), showing a clear alternation in CAP excitability from supernormality to subnormality.

At a concentration selectively blocking HCN channels in the hippocampus (Huang & Hsu 2003), ZD7288 (10 μM) had no significant effect on CAP properties over the entire train at 100 Hz stimulation (figure 3.4B,D,E,H; repeated measures ANOVA; p>0.05). Similar negative results were found with 2 mM Cs^+ both at 100 Hz (figure 3.4F,I) and at 30 Hz (figure 3.4G,J). However, statistical analysis on bins of 10 stimuli revealed consistently significant greater amplitude differences at the beginning of 100 and 30 Hz stimulation and consistently significant latency increases at the end of stimulation in the presence a HCN channel blocker.
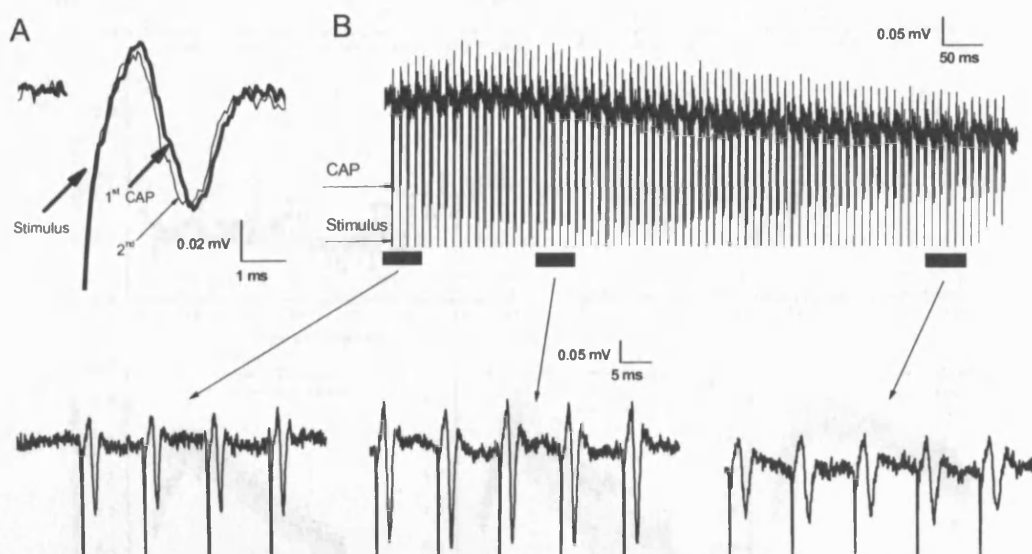
Figure 3.3 Changes in CAP amplitude and latency in response to 100 Hz stimulation

A, average traces of the first and second evoked fibre volleys by pulses of identical strength separated by 10 ms (i.e. the first and second CAPs from the train of 80 stimuli at 100 Hz in B; n=13). The amplitude was unchanged for both (p=0.89) while the latencies were significantly different (p<0.001); the stimulus artefact was cropped for clarity.

B, a typical example of 80 stimuli at 100 Hz with expanded sections as indicated. As stimulus train proceeded, a transition in the amplitude of the fibre volley was clear.

Figure 3.4 Changes in CAP amplitude and latency in response to 80 stimuli at 100 and 30 Hz with and without block of I_h

A,B, a typical example of the CAP amplitude at 0.2 Hz and at 100 Hz (as indicated by the bars). In control (black squares) and in the presence of 10 µM ZD7288 (red squares), the increase and decrease in amplitude follow the same trend.

C,D, the latency transition in the same slice as A.

E,H, mean amplitude and latency values at 100 Hz normalised to the stable mean at 0.2 Hz (n=6). * indicate significant differences in the presence of 10 µM ZD7288 (Repeated measures ANOVA; p<0.05).

F,I, mean amplitude and latency values using 2 mM Cs^+, another HCN channel blocker (n=7). * indicate significant differences between the control values and measurements in the presence of Cs^+ (Repeated measures ANOVA; p<0.05). Some sem were omitted in either the positive or negative direction for clarity of data points.

G,J, mean amplitude and latency values at 30 Hz normalised to the stable mean at 0.2 Hz (n=7). * indicate significant differences in the presence of Cs^+ (Repeated measures ANOVA; p<0.05).

5 Hz stimulation

Under control conditions, stimulating the axons with 80 pulses at 5 Hz had little effect on the CAP amplitude (figure 3.5A,E), although there was a significant increase in the latency (figure 3.5C,G). In the presence of ZD7288, the CAP recorded became significantly smaller and slower during the course of the train (figure 3.5B,D,E,G). This finding is in good agreement with previously published data (Soleng et al. 2003) and suggests that in the absence of I_h, there is a decrease in axon excitability accompanied by impaired conduction. The same results were found with Cs^+ (2 mM), whose effects were partially reversed following a 30 min wash out (figure 3.5F,H), as expected (Harris & Constanti 1995).

Regulation of axonal HCN channels by NO-cGMP pathway

Since the effect of blocking I_h was most pronounced at 5 Hz stimulation frequency, this condition was adopted for investigating the possible modulation by cGMP. Initially, given the recent precedent from optic nerve axons (Garthwaite et al. 2006), I investigated if the NO-cGMP pathway impinged on axonal function. Blockade of endogenous NO production using L-NNA at a concentration (100 μM) that inhibits all isoforms of NOS (Hopper & Garthwaite 2006) had no effect at the baseline or test frequency (figure 3.6A,C). Exogenous NO was delivered in the form of the NONOate DEA/NO, which releases authentic NO with predictable kinetics (Keefer et al. 1996; chapter 2). When applied in the presence of L-NNA, neither 0.3 μM (data not shown) nor 10 μM DEA/NO had any observable effect on the CAP amplitude or latency recorded at 0.2 or 5 Hz (figure 3.6B,D). The selected DEA/NO concentrations cover the range that cause cGMP accumulation in hippocampal slices and that are capable of substituting for endogenous NO in the induction of hippocampal synaptic plasticity (Bon & Garthwaite 2001; Bon & Garthwaite 2003; Hopper & Garthwaite 2006).

To investigate possible modulation by cyclic nucleotides more directly, analogues of cGMP, namely 8-Br-cGMP and 8-pCPT-cGMP, were used at typical concentrations of 100 μM (DiFrancesco & Tortora 1991; Pape & Mager 1992; Bains & Ferguson 1997). No effect of either analogue was seen at 0.2 or 5
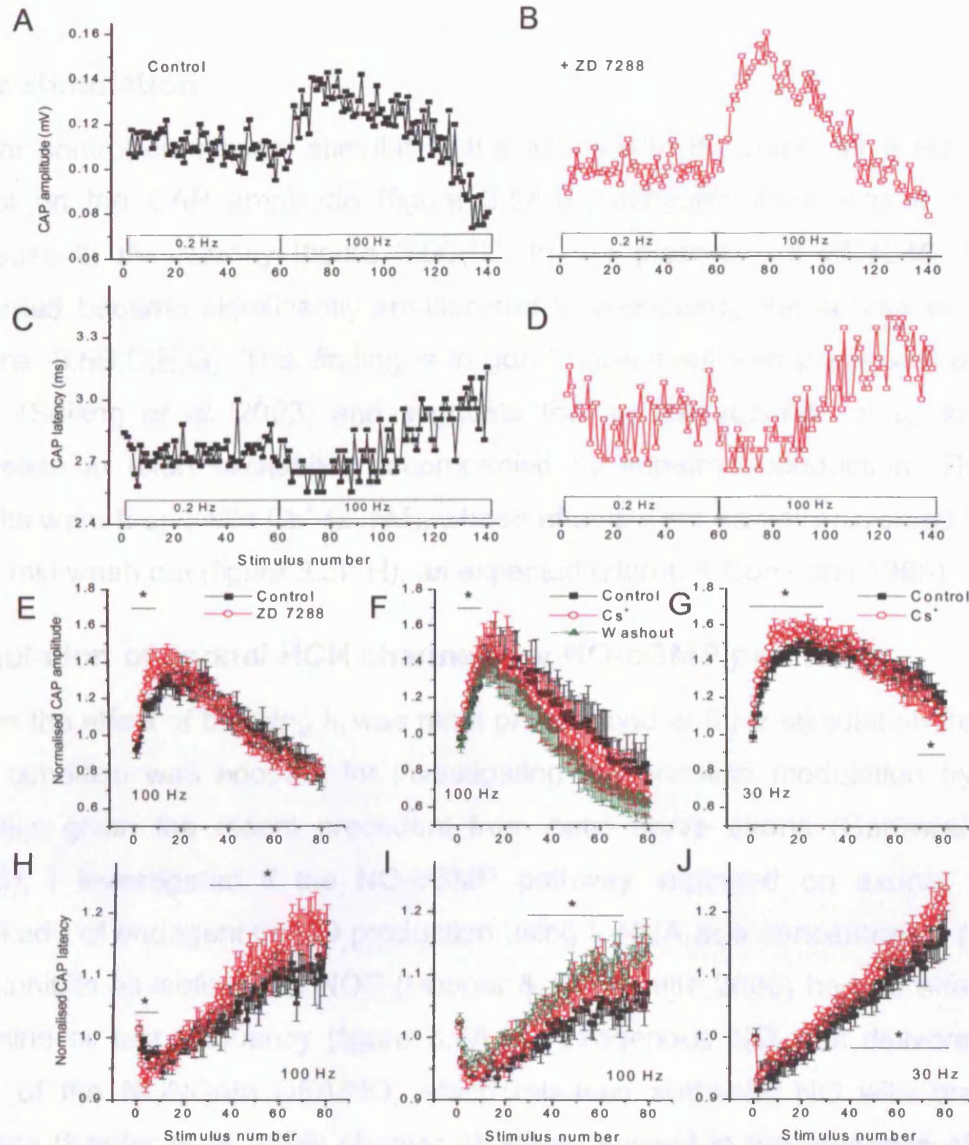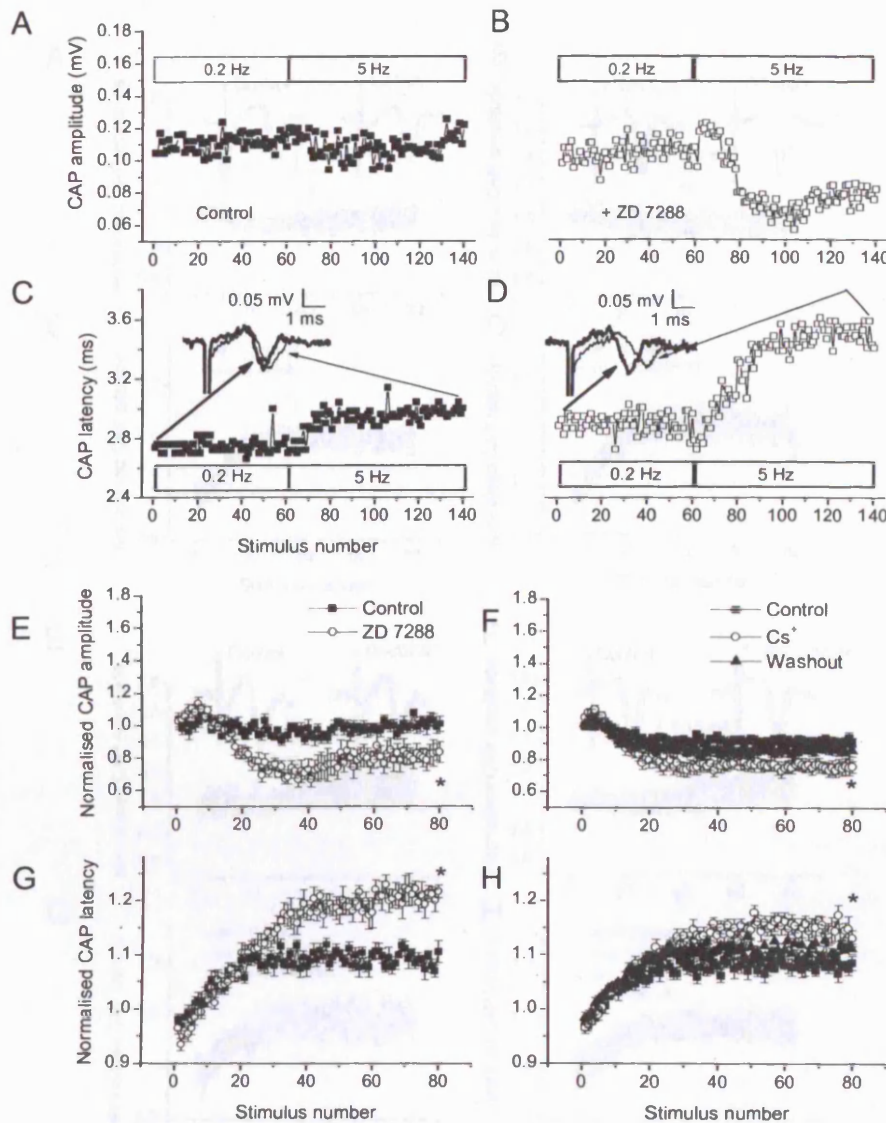
Figure 3.5. Changes in CAP amplitude and latency in response to 80 stimuli at 5 Hz with and without I_h block

A,B, a typical example of the CAP amplitude at 0.2 Hz and at 5 Hz (as indicated by the bars). In control experiments (closed squares) at 5 Hz the amplitude values ended at approximately their initial value. In the presence of 10 µM ZD7288 (open squares) the amplitude decreased considerably as the stimulation at 5 Hz progressed.

C,D, a typical example of the CAP latency at 0.2 Hz and at 5 Hz (as indicated by the bars). In control experiments (black) the latency increases at 5 Hz. ZD7288 (grey) gave a further increase.

Insets, average traces of the first (black) and the last (dashed) three CAP responses to 80 stimuli at 5 Hz.

E,G, mean amplitude and latency values at 5 Hz normalised to the stable mean at the baseline frequency, 0.2 Hz (n=6). ZD7288 had a significant effect on the amplitude and latency (*: Student's paired t-test; p<0.05)

F,H As for E & G, using 2 mM Cs$^+$ to block I_h (n=8).On wash out there was a partial reversal of the effects of the amplitude and latency.
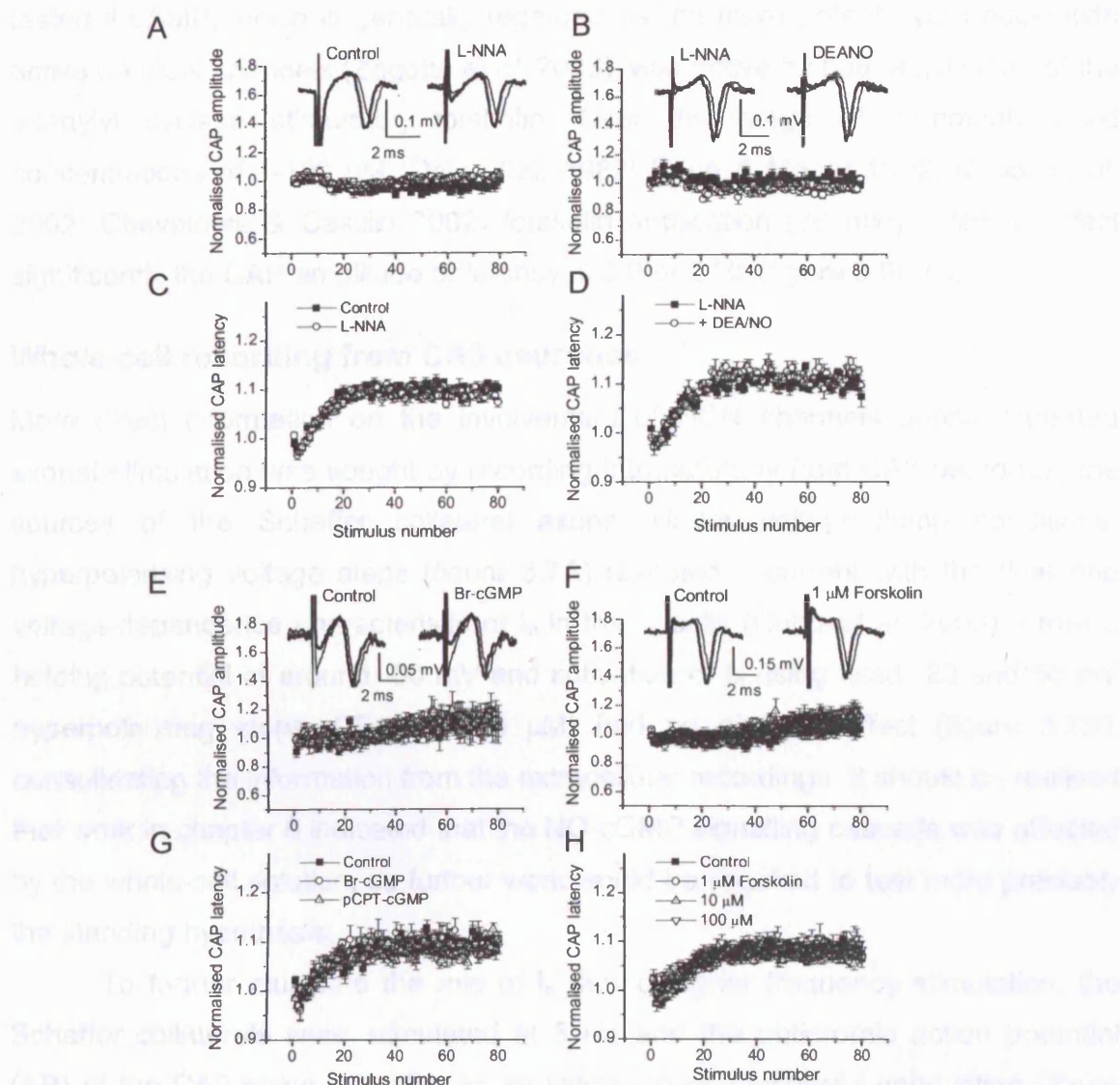
Figure 3.6. The effect of the pharmacological manipulations of the NO-cGMP and cAMP signalling pathways on CAP amplitude and latency in response to 80 stimuli at 5 Hz

Each pair of graphs show the mean amplitude and latency values at 5 Hz normalised to the stable mean at 0.2 Hz. In all cases, there were no obvious differences between drug conditions (Student's paired t-test; p.0.05).
A,C, Blockade of endogenous NO production using 100 µM L-nitroarginine (L-NNA; n=11).
B,D, Application of exogenous NO using 10 µM DEA/NO that results in maximal production of cGMP (n=4).
E,G, Increasing cGMP levels by application of membrane-permeable analogues of cGMP, 8-Br-cGMP and 8-pCPT-cGMP (both 100 µM; n=4).
F,H, Augmentation of the level of cAMP using forskolin (1, 10 or 100 µM; n=9).
Insets: typical average waveforms for fibre volleys at 0.2 (mean of all 60 stimuli; thick line) and at 5 Hz (mean of the latency plateau; thin line) from one slice.

Hz stimulation frequency (figure 3.6E,G) during perfusion for 20 min. Finally, I tested if cAMP, which is generally regarded as the more potent cyclic nucleotide active on HCN channels (Zagotta *et al.* 2003), was active by bath application of the adenylyl cyclase stimulator, forskolin. Over the range of commonly used concentrations of 1-100 µM (Daly *et al.* 1982; Pape & Mager 1992; Mellor *et al.* 2002; Chevaleyre & Castillo 2002) forskolin application (20 min) failed to affect significantly the CAP amplitude or latency at 0.2 or 5 Hz (figure 3.6F,H).

Whole-cell recording from CA3 neurones

More direct information on the involvement of HCN channels during repeated axonal stimulation was sought by recording intracellularly from CA3 neurones, the sources of the Schaffer collateral axons. Under voltage-clamp conditions, hyperpolarising voltage steps (figure 3.7A) revealed a current with the time and voltage-dependence characteristic of I_h in these cells (Cobb *et al.* 2003). From a holding potential of around -60 mV and activation of I_h using fixed 20 and 50 mV hyperpolarising steps, DEA/NO (10 µM) had no obvious effect (figure 3.7B), consolidating the information from the extracellular recordings. It should be realised that work in chapter 6 indicated that the NO-cGMP signalling cascade was affected by the whole-cell solution, so further work would be required to test more precisely the standing hypothesis.

To further elucidate the role of I_h during higher frequency stimulation, the Schaffer collaterals were stimulated at 5 Hz and the antidromic action potential (AP) at the CA3 soma recorded as an indication of successful conduction (figure 3.7C). As expected, an all-or-none response with no rise to threshold was observed. An afterdepolarisation immediately following the sodium spike and subsequent medium and slow afterhyperpolarisations were also as expected (Vervaeke *et al.* 2006). The h-current was measured following hyperpolarising steps of 20 and 50 mV before and after 80 stimuli at 5 Hz (figure 3.8A). Axon stimulation did not result in any significant changes in I_h elicited following a -20 mV step while on a -50 mV step, there was a significant decrease in amplitude (figure 3.8A-C). I_h is partially activated at the holding potential (Cobb *et al.* 2003) generating a cationic inward current that would contribute to the instantaneous current component. Therefore, a decrease on a -50 mV step is suggestive of more
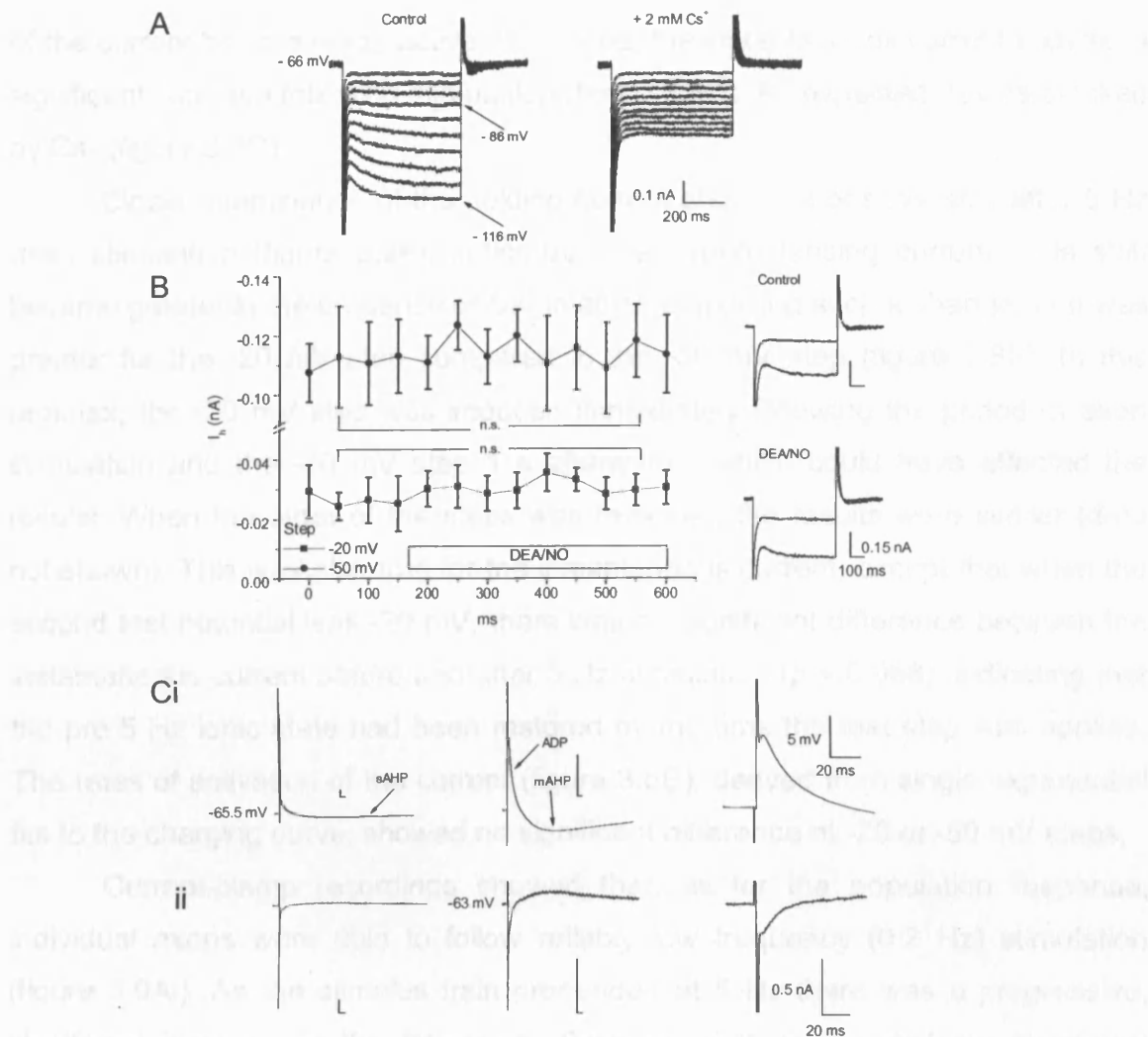
Figure 3.7. I_h and the antidromic AP in CA3 pyramidal cells

A, Under voltage clamp conditions, 600 ms voltage steps from -66 mV to -116 mV (-5 mV steps) activated an inward current with slow onset. This current was sensitive to 2 mM Cs^+. This cell, recorded in the presence of 20 μM CNQX, 50 μM D-AP5 and 50 μM picrotoxinin, had a resting membrane potential of -61 mV.

B, 10 μM DEA/NO had no effect on I_h amplitude activated by -20 and -50 mV steps (n=5; Student's paired *t*-test; p<0.05). Data points represent bins of 4 results.
Insets: typical current recorded during the experiment.

C, Antidromic activation of CA3 pyramidal neurones via stimulation of Schaffer Collaterals in the CA1 *stratum radiatum*

i, under current clamp conditions, stimulation results in a clear action potential without a rise to threshold. Immediately after there was an after-depolarisation (ADP) followed by a medium and slow afterhyperpolarisation (mAHP & sAHP). Recorded in the presence of 20 μM CNQX, 50 μM D-AP5, 50 μM picrotoxinin and 200 μM saclofen.

ii, a different cell, under voltage clamp conditions, exhibits the currents that reflect the membrane potential changes in (i). Recordings were carried out in the presence of 20 μM CNQX, 50 μM D-AP5 and 50 μM picrotoxinin.

of the current being already activated. Indeed, the instantaneous current showed a significant increase following stimulation (figure 3.8D). As expected, I_h was blocked by Cs^+ (figure 3.8C).

Closer examination of the holding current showed a positive shift after 5 Hz axon stimulation (figure 3.8F), indicative of a hyperpolarising current. This shift became greater in the presence of Cs^+ in all cells showing such a change, and was greater for the -20 mV step compared to the -50 mV step (figure 3.8F). In this protocol, the -20 mV step was imposed immediately following the period of axon stimulation and the -50 mV step 1 s afterwards, which could have affected the results. When the order of the steps was reversed, the results were similar (data not shown). This was also true for the instantaneous current, except that when the second test potential was -20 mV, there was no significant difference between the instantaneous current before and after 5 Hz stimulation (p = 0.068), indicating that the pre 5 Hz ionic state had been restored by the time the test step was applied. The rates of activation of the current (figure 3.8E), derived from single exponential fits to the charging curve, showed no significant difference at -20 or -50 mV steps.

Current-clamp recordings showed that, as for the population response, individual axons were able to follow reliably low frequency (0.2 Hz) stimulation (figure 3.9Ai). As the stimulus train proceeded at 5 Hz there was a progressive, significant increase in the latency to firing as well as an obvious, significant hyperpolarisation (figure 3.9Aii,B). As expected from the field potential results, Cs^+ had no effect on the fidelity of conduction at 0.2 Hz (figure 3.9Aiii,B,C,E). At 5 Hz, Cs^+ caused a significantly greater increase in the latency to the action potential peak and a greater, yet not significant hyperpolarisation (figure 3.9Aiv,B,C). By superimposing and aligning the baseline membrane potential of the first and last action potential, it can be seen that over the course of 80 stimuli at 5 Hz, there was a significant increase in the ADP (figure 3.9D, E). In the presence of Cs^+, the ADP was significantly larger over the 0.2 Hz period. Similarly the ADP increased following 5 Hz stimulation, but the final increase was significantly greater (figure 3.9E).
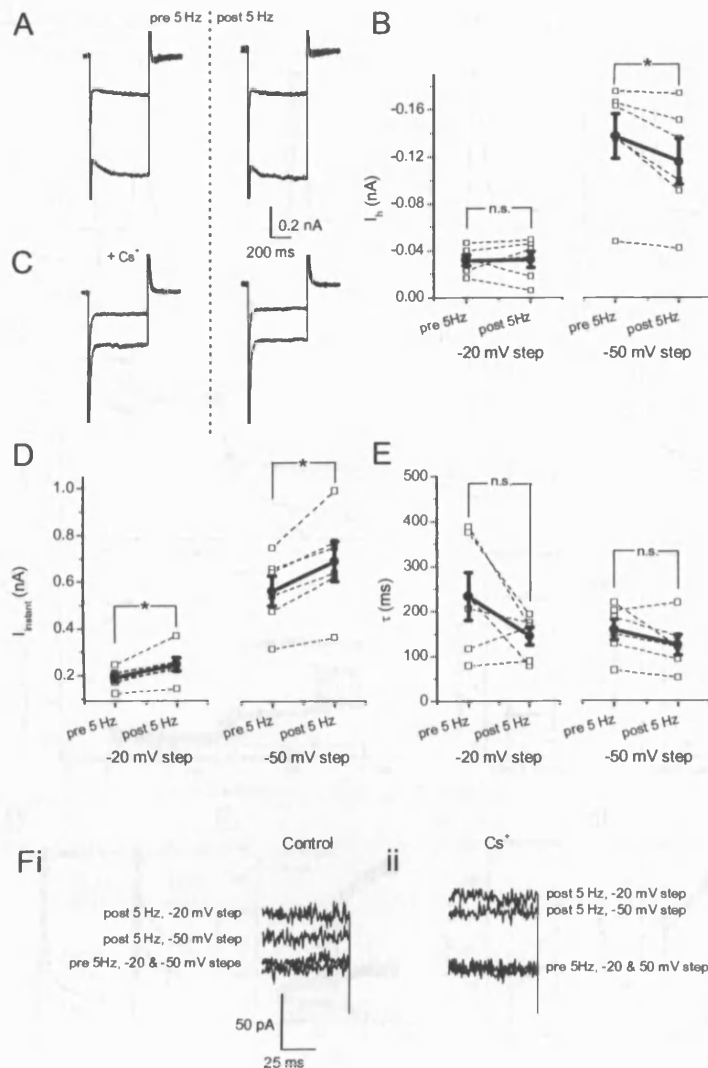
Figure 3.8 The changes in the membrane currents measured from the soma of CA3 pyramidal cell before and after 5 Hz stimulation

A, a typical response of a cell to -20 and -50 mV steps. (i) and (ii) are the responses immediately before and after 80 stimuli at 5 Hz respectively. This cell, in the presence of 20 µM CNQX, 50 µM D-AP5 and 50 µM picrotoxinin, had a resting membrane potential of -65 mV and the holding potential was − 73 mV.

B, raw (open squares) and mean (filled circles; n=6) values indicating the changes in the h-current measured at two step potentials before and after 5 Hz stimulation. For the -20 mV step, there was no significant difference (Student's paired t-test; p = 0.89) between current amplitude values before and after 5 Hz. Conversely, for the -50 mV step, there was a significant difference (Student's paired t-test, p < 0.03).

C, same as for A but in the presence of 2 mM Cs$^+$.

D, raw (open squares) and mean (filled circles; n=6) values for the instantaneous current component. Stimulation at 5 Hz resulted in significantly different values at both step potentials (Student's paired t-test, p < 0.02).

E, summary of the changes in the time constants of activation for I_h. Values are derived from exponential fits during the two voltage steps of -20 and -50 mV. There were no significant differences following stimulation at 5 Hz at either voltage step (paired student's t-test; n=6)

F, the changes in the holding current immediately before and after 5 Hz stimulation

i, following stimulation at 5 Hz, there was a change in the outward direction indicative of a hyperpolarisation.

ii, As for (i) but in the presence of 2 mM Cs$^+$. The outward changes in the holding current during the two steps were larger when I_h was blocked (Student's paired t-test; 20 mV, p<0.035; 50 mV, p<0.02). The holding current prior to the -50 mV step was significantly less positive than the holding current prior to the -20 mV (Student's paired t-test; p<0.03).
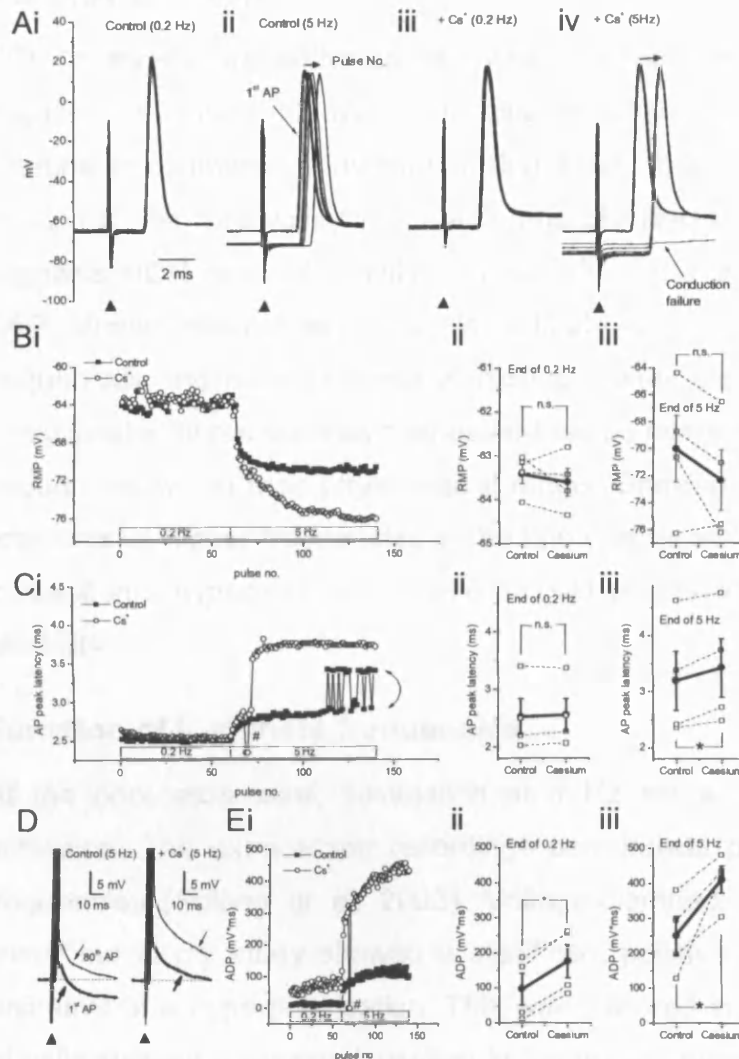
Figure 3.9 The changes in the membrane potentials recorded from the CA3 pyramidal cell soma during stimulation

A, i,ii, a series of traces from a during stimulation at 0.2 Hz (one trace every 50 s shown) and at 5 Hz (one trace every 2 sec displayed). There was little or no change at 0.2 Hz, while at 5 Hz there was a significant hyperpolarisation in the membrane potential and an obvious increase in the action potential latency (Student's paired t-test; p<0.01)

iii, iv, as for i,ii but in 2 mM Cs^+. Again at 0.2 Hz, there is apparently little/no change. At 5 Hz, irrespective of conduction failures, the hyperpolarising shift in the membrane potential is more pronounced as is the increase in latency.

B, i, an relatively non-representative example of the changes in the membrane potential during stimulation at 0.2 and 5 Hz (as indicated by the bar) with and without I_h block.

ii, iii, Cs^+ had no significant effect on the membrane potential at 0.2 Hz or at 5 Hz (Student's paired t-test; n=4).

C, i, an example of the representative changes in the latency to the peak of the action potential (AP) during stimulation at 0.2 and 5 Hz (as indicated by the bar) with and without I_h block. Cs^+ appeared to cause differences at 5 Hz. # indicates conduction failures. In the absence of Cs^+, this neurone showed some jitter after reaching a plateau at 5 Hz as indicated by the double-arrowed line.

ii, Cs^+ had no significant effect on the time to peak at 0.2 Hz (Student's paired t-test; n=4).

iii, Blocking I_h increased the peak latency (Student's paired t-test; p<0.035; n=4).

D, Alignment of the baseline membrane potential for the first and last stimulation at 5 Hz highlights a change in the afterdepolarising potential (ADP). This change seemed larger in the presence of Cs^+.

E, i, timecourse of the changes in the ADP during 0.2 and 5 Hz stimulation. # indicates conduction failures.

ii, iii, The I_h blocker increased the ADP at both frequencies of stimulation (Student's paired t-test; p<0.05; n=4)

3.5 DISCUSSION

HCN channels are activated at hyperpolarized membrane potentials (typically negative to about -60 mV), producing an inward current that depolarises the neurone to counteract a hyperpolarising input. At the baseline stimulus frequency of 0.2 Hz, the fibre volley was stable and blocking I_h had no obvious effect. This suggests HCN channel activity may not affect the action potential and therefore CAP shape; alternatively it could indicate quite low h-current levels at low frequencies and most probably at resting membrane potentials. It is known that unmyelinated fibres such as desheathed vagus nerve hyperpolarise at higher firing frequencies within their physiological range (Grafe et al. 1997). Therefore, action potentials at higher frequencies in the fine calibre SC/C axons might be expected to result in a hyperpolarisation, which could conceivably interfere with conduction reliability.

Function of I_h at theta frequencies

At the population level, stimulation at 5 Hz led to an increased threshold for activation. The extracellular recordings corroborate published findings at similar frequencies (Soleng et al. 2003). Voltage-clamped, intracellular measurements presented in my study showed a significant positive shift in the holding current, indicative of a hyperpolarisation. This was mirrored in current-clamp mode, where all cells showed a hyperpolarisation in the resting membrane potential during 5 Hz stimulation. Individual axons showed changes in the latency to peak reflecting the CAP latency increase. This intracellular information confirms and reinforces the interpretation that the activity-induced increase in threshold is a hyperpolarisation (Soleng et al. 2003; Munoz-Cuevas et al. 2004). This activity-induced hyperpolarisation has been shown to be blocked by ouabain, suggesting an involvement of the Na^+-K^+-ATPase in this process (Kobayashi et al. 1997; Munoz-Cuevas et al. 2004). Voltage-clamped measurements showed an increase in the instantaneous component during the hyperpolarising steps to activate I_h. This is suggestive of a greater standing I_h at the holding potential, presumably activated by the activity-induced hyperpolarisation.

Under current-clamp, I found an increase in somal ADP that follows the increasing spike peak latency during stimulation at 5 Hz. In many principal brain neurones, the somatic spike ADP is thought to be generated by a Ca^{2+}-activated current (Wong & Prince 1981; Jung *et al.* 2001), low voltage-gated, persistent Na^+ current (Azouz *et al.* 1996) or Na^+-activated K^+ channel (Liu & Stan Leung 2004). This change in the repolarisation of the membrane would presumably impact on the recovery from inactivation of Na^+ channels. This coupled with the activity-induced hyperpolarisation moving the membrane potential further from threshold would likely cause action potential failures and underlie the decrease in CAP. A part of the increase in ADP could also be simply due to the concomitant increase in driving force following the hyperpolarisation of the membrane potential.

When I_h was blocked, there was an increase in the CAP latency, seen also in individual somal action potential recordings; there was a decrease in the CAP amplitude, seen as a greater number of AP failures in individual axons. However, there was no significant increase in the extent of the hyperpolarisation in the presence of Cs^+. One cell (out of four) in particular hyperpolarised to the maximum level during the control stimulus train and displayed no obvious difference in the presence of Cs^+. This seems strange given the important role of I_h to act to dampen hyperpolarisation and maintain excitability; however a larger sample size would be required to elucidate the true effect. Unlike the voltage-clamp data, no cells studied under current-clamp were rejected, because the interpretation of the size of the I_h sag, which is an indirect measure of the level of current activation, is difficult (Aponte *et al.* 2006). Furthermore, it is intriguing that the soma of different cells should display such marked changes in the level of I_h. Perhaps HCN channels are mainly located on dendrites that may have been lost depending on their orientation to the slicing angle.

Given the pronounced effects of ZD7288 or Cs^+ on CAP at 5 Hz stimulation, it is possible that I_h is larger across the axon population. SC/C axons display stronger signal preservation than the soma or initial segment of CA3 pyramidal cells (Meeks *et al.* 2005), suggesting a decrease in CAP amplitude represents a marked effect. It has been shown that both granule cells and the attached mossy

fibre show ADPs (Geiger & Jonas 2000), suggesting effects at the soma may reflect changes occurring in the axon. However, the duration of axonal action potentials, ADP and the resting membrane potential, all of which will influence I_h activation, may cause subtle deviations from that recorded in the soma. Immunohistochemical localisation of channel subunits suggests a change in the HCN subunits present in the various *strata* of the hippocampus in which the CA3 soma and the Schaffer Collateral exist (Notomi & Shigemoto 2004). For this reason, there may be subtle differences in I_h in different parts of the CA3 pyramidal cell, as for the non-inactivating K^+ current, I_m (Vervaeke *et al.* 2006). This makes the interpretation of the whole-cell I_h data difficult, yet unavoidable problem given the small size of the axons precluding them from individual electrophysiological analysis. Another important caveat to the interpretation is that Cs^+ is non-specific, and ZD7288 was not used (because of the longer wash in times) to determine if the effects seen were attributable to I_h; an alternative strategy may be to block inwardly-rectifying channels, which are also blocked by Cs^+, with low micromolar Ba^{2+}.

In the presence of Cs^+ the somal ADP was increased even at the 0.2 Hz stimulation frequency. Previous work in CA1 pyramidal cells suggested that the mAHP is caused, in part, by the deactivation of I_h (Gu *et al.* 2005a). This would therefore suggest that blocking HCN channels allows the ADP to increase in size, as seen in our results. However this increase in the ADP had no effect on the ability of the axons to respond to 0.2 Hz stimulation at the individual or population level. In CA1 cells, the role of deactivation of HCN channels is only consistently important at -80 mV, not at -60 mV (Gu *et al.* 2005a). This highlights the role of I_h at 5 Hz because we find that the membrane potential hyperpolarises within this range. When I_h was unavailable, the ADP showed a further significant increase suggesting that I_h may not only be acting to reduce hyperpolarisation, but its deactivation perhaps reduces the extent of the ADP and therefore prolongs inactivation of Na^+ channels.

NO-cGMP-HCN channel signalling at theta frequencies

This obvious importance of HCN channels in the fidelity of conduction prompted investigation of modulation by the direct binding of cGMP to the C-terminal cyclic

nucleotide binding domain (CNBD; Ludwig *et al.* 1998; Zagotta *et al.* 2003). The apparent presence of HCN1 and 2 subunits within the CA1 *stratum radiatum* (Notomi & Shigemoto 2004) circumstantially implies axonal I_h would derive from a channel comprising of one or both of these subunits. HCN2, along with the HCN4 isoform, is particularly sensitive to regulation by cyclic nucleotides, which shift activation to more depolarized membrane potentials, making the resting membrane potential more depolarized. Heteromeric HCN1-HCN2 channels have a voltage dependence of activation similar to HCN2, with intermediate sensitivity to cAMP (Ulens & Tytgat 2001). Due to the proposed role of NO in hippocampal synaptic plasticity (Hopper & Garthwaite 2006) and the tonic effect on optic nerve HCN channels (Garthwaite *et al.* 2006), I_h is a realistic candidate for regulation by cGMP and therefore NO. It is surprising that pharmacological manipulations of the NO/cGMP signalling cascade had no obvious effect on CAP latency (and amplitude) via I_h or another means. The use of L-NNA indicates that there is no tonic regulation of SC/C axonal I_h, nor acute regulation by NO donors or analogues causing phasic rises in cGMP. The NO-dependent effect on axonal excitability previously reported appears to occur only at room temperature (McNaughton *et al.* 1994).

Being ten-fold more potent (DiFrancesco & Tortora 1991; Zagotta *et al.* 2003), cAMP is generally regarded as the natural CNBD ligand, yet several examples are now to be found where the NO-cGMP pathway brings about changes in neuronal excitability using HCN channels (Pape & Mager 1992; Ingram & Williams 1996). To address this issue I used the diterpene, forskolin, which is known to activate adenylyl cyclase in this region of the hippocampus (Mons *et al.* 1995; Wong *et al.* 1999), leading to an increase in the levels of intracellular cAMP. As for the results from modulation of the NO/cGMP pathway, there was no obvious effect on CAP properties. The consistent lack of effect of changing cyclic nucleotide levels is expected as both cAMP and cGMP should be able to modulate the HCN subunit, albeit with different potency, as outlined previously. These results in SC/C axons mirror those in frog sciatic nerve, where increases in cyclic nucleotide levels also had no bearing on axonal excitability (Horn & McAfee 1977).

This lack of effect of all of these pharmacological interventions on CAP properties suggests there is no modulation by the NO-cGMP pathway of the native I_h via the CNBD or other cyclic nucleotide-regulated targets like cGMP-dependent protein kinases. This suggests that the native channel possesses properties consistent with the HCN1 homomeric channels with regard to changing cyclic nucleotide level sensitivity (Ulens & Tytgat 2001; Wang *et al.* 2001). This is interesting because in the rat optic nerve, tonic NO from eNOS, directly affects I_h via cGMP. However, these channels are thought to also contain HCN4, which would confer greater sensitivity to cyclic nucleotides (Garthwaite *et al.* 2006). The lack of a positive control is problematic, but all compounds have previously been used to facilitate transmission and affect plasticity in the hippocampus in the literature (Hopper & Garthwaite 2006). Other published work from the laboratory verifies the drugs' expected activity (Garthwaite *et al.* 2006), as well as work in chapter 4. The sequestering of the signalling cascades and gradients of the cyclic nucleotides away from the I_h channels could conceivably mean that the HCN channels in the Schaffer collateral would never see the increases in cGMP or cAMP induced by treatment with DEA/NO or forskolin. However in our experiments the cGMP analogues would be expected to diffuse throughout the axon unimpeded. Therefore HCN channels in SC/C axons have properties consistent with HCN1 homomeric channels with respect to cyclic nucleotide sensitivity.

Gamma frequency stimulation

At 30 or 100 Hz, I demonstrated an initial increase in the amplitude that mirrors the decrease in latency, similar to activity seen at 10, 20 and 50 Hz (Munoz-Cuevas *et al.* 2006). Previous reports considered the rise in the extracellular potassium concentration, $[K^+]_o$, as a possible explanation of this supernormal period. This rise in amplitude may be due to the lateral diffusion of the increasing $[K^+]_o$ in the inter-axonal space (Kocsis *et al.* 1983), which would, in turn, depolarise quiescent axons as well as the previously activated fibres, resulting in an increased likelihood of firing. In addition, the recruitment of 'threshold' fibres that fail sometimes but after firing once, keep firing because of this residual depolarisation afforded by the ADP (Munoz-Cuevas *et al.* 2006) could contribute to the increased CAP amplitude. The initial decrease in latency suggests an increase in synchrony of firing (Munoz-

Cuevas *et al.* 2006), which would have important implications with regard to message transmission to CA1 pyramidal cells, particularly when theta (Morgan & Teyler 2001) and long theta-patterned (Maffei *et al.* 2003) stimulation protocols. The persistent accumulation of K^+ and hence prolonged depolarisation could then contribute to Na^+ channel inactivation, subnormality and failures.

Compared to most other ion channels, I_h has relatively slow kinetics (Accili *et al.* 2002) and therefore its role at 30 and 100 Hz, and the consequences of blocking it, may be much more subtle: Blocking I_h led to a consistently, greater increase in the CAP amplitude at the beginning of the train. At the end of the train, there was a significantly greater increase in the latency. These differences may be explained by considering that the supernormal period may, in part, also be due to an ADP (Wigstrom & Gustafsson 1981; Soleng *et al.* 2004). The intracellular recordings showed that at 5 Hz the blockade of HCN channels increased the ADP. Assuming a similar outcome at 30 and 100 Hz, this would mean that the subsequent stimulation would occur during the ADP of the previous action potential. The membrane would be closer to threshold and more likely to fire. Towards the end of the pulse train, the enhanced ADP from blocking I_h would compound the K^+-induced depolarisation, making the axons less likely to fire, increasing the latency with respect to the control.

There are dense recurrent connections within the CA3 region, in which single pyramidal cells synapse with approximately 10,000 other pyramidal cells, giving rise to an autoassociative network (Amaral & Witter 1989). Field oscillations typically at 40 Hz, indicated that neuronal synchronisation is capable of affecting spiking behaviours of other CA3 pyramidal cells (Fujisawa *et al.* 2004). Presumably this phenomenon would affect the output of the cell via the Schaffer collateral. If this was the case and a lot of neurones were indeed firing at once, the discussed effect of K^+ accumulation and activation of quiescent fibres would act to modify the signal conveyed to the CA1 pyramidal cells.

Functional considerations

These findings add to the wealth of information about synaptic plasticity within the hippocampus. Within the literature there are several LTP-inducing protocols consisting of several trains of 100 Hz, such as the well characterised theta-burst

stimulation (Morgan & Teyler 2001). High frequency stimulation-induced LTP normally requires stimuli in the 30-100 Hz range (Bliss & Collingridge 1993). Yet at these high frequencies, both of which belong to the gamma range of frequencies (Traub et al. 1998), the involvement of presynaptic axonal I_h seems somewhat irrelevant. Since NO signals are required for LTP, which can be induced at 100 Hz, and I_h is not affected by 100 Hz stimulation, then NO and I_h do not interact during LTP. Supporting this, expression of LTP has been found not to involve changes in presynaptic spike properties (Laerum & Storm 1994). On the other hand, typical protocols for inducing LTD tend to involve repetitive stimulation at lower frequencies 4-12 Hz (theta range; see review, Malenka & Bear 2004). At these frequencies, I_h is required for fidelity of signal conduction. However, as the h-current in these axons is unresponsive to modulation by changing levels of cyclic nucleotides, the axon is probably not affected during the induction, expression or maintenance of LTD.

In conclusion, the NO-cGMP-HCN channel pathway is seemingly not present in SC/C axons and plays no role in modulating firing properties at different stimulation frequencies. Therefore it is likely that, like the optic nerve, other fibre tracts and nuclei within the CNS that possess HCN channels containing HCN2 and HCN4 subunits would express a form of I_h that can be regulated by the NO-cGMP pathway.

Chapter 4 - The NO-cGMP-HCN channel pathway in the auditory brainstem and cerebellum

4.1 INTRODUCTION

Within the literature there is a precedent for modulation of HCN channels by NO
and cGMP (see chapter 1). The apparent lack of changes in hippocampal axonal
HCN channel function during pharmacological manipulation of both cGMP and
cAMP levels (chapter 3) suggests that it is most likely the particular subunit
composition of the channel that accounts for the insensitivity to cyclic nucleotides.
From immunohistochemical studies, these axonal channels are circumstantially
made up of HCN1 and 2 subunits (Notomi & Shigemoto 2004). Heterlogously-
expressed HCN4 and HCN2 homomeric channels show greater degrees of
modulation by cyclic nucleotides than HCN1 channels (Accili *et al.* 2002), with
HCN4 channels showing the greatest. Therefore the obvious progression was to
investigate the NO-cGMP-HCN channel pathway in neurones showing high levels
of HCN4 expression with minimal HCN1 subunit protein. Such areas include the
ventral group and geniculate nuclei of the thalamus, components of the olfactory
pathway (nucleus of the lateral olfactory tract and external plexiform layer of the
olfactory bulb), parts of the auditory brainstem (ventral cochlear nucleus (CN) and
medial nucleus of the trapezoid body (MNTB)) and the deep cerebellar nuclei
(DCN; Notomi & Shigemoto 2004). The thalamic and olfactory regions were
rejected because they had already been studied (Pape & Mager 1992), or had a
less well-defined function. The last two brain regions were selected to be realistic
targets for NO-cGMP signalling because of the expression of HCN4 in the MNTB
neuronal cell bodies (Leao *et al.* 2006a) or neuropil of DCN neurones (Notomi &
Shigemoto 2004).

Auditory brainstem

Principal cells of the medial nucleus of the trapezoid body (MNTB; figure 4.1) are
vital parts of a circuit in the superior olivary complex (SOC). These cells have been
postulated to convert excitatory inputs from the contralateral cochlear nucleus (CN;
(Smith *et al.* 1991) to form inhibitory projections onto principal cells in the lateral
superior olive (LSO; Glendenning *et al.* 1985; Wenthold *et al.* 1987). Cells in LSO
compare this contralateral inhibitory input from MNTB with ipsilateral excitatory

input, a configuration believed to underlie their sensitivity to interaural intensity differences (Boudreau & Tsuchitani 1968). The function of MNTB cells was therefore thought to act as a simple sign-inverting relay synapse.

MNTB neurones receive their major input from the contralateral CN via globular bushy cells (GBCs; Smith *et al.* 1991). These afferents envelop the somata of the principal cells with some of the largest synaptic terminals in the CNS, the calyces of Held. In the juvenile rat, the calyx resembles a cup covering about 40% of the MNTB cell membrane with some finger-like stalks (Satzler *et al.* 2002). MNTB neurones appear to also receive other, smaller synapses onto the principal cells (Smith *et al.* 1991).
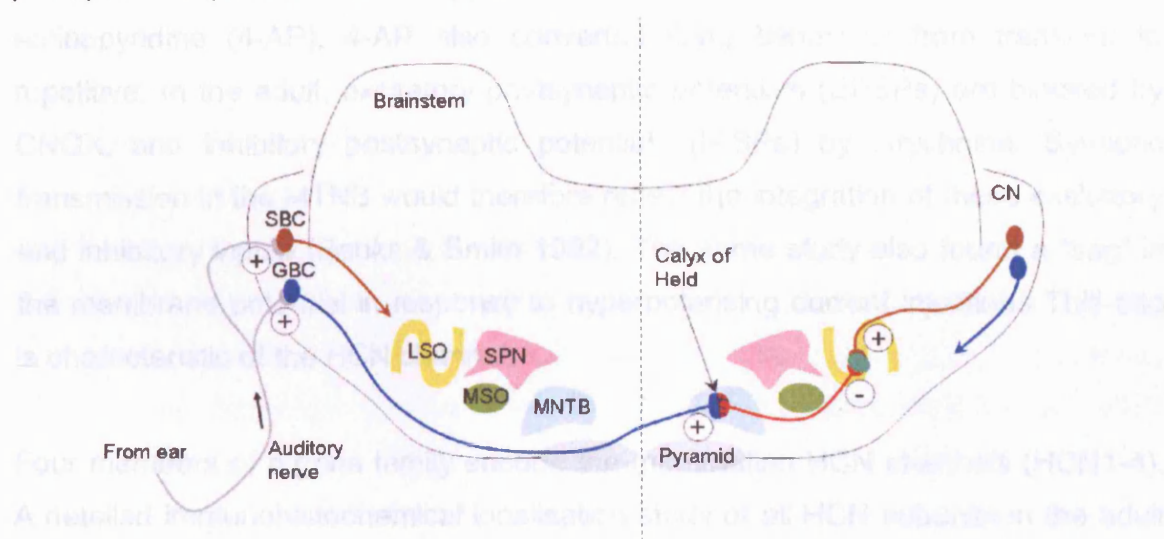
Figure 4.1 The circuitry of the auditory brainstem
Auditory stimuli are converted to signals by the cochlear hair cells and are transmitted to the ipsilateral anterior ventral cochlear nucleus (CN) by excitatory synapses onto the spherical and globular bushy cells (SBC and GBC). GBC axons (blue) cross the brainstem, decussate and synapse onto the principal neurones of the contralateral medial nucleus of the trapezoid body (MNTB). These neurones (red) in turn project to the lateral superior olive (LSO) forming an inhibitory synapse. In addition, the LSO receives excitatory input from the ipsilateral CN via the SBCs (brown). The precise timing of these two inputs at the LSO allows it to act as a coincidence detector of binaural cues. (MSO: medial superior olive; SPN: superior paraolivary nucleus; the superior olivary complex (SOC) comprises of the LSO, SPN and MSO)

The MNTB principal cells have spherical or ellipsoid somata that give rise to single large-diameter dendrites, which branch extensively and often extend beyond the borders of MNTB. The commonly observed axonal projections include not only those to the LSO, but also to the superior paraolivary nucleus (SPN), and the medial superior olive (MSO), and occasionally the lateral nucleus of the trapezoid

body. These connections with other nuclei hint that MNTB cells may play a more complicated role than simply a high-fidelity, sign-inverting synapse. The projections of individual MNTB cells show an orderly spatial arrangement of regions responsible for aural perception (Banks & Smith 1992).

The Calyx of Held is a high-fidelity synapse being able to follow reliably input in excess of 600 Hz and therefore well-suited for preserving the timing of afferent impulses from the cochlear nucleus (Wu & Kelly 1993). In response to current injection, MNTB principal cells exhibit rectification for depolarising currents. This rectification was removed on application of the potassium channel blocker, 4-aminopyridine (4-AP). 4-AP also converted firing behaviour from transient to repetitive. In the adult, excitatory postsynaptic potentials (EPSPs) are blocked by CNQX, and inhibitory postsynaptic potentials (IPSPs) by strychnine. Synaptic transmission in the MTNB would therefore reflect the integration of these excitatory and inhibitory inputs (Banks & Smith 1992). The same study also found a "sag" in the membrane potential in response to hyperpolarising current injections This sag is characteristic of the HCN channel.

Four members of a gene family encode the mammalian HCN channels (HCN1-4). A detailed immunohistochemical localisation study of all HCN subunits in the adult rat indicates a higher level of HCN2, with lower equal levels of HCN1, 3 and 4 in the MNTB (Notomi & Shigemoto 2004). In younger animals, amenable to patch-clamp analysis, strong HCN2 antibody labelling but no HCN1 staining is seen in the MNTB (Koch *et al.* 2004). *In situ* hybridisation data in adult rat also corroborates these findings of high levels of HCN2 and 4 with little or no HCN1 (Monteggia *et al.* 2000). More recently, robust membrane staining for HCN2 and HCN4 and no HCN1 is described in the young mouse (Leao *et al.* 2006a; Leao *et al.* 2006b). As the I_h in these cells should consist of mainly HCN2 and 4 subunits, it is plausible that the channels in the MNTB could be regulated by cyclic nucleotides (chapter one).

Indeed, a study investigating the enhancement of this current, I_h, by noradrenaline and 8-Br-cAMP confirmed this prediction. Sharp electrode voltage-

clamp analysis showed a depolarising shift in the steady-state activation curve (Banks *et al.* 1993). In current clamp, these effects on I_h resulted in a membrane depolarisation, an increase in input conductance, and a reduction in the voltage sag in response to hyperpolarising currents. This is an important finding because MNTB cells exhibit highly nonlinear behaviour near the resting membrane potential (RMP). Therefore this augmentation of HCN channel function could have profound effects on their responses to auditory input. In particular, the resulting depolarising shift in RMP would cause an increase in the aforementioned 4-AP-sensitive low-threshold potassium conductance. This in turn would decrease the duration of synaptic potentials and enhance the ability of MNTB cells to follow calyceal inputs at high rates. A similar role for I_h in determining the firing properties and excitability of neurones in the superior olivary complex, again augmented by cAMP, has also been shown in vivo (Shaikh & Finlayson 2003; Shaikh & Finlayson 2005).

It is therefore conceivable that the effect of cAMP on I_h could also occur when the NO-cGMP signalling pathway is engaged. Neuronal nitric oxide synthase (nNOS) has been localised to adult rat MNTB principal cells by *in situ* hybridisation, NADPH-diaphorase histochemistry and immunohistochemistry (Iwase *et al.* 1998; Fessenden *et al.* 1999; Schaeffer *et al.* 2003). The presence of mRNA for the β-subunit of sGC or $NO_{GC}R$, the physiological receptor for nitric oxide, has also been confirmed (Fessenden *et al.* 1999). Therefore it could be postulated that nitrergic transmission and furthermore the NO-cGMP-HCN channel pathway may be present in the Calyx of Held.

Unlike the adult, the young rodent (up to post-natal day 12 (P12)) has a large NMDA-R-mediated EPSC which subsequently decreases markedly with age (virtually undetectable at P16; Joshi & Wang 2002). In P8-12 rats, approximately 30 % of the total Ca^{2+} that enters the principal cell during an EPSC occurs via the NMDA receptor (Bollmann *et al.* 1998). Elsewhere NMDA-R activation is known to engage the NO/cGMP pathway by preferentially activating the calcium-sensitive nNOS, which is physically coupled to NMDA receptors (Kornau *et al.* 1995; Brenman *et al.* 1996; Christopherson *et al.* 1999). Given the high incidence of

nNOS in MNTB principal cells (Fessenden *et al.* 1999), as well as the expression of NMDA receptors (Sato *et al.* 1999), there is a high probability that both proteins are coexpressed in this nucleus. During this critical period when the auditory brainstem becomes capable of high-frequency transmission coinciding with the onset of responses to tone-pips at P12 (Blatchley *et al.* 1987), nitrergic transmission via cGMP may play an important role at this giant synapse by affecting HCN channels.

Cerebellum

The deep cerebellar nuclei (DCN) are the primary output structure of the cerebellum (figure 4.2). Purkinje cells, the sole output of the cerebellar cortex, send inhibitory GABAergic projections to the DCN. They account for about 70 % of the synapses onto DCN neurones (De Zeeuw & Berrebi 1995). In addition, the DCN receive excitatory glutamatergic inputs from various extra-cerebellar sources via the mossy fibres as well as from the inferior olive via the climbing fibres (Llinas & Muhlethaler 1988). Therefore the firing properties of these cells will reflect the net effect of all these inputs and neural computations carried out in the cerebellum.

The cells of the DCN are seemingly heterogeneous, consisting of both large and small projection neurones as well as local circuit GABAergic neurones. Anatomically, the large projection neurones have fusiform or multipolar shaped somata, with diameters ranging from 15 to 35 µm, are immunoreactive for glutamate and project to a variety of premotor centres. In addition, there are smaller projection GABAergic neurones. They too have fusiform or multipolar somata, with smaller diameters of 5 to 20 µm, sending axons to the inferior olive. These different cell types are heterogeneously distributed throughout the DCN (Beitz & Chan-Palay 1979; Kumoi *et al.* 1988; Batini *et al.* 1992).
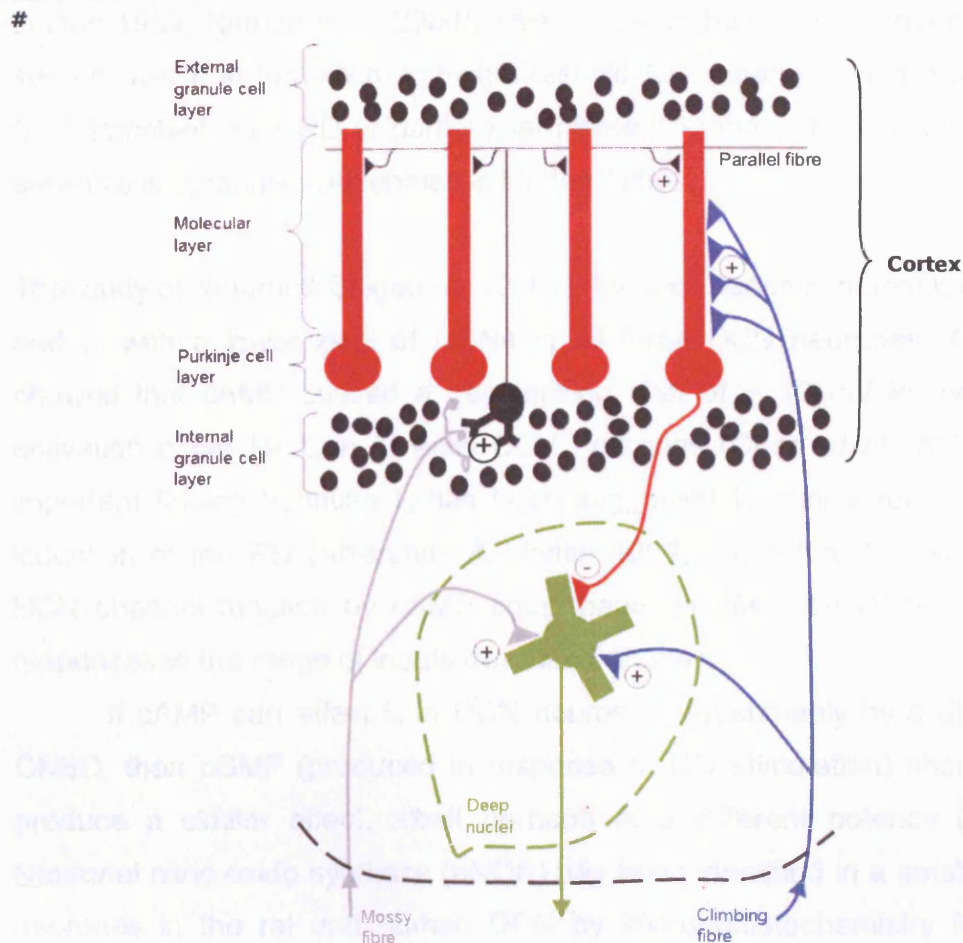
Figure 4.2 Diagram of the core cerebellar pathways

The cortex receives two major excitatory inputs. The first is from the climbing fibres (blue) that form multiple synapses with a single Purkinje cell. The second is from the mossy fibres (grey) that synapse onto granule cells, the axons of which, known as parallel fibres, form excitatory synapses with Purkinje cells in the molecular layer. Both of these inputs act to modulate the Purkinje cell response, the sole output of the cortex to the deep cerebellar nuclei. These nuclei convey cerebellar output to other brain regions.

The large glutamatergic projection neurones are very active at rest and either spike regularly or burst spontaneously (Jahnsen 1986b; Aizenman & Linden 1999). An important electrophysiological property of DCN neurones is the presence of a pronounced rebound depolarisation (RD) that typically triggers a series of action potentials immediately after the offset of a hyperpolarising pulse or a train of IPSPs. A number of conductances underlie this RD, including low-threshold, voltage-gated Ca^{2+} channels, the persistent Na^+ channel and the hyperpolarisation-activated current, I_h (Jahnsen 1986a; Llinas & Muhlethaler 1988; Aizenman &

Linden 1999; Raman *et al.* 2000). This so-called depolarising envelope drives Na^+ spiking, which in turn recruits high-threshold Ca^{2+} channels and results in a large Ca^{2+} transient. The RD is partially terminated by the activation of SK-type Ca^{2+}-sensitive K^+ channels (Aizenman & Linden 1999).

The study of Notomi & Shigemoto (2004) reveals intense immunolabelling of HCN1 and 2, with a lower level of HCN4 in all three DCN neurones. A recent study showed that cAMP caused a depolarising shift of ~ 10 mV in the steady-state activation curve for I_h in juvenile DCN neurones (Chen *et al.* 2005). This is an important finding because I_h has been suggested to play a role in boosting the induction of the RD (Aizenman & Linden 1999). Therefore this augmentation of HCN channel function by cAMP could have an effect on DCN neurone output responses to the range of inputs described above.

If cAMP can affect I_h in DCN neurones, presumably by a direct action on CNBD, then cGMP (produced in response to NO stimulation) should be able to produce a similar effect, albeit perhaps at a different potency (chapter one). Neuronal nitric oxide synthase (nNOS) has been identified in a small subset of the neurones in the rat and human DCN by immunohistochemistry (Rodrigo *et al.* 1994; Bernstein *et al.* 2001). The presence of the α- and β-subunit of sGC or $NO_{GC}R$, the physiological receptor for NO with different intensities, has also been confirmed again by immunohistochemistry (Ding *et al.* 2004). Therefore it could be postulated that the NO-cGMP-HCN channel pathway may play a role in the DCN and ultimately the entire output of the cerebellum.

4.2 AIM

Given the favourable HCN subunit expression profile and the previously established modulation of I_h by cAMP in the MNTB and DCN neurones, I investigated the presence of NO-cGMP-HCN channel cascade.

HYPOTHESIS: The NO-cGMP signalling pathway modulates HCN channel function in the principal neurones of the MNTB and DCN.

4.3 METHODS

Tissue preparation

All procedures were in accordance with regulations given by the UK Home Office.

Post-natal day 8-13 (P8-13) Sprague-Dawley rats were killed by cervical dislocation and decapitation. Juvenile rats were used because beyond this age the extent of myelination is much greater, which diminishes both visibility and viability of the neurones after slicing (Gauck & Jaeger 2003).

The brain was rapidly removed and the brainstem or the cerebellum (as appropriate) dissected out, taking care to remove the meninges, and placed in iced (4 °C) sucrose-substituted low Na^+ artificial cerebrospinal fluid (aCSF) containing (mM): 250 sucrose, 2.5 KCl, 1.3 (for MNTB) or 6 (for DCN) $MgCl_2$, 2.0 $CaCl_2$, 1.0 $NaH_2PO_4.H_2O$, 26.2 $NaHCO_3$, and 11 glucose, equilibrated with 95% O_2 - 5% CO_2. By trial-and-improvement, I found that using a higher concentration of $MgCl_2$ increased the number of viable DCN neurones, presumably by blocking NMDA-R activity. Coronal slices (200-350 µm thick) were prepared using a vibroslicer and maintained in an interface holding chamber containing normal aCSF at room temperature. For brainstem slices, the level of the 7th nerve was used as a guide for the presence of the MNTB. After a period of recovery (at least 60 min), one slice was transferred into a submerged chamber and continuously perfused with gassed normal aCSF.

Electrophysiological recordings

Whole-cell recordings were made at 30 - 32 °C from individual MNTB cells or large-diameter DCN (dentate or interposed) neurones, visually identified using normal optics and a x40 water-immersion objective (NA .75, Zeiss). Pipette solutions contained (in mM): 150 $KMeSO_4$, 10 KCl, 10 Hepes, 4 NaCl, 4 or 1 MgATP, 0.4 NaGTP. The pH was adjusted to 7.39 - 7.4 and the osmolarity to 280-290 mOsm / l. Open pipette resistance was 2-4 MΩ. Under voltage clamp conditions, currents were recorded using an Axopatch 1D amplifier and pClamp7 (Axon Instruments,

Foster city, CA) in neurones clamped at holding potentials from -40 to -75 mV. Resting membrane potentials (RMP; observed before and after TTX application) were between -51 and -70 mV for MNTB neurones. The RMP of DCN neurones showed regular cycling, between -37 and -68 mV. In all experiments 80% compensation of the series resistance was used; junction potentials were not compensated. The recordings were filtered at 1 kHz and sampled at 2 kHz. Patch longevity was usually a maximum of 30 min, so Cs^+ (2 mM) was used to block I_h because of the long wash in times required for ZD7288 and other organic blockers.
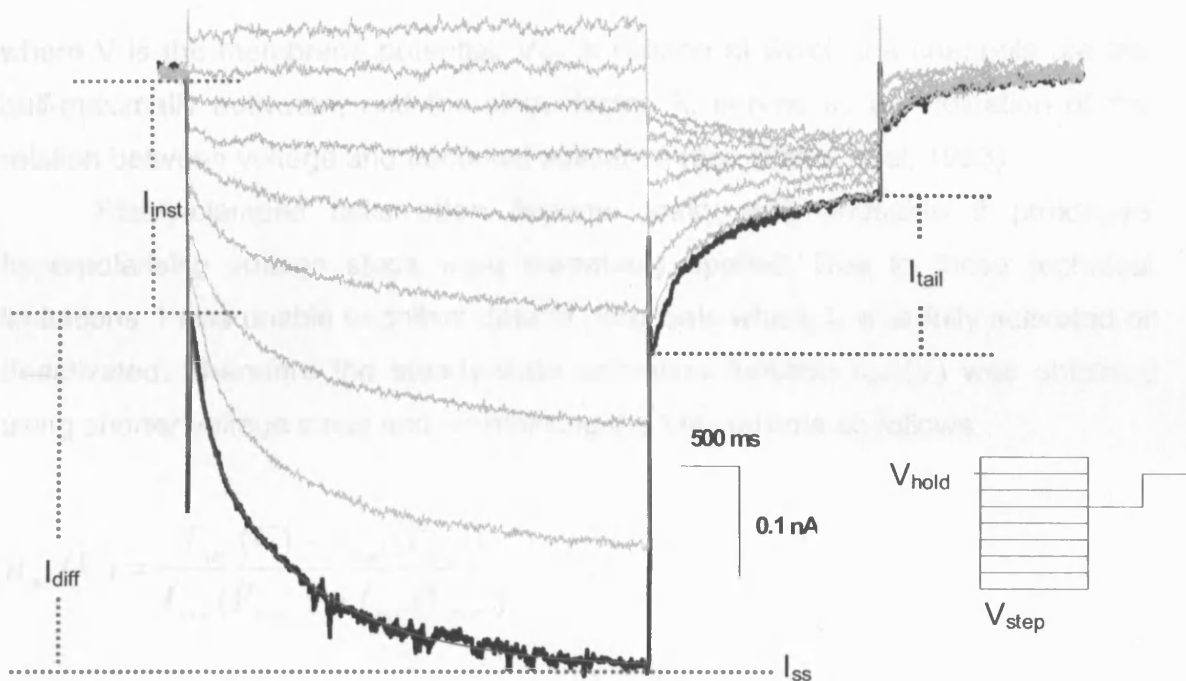
Figure 4.3 A current response to the typical voltage step protocol (inset).

A series of long (3-4 s) voltage steps (inset, figure 4.3) were used to study I_h. The current amplitudes were obtained by double exponential fits (solid red line) to the charging curve; I_h amplitude (I_{diff}) was measured as the difference between the plateau steady-state current level (I_{ss}) at the end of the hyperpolarising step and the point where the extrapolated fitted line intersected with the capacitative transient; the instantaneous current (I_{inst}) component was measured as the difference between this point of intersection and the holding current. The voltage

dependence of I_h activation was assessed by measuring the activation and deactivation tail currents upon return to a fixed holding potential to remove the effect of the driving force. The tail current values were used to construct steady-state activation curves, which showed a typical S-shaped dependence on the hyperpolarising voltage and quantified by fitting with the Boltzmann function:

$$ n_{\text{inf}}(V) = \frac{1}{1+e^{\frac{V-V_{1/2}}{k}}} $$

where V is the membrane potential, $V_{1/2}$ is voltage at which the channels are the half-maximally activated, and the slope factor, k, serves as an indication of the relation between voltage and fractional activation (see Banks *et al.* 1993).

Stably-clamped cells often became leaky and unusable if prolonged hyperpolarising voltage steps were repeatedly applied. Due to these technical limitations, I was unable to collect data at potentials where I_h was fully activated or deactivated. Therefore the steady-state activation function $n_{\text{inf}}(V)$ was obtained using shorter voltage steps and normalising the tail currents as follows:

$$ n_{\text{inf}}(V) = \frac{I_{tail}(V) - I_{tail}(V_{\min})}{I_{tail}(V_{\max}) - I_{tail}(V_{\min})} $$

where $V_{\max}$ and $V_{\min}$ are the voltages corresponding approximately to maximum and zero activation of I_h respectively.

Pharmacological manipulation of HCN channels was examined by bath application of compounds over a short time, typically 3 to 7 minutes, before applying the above step protocol to study the function of HCN channels. In order to follow the timecourse of wash in (and wash out), a small (~ 40 mV), short (typically 500 ms) hyperpolarising step from the holding potential was applied every 10 s to activate sufficient HCN channels to observe any changes. I_h was approximately measured

as the difference between the point following the capacitative transient and the plateau prior to the offset of the voltage step.

Analysis was performed offline using Clampfit 8.0 (Axon Instruments, Foster City, CA).
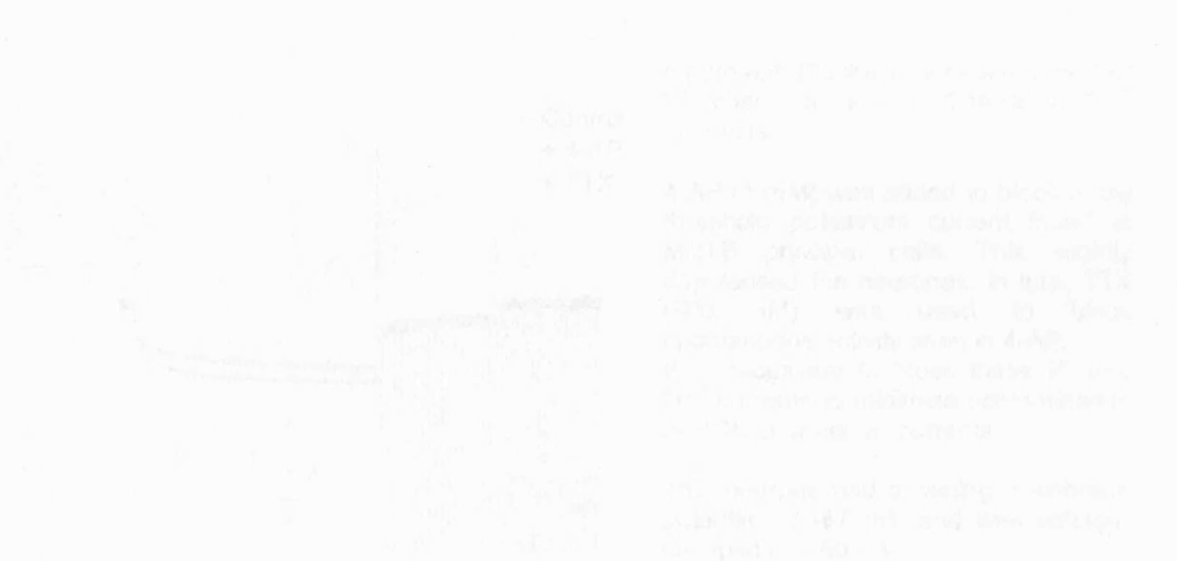
4.4 RESULTS

I_h was first recorded from voltage-clamped MNTB principal cells. Preliminary experiments in these neurones indicated that there was a marked rundown of HCN channels particularly at the beginning of the recording (n=3), a common problem of the whole-cell technique. Therefore to minimise variation, an equilibration period of 3 - 5 min was introduced after obtaining the whole-cell configuration. In line with previous results, I found it necessary to block K^+ channels using 1 mM 4-AP as they contaminate the HCN channel tail currents. A consequence of the loss of K^+-conductances was unclamped TTX-sensitive Na^+-influx (figure 4.4). Therefore all subsequent measurements were made in 1 mM 4-AP and 500 nM TTX.

Control
+ 4-AP
+ TTX

0.5 nA

1 s
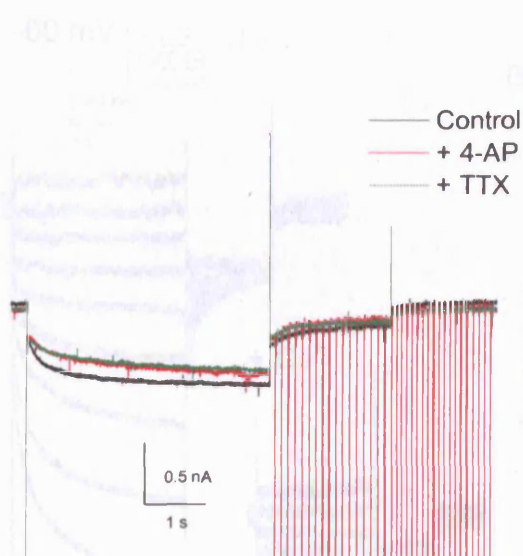
Figure 4.4. Blockade of delayed rectifier K^+ channels and TTX-sensitive Na^+ channels

4-AP (1 mM) was added to block a low threshold potassium current found in MNTB principal cells. This slightly depolarised the neurones. In turn, TTX (500 nM) was used to block spontaneous activity seen in 4-AP.
It is necessary to block these K^+ and Na^+ currents to minimise contamination of HCN channel tail currents.

This neurone had a resting membrane potential of -67 mV and was voltage-clamped at – 60 mV.

The whole-cell voltage-clamp technique was employed to investigate the effect of the NO-cGMP signalling pathway on the properties of I_h in MTNB principal cells. I was unable to apply strong hyperpolarising voltage step (more negative than -105 mV) to ensure maximum activation of I_h because this sustained hyperpolarisation, particularly with repeated steps for multiple drug conditions, led to loss of a stable recording. Therefore a compromise of a much longer 4 s pulse with less negative

voltage step was used to activate HCN channels. As far as possible, drug applications were done in series on the same neurones.

I_h was found in every cell in which a stable voltage clamp was obtained. Smaller hyperpolarising steps elicited currents composed primarily of linear leakage currents, because the steady-state and instantaneous current were approximately equal. Larger voltage steps elicited a slow inward, non-inactivating current (figure 4.5). These currents traces approach their steady-state values more rapidly for larger hyperpolarising steps due to voltage-dependent activation kinetics. For example, τ_{slow} and τ_{fast} were 1320 ± 94 and 166 ± 12 ms at -90 mV, and increasing to 1539 ± 74 and 235 ± 23 at -80 mV (n=4; Student's paired t-test; p<0.05). As expected the current was blocked by 2 mM Cs^+.
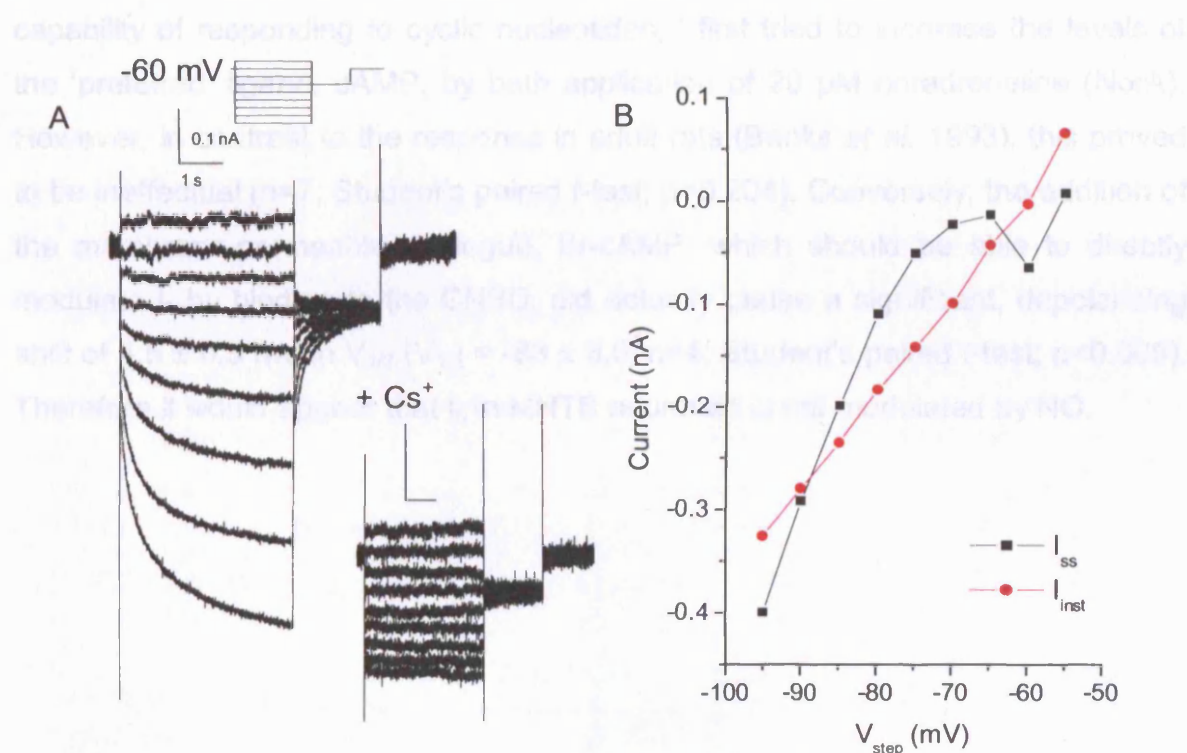
Figure 4.5 A typical current response from a voltage-clamped MNTB principal cell

A, The current response to 4 s voltage steps to activate I_h in 5 mV increments i.e -55 to -95 mV. The membrane potential was then stepped to -70 mV for 2 s to obtain I_h tail currents and then back to the holding potential (-60 mV). This current was blocked by 2 mM Cs^+.

B, The current-voltage relationship derived from A.

This cell had a resting membrane potential of -68 mV.

The activation curve for I_h was derived from tail currents (see Methods) and fitted with a Boltzmann function; the voltage causing half-maximal activation ($V_{1/2}$) was -85 ± 1.0 mV (n=8; see figure 4.6 for a representative example). The application of 100 μM DEA/NO, a supramaximal concentration for stimulating maximal cGMP accumulation in the hippocampus (Bon & Garthwaite 2001), caused a significant hyperpolarising shift in $V_{1/2}$ (-90 ± 1.5 mV; n=8; Student's paired t test; p<0.005). However this effect was attributable to rundown as seen in the timecourse, because it did not reverse on wash out ($V_{1/2}$ = -90 ± 1.6 mV; n=4; Student's paired t-test; p=0.379).

To ensure that HCN channels in the MNTB cells had the functional capability of responding to cyclic nucleotides, I first tried to increase the levels of the 'preferred' ligand, cAMP, by bath application of 20 μM noradrenaline (NorA). However, in contrast to the response in adult rats (Banks *et al.* 1993), this proved to be ineffectual (n=7; Student's paired t-test; p=0.204). Conversely, the addition of the membrane-permeable analogue, Br-cAMP, which should be able to directly modulate I_h by binding to the CNBD, did actually cause a significant, depolarising shift of 4.5 ± 0.5 mV in $V_{1/2}$ ($V_{1/2}$ = -83 ± 3.0; n=4; Student's paired t-test; p<0.005). Therefore it would appear that I_h in MNTB neurones is not modulated by NO.
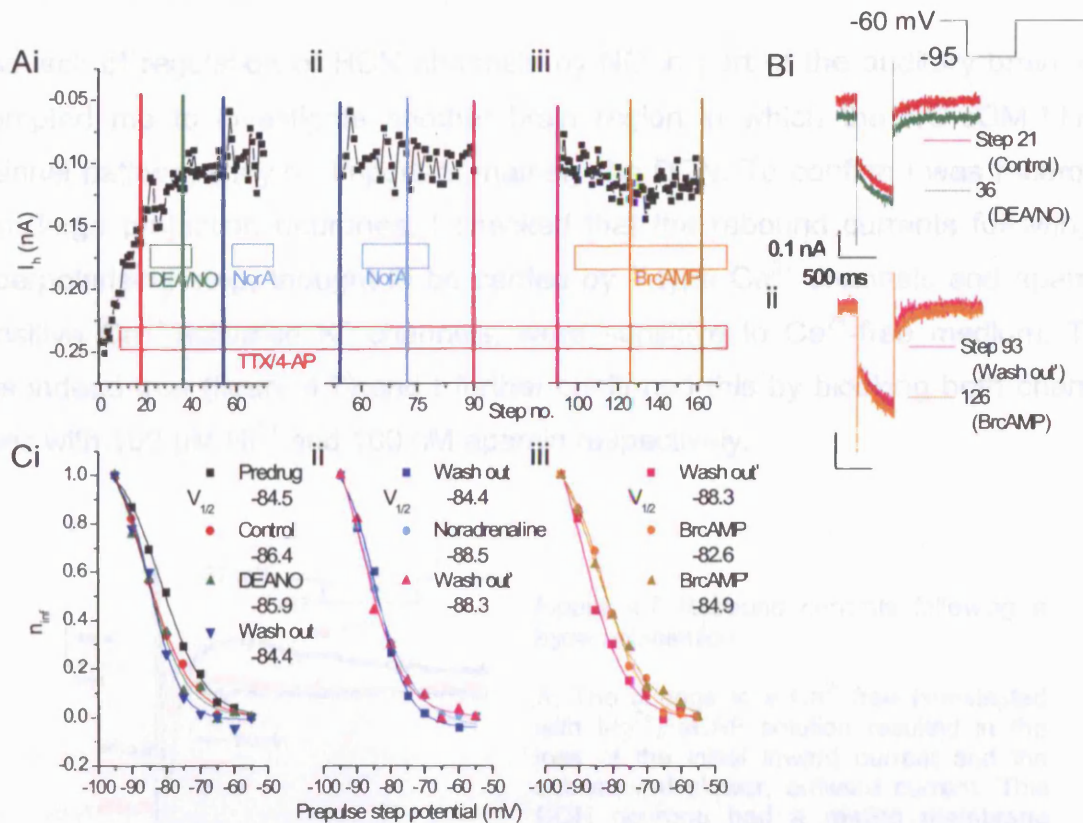
Figure 4.6 An individual example (same cell as figure 4.3) of the apparent lack of receptor-mediated modulation of I_h in MNTB principal cells

A, Timecourse for effect of drug manipulations on I_h. Drug effect was followed by measuring I_h activated by a short (500 ms) hyperpolarising step to -95 mV every 10 s. Coloured vertical lines correspond to the step immediately prior to the protocol to generate activation curves in C.
i, initially there was a clear rundown in the current after obtaining the whole-cell configuration. The 3 min exposure to 100 µM DEA/NO had no obvious effect on the current.
ii, 3 min application of 20 µM noradrenaline (NorA) had no apparent effect on I_h
iii, The wash in of 1 mM Br-cAMP caused an increase in the current activated by the short hyperpolarising step.

B, Raw traces for the current activated by 500 ms hyperpolarising step to -95 mV. The same colours are used as A . Notice the increase in current amplitude and the small depolarising shift in the holding current in the presence of Br-cAMP (ii).

C, Steady-state activation curves derived from tail currents from voltage step protocols to activate I_h. Lines are Boltzmann fits to the data. Legend gives values for half-maximal voltage ($V_{1/2}$) in mV
i, The wash in and wash out of 100 µM DEA/NO had little obvious effect.
ii, The wash in and wash out of 20 µM noradrenaline had little obvious effect
iii, The wash in of 1 mM Br-cAMP caused a positive shift in the curve.

'Predrug' was prior to continuous application of 4-AP (1 mM) and TTX (500 nM).

This lack of regulation of HCN channels by NO in part of the auditory brainstem prompted me to investigate another brain region in which the NO-cGMP-HCN channel pathway may be important, namely the DCN. To confirm I was recording from large projection neurones, I checked that the rebound currents following a hyperpolarising step, thought to be carried by T-type Ca^{2+} channels and apamin-sensitive Ca^{2+}-activated K^+ channels, were sensitive to Ca^{2+}-free medium. This was indeed true (figure 4.7) and I further confirmed this by blocking both channel types with 100 μM Ni^{2+} and 100 nM apamin respectively.
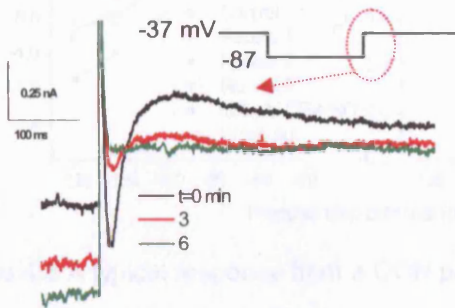
Figure 4.7 Rebound currents following a hyperpolarisation

A, The change to a Ca^{2+}-free (substituted with Mg^{2+}) aCSF solution resulted in the loss of the initial inward current and the subsequent slower, outward current. This DCN neurone had a resting membrane potential (RMP) of -57 mV.

I then repeated the voltage step protocols in large diameter DCN cells as for the MNTB. I_h was observed in all neurones from which stable recordings were obtained. As can be seen from figure 4.8 , there was no effect of 100 μM DEA/NO on steady-state activation curve of I_h (n=3; $V_{1/2}$: control -85 ± 3.7, DEA/NO -87 ± 3.8; Student's paired t-test; p=0.358). As in the case of the MNTB, I tried to modulate HCN channel function by increasing the level of cAMP. Bath application of 10 μM isoprenaline (figure 4.9), a β-adrenergic receptor agonist, caused a significant positive shift in the voltage-dependence of activation (n=4; $V_{1/2}$: control -91 ± 2.7, isoprenaline -86 ± 3.0; Student's paired t-test; p<0.02).
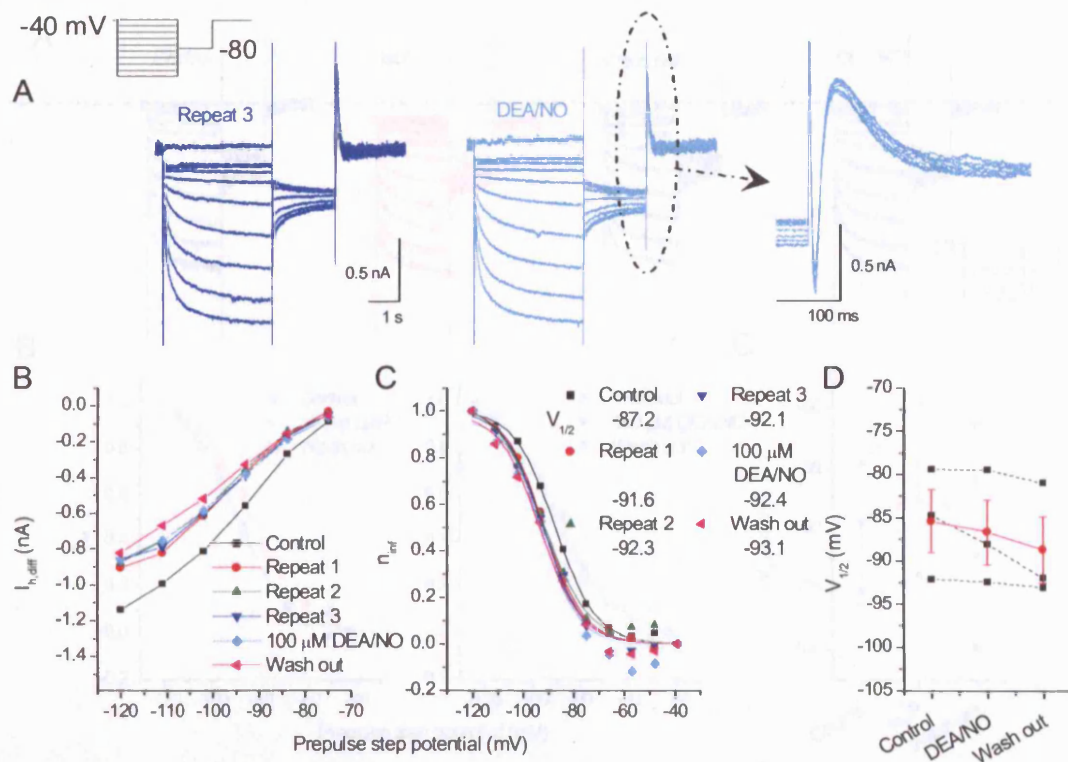
Figure 4.8 A typical response from a DCN principal cell

A, The current response to 3.5 s voltage steps to activate I_h in 9 mV increments i.e -120 to -39 mV. The membrane potential was then stepped to -80 mV for 2 s to obtain I_h tail currents and then back to the holding potential (-40 mV). The protocol was repeated every 3 min to gauge the degree of run-down. In the presence of 100 µM DEA/NO there was no obvious change in the current response measured. The rebound currents activated on stepping back to the holding potential are more clearly shown on the right hand side.

B, The voltage-I_h relationship obtained from double exponential fits to the charging curves in A. It can be seen that the current stabilised after the first repeat i.e. approximately 5 minutes after obtaining the whole-cell configuration. 100 µM DEA/NO did not appear to affect the amplitude of I_h

C, The steady-state activation curves constructed from tail currents in A. Again the initial rundown can be seen and also the fact that DEA/NO had no obvious effect on voltage-dependence of activation

D, Summary of the values for $V_{1/2}$ (raw data in black, mean ± sem in red). There was no significant effect of DEA/NO application (n=3; Student's paired t-test; p=0.358)

1 mM 4-AP and 500 nM TTX were present throughout; 4 mM ATP was used in the whole-cell solution.
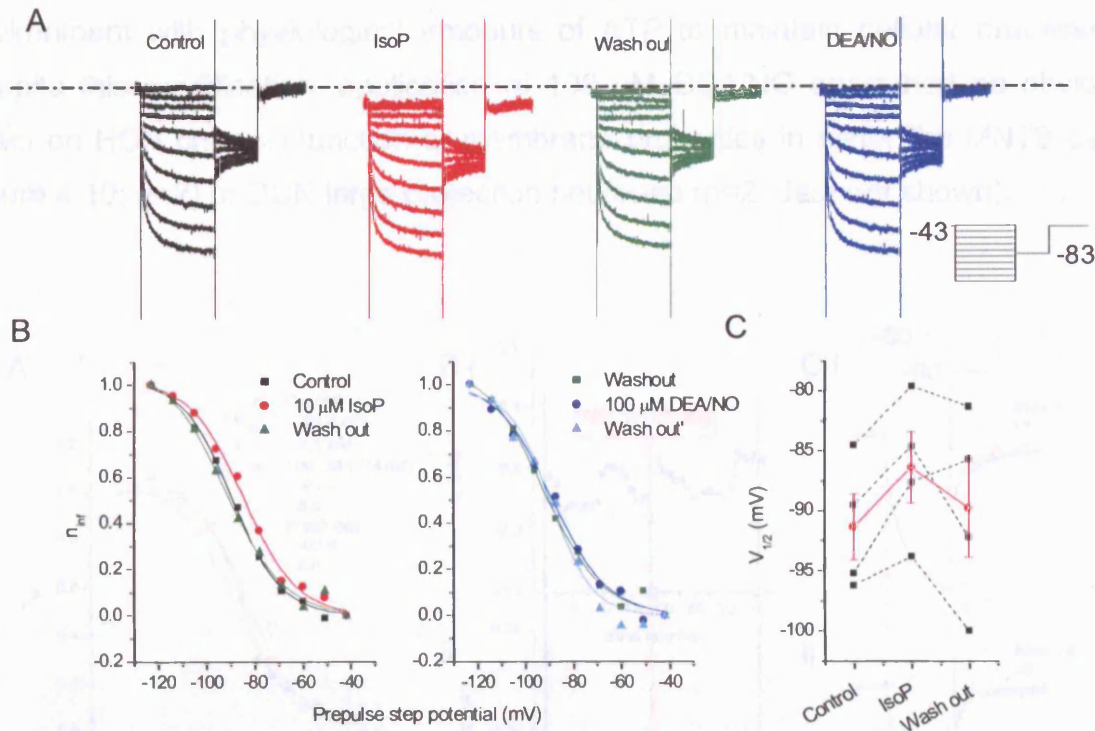
Figure 4.9 The effect of isoprenaline on I_h in DCN neurones

A, 10 µM isoprenaline (IsoP) caused a reversible, negative shift in the holding current, while 100 µM DEA/NO had no obvious effect.
B, The steady-state activation curves constructed from tail currents in A. Isoprenaline caused a reversible, depolarising shift; DEA/NO had no effect on voltage-dependence of activation
C, Summary of the values for $V_{1/2}$ (raw data in black, mean ± sem in red). Isoprenaline caused a significant depolarising shift in $V_{1/2}$ (n=4; Student's paired t-test; p<0.02).

1 mM 4-AP and 500 nM TTX were present throughout; 4 mM ATP was used in the whole-cell solution.

Therefore it seemed that despite the ability to respond to cAMP, the HCN channels in the MNTB and DCN were not modulated following stimulation of the cell with NO. However, around this same time, biochemical measurements of cGMP levels following activation of purified $NO_{GC}R$ in the laboratory showed that 4 mM ATP reduced enzyme activity to about 10% of control at a range of GTP concentrations (B. Roy, personal communication). This would mean that little cGMP would be generated in response to application of NO to the MNTB or DCN. Physiological ATP concentrations are thought to be around 1 mM (Gribble et $al.$ 2000). This concentration causes about 50 % inhibition of $NO_{GC}R$ fractional activity (Ruiz-Stewart et $al.$ 2004). 1 mM ATP was selected to use in the whole-cell solution in

order to permit NO-stimulated cGMP production, but still to supply the intracellular environment with physiological amounts of ATP to maintain cellular processes. Despite this modification, application of 100 μM DEA/NO again had no obvious effect on HCN channel function or membrane properties in either the MNTB cells (figure 4.10; n=2) or DCN large projection neurones (n=2; data not shown).
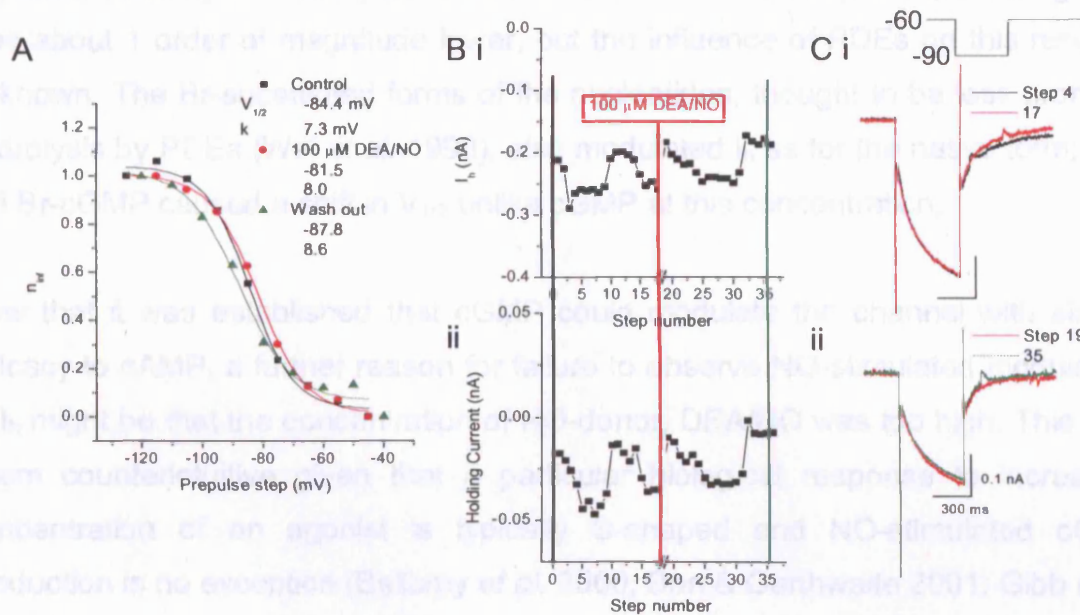
Figure 4.10 The NO-cGMP-HCN channel pathway in voltage-clamped MNTB principal cells using 1mM ATP in the whole-cell solution
A, Steady-state activation curve constructed from tail currents. Values for $V_{1/2}$ and k are as legend.
B, Timecourse for effect of 100 μM DEANO on I_h (i) and the holding current (ii) measured a short (500 ms) hyperpolarising step to -90 mV every 10 s. Coloured vertical lines correspond to the step immediately prior to voltage-step protocol to generate activation curves in A.
C, Example raw traces from timecourse (B).

This cell had a resting membrane potential of -63 mV and was clamped at -60 mV.

One explanation for the lack of modulation of I_h by NO could be that the HCN channel in both of two sets of neurones may be incapable of responding to cGMP on a molecular basis, as for sea urchin sperm HCN channels, spHCN (Gauss *et al.* 1998). To address this possibility, I carried out a series of interleaved experiments in which the cyclic nucleotide or analogue was directly delivered to the intracellular milieu by inclusion with the whole-cell solution. These experiments were initially

performed in DCN cells because rundown is less of a problem. Each 'n' number represents an individual cell, which was exposed to only a single whole-cell solution I.e. no repeated measures.

100 µM cGMP had no apparent effect on $V_{1/2}$, while 100 µM cAMP caused a depolarizing shift of ~ 10 mV (figure 4.11). Increasing the concentration of cGMP to 1 mM caused a similar positive shift in the steady activation curve and $V_{1/2}$. The apparent potency of cGMP, compared to cAMP, for inducing a depolarising shift was about 1 order of magnitude lower, but the influence of PDEs on this result is unknown. The Br-substituted forms of the nucleotides, thought to be less prone to hydrolysis by PDEs (Wei *et al.* 1998), also modulated I_h as for the native form; 100 µM Br-cGMP caused a shift in $V_{1/2}$ unlike cGMP at this concentration,

Now that it was established that cGMP could modulate the channel with similar efficacy to cAMP, a further reason for failure to observe NO-stimulated modulation of I_h might be that the concentration of NO-donor, DEA/NO was too high. This may seem counterintuitive given that a particular biological response to increasing concentration of an agonist is typically S-shaped and NO-stimulated cGMP production is no exception (Bellamy *et al.* 2000; Bon & Garthwaite 2001; Gibb *et al.* 2003; Hopper *et al.* 2004). It would appear that after reaching the maximal production of cGMP in response to NO, greater concentrations of NO apparently decrease the rate of ensuing cGMP accumulation below this maximum. Extrapolating this trend would mean that the concentration-effect curve would become bell-shaped, such that if the concentration was too high, no cGMP would be produced within the measurable limits.
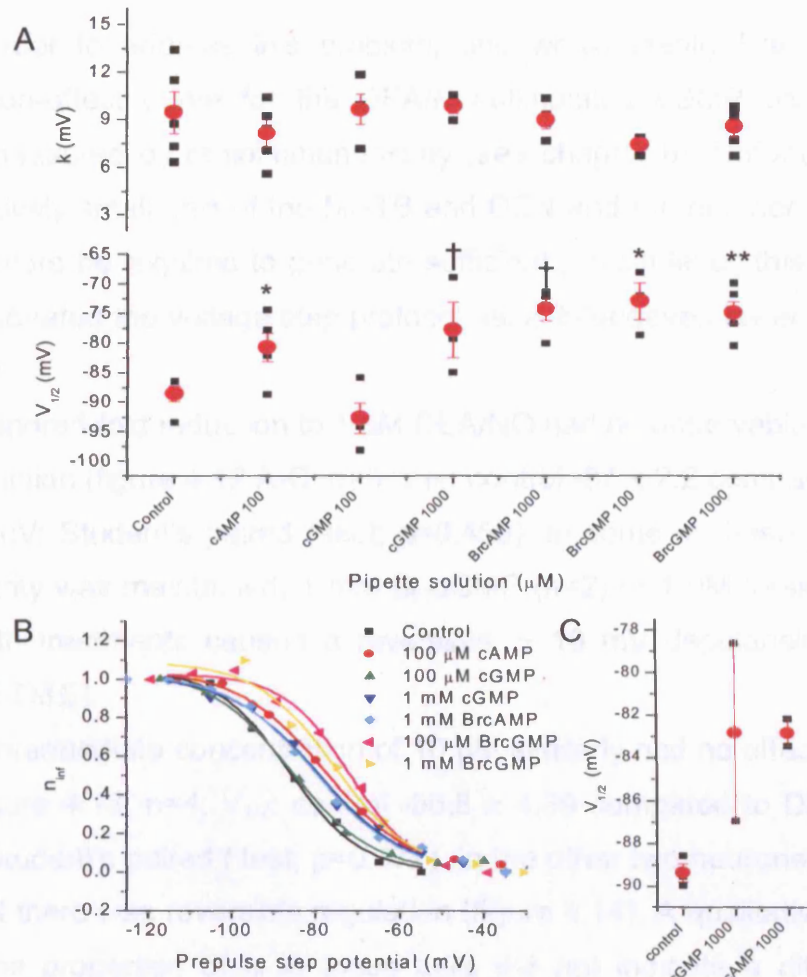
Figure 4.11 Sensitivity of I_h to cyclic nucleotides (and analogues)

A, A series of interleaved experiments in voltage-clamped DCN neurones to show the extent of modulation of HCN channel function by cyclic nucleotides directly in the whole-cell solution. Individual values are in black and mean ± sem in red.

Top panel: none of the different cyclic nucleotides had an effect on k.

Bottom panel: 100 μM cGMP had no apparent effect on $V_{1/2}$. All other treatments significantly shifted $V_{1/2}$ in a depolarised direction (n=3-5 separate cells in different slices; Student's unpaired t-test compared control and test values; * p< 0.03, ** p< 0.002, † p<0.0005).

B, Representative steady-state activation curves for each of the conditions in A. Notice the almost overlay of control and 100 μM cGMP. All other treatments shift the curve to more positive potentials for a given level of activation.

C, A limited set of experiments in MNTB principal cells to show that these neurones are indeed capable of responding to cGMP and cAMP (n=2-3).

4 mM ATP in the whole-cell solution throughout.

In order to address this problem, one would ideally like to carry out a concentration-effect curve for the DEA/NO-stimulated cGMP production in the DCN, as measured by radioimmunoassay (see chapter 6). Unfortunately, due to the prohibitively small size of the MNTB and DCN and the number of animals that would therefore be required to generate sufficient protein level, this was not done. Instead I repeated the voltage step protocol using interleaved lower concentrations of DEA/NO.

A hundred-fold reduction to 1 μM DEA/NO had no observable effect on HCN channel function (figure 4.12 A-C; n=5; $V_{1/2}$: control -87 ± 2.2 compared to DEA/NO -86 ± 2.4 mV; Student's paired t-test; p=0.459). In some of these experiments, if patch integrity was maintained, 1 mM Br-cGMP (n=2) or 1 μM forskolin (n=1) was added. Both treatments caused a reversible, ~ 10 mV depolarising shift in $V_{1/2}$ (figure 4.12 D&E).

An intermediate concentration of 10 μM similarly had no effect in 4 of 6 cells studied (figure 4.13; n=4; $V_{1/2}$: control -96.8 ± 4.39 compared to DEA/NO -98.0 ± 3.66 mV; Student's paired t test; p=0.477). In the other two neurones, interestingly, I found that there was reversible regulation (figure 4.14). A qualitative inspection of some of the properties of I_h in these cells did not indicate a difference in the properties of I_h to account for the different responses to NO application (table 4.1).

Cell	RMP (mV)	I_h amplitude at -100 mV (nA)	Time constants (ms)	$V_{1/2}$ (mV)
A	-58	-0.301	1371 255.5	-90.2
B	-47	-0.172	1261.0 198.2	-89.5
C	-47	-0.152	1603.9 336.7	-99.6
D	-57	-0.212	1440.3 250.4	-108.1
1	-44	-0.190	916.7 271.8	-93.5
2	-43	-0.180	1104.3 551.2	-88.6

Table 4.1 Collection of properties for cells in which I_h was (1&2) and was not (A-D) regulated by NO
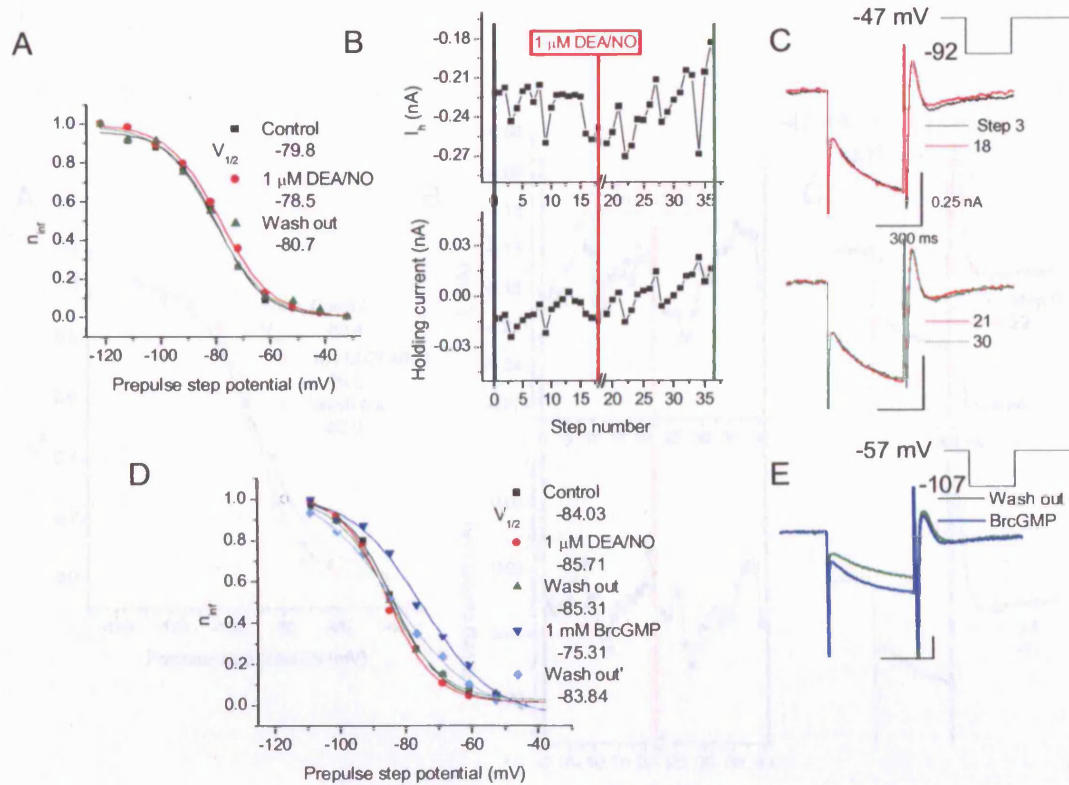
Figure 4.12 The lack of effect of 1 µM DEA/NO on I_h in DCN principal cells (n=5)

A, A typical example of a steady-state activation curve constructed from tail currents. Values for $V_{1/2}$ are as legend.

B, Timecourse for effect of 1 µM DEANO on (i) I_h and (ii) the holding current measured during a short (500 ms) hyperpolarising step to -90 mV every 10 s. Coloured vertical lines correspond to the step immediately prior to voltage-step protocol used to generate activation curves in A.

C, Example raw traces from timecourse (B).

This cell was clamped at -47 mV and 1 mM ATP was used in the whole-cell solution.

D, Bath application of 1 mM Br-cGMP produced a depolarising shift in the activation curve.
E, Example raw traces showing the effect of Br-cGMP following wash in.

This cell was clamped at -57 mV and 1mM ATP was used in the whole-cell solution.
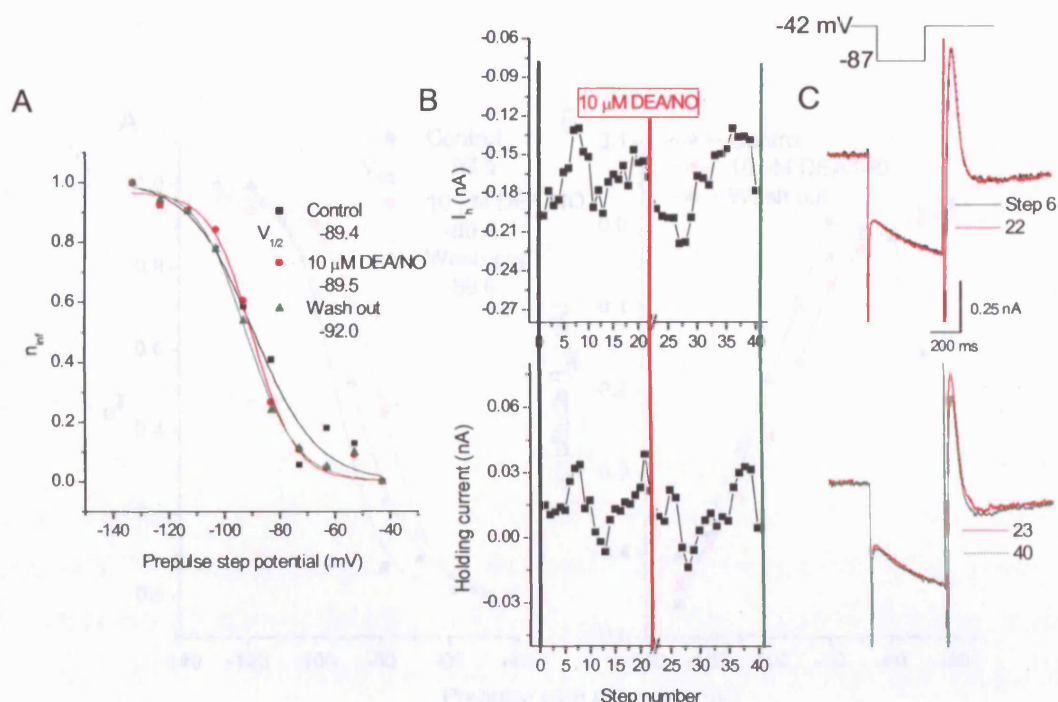
Figure 4.13 The lack of effect of 10 µM DEA/NO on I_h in DCN principal cells

A, A typical example of a steady-state activation curve constructed from tail currents. Values for $V_{1/2}$ are as legend.

B, Timecourse for effect of 10 µM DEANO on (i) I_h and (ii) the holding current measured during a short (500 ms) hyperpolarising step to -90 mV every 10 s. Coloured vertical lines correspond to the step immediately prior to voltage-step protocol to generate activation curves in A.

C, Example raw traces from timecourse (B).

This cell had a resting membrane potential of -58 mV and was clamped at -42 mV. 1mM ATP in the WCS.

Figure 4.14 The regulation of I_h by NO in the minority of DCN principal cells

A, An example from a minority of cells (total n=2) showing reversible regulation of the steady-state activation curve for HCN channels. Lines are Boltzmann fits to the data; values for $V_{1/2}$ are as legend.

B, Current-voltage plots derived from voltage step protocol show the reversible increase in I_h amplitude (up to approximately -120 mV when HCN channels are fully activated) in the presence of NO.

This cell was clamped at -49 mV. There was 1 mM ATP in the WCS.

4.5 DISCUSSION

The modulation of I_h by the NO-cGMP signalling pathway was investigated in the MNTB and DCN neurones. Kinetics of activation were of the appropriate range to confirm that the HCN channels in these neurones were likely to contain HCN4 and HCN2 subunits (Accili *et al.* 2002).

The $V_{1/2}$ for MNTB neurones (around -85 mV) was more hyperpolarised than previously reported values in the adult rat but is in agreement to measurements in similarly aged mice. As well as a difference in voltage-dependence, I_h amplitude was also much smaller in the juvenile neurones (about 200 pA compared to 2 nA) but similar to that in mice of the same age (Banks *et al.* 1993; Leao *et al.* 2006a). This may present a change during maturation into an adult.

HCN channel function was not modulated by application of noradrenaline at this age unlike the adult (Banks *et al.* 1993). This was presumably due to a lack of expression of relevant adrenergic receptors or a lack of coupling of an increase in noradrenaline-stimulated cAMP accumulation to HCN channel function, because bath application of Br-cAMP caused a depolarising shift in voltage dependence. This shift of ~ 4.5 mV was smaller than that seen in the adult (~ 17 mV). This may represent a difference in drug potency or efficacy and/or the exact subunit composition of the HCN channel.

The attempt to modulate the voltage-dependence of I_h by NO yielded no positive results. This was not due to the channel properties being maximally modulated i.e. the maximal positive shift in $V_{1/2}$, because subsequent application of Br-cAMP lead to a positive shift in the voltage dependence. The initial conclusion would be that the NO-cGMP-HCN channel pathway is not active in the MNTB. This is a disappointing finding because an increase in the kinetics and amplitude of I_h is known to affect the delay to firing of an action potential which would have implications for binaural processing at LSO (Leao *et al.* 2006a; Leao *et al.* 2006b).

Turning next to the DCN, values for $V_{1/2}$ and current amplitudes were comparable to reported values (Chen *et al.* 2005), as were 'resting' membrane potentials

(Aizenman *et al.* 2003). I found a comparable lack of modulation of I_h in DCN neurones by NO as in the MNTB. Again, this was not due to the voltage-dependence of activation already being shifted to the maximally depolarised position because the addition of isoprenaline caused a depolarising shift in $V_{1/2}$.

The almost consistent lack, so far, of modulation by NO could be due to a lack of modulation by cGMP. This was found not to be the case because inclusion of cGMP in the patch pipette modulated I_h. Therefore, like other native channels, HCN channels in the MNTB and the DCN can be modulated by both cAMP and cGMP (DiFrancesco & Tortora 1991; Ludwig *et al.* 1998; Zagotta *et al.* 2003).

One important assumption that is not confirmed for both the DCN and MNTB is that the entire NO-cGMP-HCN channel pathway is expressed in these neurones at this particular range of post-natal days used. This is to say that the NO-synthesising enzyme (NOS), the NO-receptor ($NO_{GC}R$) and HCN channels are present. The occurrence of the HCN channels is not so problematic, as the electrophysiological recordings presented here confirm the presence of a current resembling that previously described. The occurrence of $NO_{GC}R$ is of paramount importance, otherwise there is no apparatus for the transduction of an NO signal. The presence of NOS within the vicinity of the nuclei would be required to indicate an endogenous source of NO and a potential, physiological relevance of the NO-cGMP-HCN channel pathway.

In the case of the DCN, mixed results using 10 µM DEA/NO as well as the seemingly homogeneous properties of I_h in the neurones recorded are at first confusing. One explanation for the inconsistently negative results could be that the large projection cells show heterogeneity in terms of NO-cGMP pathway. For example, only a minority of cells may express $NO_{GC}R$ and therefore generate cGMP. In the DCN, the cyclase might not be abundant even in the adult (Matsuoka *et al.* 1992). On the other hand, assuming that all necessary proteins are expressed, it is possible that in the majority of the DCN neuronal population there is no coupling between cGMP production and downstream HCN channels.

Little is known about PDEs expressed in the DCN or the MNTB. Particularly in regard to cGMP-hydrolysing PDE isoforms, mRNA for PDE2 and PDE9 are found in the DCN but not PDE5 (van Staveren *et al.* 2002; van Staveren *et al.* 2003). This could reduce the amplitude and spread of NO-stimulated cGMP such that the HCN channels do not detect a change during a NO signal; in cardiac myocytes, PDE5 and to a lesser extent, PDE2 act to prevent access of the $NO_{GC}R$-synthesised cGMP pool to expressed CNG channels (Castro *et al.* 2006). The apparently higher potency of PDE-resistant Br-cGMP in my experiments could indicate that PDE activity is quite high in DCN and that HCN channels might be compartmentalised away from the cGMP pools controlled by $NO_{GC}R$. Some preliminary data (n=4; not shown) using the non-selective PDE-inhibitor, 3-Isobutyl-1-methylxanthine (IBMX), showed that inhibition of PDEs resulted in a depolarising shift of HCN channel voltage dependence. I considered that testing the hypothesis that the activity of certain PDE-isoforms compartmentalises HCN channels away from cyclic nucleotide pools could result in an expensive pharmacological 'fishing' exercise, which may not yield useful information, particularly given the lack of inhibitors for certain PDEs.

If PDE activity is an explanation of the results, why do two neurones show positive regulation of I_h by NO? For one, they could have simply occurred by chance, but this seems unlikely because the effect was reversible on removal of NO. Therefore, this could represent recordings from two different populations of large projection cells within the DCN differing in PDE expression and/or activity. This level of differential expression is seen in cerebellar Purkinje cells, which all express PDE5, but only a subset express PDE1B (Bender & Beavo 2004). However the functional implications are unknown.

Alternatively, the differences in the NO-cGMP-HCN channel pathway may reflect two electrophysiologically-distinct neuronal populations. Despite providing the major output of the cerebellum and playing a crucial function in motor control and learning, the populations of DCN neurones remain poorly characterised and defined. Identification of two types of neurones in the DCN failed to make a strong correlation between morphological and electrophysiological parameters (Czubayko

107

et al. 2001), but subsequent work suggests that one type are small interneurones and the rest the larger projection neurones (Aizenman *et al.* 2003). Most recently, the 'large' glutamatergic neurones have been further classified into two distinct populations according to cell size and electrophysiological features. GABAergic neuronal size also appears to show some overlap with glutamatergic neurones (17 ± 1.1 vs 26 ±1.5 µm respectively (Uusisaari *et al.* 2007). In this case, the characterised cell-types all displayed similar I_h-attributed depolarising sags, indicative of homogeneous I_h profiles. Therefore I could have been recording from the GABAergic neurones or a distinct set of glutamatergic cells in the two examples of reversible modulation of HCN channels.

Lastly, it may be that there is a methodological problem with the electrophysiological recordings. The run-down in I_h seen in the recordings after obtaining the whole-cell configuration may be due to the equilibration with the solution in the patch pipette. One could hypothesise that dialysis of the intracellular milieu disrupts the coupling in the signalling pathway. In the 2 cells displaying positive regulation, this dialysis may not (yet) have occurred; perhaps increasing the duration of baseline recording may have been necessary to allow dialysis to occur; another possibility is that for the recordings of these 2 cells, the series resistance was higher, although this did not appear to be the case.

The following chapters explore and discuss some of these possible explanations using immunohistochemical, biochemical and electrophysiological techniques.

Chapter 5 - The NO-cGMP-HCN channel pathway in brainstem and cerebellum: immunocytochemical studies and sharp electrode recordings

5.1 INTRODUCTION

To complement the study in chapter 4, the presence of the NO-cGMP-HCN pathway was examined by immunohistochemical and less-invasive electrophysiological means.

nNOS (Vincent & Kimura 1992; Rodrigo *et al.* 1994; Iwase *et al.* 1998; Fessenden *et al.* 1999; Gotti *et al.* 2005), $NO_{GC}R$ (Ariano *et al.* 1982; Fessenden *et al.* 1999; Gibb & Garthwaite 2001; Ding *et al.* 2004; Pifarre *et al.* 2007) and HCN channel subunits (Monteggia *et al.* 2000; Moosmang *et al.* 2001; Notomi & Shigemoto 2004) have been previously identified in the adult MNTB and DCN. The possibility remains that part of the NO-cGMP-HCN channel pathway may be missing in these brain regions in juvenile rats. The kinetics of activation suggest HCN channels in these regions contain HCN2 and HCN4 subunits and are therefore liable to modulation by cGMP (chapter 1). The lack of modulation of HCN channels in the MNTB and DCN by NO (chapter 4) may arise from the lack of expression of $NO_{GC}R$ at this age, which would mean a NO signal could not be transduced to cause rises in cGMP.

Alternatively, the signalling pathway may be present but the whole-cell technique used to measure the functionality of the pathway may cause dialysis or uncoupling (Sakmann & Neher 1984) of NO-stimulated cGMP and HCN channel function. This could be overcome by using a method that limits the perturbation of the intracellular contents.

5.2 AIM

The principal aim of this study was to determine the presence of the components of the NO-cGMP-HCN channel pathway in the MNTB and DCN neurones and to investigate the functioning of the pathway using less invasive recording methods than the whole-cell technique.

HYPOTHESIS: The NO-cGMP-HCN channel signalling pathway is present in the principal cells of the MNTB and DCN.

5.3 METHODS

Immunohistochemistry

Antibody	Concentration	Source
Primary:		
Mouse anti-eNOS	1:200	BD Biosciences Ltd, UK (Catalogue #610296)
Rabbit anti-nNOS	1:500	Zymed, San Francisco, CA (#61-700)
Sheep anti-nNOS	1:20,000	Gift from Dr. P.C. Emson, The Babraham Institute, Cambridge, UK
Rabbit anti-sGCβ_1 subunit	1:500	Cayman Chemical, Ann Arbor, MI (#160897)
Sheep anti-cGMP	1:40,000	Gift from Dr. J. de Vente, Maastricht, Netherlands
Rabbit anti-HCN1	1:800	Alomone labs Ltd., Jerusalem, Israel (#APC-056)
Rabbit anti-HCN2	1:500	Alomone labs Ltd., Jerusalem, Israel (#APC-030)
Rabbit anti-HCN4	1:200	Alomone labs Ltd., Jerusalem, Israel (#APC-052)

Table 5.1 Summary of antibodies used

All secondary antibodies were from Chemicon International, Harlow, UK. They were raised in a donkey host and used at 1:200.

Slices containing the MNTB or DCN, prepared as before (chapter 4), were fixed in ice-cold, freshly depolymerised paraformaldehyde (1 or 4 %) in 0.1 M phosphate buffer (PB; pH 7.4) for 2 h. Tissue was cryoprotected using ice-cold sucrose solution at 5 % for 3 h and then at 20 % in PB overnight. The slices were quickly frozen under dry ice in OCT, then frozen on a cryostat chuck and sectioned coronally at 10 µm intervals onto chrome alum/gelatin-coated slides. Slides were allowed to dry before being stored at -20 °C.

For fluorescence immunostaining, the slides were rehydrated in 0.1 % Triton X-100 in 0.1 M Tris-buffered saline (TBS-T) twice for 5 min. After rinsing, the slides were incubated with 20 % donkey serum (DS) in 0.1 M TBS-T for 1 h and then with primary antibody in 1% DS / 0.1 M TBS-T overnight at 4 °C. To characterise the

location of $NO_{GC}R$, I decided to use an antibody raised against a synthetic peptide from the β_1 subunit of the cyclase because all functional enzymes in the brain are thought to consist of this subunit with either α_1 or α_2 subunits (chapter 1), and therefore should detect all known heterodimers. nNOS detection was performed using two different antibodies. After rinsing (4 x 10 min with 0.1 M TBS-T) and incubation with FITC- or TRITC-labelled secondary antibodies raised in donkey (1:200) for 1 h, the slides were again rinsed (4 x 10 min with 0.1 M TBS-T) before mounting in Vectashield (Vector Laboratories Inc., Burlingame, CA) with DAPI, which binds tightly to DNA, hence staining effectively the nucleus; this allows for discerning qualitatively if immunolocalisation of the other proteins is extra-nuclear or not. The sections were visualised under confocal fluorescence optics (Leica Microsystems, UK).

To further characterise the location of nNOS and $NO_{GC}R$, an immunoperoxidase staining procedure was applied. To do this a peroxidase suppressor in a methanol solution (Pierce, Rockford, II, USA) was used to inhibit endogenous peroxidase activity in order to avoid false positives. As the exact requirements for inhibition vary with the tissue and sometimes the primary antibody, two parallel sets of slides were employed to allow the inhibitor to be applied before the primary antibody incubation in one set and immediately afterwards in another. The presence of $NO_{GC}R$ was probed using a rabbit polyclonal antibody raised against a synthetic peptide corresponding to the rat sGC β_1 subunit (1: 500, Cayman Chemical, MI, USA), while using the Zymed rabbit anti-rat antibody for nNOS. The staining procedure was carried out on tissue fixed with 1 % PFA. Again this involved rehydration of the slides with 0.1 % TBS-T. Following that, one set of slides were incubated with suppressor, the other with TBS-T, for 15 min. After rinsing twice with TBS-T for 3 min, the tissue was blocked with 20 % donkey serum and then incubated with primary antibody and 1 % donkey serum overnight at 4 °C. The slides were rinsed at 10 min intervals, twice with TBS-T and then once with TBS, followed by peroxidase suppressor or just TBS for 15 min as appropriate. After rinsing with TBS, twice for 3 min, the sections were incubated with donkey anti-rabbit biotinylated secondary antibody for 1 h at room temperature. Slides were washed (3 x 10 min with TBS) and incubated with Vectastain elite ABC

(Vecto Labs Ltd, Peterborough, UK) for 45 min, stained for 4 min with 0.05 % DAB (3,3'-diaminobenzidine; Sigma, Dorset) then counterstained with Mayer's haemalum (Raymond A Lamb Ltd., Eastbourne) for 15 s. Finally slides were air-dried and mounted in DPX medium (Agar Scientific, Stansted).

All results presented are representative examples of sections from two or more animals.

The qualitative effect of NO-stimulation in the MNTB was detected using cGMP immunohistochemistry following different experimental conditions. Slices were exposed to the NO donor, DEA/NO (100 µM) for 5 min at 37 °C. The general phosphodiesterase inhibitor, 3-isobutyl-1-methyl-xanthine (IBMX, 1 mM) was added 15 min before exposure to the NO donor. Sections were incubated with primary sheep anti-cGMP antibody at 1:40,000 and donkey anti-sheep FITC-labelled secondary antibody as described above. Resents presented are representative example of three slices from three different animals.

The presence of specific HCN subunits was probed using the appropriate antibody raised in rabbit from Alomone Labs. HCN 1, 2 and 4 antibodies were used at 1:800, 1:500 and 1:200 respectively as optimised previously in the laboratory. In an attempt to improve the ratio of specific-to-background staining, increased permeabilisation and an amplification step were implemented. Following the overnight incubation with primary antibody, the slides were rinsed first twice with 0.3 % TBS-T for 10 min and then once with just TBS. After rinsing, the sections were incubated with donkey anti-rabbit biotinylated secondary antibody (1:100) for 1 h at room temperature. The slides were then washed 3 times with TBS for 10 min each, with a subsequent incubation with avidin-Texas Red (1:200; Vector Laboratories Inc., Burlingame, CA) for 1 h at room temperature. The slides were rinsed again (3 x 10 min with TBS) and mounted in DAPI-containing Vectashield.

Electrophysiology

Rat pups (9 - 13 days old) were killed, and the brains promptly removed and immersed in ice-cold high Mg^{2+}/low Na^+ aCSF containing (in mM): 250 sucrose, 2.5 KCl, 6 $MgCl_2$, 2.0 $CaCl_2$, 1.0 $NaH_2PO_4.H_2O$, 26.2 $NaHCO_3$, and 11 glucose, equilibrated with 95% O_2 - 5% CO_2. Coronal slices (400 µm) from the cerebellum were cut using a McIlwain chopper. Slices were then incubated at 37 °C for one hour, and at room temperature thereafter, in gassed normal aCSF. After this period of recovery (at least 60 min), one slice was transferred into a submerged chamber and continuously perfused with aCSF. Borosilicate microelectrodes (100-160 MΩ; Clark capillaries, Reading) were filled with 2 or 3 M KAc. Blind recordings were made in either the lateral or interposed DCN. Upon entry into the cell, a strong hyperpolarising current bias was applied to promote stability. Membrane voltage was filtered at 1 kHz and sampled at 2 kHz using an Axoclamp-2B amplifier (Axon instruments, Foster City, CA) in bridge mode. The neuronal membrane potential was clamped at around -62 mV (irrespective of offset), as this potential was sufficiently hyperpolarising to prevent spontaneous, rhythmic firing. The bridge balance was constantly monitored throughout the experiment and adjusted appropriately. A 3750 ms hyperpolarising step (figure 5.1) was applied to activate I_h every 10 s. Prior to this a short (500 ms), small hyperpolarising step was applied for calculation of the neuronal input resistance (R_{in}). Analysis was performed offline using Clampfit 8.0 (Axon Instruments, Foster City, CA).
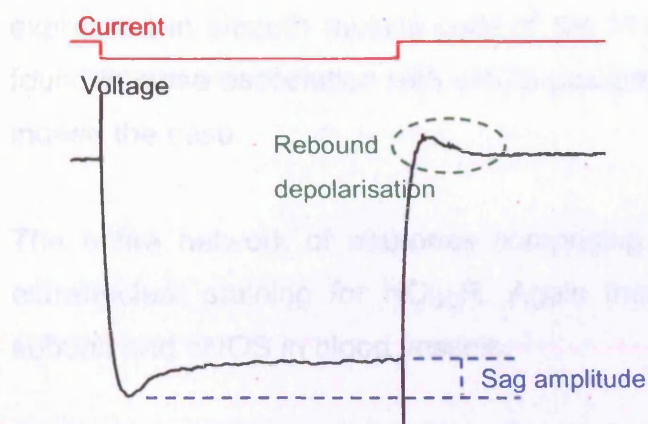
Figure 5.1 A schematic of the membrane response to a hyperpolarising current injection

There is a depolarising sag in the membrane potential, indicative of I_h activation.

5.4 RESULTS

NO$_{GC}$R and eNOS immunofluoresence

Cerebellar cortex – a positive control (figure 5.2) and DCN (figure 5.3)

The presence of the receptor for NO has been well characterised in the cerebellar cortex and therefore this brain region was used to test the sGCβ_1 antibody for immunocytochemistry. The external granule cell layer, a germinal layer consisting mainly of a replicating granule cell precursor pool, showed weak staining. There appeared to be fine processes stretching out from the molecular layer and extending into this layer. There was a robust staining of the internal granule cell layer, which ceases at its boundary with the white matter tracts leading to the deep cerebellar nuclei. The Purkinje cell bodies showed weakly granular staining throughout the soma; it was difficult to discern the staining of the (proximal) dendritic tree because of the coronal sectioning of the cerebellum. This staining pattern was consistent with previously, well-established localisation of NO$_{GC}$R expression (Ariano *et al.* 1982; Ding *et al.* 2004) or mRNA transcript distribution (Gibb & Garthwaite 2001; Pifarre *et al.* 2007) in the folia.

The anti-eNOS antibody stained the blood vessels as to be expected. In addition there was a low-level specific staining throughout the parenchyma of the slice, probably representing the endothelial cells of the microvasculature extending throughout the cerebellum and the brain as a whole. Co-staining with eNOS was used as an additional control for the selectivity of sGCβ_1 antibody. NO$_{GC}$R is expressed in smooth muscle cells of the blood vessels and therefore should be found in close association with eNOS-positive vascular endothelial cells. This was indeed the case.

The entire network of neurones comprising the DCN appeared to show weak, extranuclear staining for NO$_{GC}$R. Again there was co-expression of NO$_{GC}$R β-subunit and eNOS in blood vessels.
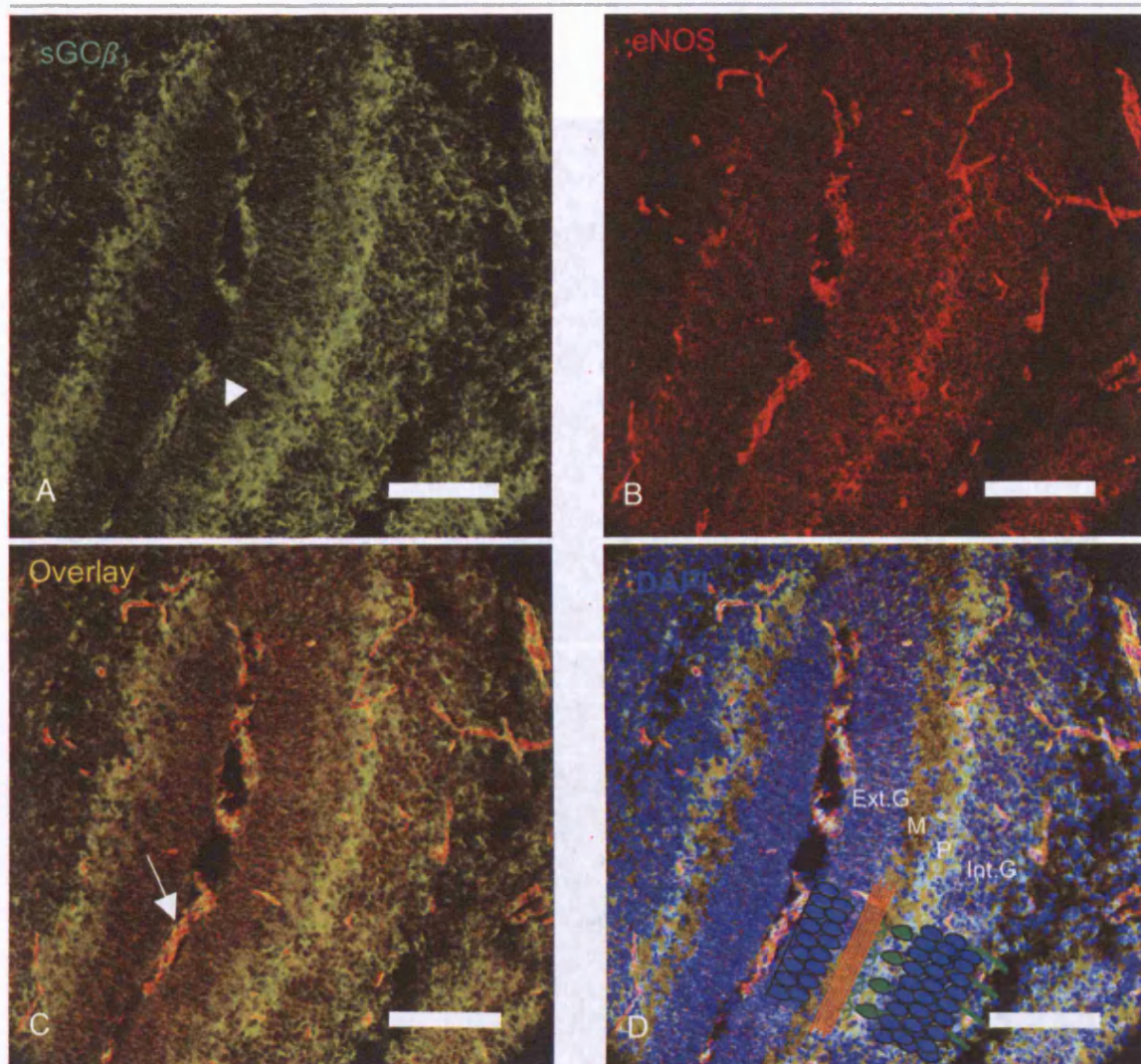
Figure 5.2 Immunofluorescent double labelling for sGCβ_1 and eNOS in the cerebellar cortex.

A-D, Both proteins were found throughout the folia. In most layers, the two proteins colocalised, particularly in the blood vessels (arrows). sGCβ_1 immunoreactive fibres can be seen extending into the external granule cell layer (arrow head) which are probably Bergmann glial processes.

E,F Controls in which sections were exposed only to secondary antibody. There was a very low background of non-specific binding.

Scale bar = 100 µm; Ext G = external granule cell layer; M = molecular layer; P = Purkinje cell layer; Int G = internal granule cell layer.

G, Key to the schematic overlay in D to outline the anatomy of the cerebellar cortex.
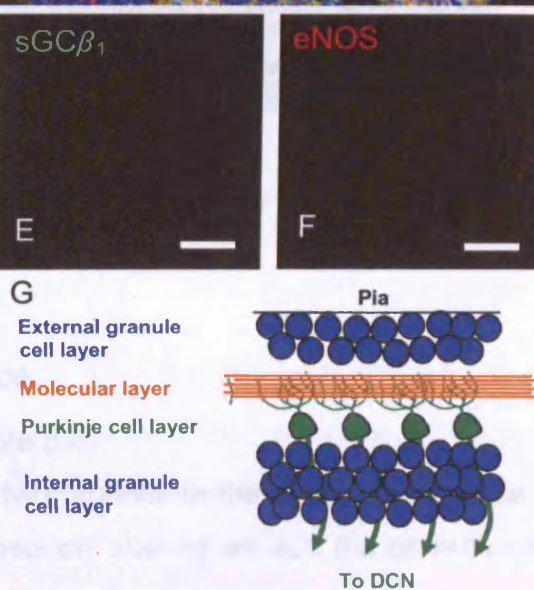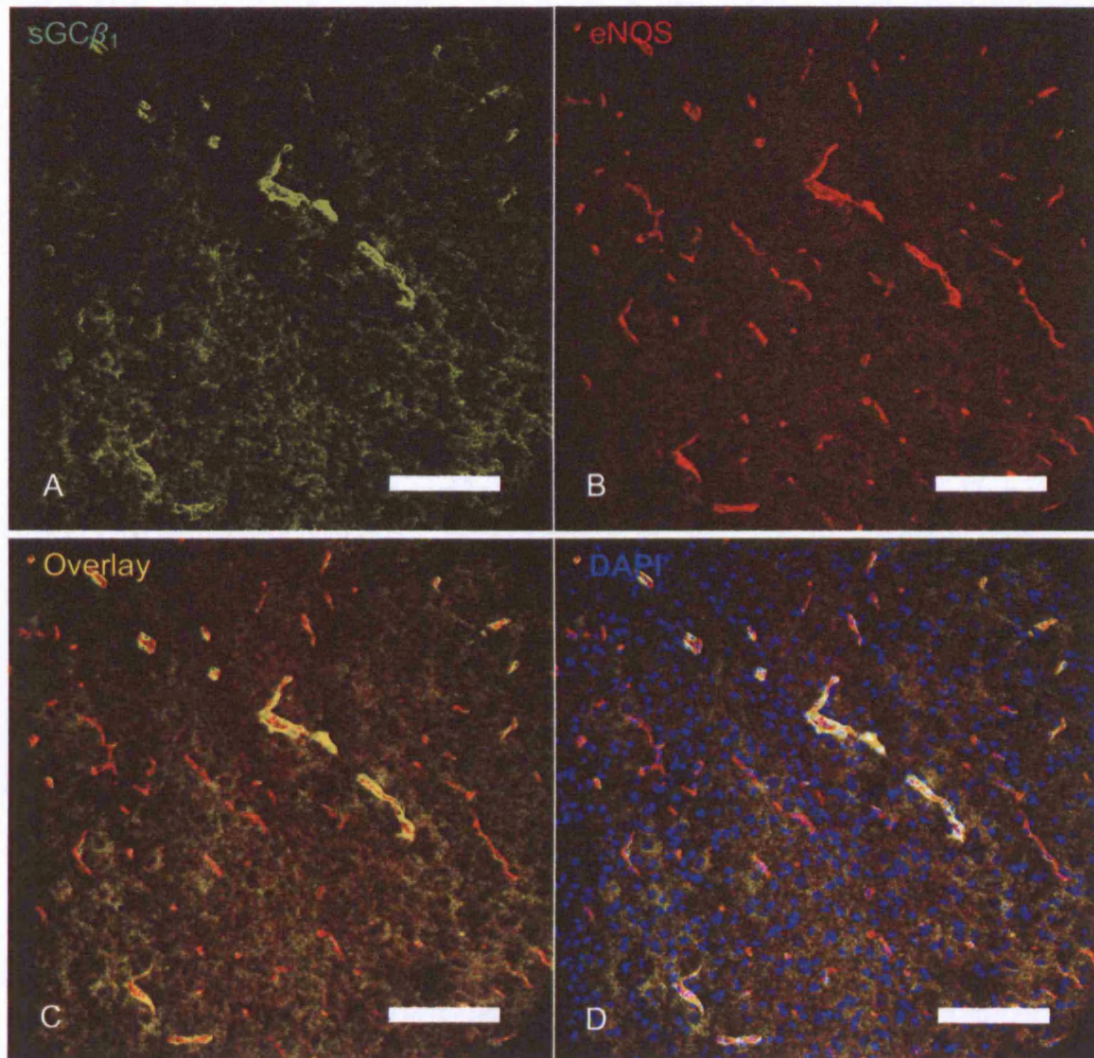
Figure 5.3 Double immunostaining in the DCN

There was diffuse, extranuclear expression of $NO_{GC}R$ in the parenchyma of the DCN.
There was some degree of overlap with eNOS in blood vessels.
Scale bar = 100 μm.

$NO_{GC}R$ and nNOS immunofluorescence

Cerebellar cortex (figure 5.4) and DCN (figure 5.5)

There was a good overlap between these two proteins in the cortex as a whole –
the molecular layer neuropil was homogeneously stained as was the granule cell

layer. The Purkinje cells were devoid of nNOS staining as in adult tissue (Vincent & Kimura 1992; Rodrigo *et al.* 1994). Cells in the inner part of the molecular layer, around the Purkinje cells were heterogeneous in their staining for nNOS. The distribution of nNOS was consistent with that found in the aforementioned studies.

In the DCN, strong nNOS immunoreactivity was found in a few large cells and also as a sparse network of fibres and punctae radiating throughout the nucleus. Neurones showing positive signal for nNOS did not show expression of $NO_{GC}R$. As for figure 5.3, there was a weak, homogeneous extranuclear $sGC\beta_1$ staining in the DCN neuronal population.

$NO_{GC}R$ and nNOS immunohistochemistry in the cerebellum

The relatively weak, but specific staining in the DCN for $NO_{GC}R$ and nNOS prompted the use of the peroxidase technique that improves resolution of a particular epitope by virtue of its intrinsic property of signal amplification.

$NO_{GC}R$ staining in the cerebellar cortex was as for the fluorescence data (figure 5.6A). In particular it was clear that the granule cells and the glomeruli, where granule cell dendrites are contacted by incoming mossy fibres expressed $NO_{GC}R$. The white matter tracts connecting the cortex and DCN were virtually devoid of receptor for NO. In contrast, the outline of the DCN was clearly discernable by the presence of $NO_{GC}R$ immunoreactivity throughout the nuclei. The larger DCN neurones showed dense staining throughout their cytoplasm (figure 5.6B).

nNOS staining (figure 5.7) was similar to that found using immunofluorescence patterns. Staining in the somata of Purkinje cells was faint or absent. In the DCN, the sparse network of positive fibres was more clearly seen as a widely-distributed plexus of varicose fibres seemingly contacting every neurone.

$NO_{GC}R$ and nNOS immunohistochemistry in the brainstem

There was intense $sGC\beta_1$ staining in descending motor fibres of the pyramid, while the decussating axons running to the MNTB were immunonegative (figure 5.8A-C). The principal cells of the MNTB showed expression of $NO_{GC}R$ throughout the nucleus (figure 5.8D) as seen before in the adult (Fessenden *et al.* 1999).
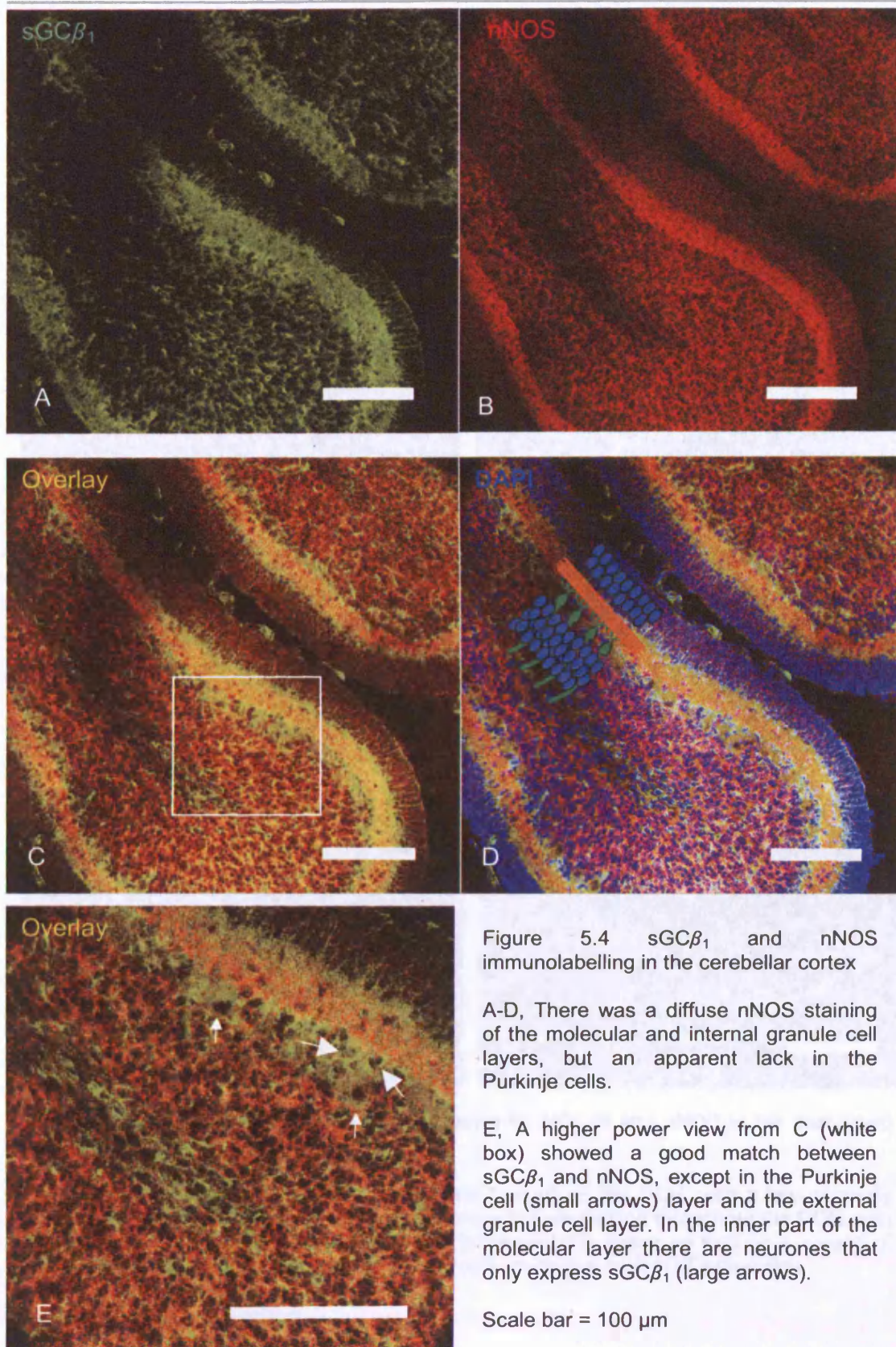
Figure 5.4 sGCβ_1 and nNOS immunolabelling in the cerebellar cortex

A-D, There was a diffuse nNOS staining of the molecular and internal granule cell layers, but an apparent lack in the Purkinje cells.

E, A higher power view from C (white box) showed a good match between sGCβ_1 and nNOS, except in the Purkinje cell (small arrows) layer and the external granule cell layer. In the inner part of the molecular layer there are neurones that only express sGCβ_1 (large arrows).

Scale bar = 100 μm
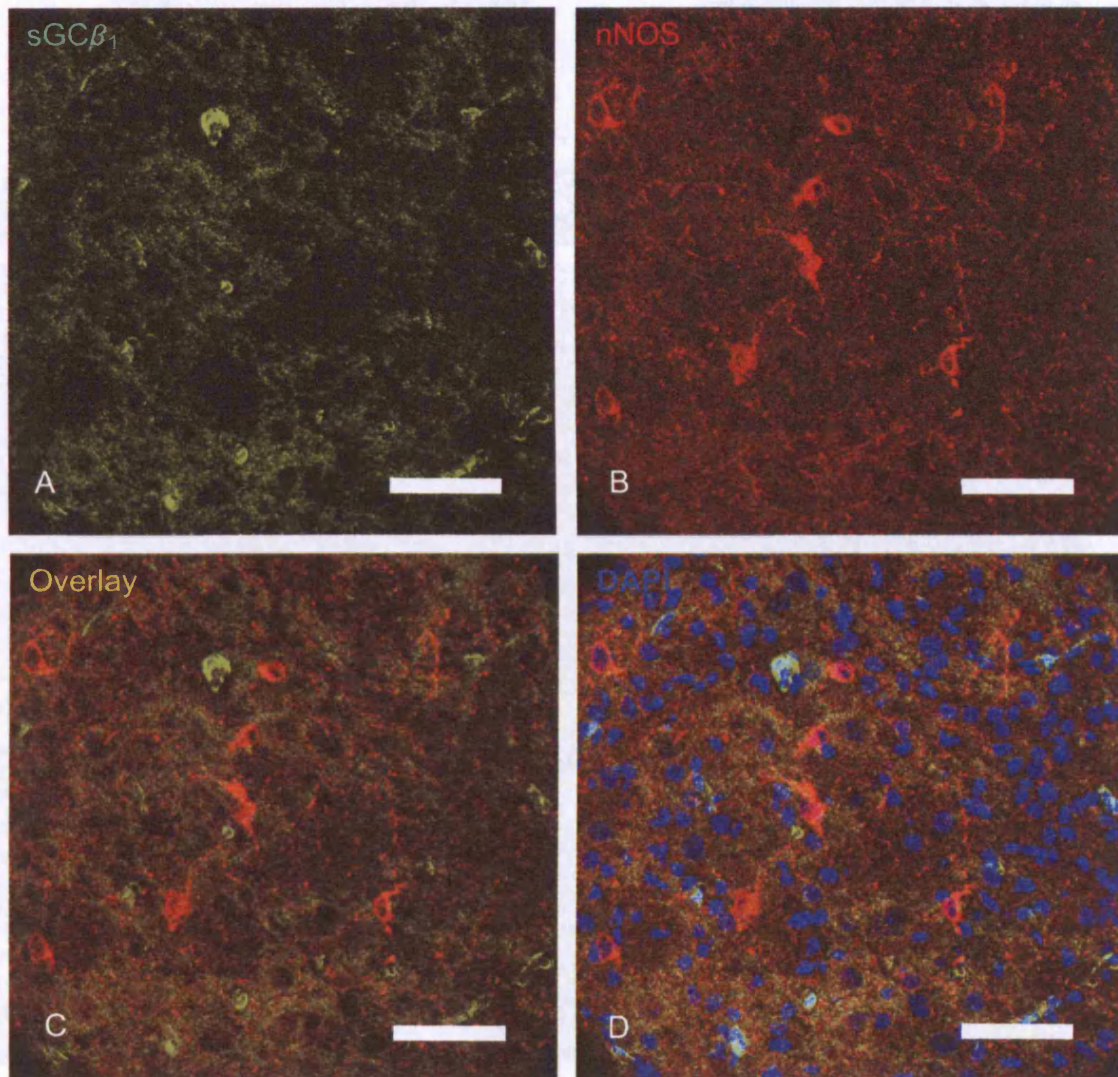
Figure 5.5 Double-labelling immunofluorescence for $NO_{GC}R$ and nNOS in the interposed DCN

A diffuse staining of $sGC\beta_1$-subunit was seen throughout the DCN, with a few intensely staining nuclei. Similarly nNOS showed a low level of expression throughout the DCN, with a number of positive neurones distributed throughout the tissue as well as a spread of unconnected tendrils. Proteins showed a mutually-exclusive pattern of expression.
Scale bar = 50 µm
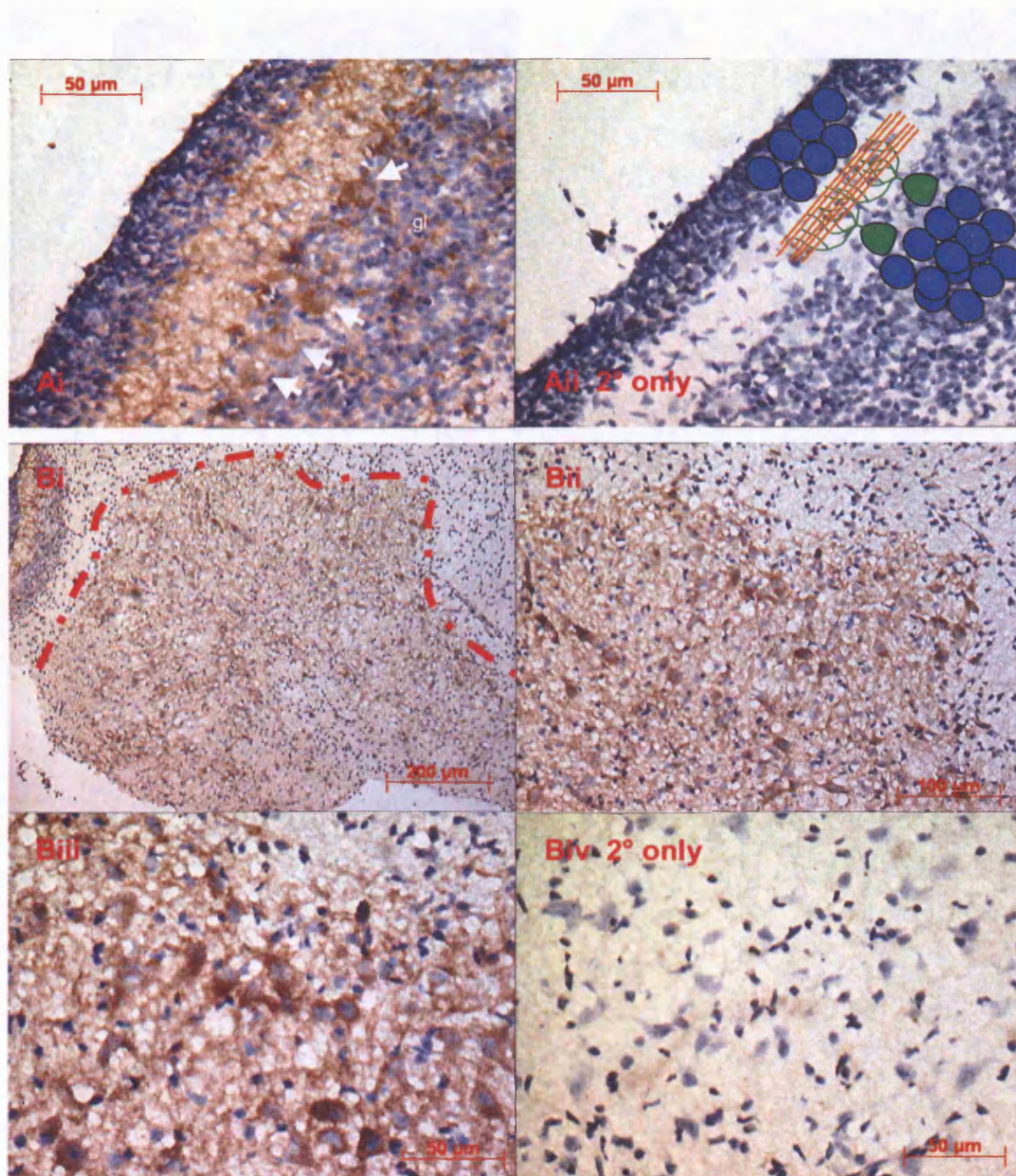
Figure 5.6 sGCβ_1-immunoreactivity in the cerebellum

Ai, The NO$_{GC}$R appeared to be expressed in all layers of the cortex. Arrows: Purkinje
cells; gl: glomerulus

Aii, A control in which the section was incubated with secondary antibody only; there
was a very low background of non-specific binding.

B, sGCβ_1 staining, at various magnifications (i-iii), was seen throughout the cytoplasm of
the majority of the dentate DCN (outline marked by dashed red line) neurones. The
prominent staining in the DCN makes it clearly discernable from the surrounding white
matter tracts (Bi) connecting the DCN to the cortex.
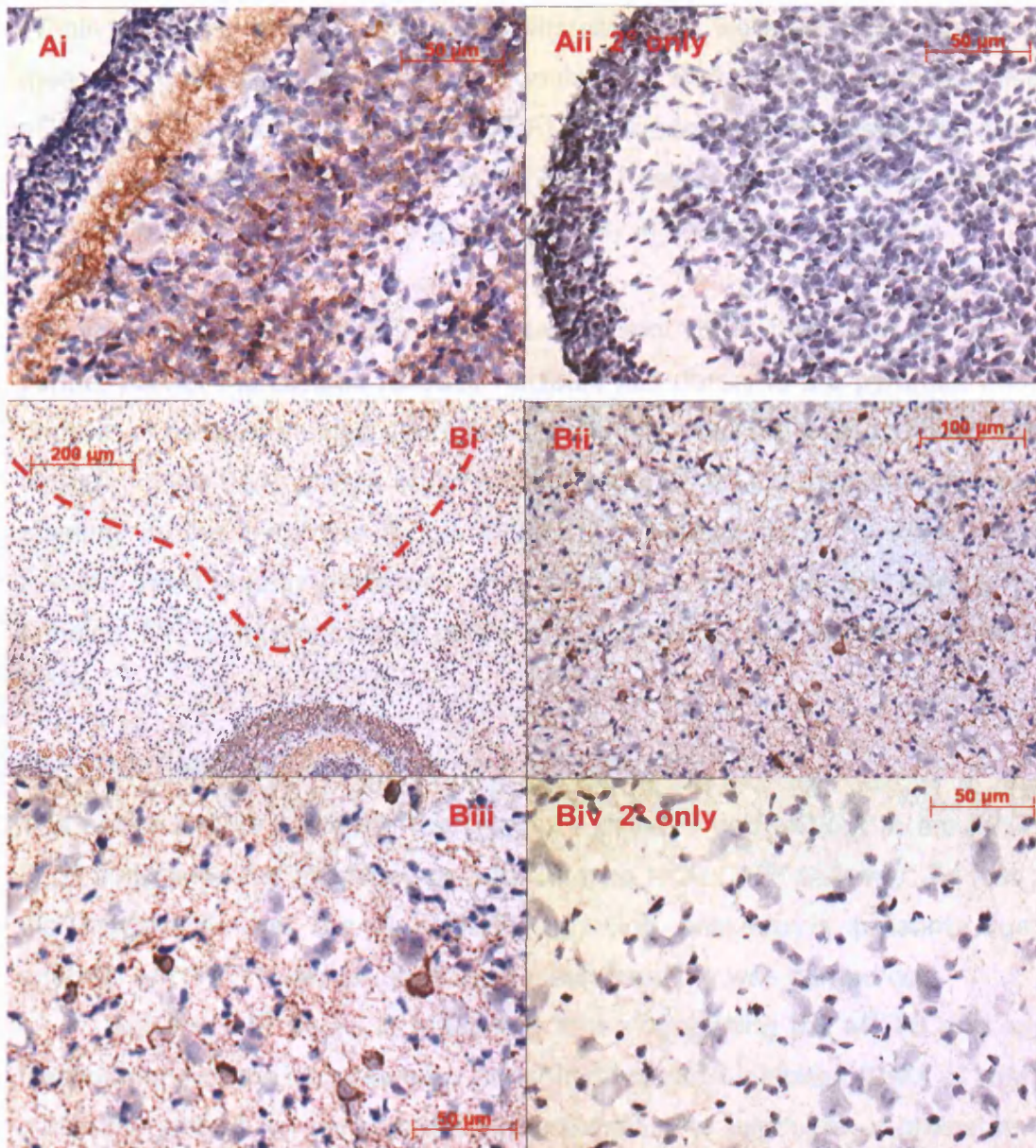
Figure 5.7 nNOS-immunohistochemistry in the cerebellum

A, Specific staining in the molecular and granule cell layer as seen in figure 5.3. There was little-to-no signal in the Purkinje cells.
B, Within the dentate and interposed DCN, there was a distinct subset of nNOS-expressing neurones, from which a network of varicose fibres extend throughout the tissue. There was no nNOS staining in the white matter between the cortex and DCN (B1; red dashed line traces the outline of the DCN).

Within the same coronal section of brainstem, there were the trigeminal motor and mesencephalic trigeminal neuronal populations. Both sets of neurones displayed sGCβ_1-immunoreactivity (figure 5.8E,F) as expected from previously published data on NO regulation (Abudara *et al.* 2002; Pose *et al.* 2003). This suggests that the sGCβ_1 antibody was staining appropriately in brainstem sections.

nNOS expression (figure 5.9) was much weaker than that seen for sGCβ. The ventral part of the pontine reticular nucleus, just dorsal to the pyramid, showed a number of densely stained neurones from which a net of varicose fibres extended throughout the parenchyma of the nucleus (figure 5.9B,C). There was a very weak staining in the pyramids (figure 5.9D,E), complementing the NO$_{GC}$R pattern. Positive nNOS-immunoreactivity was seen at a very low level throughout the principal MNTB neurones and as distinct, apparently cytoplasmic granules (figure 5.10).

NO-stimulated cGMP immunohistochemistry

The above results indicating the presence of NOS and NO$_{GC}$R in the MNTB and DCN suggested the existence of a functioning NO-cGMP pathway. To test further the hypothesis that the NO-cGMP signalling cascade is present, qualitative analysis of cGMP levels using immunohistochemistry was carried out.

Basal cGMP levels in brainstem slices containing the MNTB and levels in the presence of the non-selective phosphodiesterase inhibitor, IBMX (1 mM) were quite low, just above background fluorescence. The exposure of brainstem slices for 5 min to 100 µM DEA/NO, in the presence of IBMX, resulted in an obvious elevation of cGMP levels in MNTB neurones and the pyramids (n=3; figure 5.11). This result also confirms that slices prepared using this method, as for electrophysiological recordings, are indeed capable of responding to NO with a rise in cGMP levels.
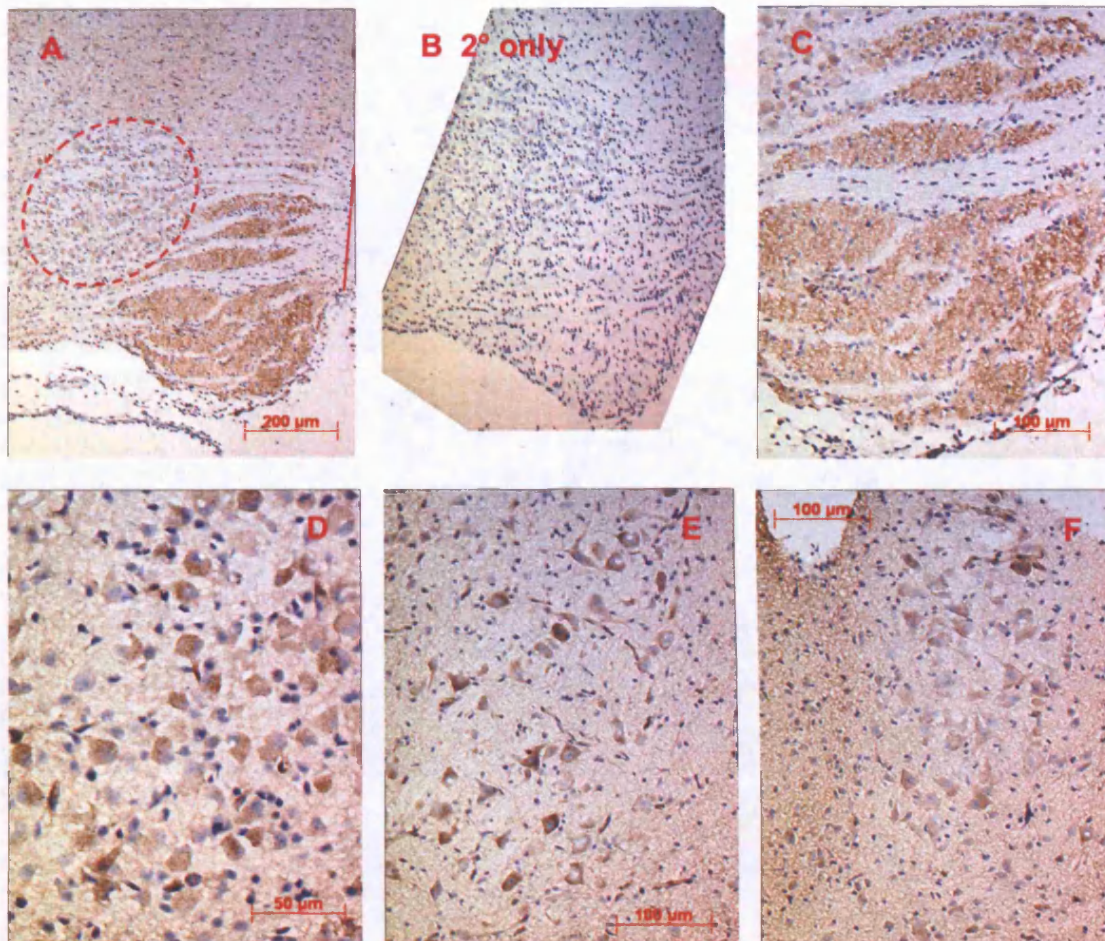
Figure 5.8 NO$_{GC}$R immunoreactivity in the auditory brainstem
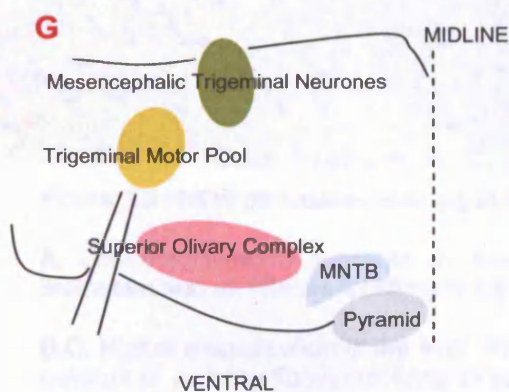
A, Low-power field of the pyramid and MNTB (dashed oval) on one side of the trapezoid body (solid red line indicates the midline).

B, Little-to-no non-specific background signal using the secondary antibody only.

C, Intense sGCβ_1 staining appeared to be found in the motor fibre pyramidal tract, but none in the fibres running to and from the midline.

D, Obvious, granular staining in the principal cells of the MNTB.

E, F, Prominent NO-receptor staining was found in the trigeminal motor pool and mesencephalic trigeminal neurones respectively.

G, Schematic diagram highlighting the anatomy of the auditory brainstem, and the regions discussed above.
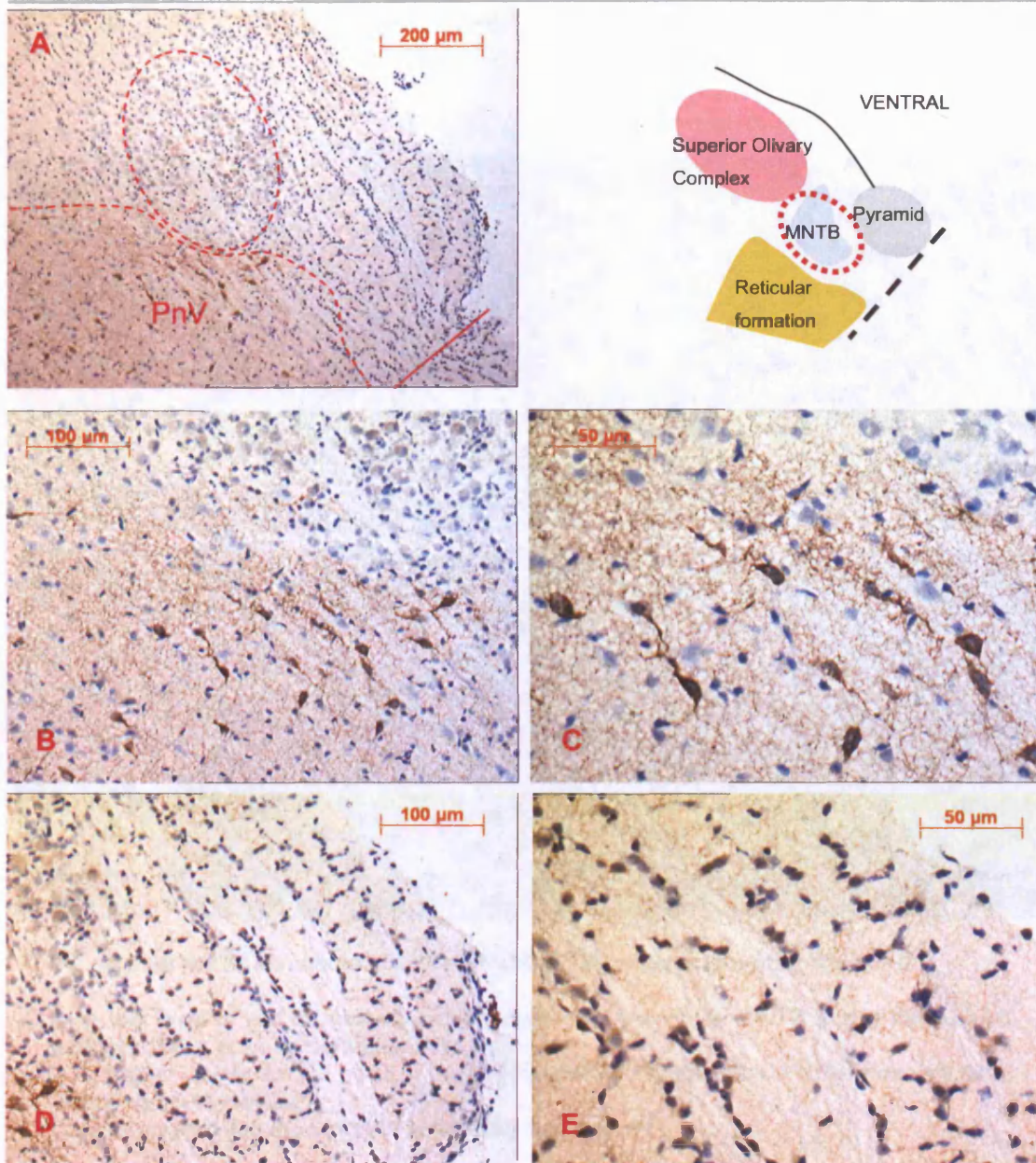
Figure 5.9 nNOS peroxidase staining in the brainstem

A, Low magnification indicated a low-level, diffuse staining throughout the auditory brainstem and an intense labelling in the ventral pontine reticular nucleus (PnV).

B,C, Higher magnification of the PnV. Prominently stained neurones can be seen with a network of varicose fibres ramifying throughout the nucleus.

D,E, Within the pyramid, there was a weak staining in the motor fibre pyramidal tract but not in the decussating fibres running across the field of view.
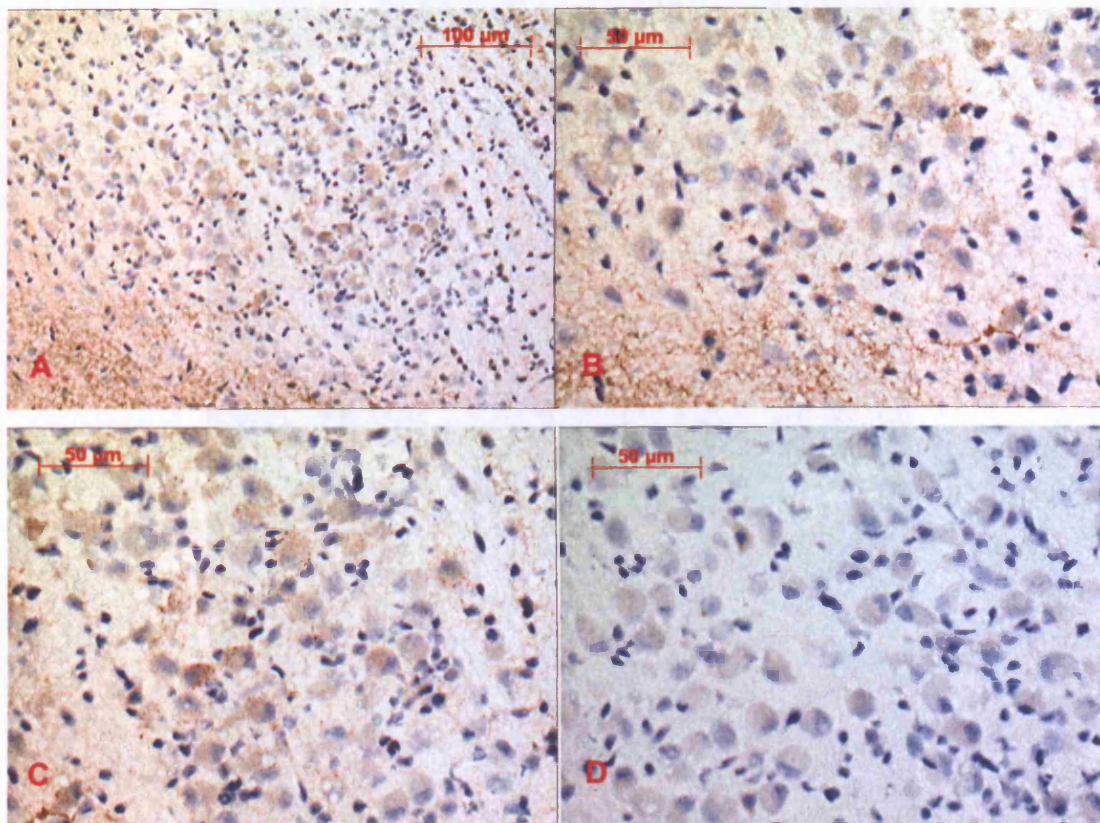
Figure 5.10 nNOS immunoreactivity in MNTB principal neurones from figure 5.9

A, A low level of nNOS staining can be seen over the entire MNTB and a network of
varicose fibres at its dorsomedial edge.
B,C, Higher power field of parts of the MNTB. Principal cells show a diffuse as well as a
distinct granule staining.
D, Background staining from the secondary antibody only.
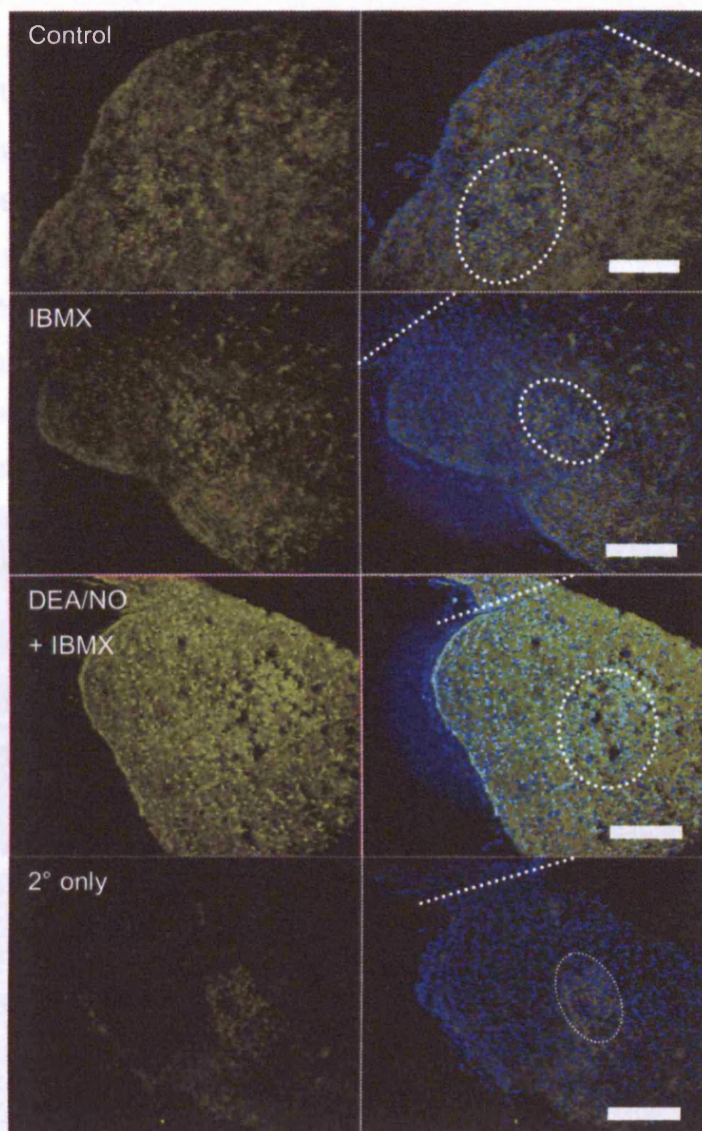
Figure 5.11 cGMP immunohistochemistry in MNTB slices

cGMP levels under basal conditions and in the presence of 1 mM IBMX are both low, similar to background with the secondary (2°) antibody only. cGMP levels are greatly increased in the presence of 100 µM DEA/NO.

Panels on the right show nuclear staining using DAPI; white dashed line indicates the midline; dashed oval indicates MNTB; scale bar = 200 µM

127

HCN immunofluoresence

In order elucidate the hypothesised composition of HCN channels in the MNTB and DCN, I used polyclonal antibodies against HCN1, HCN2 and HCN4 that yielded positive results in the literature (Koch *et al.* 2004; Leao *et al.* 2005). Anti-HCN2 stained the cytoplasm and plasma membrane of the entire MNTB as well as the surrounding regions (figure 5.12A). To improve the signal-to-noise ratio, I used an amplification step, but this yielded only non-specific binding (figure 5.12B). All batches of HCN antibodies subsequently received were ineffectual, and it appeared that other researchers that had previously demonstrated successful stainings were now experiencing the same problems (K.E. Leao, personal communication). Therefore further attempts at HCN staining were abandoned.
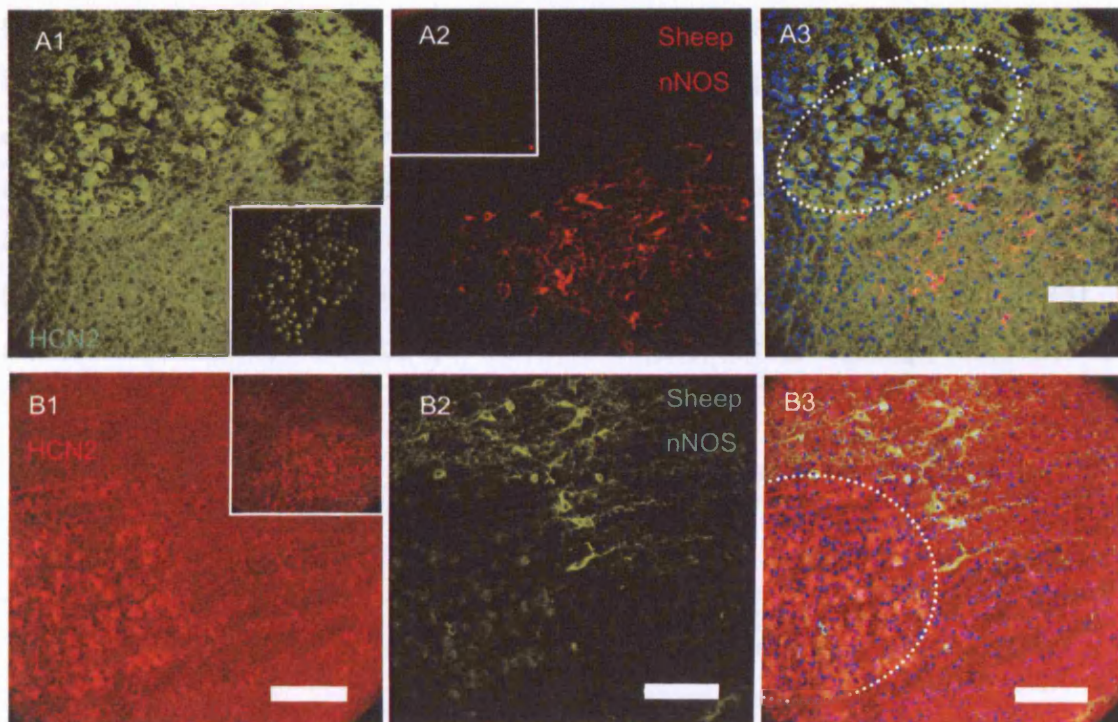
Figure 5.12 HCN immunohistochemistry was inconclusive
A, HCN2 immunoreactivity was found diffusely in the MNTB, both cytoplasmic and on the cell membrane. There was also a lot of staining in the surrounding parenchyma. Double labelling with a different nNOS antibody to that shown prior figures confirmed the strong staining in the ventral pontine reticular nucleus (PnV) and little in the MNTB.
B, An additional amplification step failed to improve the signal-to-noise of HCN2. Again, double-labelling with nNOS showed a low level in the MNTB with an intense network of nNOS-positive cells in the PnV.
Scale bar = 100 μm; dashed white line indicates the location of MNTB; insets are secondary antibody only.

Microelectrode recordings

The expression of NOS and $NO_{GC}R$ at this age of rats suggested that the level of cGMP should be elevated in response to an NO signal. To test if the lack of NO-stimulated modulation of HCN channels seen in chapter 4 was due to whole-cell dialysis of intracellular contents, the apparently less disruptive sharp microelectrode current-clamp technique was employed. nNOS staining in the MNTB was quite light, while the presence of a mesh of nNOS-positive varicose fibres ramifying throughout the DCN suggested that NO is likely to play an important physiological role in this part of the cerebellum. For these reasons, the recordings were made in the interposed or dentate DCN.

In the presence of 500 nM TTX and 1 mM 4-AP, there was a depolarising sag, an index of I_h, in the membrane voltage during a long hyperpolarising step. After cessation of the hyperpolarising step, there was a prominent rebound depolarisation with one or more associated spikes presumably caused by activation of Ca^{2+} channels (chapter 4). The mean R_{in} of the cells was 63 ± 8.6 MΩ (range 33-92; n=7), comparable to previous reports (Aizenman *et al.* 2003). The addition of 2 mM Cs^+ to block I_h removed the depolarising sag (figure 5.13).
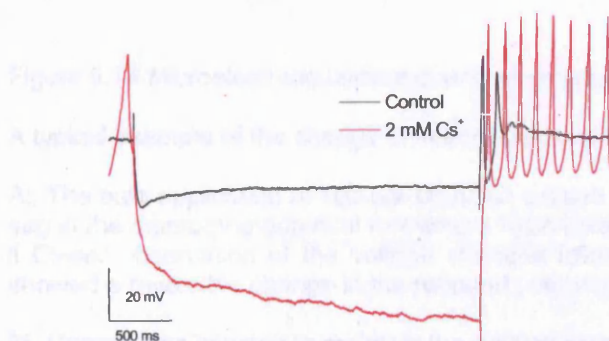
Figure 5.13 Removal of the depolarising sag by 2 mM Cs^+

The negative current injection caused a much greater hyperpolarisation in the membrane potential, likely due to block of I_h. There was also repetitive spiking activity.

The application of 100 µM DEA/NO resulted in a decrease in the depolarising sag (n=5 of 5; figure 5.14A; 10 ± 1.3 mV significantly decreased to 4 ± 0.5 mV: Student's paired *t*-test; p<0.02). This change was completely reversible following wash out of NO. The amplitude of the depolarising sag reflects the

disparity in the activation level of I_h at the holding potential and at the membrane
potential in response to the negative current step. During the application of NO,
there was also a decrease in the R_{in} (figure 5.14B), indicative of an increase in a
membrane conductance, probably carried by HCN channels. If the recording was
sufficiently stable, reapplication of NO caused a similar reproducible decrease in
the depolarising sag and input resistance (figure 5.15).
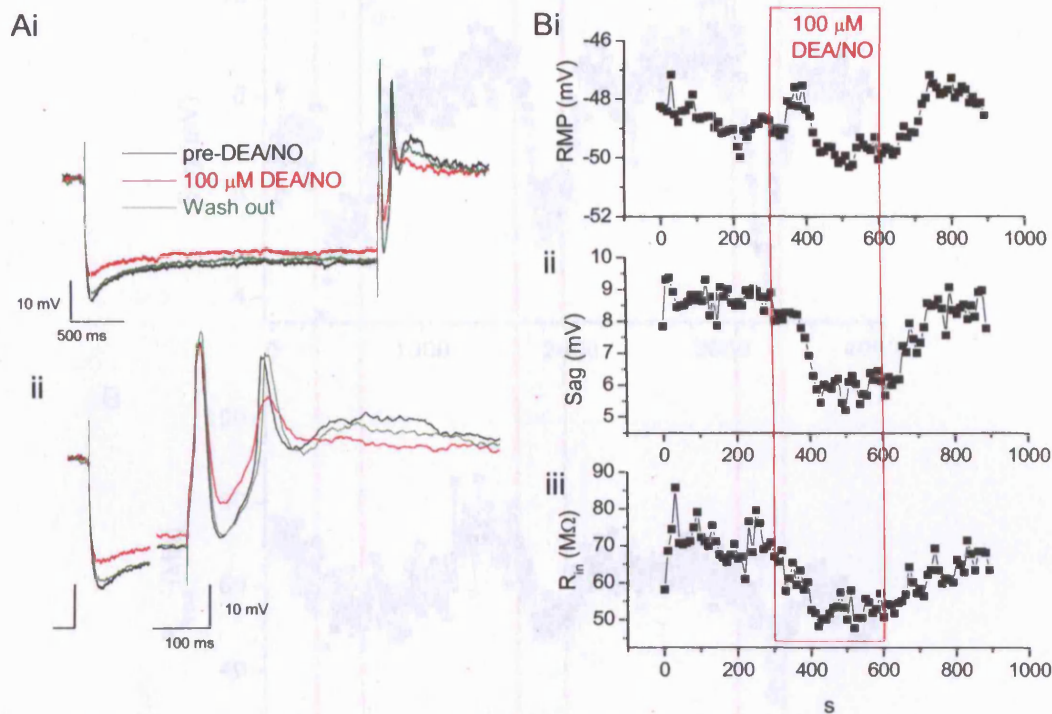
Figure 5.14 Microelectrode current-clamp recordings of DCN neurones (n=5)

A typical example of the change in membrane properties

Ai, The bath application of 100 µM DEA/NO caused a reversible decrease in the depolarising
sag in the membrane potential following a hyperpolarising current injection.
ii Closer observation of the voltage changes following offset of the negative current step
showed a reversible change in the rebound potentials.

Bi, Current was injected to maintain the holding potential around -49 mV.
ii, The depolarising sag in the membrane potential during a long hyperpolarising current (-0.4
nA) injection.
iii, There was a concomitant decrease in input resistance during the presence of NO.

This cell was recorded in the presence of 1 mM 4-AP and 500 nM TTX.

Closer interrogation of the rebound depolarisation after termination of the hyperpolarising step showed that there were reproducible, reversible changes in the Ca^{2+} spikes following NO application (figure 5.14Aii). There was an obvious decrease in the amplitude, with little increase in the time to peak (figures 5.16 and 5.17).
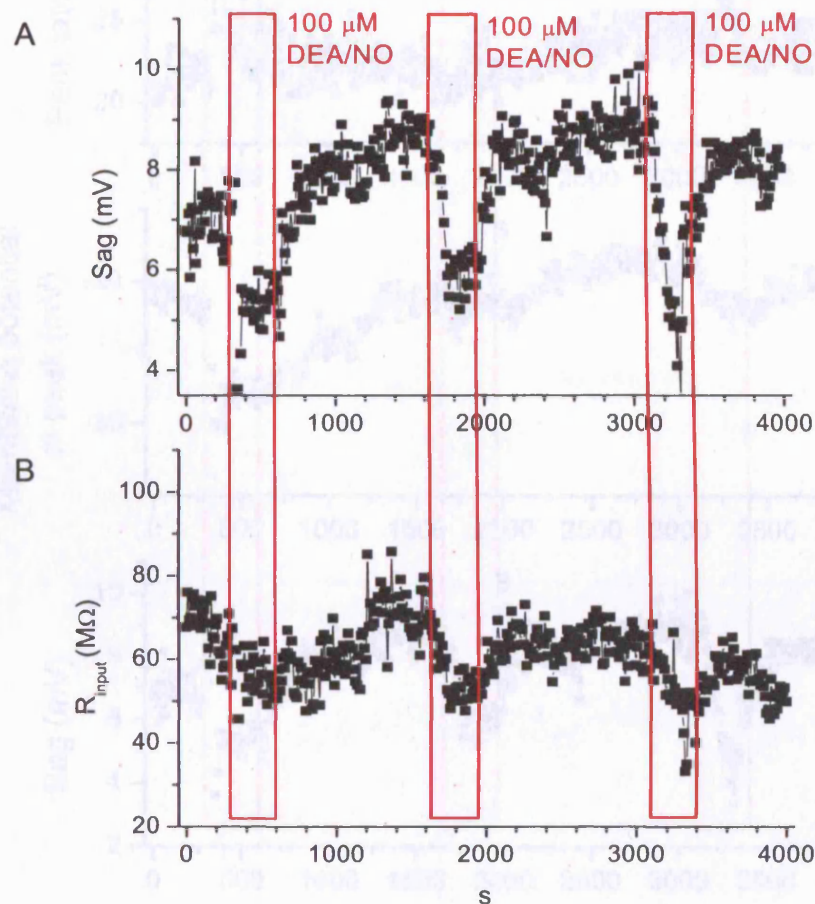
Figure 5.15 The time course of reproducible changes in DCN neurones during NO application

The same neurone as figure 5.14; values are taken from voltage traces recorded every 10 s.

A, 3 applications of 100 μM DEA/NO lead to similar decreases in sag amplitude. These changes reversed on wash out.
B, The decreases in sag amplitude mirrored the decreases in input resistance during the presence of NO.

First Ca^{2+} spike
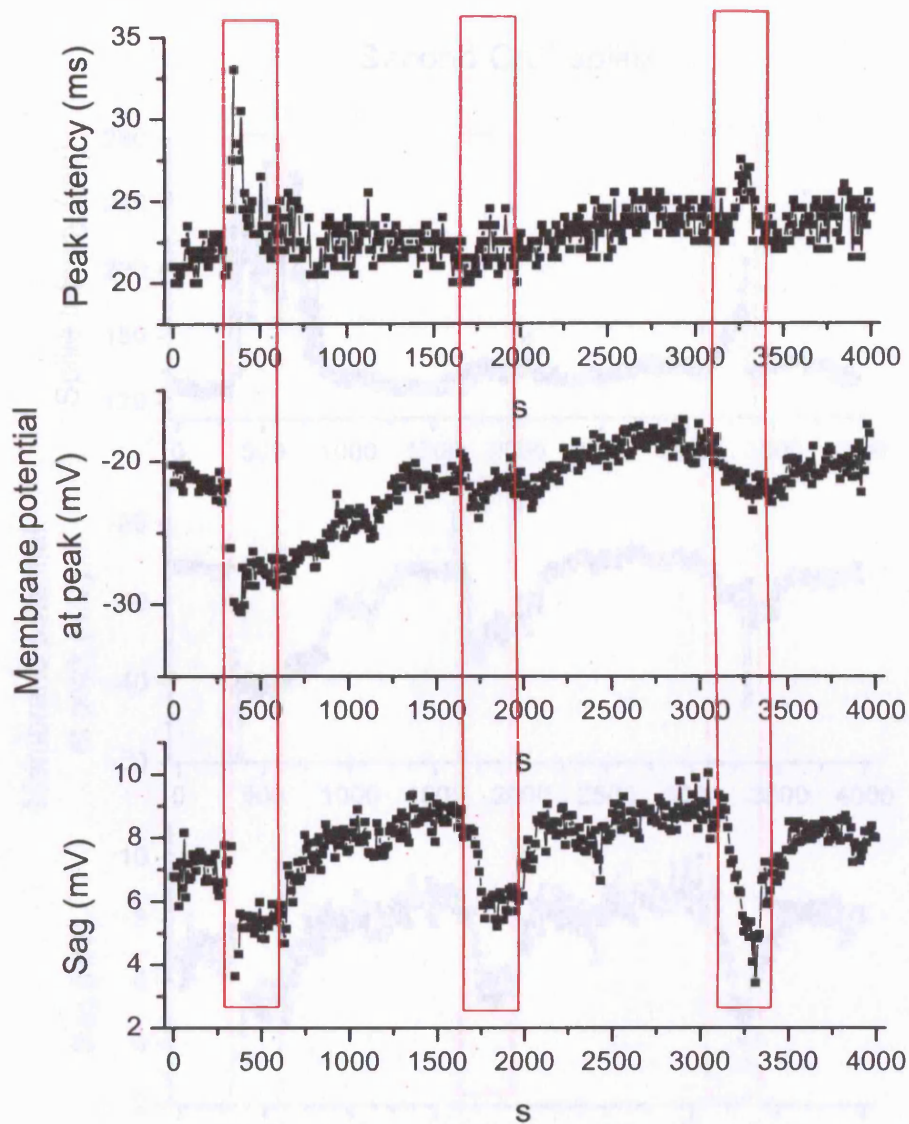
Figure 5.16 The changes in the first Ca^{2+} spike of the rebound depolarisation

From the same cell as figure 5.14, the time to peak and the peak potential of the first spike
of the rebound depolarisation are displayed with the changes in the depolarising sag from
figure 5.13. Red rectangles denote the presence of 100 µM DEA/NO.
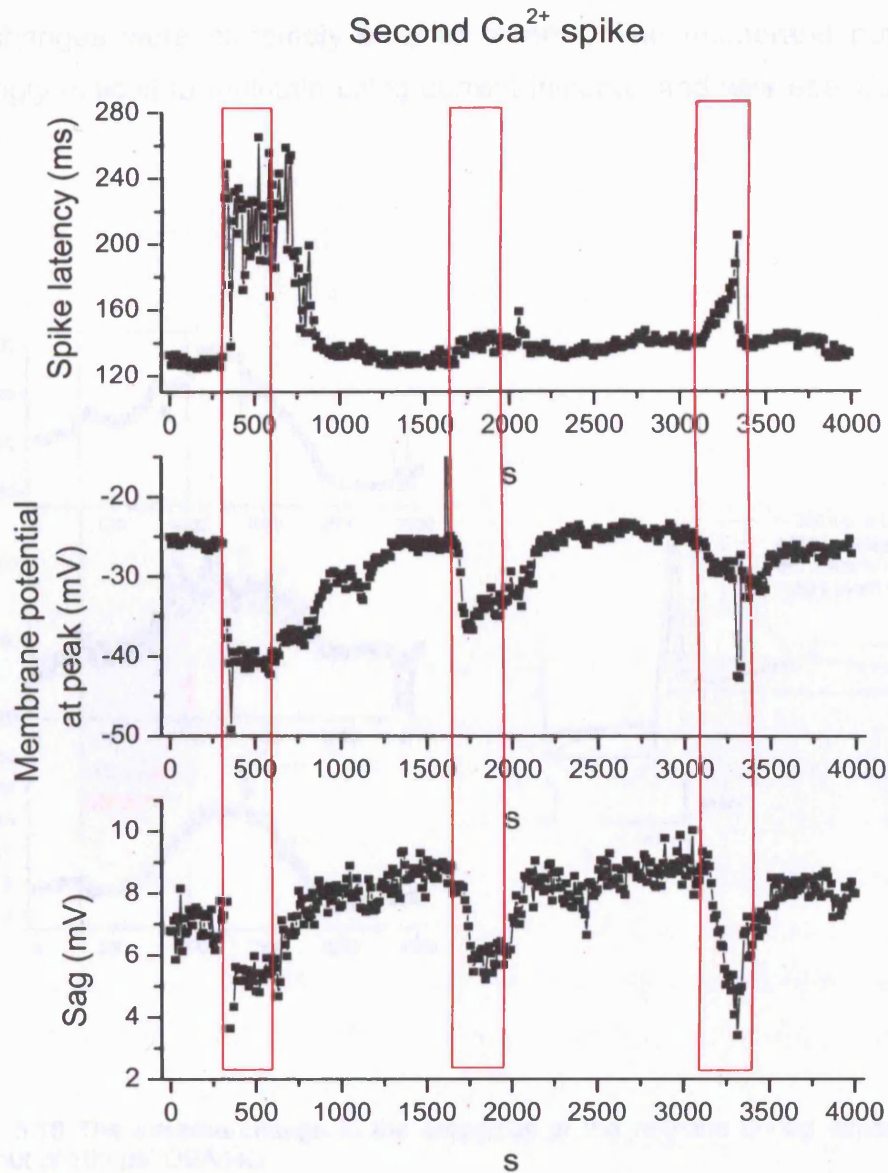
Figure 5.17 The changes in the second Ca^{2+} spike of the rebound depolarisation

From the same cell as figure 5.14, the time to peak and the peak potential of the second spike of the rebound depolarisation are displayed with the changes in the depolarising sag from figure 5.13. Red rectangles denote the presence of 100 µM DEA/NO.

In two cells, application of NO caused a different series of changes including a marked membrane depolarisation and accompanying changes in R_{in} (figure 5.18). These changes were extremely slow to reverse. The membrane potential was exceedingly difficult to maintain using current injection and was abandoned in this case.
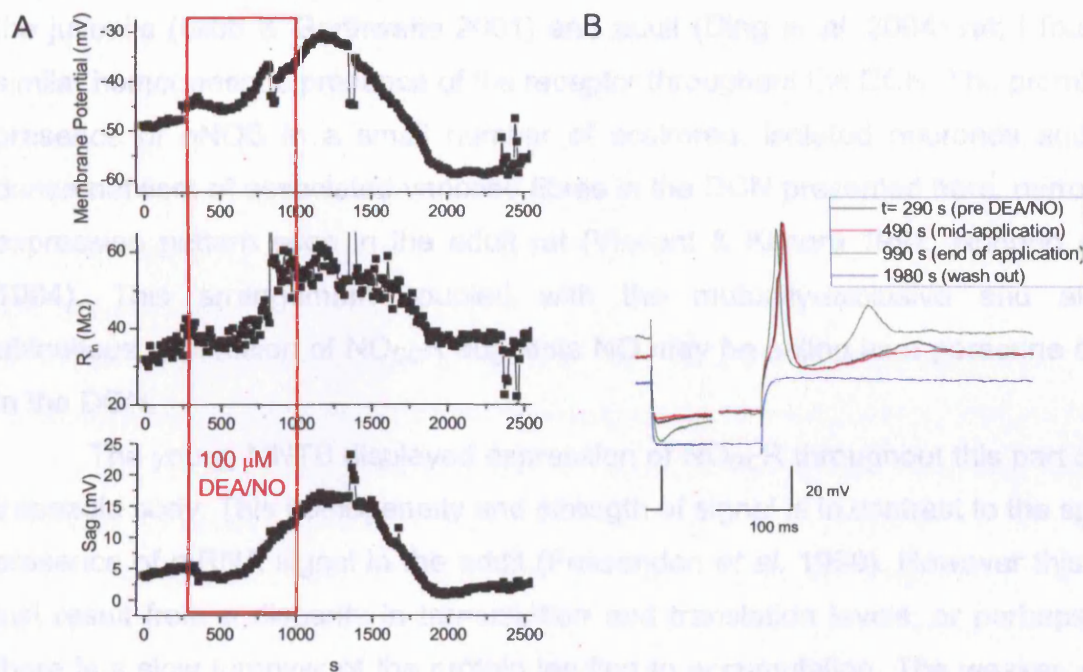
Figure 5.18 The adverse change in the properties of the neurone during exposure and wash out of 100 µM DEA/NO

A, Initially there was a small decrease in the sag followed by a 3-fold increase. This was in concert with a rise in input resistance and excess depolarisation of the membrane potential. B, Example traces before, during and after DEA/NO application.

5.5 DISCUSSION

This chapter focused on the presence of NO-cGMP-HCN channel pathway in the MNTB and DCN. The results of immunological detection of the proteins in the NO-cGMP pathway in the MNTB and DCN suggest that in the juvenile rat, both nNOS and $NO_{GC}R$ are expressed.

The juvenile cerebellar cortex displayed a pattern of $sGC\beta_1$-immunoreactivity similar to that of the adult (Ding et al. 2004). The presence of $NO_{GC}R$ in the DCN has been demonstrated in whole brain parasagittal sections in the juvenile (Gibb & Garthwaite 2001) and adult (Ding et al. 2004) rat; I found a similar homogeneous presence of the receptor throughout the DCN. The prominent presence of nNOS in a small number of scattered, isolated neurones and the dense network of associated varicose fibres in the DCN presented here, mirror the expression pattern seen in the adult rat (Vincent & Kimura 1992; Rodrigo et al. 1994). This arrangement coupled with the mutually-exclusive and almost ubiquitous expression of $NO_{GC}R$ suggests NO may be acting as a paracrine agent in the DCN.

The young MNTB displayed expression of $NO_{GC}R$ throughout this part of the trapezoid body. This homogeneity and strength of signal is in contrast to the sparse presence of mRNA signal in the adult (Fessenden et al. 1999). However this may just result from a disparity in transcription and translation levels, or perhaps that there is a slow turnover of the protein leading to accumulation. The weaker, more diffuse staining of nNOS in the juvenile MNTB mirrors the adult NADPH-diaphorase activity and mRNA transcript levels (Fessenden et al. 1999). The apparent presence of both proteins in the MNTB suggests that it may be acting as an autocrine factor. The stimulation of native $NO_{GC}R$ by DEA/NO resulted in an elevation in the cGMP levels throughout the superior olivary complex, previously seen in the adult (Southam & Garthwaite 1993) suggesting a functional NO-cGMP pathway.

This apparent presence of the proteins of the NO-cGMP pathway in the DCN prompted further electrophysiological investigation, but using the less disruptive recording technique of high resistance microelectrodes. Utilising this

method, there was a reproducible regulation by NO of the slow depolarising sag in membrane potential during a negative current step. These effects occurred with little delay on application of DEA/NO and reversed almost immediately following wash out. This would suggest that the changes are caused by the acute formation of cGMP, although no attempt was made to inhibit $NO_{GC}R$ using ODQ to test this hypothesis (Garthwaite *et al.* 1995). The depolarising sag is an index of the activation of I_h; the opening of HCN channels causes an inward current following a hyperpolarising stimulus. A decrease in sag size is indicative of less I_h being available to be activated by the hyperpolarising step. This suggests there was a larger I_h at the holding potential suggesting a depolarising shift in the voltage dependence of I_h. In tandem with the decrease in sag size, there was also a decrease in the input resistance consistent with elevated HCN channel activity. Therefore, current-clamp measurements made without vastly perturbing the intracellular milieu indicate a functional NO-cGMP-HCN channel pathway in these neurones.

In addition to changes in the magnitude of the voltage sag, there were reversible depressions in the peak potentials of the rebound depolarisation. These peaks are presumably carried by a low-threshold T-type Ca^{2+} channel as TTX-sensitive Na^+ channels are blocked. The decrease in the peaks could be a direct effect of increases in cGMP; there is some evidence in the literature of the acute inhibition of L-type Ca^{2+} channels by cGMP and cGK (Quignard *et al.* 1997; Liu *et al.* 1997); however reports on the effects of cGMP on T-type channels are sparse and appear to involve transcriptional regulation (Zeng *et al.* 2005). Alternatively the apparent effects of NO on I_h and therefore the voltage sag and input resistance may have caused these changes because the rebound depolarisation is known to be driven by interplay between HCN and T-type channel activity (Aizenman & Linden 1999). Further work in voltage-clamp mode would be required to elucidate this relationship. A potential link would be very interesting because LTP at the inhibitory synapse between the Purkinje cell and DCN neurones requires a sufficient rebound depolarisation to elicit Na^+ spikes as well as a rise in Ca^{2+} in the dendrites (Aizenman *et al.* 1998). It has also been shown that *in vivo* injection of a NOS inhibitor into the interpositus nucleus of the DCN delays the formation of

learning-related neuronal activity in the interpositus as well as the conditioned response of rabbit classical eyelid conditioning (Allen & Steinmetz 1996). Therefore an effect on HCN channels and/or T-type channel function may provide a means for NO to play a role in plasticity in the DCN.

In two cells, the profound depolarisation of the membrane potential and increased input resistance suggests that NO could be engaging a different signalling cascade. Another putative target, in addition to $NO_{GC}R$, is cytochrome c oxidase, which is the terminal component in the mitochondrial respiratory train (Cooper 2002). By competing with oxygen at this site, NO inhibits oxidative phosphorylation and hence, decreases ATP levels with various pathological repercussions (Erecinska & Silver 2001; Brown 2001; Moncada & Erusalimsky 2002). For example, decreases in available ATP would decrease the activity of the Na^+-K^+ ATPase, explaining the depolarisation in membrane potential. This action of NO occurs at a concentration about thirty-fold greater than that necessary to engage $NO_{GC}R$ activity (Bellamy *et al.* 2002). The magnitude of the NO signal in the neurone will depend on its spatial location because of diffusion and inactivation of NO by the slice (Hall & Garthwaite 2006). Therefore if the cell is nearer to the surface of the slice, it will experience a much greater concentration of NO and therefore be more prone to metabolic inhibition.

The results presented here suggest a functional NO-cGMP-HCN channel pathway in the DCN and most probably in the MTNB. Further study of the pathway by voltage-clamp will be necessary to confirm this function. This is described in the following chapter.

Chapter 6 - Optimising patch pipette solutions for studying the NO-cGMP-HCN channel pathway

6.1 INTRODUCTION

In regard to the NO-cGMP-HCN channel pathway, the inconsistently negative results recorded in voltage-clamp mode (chapter 4) in tandem with the consistently positive regulation of the voltage sag using sharp electrode current-clamp (chapter 5) suggest a methodological problem intrinsic to the whole-cell technique. This 'whole-cell' discrepancy is usually explained by the invasiveness of the technique as it causes 'wash out' of the intracellular milieu; after formation of a tight high resistance seal, the rupture of the membrane encircled by the patch pipette exposes the cellular contents to the pipette whole-cell solution (WCS); the WCS is far larger in terms of volume and results in rapid equilibration by diffusion (Sakmann & Neher 1984). On the other hand, sharp electrodes have a much smaller diameter usually about 0.1 - 0.01 µm compared to 1 - 2 µm for patch pipettes. Therefore, not only do sharp electrodes cause less physical damage to the cell, but they also decrease the extent of diffusion of contents of the pipette into the cell. Therefore it is quite conceivable that in the whole-cell configuration, dialysis of the normal sub-cellular molecular gradients could occur.

This scenario is particularly true for HCN channels. Since the discovery and characterisation of I_h, the initial rundown of the current caused by a hyperpolarising shift in the steady-state activation curve has been well documented (Ludwig et al. 1998; Wainger et al. 2001; Wang et al. 2001; Zagotta et al. 2003). In these whole-cell and inside-out patch studies, the investigation of channel properties and its modulation were performed after a 10 min period to allow stabilisation of the response to voltage steps. I too found an intial shift in the voltage-dependence of I_h in MNTB and DCN neurones (chapter 4) This particular 'in vitro' phenomenon has recently been ascribed, in part, to the loss of the regulatory factor, PI(4,5)P$_2$, from the phospholipid membrane in the vicinity of the HCN channel (Pian et al. 2006; Zolles et al. 2006). Therefore it is apparent that the specific contents of the whole-cell solution are particularly important in affecting normal cellular function and therefore the results recorded and interpretations formed.

In the case of the NO-cGMP signalling pathway, the production of cGMP from GTP by NO$_{GC}$R is dependent upon and regulated by a number of inter-related factors, namely Ca^{2+}, Mg^{2+} ATP and GTP. At physiological concentrations of Mg^{2+}

(~300 µM; Traut 1994), Ca^{2+} binds to a high affinity site on the enzyme, inhibiting its activity (Kazerounian *et al.* 2002). The extent of inhibition is concentration-dependent being about 10 % at 100 nM and 90 % at 1 µM. These Ca^{2+} concentrations straddle much of the physiologically relevant range (Clapham 1995) meaning that this inhibitory site is perfectly tuned to regulate $NO_{GC}R$ in response to (sub-)cellular calcium fluctuations. ATP also acts as an inhibitor, decreasing $NO_{GC}R$ activity by 50 % at 1 mM in the presence of 100 µM GTP (B. Roy, Personal Communication), both of which are thought to be the physiological concentrations (Horie & Irisawa 1989; Gribble *et al.* 2000); maximal inhibition occurred at 10 mM. The mode of action for ATP is thought to be through binding to an allosteric site, perhaps the pseudosymmetric site (Chang *et al.* 2005).

Clearly, the precise components, particularly the concentrations of these four species, making up the whole-cell solution will therefore affect the ability of the $NO_{GC}R$ to respond to a NO signal and the subsequent signalling to the HCN channels.

6.2 AIM

This chapter investigated the WCS using a standard biochemical assay for $NO_{GC}R$ activity and cGMP production as measured by radioimmunoassay. The WCS was optimised and modified to yield good cyclase activity and then used in electrophysiology to study the modulation of HCN channels by NO.

HYPOTHESIS: The whole-cell solution affects the NO-cGMP-HCN channel signalling pathway.

6.3 METHODS

Enzyme Activity Assay

From other work within the laboratory, a buffer that yields excellent activity from isolated, purified $NO_{GC}R$ was chosen as a benchmark of good activity for optimisation of the whole-cell solution. This normal assay buffer (NAB) had the following composition: 50 mM Tris/HCl, 3 mM $MgCl_2$ (which is in excess of nucleoside triphosphates), 0.1 mM EGTA, 1 mM GTP, and 0.5 mg/ml bovine serum albumin (BSA), prewarmed to 37 °C and at pH 7.4.

50 ng/ml of purified $NO_{GC}R$ in 100 µl NAB were exposed to 20 µM DEA/NO for 2 mins. 50 µl of the reaction mixture was inactivated by immersion in 200 µl of inactivation buffer, preheated to 90 °C. The composition of inactivation buffer was 50 mM Tris, 4 mM EDTA at pH 7.4. The inactivated sample was mixed and frozen at -20 °C until use. The levels of cGMP per sample were measured by radioimmunoassay, using an antibody generated in house by Dr Giti Garthwaite, and expressed relative to the amount of protein. In every case, three independent trials were carried out for each experiment and the resulting data expressed as mean ± sem.

Bound and Determined

During the optimisation of WCS, the free concentrations of Mg^{2+} were calculated using the computer program, Bound and Determined (Brooks & Storey 1992). This tool facilitated the preparation of solutions containing known concentrations of Mg^{2+}-ligand (ATP, GTP and EGTA) complexes.

Electrophysiology

Following the outcome of the biochemical investigation, the optimised WCS was used to investigate the NO-cGMP-HCN channel pathway in DCN and MNTB neurones under whole-cell voltage-clamp as described in chapter four. Briefly, the effects of the NO donors, DEA/NO and PAPA/NO were assessed by constructing steady-state activation curves to tail currents in response to voltage steps.

Gramicidin- and amphotericin-based perforated-patch recordings were also made from visually-identified large DCN neurones. The pipette solution contained (in mM): 150 $KMeSO_4$, 10 KCl, 10 HEPES, 4 NaCl, 0.1 EGTA, 1 $MgCl_2$. The pH was adjusted to 7.39 - 7.4 and the osmolarity to 280-290 mOsm / l. Open pipette resistance was 2-4 MΩ. A gramicidin stock solution was made in DMSO at 1 g / ml. Gramicidin or amphotericin was added to the pipette solution to a final concentration of 120-200 or 90 μg / ml respectively just before use and clarified through a 0.45 or a 0.8 μm filter. Stable access resistances were obtained 20-90 min after forming a gigaohm seal. If there was an abrupt increase in the amplitude of recorded current, signalling that the membrane had ruptured, the experiment was terminated.

Acutely dissociated cells were prepared from cerebellar slices containing the DCN using a technique used to record I_h previously (Simeone *et al.* 2005). PIPES buffer, at pH 7.4 and 290-300 mOsm / l, contained (in mM): 86 PIPES, 30 NaCl, 3 KCl, 2 $MgCl_2$, 10 glucose. A small volume of this solution in a Petri dish was heated to 37 °C in a water bath. Protease XXIII was added at 0.33 mg / ml of PIPES and equilibrated for 5 min. Cerebellar slices were placed into this solution for 10 min to allow sufficient chemical breakdown of the extracellular matrix. This reaction was stopped by transferring the slices into an oxygenated PIPES solution containing 1 mg / ml Protease XXIII inhibitor and 1 mg / ml BSA. Using a dissecting microscope, the DCN was 'cored' out using an adapted hypodermic needle and placed into an eppendorf tube with 0.5 ml of the same solution. The DCN tissue was triturated using three glass pipettes of decreasing diameters, each for ~ 1 min. The dissociated tissue was dropped onto glass coverslips coated in poly-D-lysine and at least 15 min was allowed for the neurones to adhere to coverslip. The oxygenated external solution contained (in mM): 80 NaCl, 2.5 KCl, 1.3 $MgCl_2$, 0.5 $CaCl_2$, 0.1 $CdCl_2$, 11 glucose, 5 HEPES. The WCS contained (in mM): 150 $KMeSO_4$, 10 KCl, 10 HEPES, 4 NaCl, 4 MgATP, adjusted to pH 7.4 and had an osmolarity of ~290 m0sm / l. The largest cells, that were reasonably isolated and agranular, with several processes were selected for electrophysiological investigation. All recordings were performed at room temperature to prolong the lifetime of the cells (B. Lancaster, personal communication). The neurones were

photographed using a Hamamatsu C4742-95 camera and the Kinetic Imaging Lucida 2000 system.

Modelling the NO profile across the slice

Diffusion of NO into the slice from the aCSF approximates to the one-dimensional diffusion from one infinite planar source of NO. This is because the bulk of NO entering the slice will be on the top cut surface, as the under surface of the slice is in contact with the bottom of the bath and the sides are relatively small compared to the entire surface area of the coronally-cut surface. Intuitively, the concentration of NO at a certain point in the slice (x) will be determined by the difference in diffusion into the slice, as described by Fick's law, and inactivation by the slice. If inactivation is assumed to be first order with respect to NO and to be Michaelis-Menten in nature:

$$\frac{\partial [NO]}{\partial t} = D \frac{\partial^2 [NO]}{\partial x^2} - \frac{V_{max}[NO]}{K_m + [NO]}$$

D is the diffusion constant for NO (3.3×10^{-5} cm^2 / s); V_{max} and K_m are approximately 1.5 µM / s and 10 nM respectively as measured recently in rat cerebellar slices (Hall & Garthwaite 2006). Numerically solving this equation to steady state, with NO at the edge of the slice fixed as the bath NO concentration, generates predicted profiles of NO concentration across the slice. All partial differential equations were solved using the pdepe function in MATLAB 6.5 (The Mathworks Inc., MA, USA); this gave a read out of concentration of NO as a function of the distance into the brain slice.

6.4 RESULTS

In the first instance, each of the individual constituents of the previously used WCS solution was added separately to NAB in order to see if one particular component inhibited $NO_{GC}R$. The widespread presence of NaCl and KCl in biology suggested that perhaps the $MeSO_4^-$ anion or the HEPES buffer species may have been interfering with the NO-induced cGMP production. It is known that HEPES buffer, unlike Tris buffer, has been implicated in a process that consumes NO by reaction with the superoxide ion, O_2^{--} (Keynes et al. 2003). However, the individual WCS components had no significant detrimental effect on the cGMP produced from a 2 min exposure to 20 µM DEA/NO (figure 6.1A).

To try to replicate the conditions to which the cellular cyclase enzyme would be exposed during the whole-cell recordings, the purified $NO_{GC}R$ was added directly to the WCS. The original WCS contained 4 mM ATP and being mindful of the concentration-dependent inhibitory actions of ATP previously described, I examined the effect on cGMP production of the original 4 mM concentration, the highly unphysiological, zero ATP situation as well as an apparent physiological concentration of 1 mM (Gribble et al. 2000) that should only inhibit $NO_{GC}R$ by approximately 50 % (Ruiz-Stewart et al. 2004). None of these three conditions yielded results comparable to the NAB (figure 6.1B). In fact, cGMP production was almost reduced to zero.

To optimise the WCS, direct comparisons with NAB were made in order to identify the key deficiencies in the WCS. The NAB, like many other buffers employed in biochemistry, is used as it provides conditions for excellent cyclase activity, rather than reflecting true intracellular conditions. I therefore tested various identified components at concentrations intermediate to the optimal (NAB) values and to the published and reasonably well accepted physiological levels (table 6.1).
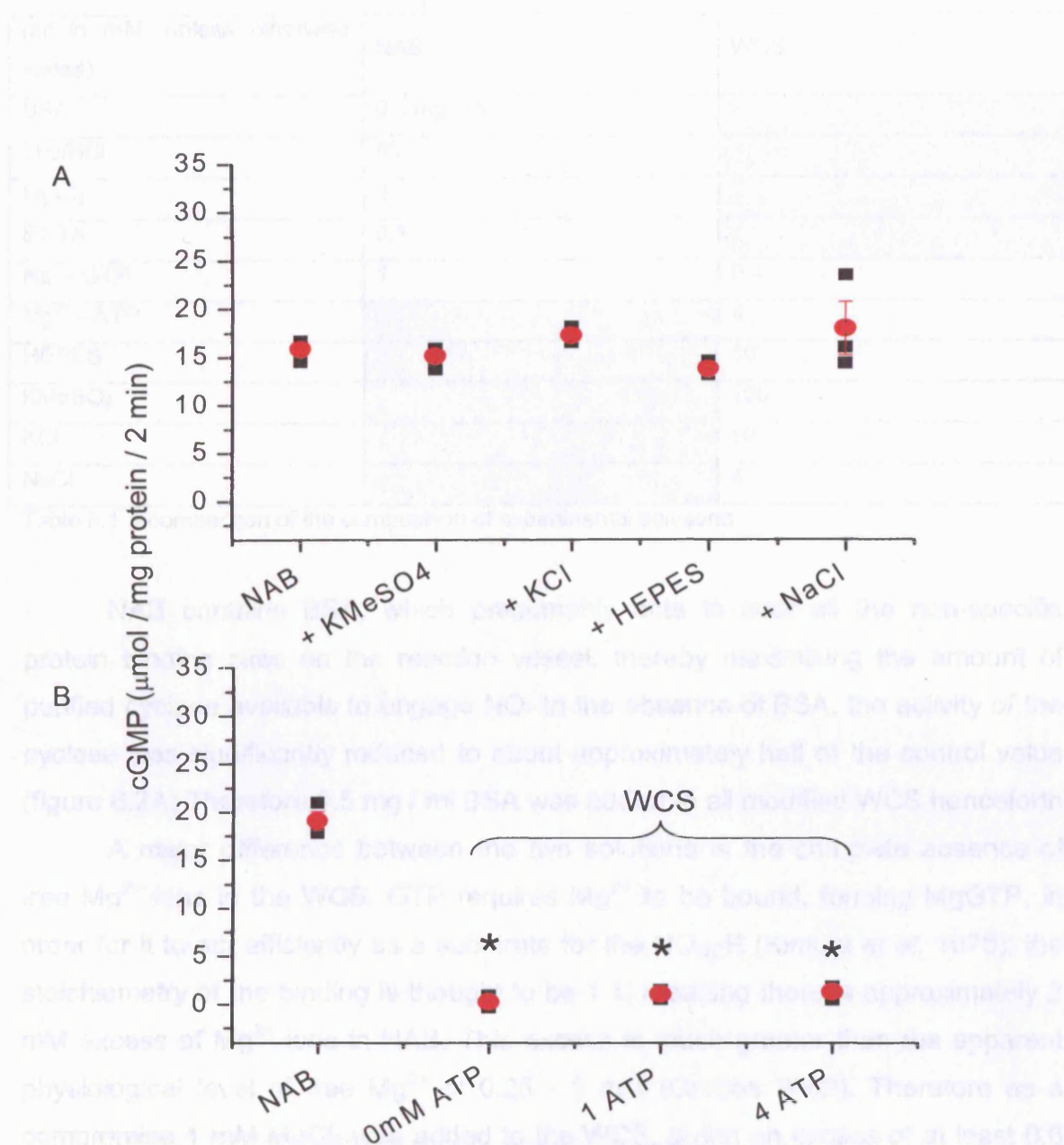
Figure 6.1 The effect of the whole-cell solution on cGMP production by purified NO$_{GC}$R during 2 min exposure to 20 µM DEA/NO at 37 °C

A, The individual constituents of the WCS, namely (in mM) 150 KMeSO$_4$, 10 KCl, 10 HEPES and 4 NaCl, added separately to NAB, had no significant effect on the production of cGMP by the purified enzyme (n=3; mean ± sem in red; student's unpaired *t*-test).

B, NO$_{GC}$R was added either to NAB or the entire WCS with 0, 1 or 4 mM ATP. Generation of cGMP by the cyclase was significantly inhibited to virtually nothing irrespective of ATP concentration (n=3; mean ± sem in red; student's unpaired *t*-test, p<0001 (*)).

(all in mM, unless otherwise stated)	NAB	WCS
BSA	0.5 mg / ml	
Tris/HCl	50	
$MgCl_2$	3	
EGTA	0.1	
Na^+ - GTP	1	0.4
Mg^{2+} - ATP		4
HEPES		10
$KMeSO_4$		150
KCl		10
NaCl		4

Table 6.1 A comparison of the composition of experimental solutions

NAB contains BSA, which presumably acts to coat all the non-specific protein binding sites on the reaction vessel, thereby maximising the amount of purified cyclase available to engage NO. In the absence of BSA, the activity of the cyclase was significantly reduced to about approximately half of the control value (figure 6.2A) Therefore 0.5 mg / ml BSA was added to all modified WCS henceforth.

A major difference between the two solutions is the complete absence of free Mg^{2+} ions in the WCS. GTP requires Mg^{2+} to be bound, forming MgGTP, in order for it to act efficiently as a substrate for the $NO_{GC}R$ (Kimura *et al.* 1976); the stoichiometry of the binding is thought to be 1:1, meaning there is approximately 2 mM excess of Mg^{2+} ions in NAB. This excess is much greater than the apparent physiological level of free Mg^{2+} of 0.25 - 1 mM (Grubbs 2002). Therefore as a compromise 1 mM $MgCl_2$ was added to the WCS, giving an excess of at least 0.6 mM after equilibration with 0.4 mM GTP. This excess is similar to the apparent free Mg^{2+} in cultured dorsal root ganglion neurones (Gotoh *et al.* 1999). The ATP used is added as a Mg-salt, unlike GTP which is a Na-salt, and therefore should not affect the free Mg^{2+} (Bound and Determined). In the presence of 0 or 1 mM ATP, the addition of $MgCl_2$ resulted in little or no production of cGMP (figure 6.2A).
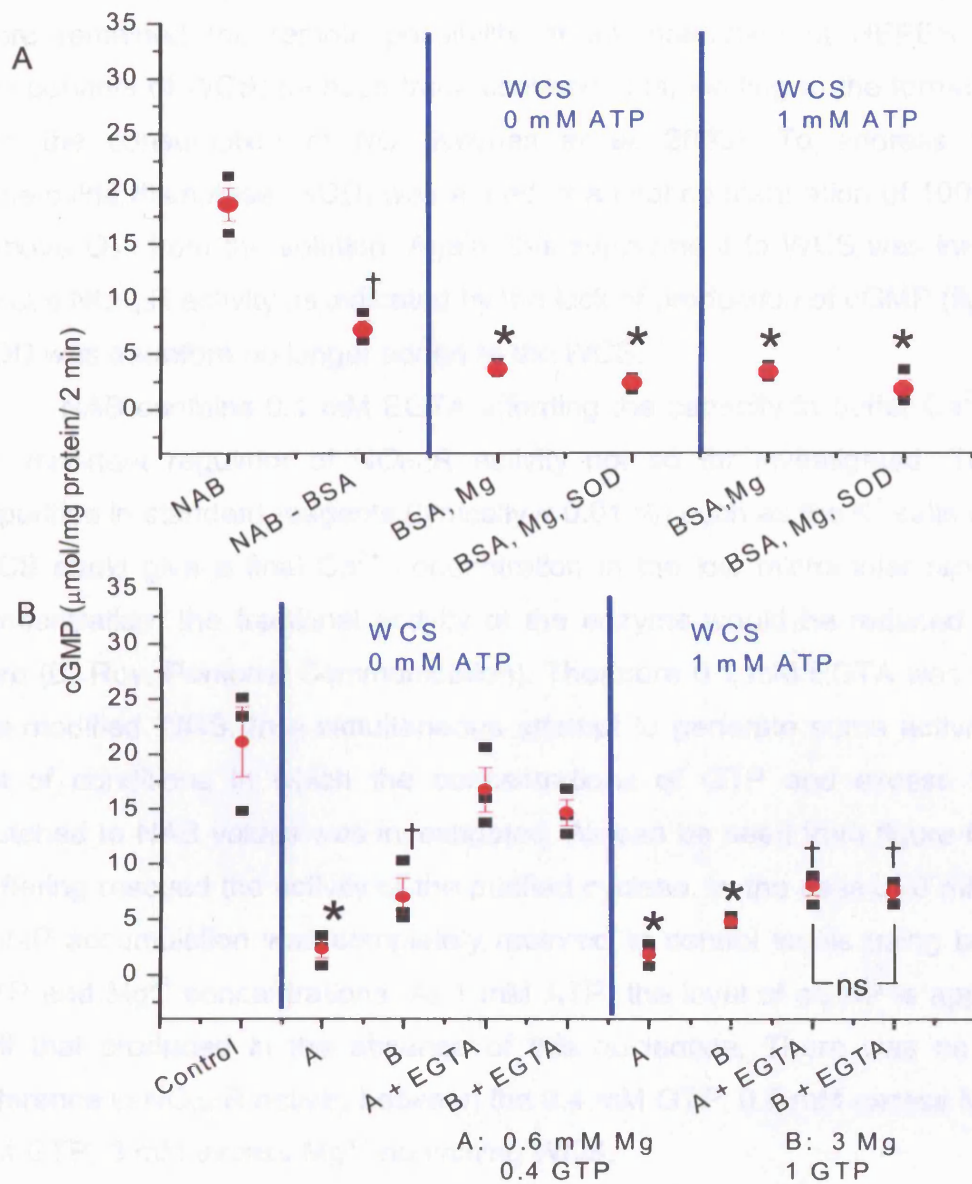
Figure 6.2 Further optimisation of WCS for cGMP production by purified $NO_{GC}R$

A, The importance of BSA (0.5 mg / ml) being present in the NAB was addressed on the left of the panel. It was therefore added to all reaction vessels henceforth. Adding 0.6 mM excess $MgCl_2 \pm 1000$ units / ml SOD to WCS did not significantly rescue the production of cGMP by the purified enzyme compared to control NAB levels. This result was the same at 0 and 1 mM ATP (n=3; mean ± sem in red; student's unpaired t-test, p<0.003 (†), p<0.0001 (*)).

B, The introduction of 0.1 mM EGTA, to buffer Ca^{2+}, restored the ability of $NO_{GC}R$ to produce cGMP in WCS compared to NAB. In addition to the Mg^{2+} and GTP concentrations in (A), similar values to NAB levels were tried, as indicated by the legend (n=3; mean ± sem in red; student's unpaired t-test, p<0.02 (†), p<0.01 (*)). 0.5 mg / ml BSA was added to every tube.

Although HEPES individually had no effect on the cGMP accumulation, there remained the remote possibility of an interaction of HEPES with other components of WCS, perhaps trace contaminants, leading to the formation of $O_2^{\cdot-}$ and the consumption of NO (Keynes *et al.* 2003). To address this issue, superoxide dismutase (SOD) was added at a final concentration of 1000 U / ml to remove $O_2^{\cdot-}$ from the solution. Again, this supplement to WCS was insufficient to rescue $NO_{GC}R$ activity as indicated by the lack of production of cGMP (figure 6.2A). SOD was therefore no longer added to the WCS.

NAB contains 0.1 mM EGTA affording the capacity to buffer Ca^{2+}, which is an important regulator of $NO_{GC}R$ activity not so far investigated. Trace Ca^{2+}-impurities in standard reagents (typically < 0.01 %) such as the K^+ salts used in the WCS could give a final Ca^{2+} concentration in the low micromolar range. At this concentration, the fractional activity of the enzyme would be reduced to virtually zero (B. Roy, Personal Communication). Therefore 0.1 mM EGTA was included in the modified WCS. In a simultaneous attempt to generate some activity, another set of conditions in which the concentrations of GTP and excess Mg^{2+} were matched to NAB values was investigated. As can be seen from figure 6.2B, Ca^{2+}-buffering rescued the activity of the purified cyclase. In the case of 0 mM ATP, the cGMP accumulation was completely restored to control levels using both sets of GTP and Mg^{2+} concentrations. At 1 mM ATP, the level of cGMP is approximately half that produced in the absence of this nucleotide. There was no significant difference in $NO_{GC}R$ activity between the 0.4 mM GTP, 0.6 mM excess Mg^{2+}- and 1 mM GTP, 3 mM excess Mg^{2+}-containing WCS.

It now appeared that the problem of chemical dialysis or inhibition of the NO-cGMP pathway by the original WCS had been solved. Therefore the next logical step was to use the new, modified WCS for whole-cell voltage-clamp electrophysiology in order to study the NO-cGMP-HCN channel pathway. For this, the composition of the WCS was (in mM): 150 $KMeSO_4$, 10 KCl, 10 HEPES, 4 NaCl, 1 $MgCl_2$, 0.1 EGTA, 1 MgATP, 0.4 NaGTP at pH 7.4 and 285 ± 5 mOsm / l. Despite reproducible success in the isolated biochemical assay, the new WCS failed to
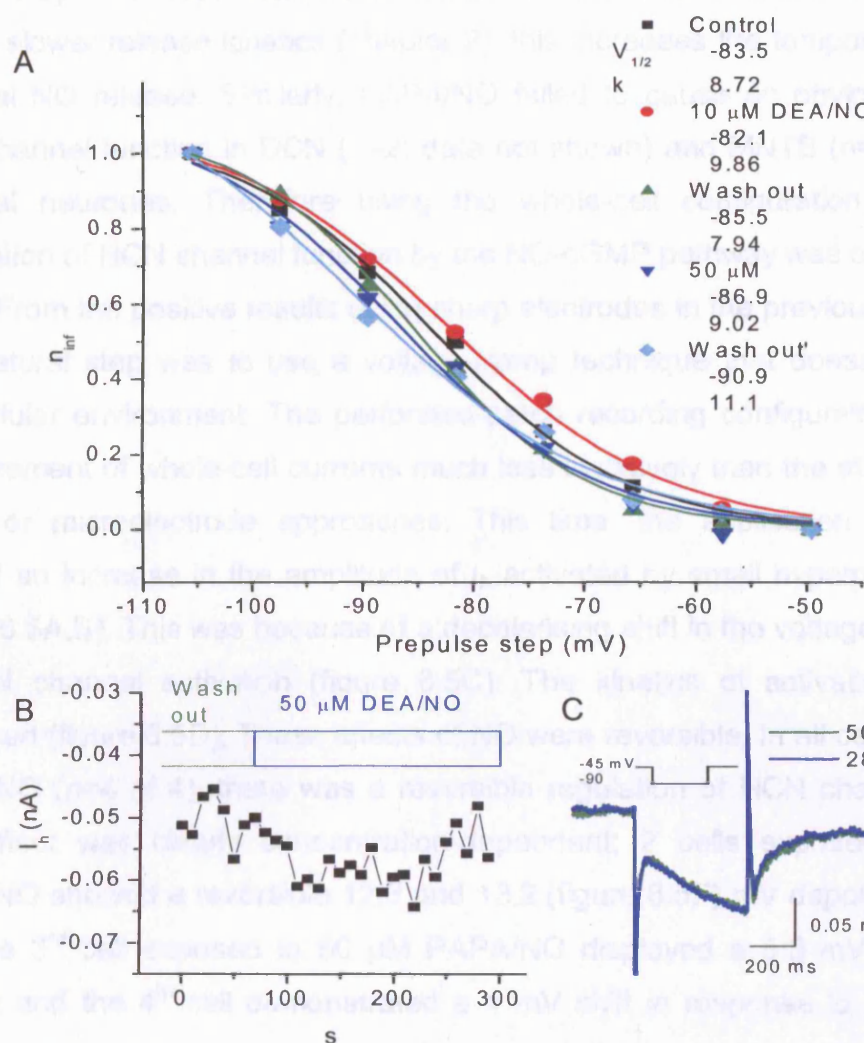
Figure 6.3 Lack of effect of DEA/NO application on I_h in DCN principal neurones using the optimised WCS (n=2)

A, The steady-state activation curves constructed from tail currents following a series of voltage steps. It can be seen that there is no obvious shift in the curve in response to 10 or 50 µM DEA/NO.
B, The timecourse for wash in of 50 µM DEA/NO. Each point represents the I_h activated following a 500 ms-long, small hyperpolarising voltage step (see C) at 10 s intervals. There was little-to-no change in the current amplitude, mirroring the lack of change in a.
C, Sample recordings prior to and during DEA/NO application at 50 and 280 s (see B) respectively.
This neurone was clamped at -45 mV in the presence of 1 mM 4-AP and 500 nM TTX .

produce depolarising shifts in the HCN channel activation curves or changes in I_h amplitude following wash in of the DEA/NO in DCN projection neurones (n=2; figures 6.3). PAPA/NO was used instead of DEA/NO because this donor has slightly slower release kinetics (chapter 2); this increases the temporal window for maximal NO release. Similarly, PAPA/NO failed to cause an obvious change in HCN channel function in DCN (n=2; data not shown) and MNTB (n=2; figure 6.4) principal neurones. Therefore using the whole-cell configuration, no obvious modulation of HCN channel function by the NO-cGMP pathway was observed.

From the positive results using sharp electrodes in the previous chapter, the next natural step was to use a voltage-clamp technique that doesn't disturb the intracellular environment. The perforated-patch recording configuration allows the measurement of whole-cell currents much less invasively than the standard patch-clamp or microelectrode approaches. This time, the application of PAPA/NO caused an increase in the amplitude of I_h activated by small hyperpolarising step (figure 6.5A,B). This was because of a depolarising shift in the voltage-dependence of HCN channel activation (figure 6.5C). The kinetics of activation were also increased (figure 6.5D). These effects of NO were reversible. In all cells exposed to PAPA/NO (n=4 of 4), there was a reversible regulation of HCN channel function. This effect was clearly concentration-dependent; 2 cells exposed to 100 µM PAPA/NO showed a reversible 12.3 and 13.2 (figure 6.5F) mV depolarising shift in $V_{1/2}$; the 3rd cell exposed to 50 µM PAPA/NO displayed a 5.3 mV (figure 6.5E) change and the 4th cell demonstrated a 4 mV shift in response to 10 µM (figure 6.5C).

The most desirable thing would be to elucidate these concentration-dependent effects on $V_{1/2}$ curves, but a major deficit in the current approach was the inability to know the concentration of NO to which the cells are exposed. As described in chapter 1, there are a number of processes, both characterised and uncharacterised, that lead to the inactivation of the NO signal. Recent work using indirect measurements of NO levels in the brain led to the construction of a model for the inactivation of NO by cerebellar slices (Hall & Garthwaite 2006). Adapting this model, it was clear that concentrations drop steeply from the outside to the
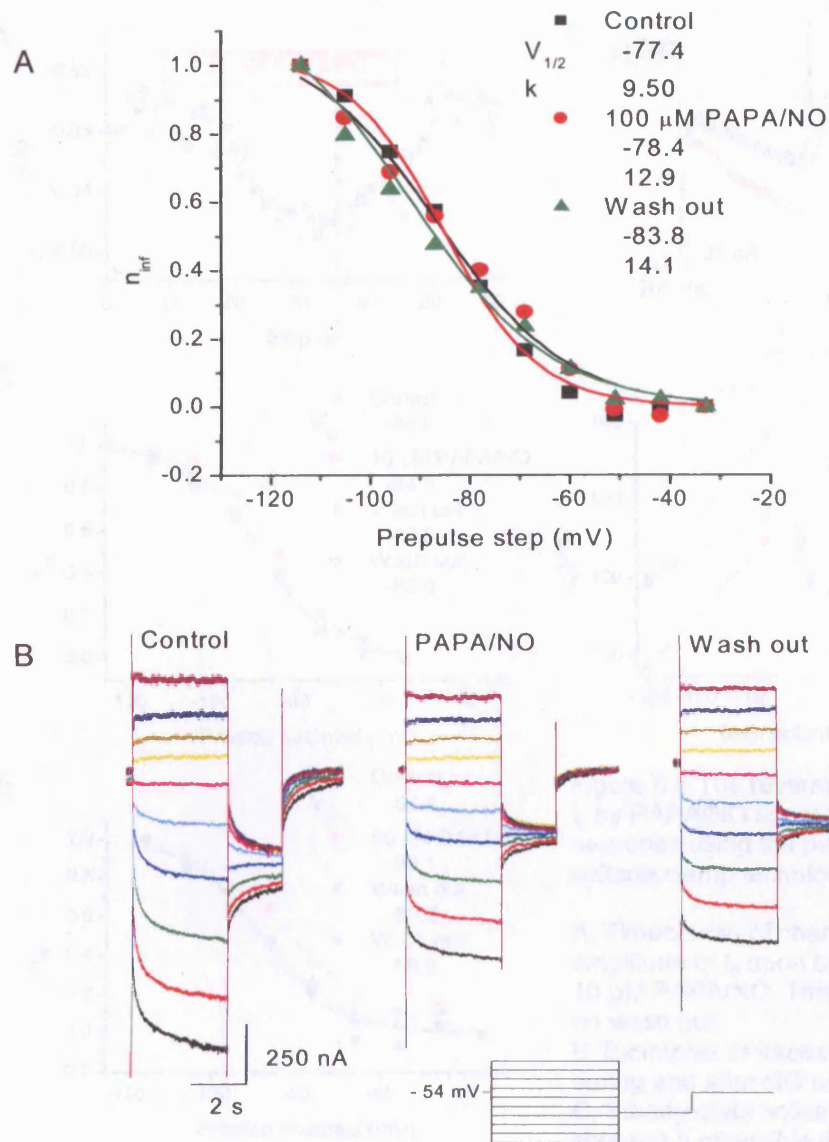
Figure 6.4 The lack of effect of PAPA/NO application on I_h in MNTB neurones at 30 - 32 °C using the optimised WCS (n=2)

A, The steady-state activation curves constructed from tail currents following a series of voltage steps. It can be seen that there is no obvious shift in the curve in response to 100 µM PAPA/NO.

B, The currents generated in response to the voltage steps (see inset) used to generate tail currents to construct the activation curve. There is a clear initial run-down of the current.

1 mM 4-AP and 500 nM TTX were present throughout.
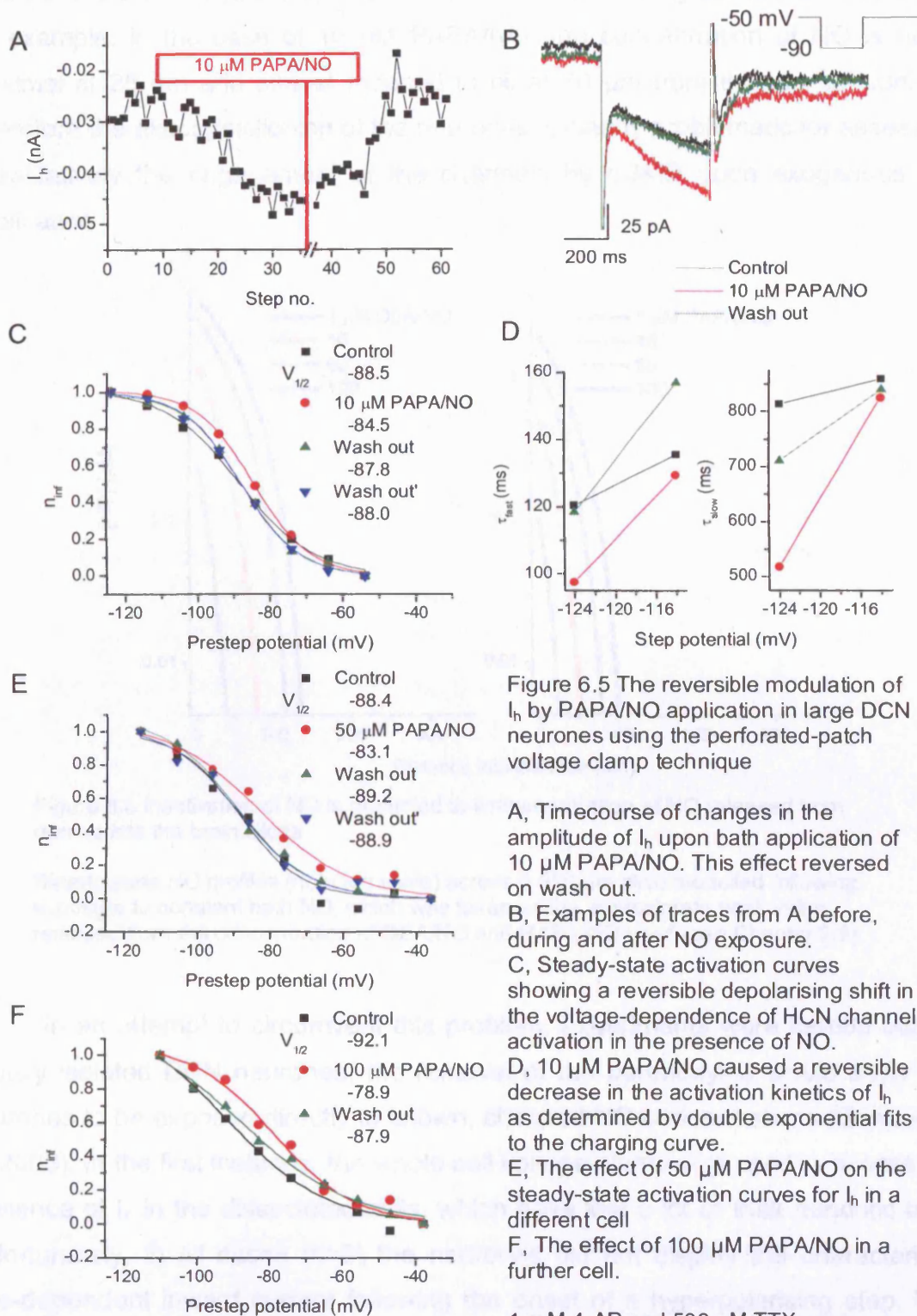
Figure 6.5 The reversible modulation of I_h by PAPA/NO application in large DCN neurones using the perforated-patch voltage clamp technique

A, Timecourse of changes in the amplitude of I_h upon bath application of 10 µM PAPA/NO. This effect reversed on wash out.
B, Examples of traces from A before, during and after NO exposure.
C, Steady-state activation curves showing a reversible depolarising shift in the voltage-dependence of HCN channel activation in the presence of NO.
D, 10 µM PAPA/NO caused a reversible decrease in the activation kinetics of I_h as determined by double exponential fits to the charging curve.
E, The effect of 50 µM PAPA/NO on the steady-state activation curves for I_h in a different cell
F, The effect of 100 µM PAPA/NO in a further cell.

1 mM 4-AP and 500 nM TTX were present throughout.

inside of the slices (figure 6.6) The marked nature of these gradients is noteworthy; for example, in the case of 10 µM PAPA/NO, the concentration of NO is near-maximal at 25 µm and almost reduced to nil at 50 µm from the top cut-surface. Therefore the exact positioning of the neurones is clearly problematic for assessing quantitatively the engagement of the channels by cGMP upon exogenous NO application.
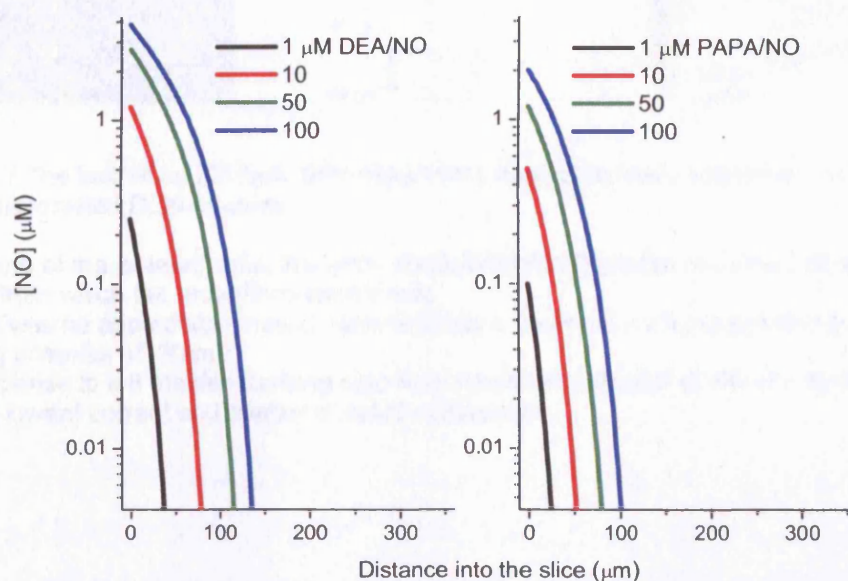
Figure 6.6 Inactivation of NO is predicted to limit penetration of NO released from donors into the brain slices

Steady-state NO profiles (note log scale) across a 350 µm slice modelled following exposure to constant bath NO, which was taken as the approximate peak value released from the concentration of DEA/NO and PAPA/NO used (see Chapter 2.2).

In an attempt to circumvent this problem, experiments were carried out on acutely isolated DCN neurones; the removal of the parenchyma would allow the neurones to be exposed directly to known, clamped NO concentrations (Griffiths *et al.* 2003). In the first instance, the whole-cell voltage-clamp was used to assess the presence of I_h in the dissociated cells, which have lost a lot of their dendritic tree. Unfortunately, in all cases (n=6) the neurones did not display the characteristic time-dependent inward current following the onset of a hyperpolarising step. The cells did however display prominent Na^+ currents (figure 6.7).
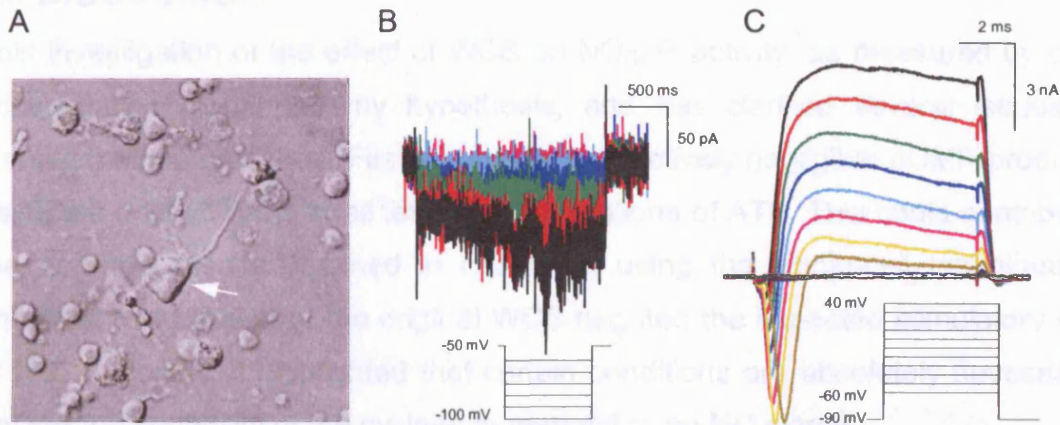
Figure 6.7 The lack of an obvious, time-dependent, hyperpolarisation-activated current in an acutely dissociated DCN neurone

A, A picture of the isolated cells; the white arrow indicates the large neurone with a large process from which the recordings were made.
B, There was no appreciable inward current during a series of 2 s hyperpolarising steps from a holding potential of -50 mV.
C, In response to a 8 ms depolarising step from a holding potential of -90 mV, there was a sizeable inward current and a latter outward component.

6.5 DISCUSSION

This investigation of the effect of WCS on $NO_{GC}R$ activity, as measured by cGMP accumulation, confirmed my hypothesis, and has clarified several issues and identified some problems. Firstly, there was effectively negligible cGMP production using the original WCS at all tested concentrations of ATP. This could contribute to the negative results obtained in chapter 4 using the whole-cell technique; the chemical composition of the original WCS negated the expected stimulatory effect of NO. Secondly, it highlighted that certain conditions are absolutely necessary to ensure the capability of the cyclase to respond to an NO signal.

The body of literature on NO-cGMP signalling reports different experimental techniques and solutions. Extracellular recording techniques are particularly beneficial in that they are completely non-invasive, thereby maintaining the cellular contents, as well as permitting one to follow changes over a long timescale. This has been used successfully, for example, to look at the role of NO in hippocampal LTP (Musleh *et al.* 1993), the part played in the spontaneous activity of the medial vestibular nuclei (Podda *et al.* 2004) and the effect of NO on HCN channels in the optic nerve (Garthwaite *et al.* 2006). Despite the aforementioned benefits, further and more detailed information on individual neurones requires the use of the highly invasive whole-cell technique.

Previous published work studying the NO-cGMP signalling pathway using the whole-cell technique had outcomes that in the light of my results now seem quite difficult to interpret given the chemical dialysis of the intricate conditions required for $NO_{GC}R$ activation and cGMP production. For example, the role of NO in the sensitisation of the TTX-resistant Na^+ current (TTX-R I_{Na}) was recorded in the presence of 3 mM ATP and 0 mM GTP with sufficient EGTA and Mg^{2+}. It is claimed that this process requires a low basal level of NO that is independent of $NO_{GC}R$ activation and cGMP as indicated by use of the specific cyclase blocker, ODQ (Aley *et al.* 1998). This interpretation is difficult to accept in that the fractional activity of the cyclase would have been reduced by ~ 25 % using 3 mM ATP; there was also no GTP substrate available for cyclisation. More recently, a novel NO indicator, formed by concatenating part of the haem domain of the cyclase and GFP, was introduced virally into murine cerebellar Purkinje cells *in vivo* to measure

changes in NO during parallel fibre stimulation. The LTP produced required NO, but was cGMP independent (Namiki *et al.* 2005). Despite the WCS containing the necessary calcium buffering and sufficient GTP, there was no Mg^{2+} to bind to the GTP and 4 mM ATP will greatly inhibit the cyclase meaning that the possible cGMP-dependent role had been occluded.

Despite my best efforts to optimise the WCS in order to create prime conditions within physiological limits for NO-stimulated cGMP production, I was still unable to measure an appreciable effect on HCN channel function. It seems unlikely that this is due to the chemical dialysis of the NO-cGMP pathway. Previous work using WCS containing appropriate ATP, GTP and Mg^{2+} concentrations with Ca^{2+}-buffering have shown positive effects of exogenous NO involving other end targets such as cGK (Arancio *et al.* 1996; Arancio *et al.* 2001). Therefore it seems that the whole-cell technique disrupts the NO-cGMP-HCN channel pathway in some way. This problem has been hinted at in the study of this pathway in the trigeminal motor pool (Abudara *et al.* 2002). However, the I_h of the neurones of the substantia gelatinosa show positive regulation by an NO donor, and mimicked by Br-cGMP, under the whole-cell voltage clamp (Kim *et al.* 2005). The WCS contained (in mM): 2 MgATP, 0.1 Na_2GTP, 1 $MgCl_2$ and 0.5 EGTA. This reinforces and confirms my biochemical results of the conditions required for good $NO_{GC}R$ activation; an intermediate level of ATP to maintain the cell energetically, while not extensively inhibiting the cyclase; a representative physiological level of GTP with an excess of Mg^{2+}; sufficient calcium buffering. Similarly, NO was able to positively shift the activation curve of HCN channels in SAN cells using a WCS of comparable composition (Barbuti *et al.* 2004). In these two examples there is not a disruption of the entire NO-cGMP-HCN pathway unlike that seen here in the DCN.

In some neurones such as those in the MTNB, DCN and perhaps the trigeminal motor pool, the WCS may affect how the NO-cGMP pathway interacts with HCN channels. The ability of HCN channels to respond to cGMP is not affected by the whole-cell technique as indicated by results using WCS loaded with the nucleotide (chapter 4). Therefore perhaps it is a physical disruption, rather than a chemical wash out. This may explain the out-of-place positive effect, in only two cases, of NO application on I_h, if this disruption had not fully occurred. If the

disruption is indeed physical, it suggests perturbations in normal localisation of the proteins involved. HCN4 subunits have been shown to co-localise with caveolin-3 in SAN cells (Barbuti *et al.* 2004). Caveolin is an integral membrane protein found throughout the cerebral cortex and cerebellum (Cameron *et al.* 1997) that gives rise to small invaginations of plasma membrane known as caveolae. These are flask-shaped microdomains particularly rich in, and functionally heavily dependent upon cholesterol (Allen *et al.* 2007). In the cardiovascular system, eNOS is localised in caveolae (Garcia-Cardena *et al.* 1996), which compartmentalise $NO_{GC}R$ and PKG (Linder *et al.* 2005). Indeed, activation of $NO_{GC}R$ has been shown to activate its translocation to the NOS-containing caveolar fraction (Zabel *et al.* 2002). Therefore it is possible that these structures tie the NO-cGMP-HCN pathway together. Perhaps the establishment of the whole-cell mode results in the loss of cholesterol as is the case for another membrane lipid, PIP_2, which also regulates HCN channels (Pian *et al.* 2006). This loss of caveolar function may disrupt the connection of the NO-cGMP and HCN channels or perhaps prevent the translocation of $NO_{GC}R$ to the area of membrane where the HCN channels are present.

The implication of this biochemical investigation is that greater care will have to be taken when studying the NO-cGMP signalling pathway using whole-cell intracellular recordings, particularly for the NO-cGMP-HCN channel pathway. For example, perforated-patch recordings have been used successfully to study NO-cGMP-HCN function in SAN/atrial preparations (Herring *et al.* 2001). It will be necessary to always perform a non-invasive voltage-clamp technique to eliminate the possibility of losing activity or connectivity of certain signalling cascades and pathways.

This use of the perforated-patch technique finally suggests that HCN channels in DCN principal neurones are indeed regulated by exogenous NO, confirming the interpretation of the sharp electrode recordings in chapter five. From the whole-cell results in chapter four, this is presumably through cGMP. The inactivation of NO by the brain tissue, as well as the inability to discern the precise position of the cell within the slice, precludes the collection of useful, quantitative data, such as the EC_{50} for positive shifts in $V_{1/2}$. In an attempt to surmount this

obstacle, recordings were made from acutely dissociated neurones. Unfortunately I was unable to obtain a current recording with an obvious time-dependent, hyperpolarisation-activated component. This is in contrast to HCN single channel recordings in isolated CA1 pyramidal cells (Simeone *et al.* 2005) and the Cs^+-sensitive current in dissociated cerebellar Purkinje cells (Swensen & Bean 2003). One explanation for this disparity may be that in these studies, there were sufficient channels in the remaining soma and remnants of the apical dendritic tree and basal processes. However, I tried to pick large cells with a relatively long dendrite or process, yet the neurones displayed negligible I_h, suggesting HCN channels were mainly located in the processes sloughed off during the isolation and trituration. The cells appeared classically 'axonal' displaying a prominent Na^+ current and as such are quite often used for the study of Na^+ channel function (Kuo & Lu 1997; Gu *et al.* 2005b). Therefore another method would be required to 'isolate' the principal neurones in a manner amenable to using known NO concentrations. One such means is the 'rollerdrum' organotypic slice culture that causes the neurones to spread out into a monolayer, while relatively maintaining the original cellular architecture depending on the age of animal used (Gahwiler 1981).

Summary

7.1 THE ENIGMATIC NATURE OF NO

Being such an unconventional transmitter, developing a conceptual framework for synaptic NO signalling has been problematic, not least because NO is very difficult to measure at physiological concentrations and in discrete synaptic locations. By analogy with the numbers of NMDA receptors, there may only be 10-100 nNOS molecules per synapse. Assuming that native nNOS has a similar activity to that exhibited by the purified enzyme and that, once made, it is dispersed by diffusion, active NO concentrations (in the 0.1-1 nM range) would only be found very locally, within a submicrometer radius (Garthwaite 2005; Hall & Garthwaite 2006). Hence, NO from nNOS may only be able to function in subsynaptic dimensions, implying that it signals between closely juxtaposed elements, such as the pre- and postsynaptic specializations. Recently, a tonic source of NO, via cGMP, persistently engages HCN channels (at least, *in vitro*) in optic nerve (Garthwaite *et al.* 2006). The aim of this study was to attempt to identify the connection between NO signalling and HCN channel function in other brain regions.

7.2 THE NO-cGMP-HCN CHANNEL PATHWAY IN HIPPOCAMPAL AXONS

The background to this line of enquiry identifies tonic (endothelial) and phasic (neuronal) sources of NO; these complementary supplies must synergise in order to generate LTP in the CA1 area (Hopper & Garthwaite 2006). Synaptic plasticity typically depends on activation of afferent axons at different frequencies, and on cyclic nucleotides. Using hippocampal slices, I examined the hypothesis that these properties may be linked at the level of axonal HCN channels. Extracellular field recordings of the fibre volley in the Schaffer collaterals, indicated HCN channels to be important in conduction at 5 Hz, but much less so at 30-100 Hz. Tests using NO as well as cGMP analogues indicated that, at 5 Hz, there was little or no modulation of axon conduction by cGMP. Whole-cell recordings from the somata of CA3 neurones were used to investigate HCN channels more directly. When the axons were stimulated at 5 Hz under control conditions, there was a hyperpolarisation of the membrane, increased latency to peak of the action potential, and an increase in the amplitude of the after-depolarization, but no

change in the amplitude of the hyperpolarisation-activated current at physiological membrane potentials. After block of HCN channels, there was an increase in the amplitude of the spike after-depolarization during baseline (0.2 Hz) stimulation. At 5 Hz, the after-depolarization amplitude increased further and there was an increase in latency for action potential firing and in the holding current. Confirming the extracellular recordings, exogenous NO had no effect on the hyperpolarisation-activated current. In conclusion, although HCN channels are important in maintaining the fidelity of axon conduction during relatively low frequencies, they are unlikely to be cyclic nucleotide-sensitive isoforms, suggesting that the actions of cAMP or cGMP in synaptic plasticity are exerted elsewhere.

It is disappointing that the function of vascular endothelial-derived, tonic NO, seen in the optic nerve (Garthwaite *et al.* 2006), was not present in the Schaffer collateral/commissural axons. Perhaps the investigation of the distribution of HCN channel subunits, with sufficiently high resolution immunolabelling, in other nerve fibres to identify HCN2- or HCN4-containing channels could be used to further study this particularly revolutionary mechanism of blood vessels signalling to CNS axons through NO.

7.3 THE NO-cGMP-HCN CHANNEL PATHWAY IN THE DEEP CEREBELLAR NUCLEI

Subsequent to the work within the hippocampus, the aim was to identify CNS neurones in which the hypothesis that endogenous NO regulates HCN channels can be directly tested. Dense immunostaining for $NO_{GC}R$ was found in the principal neurones of the DCN and throughout the neuropil. Whole-cell and perforated-patch voltage-clamp recordings showed that perfusion of Br-cGMP or NO produced a positive shift in the activation curve by ~10 mV in both cases, consistent with potential regulation by the endogenous NO-cGMP pathway. Current-clamped measurements indicated a reproducible and reversible effect of NO on the membrane sag, an index of HCN channel activation; there was also an apparent effect on the rebound depolarisation, which would be particularly pertinent during the cessation of GABAergic input from Purkinje cells in the cortex.

This identification of a set of CNS neurones regulated by bath-applied NO provides a system in which HCN channel function could act as a readout for NO signalling. The identified susceptibility of the signalling pathway to dialysis by the whole-cell solution using patch pipettes necessitates the use of the perforated patch technique, which would likely provide a better (more stable) estimate of the efficacy of NO for causing a depolarising shift in the voltage dependence of I_h. Transduction through $NO_{GC}R$ could be confirmed using ODQ (Garthwaite et al. 1995). The use of the roller-drum organotypic method (Gahwiler 1981) will minimise the problem of NO consumption generating steep gradients across the depth of the slice.

By analogy with optic nerve recordings, tonic NO from the capillary network may modulate the channels, which could be examined in the organotypic slice cultures, although it would probably be simpler in acutely-prepared slices. Bath application of L-NNA to block NOS could identify if there is a tonic NO source acting on the neurones. Immunocytochemical studies identified a network of nNOS-positive neurones and ramifying fibres in the DCN, as in the adult, representing a further potential physiological source of NO. To study this in the first instance, one could electrically activate these cells using a stimulation electrode as used before in the cerebellum (Anchisi et al. 2001) after pharmacologically blocking glutamatergic and GABAergic transmission. Ultimately, in vivo recordings from the DCN would be required to determine the influence of the nNOS-derived NO on the large, projection DCN neurones in the intact architecture containing the physiologically-relevant cellular connections and networks.

The lack of information on endogenous NO signals is the major deficit in the current understanding of NO signalling within the nervous system and beyond. The prior determination of the concentration-effect relationship for NO and the $V_{1/2}$ of HCN channels in the DCN neurones will provide a means to quantify the NO produced from both constitutively-expressed forms of NOS. In turn, this will give a great insight into the endogenous NO signals in terms of their amplitude, duration, distance or frequency.

7.4 PHYSIOLOGICAL SIGNIFICANCE OF THE DATA

The molecular targets and site of action of the eNOS-derived tonic source of NO in Schaffer Collateral-CA1 LTP are unknown. The work in my thesis goes some way to suggest that the presynaptic axon is not a target for regulation by this constitutive level of NO, nor by a phasic source such as that from nNOS activation. NO may therefore be acting only at the activated synapse. Recently it was described that hippocampal GABAergic interneurones express $NO_{GC}R$ (Szabadits et al. 2007). The greater electrophysiological implications have not as yet been elucidated, but the presence of NO-cGMP signalling in these interneurones is likely to have important implications for NO and synaptic plasticity (Makara et al. 2007). Furthermore, interneurones are known to transcribe mRNA encoding HCN channel subunits (Bender et al. 2001), and therefore the NO-cGMP-HCN channel pathway may be of significance in these cells.

My preliminary data indicated that HCN channel function in MNTB principal cells was modulated by cGMP. If one assumes that the apparent lack of modulation by NO was due to whole-cell dialysis, then there could be an important role played by this signalling molecule in the juvenile brainstem: At this age, the glutamate-stimulated excitatory current in the MNTB neurones is mainly carried by NMDA receptors (Joshi & Wang 2002), and the NMDA receptor-NO-cGMP signalling cascade has been well characterised elsewhere (Christopherson et al. 1999). The cGMP-mediated positive shift in the activation curve of I_h usually results in an increased rate of activation and current amplitude, both of which are known to decrease the delay to the initiation of an action potential in MNTB neurones (Leao et al. 2006a); this could have important implications in the processing of auditory information at the downstream lateral superior olivary nucleus.

In the principal neurones of the DCN, the polarity of synaptic plasticity is affected by the degree of rebound depolarisation-driven postsynaptic spiking (Aizenman et al. 1998). The induction of the rebound depolarisation is dependent on the size and duration of hyperpolarising prepulse (Aizenman and Linden 1999), two factors that have clear implications for the activation of HCN channels, which are known to

contribute to the depolarising envelope. My results suggest that NO signalling within the DCN modulates HCN channel function shifting the steady-state activation curve to more positive voltages; this would be expected to increase the total I_h, and therefore increase the rebound depolarisation and spiking. The NO-cGMP-HCN channel pathway may play an important role in modulating the polarity of synaptic plasticity. It has also been shown that in vivo injection of a NOS inhibitor into the interpositus nucleus of the DCN delays the formation of learning-related neuronal activity in the interpositus as well as the conditioned response of rabbit classical eyelid conditioning (Allen & Steinmetz 1996). Therefore the NO-cGMP-HCN channel pathway may have an important function in the DCN, particular the interposed and dentate nuclei, which are known to be concern motor learning, certain reflexes and voluntary movement.

Reference List

Abudara V, Alvarez AF, Chase MH & Morales FR (2002). Nitric oxide as an anterograde neurotransmitter in the trigeminal motor pool. *J Neurophysiol* **88**, 497-506.

Accili EA, Proenza C, Baruscotti M & DiFrancesco D (2002). From funny current to HCN channels: 20 years of excitation. *News Physiol Sci* **17**, 32-37.

Ahern GP, Hsu SF, Klyachko VA & Jackson MB (2000). Induction of Persistent Sodium Current by Exogenous and Endogenous Nitric Oxide. *J Biol Chem* **275**, 28810-28815.

Ahmad I, Leinders-Zufall T, Kocsis JD, Shepherd GM, Zufall F & Barnstable CJ (1994). Retinal ganglion cells express a cGMP-gated cation conductance activatable by nitric oxide donors. *Neuron* **12**, 155-165.

Aizenman CD, Manis PB & Linden DJ (1998). Polarity of long-term synaptic gain change is related to postsynaptic spike firing at a cerebellar inhibitory synapse. *Neuron* **21**, 827-835.

Aizenman CD & Linden DJ (1999). Regulation of the Rebound Depolarization and Spontaneous Firing Patterns of Deep Nuclear Neurons in Slices of Rat Cerebellum. *J Neurophysiol* **82**, 1697-1709.

Aizenman CD, Huang EJ & Linden DJ (2003). Morphological correlates of intrinsic electrical excitability in neurons of the deep cerebellar nuclei. *J Neurophysiol* **89**, 1738-1747.

Alderton WK, Cooper CE & Knowles RG (2001). Nitric oxide synthases: structure, function and inhibition. *Biochem J* **357**, 593-615.

Aley KO, McCarter G & Levine JD (1998). Nitric oxide signaling in pain and nociceptor sensitization in the rat. *J Neurosci* **18**, 7008-7014.

Allen JA, Halverson-Tamboli RA & Rasenick MM (2007). Lipid raft microdomains and neurotransmitter signalling. *Nat Rev Neurosci* **8**, 128-140.

Allen MT & Steinmetz JE (1996). A nitric oxide synthase inhibitor delays the formation of learning-related neural activity in the cerebellar interpositus nucleus during rabbit eyelid conditioning. *Pharmacol Biochem Behav* **53**, 147-153.

Altenhofen W, Ludwig J, Eismann E, Kraus W, Bonigk W & Kaupp UB (1991). Control of ligand specificity in cyclic nucleotide-gated channels from rod photoreceptors and olfactory epithelium. *Proc Natl Acad Sci U S A* **88**, 9868-9872.

Altomare C, Bucchi A, Camatini E, Baruscotti M, Viscomi C, Moroni A & DiFrancesco D (2001). Integrated allosteric model of voltage gating of HCN channels. *J Gen Physiol* **117**, 519-532.

Altomare C, Terragni B, Brioschi C, Milanesi R, Pagliuca C, Viscomi C, Moroni A, Baruscotti M & DiFrancesco D (2003). Heteromeric HCN1-HCN4 channels: a comparison with native pacemaker channels from the rabbit sinoatrial node. *J Physiol* **549**, 347-359.

Amaral DG & Witter MP (1989). The three-dimensional organization of the hippocampal formation: a review of anatomical data. *Neuroscience* **31**, 571-591.

Anchisi D, Scelfo B & Tempia F (2001). Postsynaptic currents in deep cerebellar nuclei. *J Neurophysiol* **85**, 323-331.

Aponte Y, Lien CC, Reisinger E & Jonas P (2006). Hyperpolarization-activated cation channels in fast-spiking interneurons of rat hippocampus. *J Physiol* **574**, 229-243.

Arancio O, Kiebler M, Lee CJ, Lev-Ram V, Tsien RY, Kandel ER & Hawkins RD (1996). Nitric oxide acts directly in the presynaptic neuron to produce long-term potentiation in cultured hippocampal neurons. *Cell* **87**, 1025-1035.

Arancio O, Antonova I, Gambaryan S, Lohmann SM, Wood JS, Lawrence DS & Hawkins RD (2001). Presynaptic role of cGMP-dependent protein kinase during long-lasting potentiation. *J Neurosci* **21**, 143-149.

Ariano MA, Lewicki JA, Brandwein HJ & Murad F (1982). Immunohistochemical localization of guanylate cyclase within neurons of rat brain. *Proc Natl Acad Sci U S A* **79**, 1316-1320.

Arnold WP, Mittal CK, Katsuki S & Murad F (1977). Nitric oxide activates guanylate cyclase and increases guanosine 3':5'-cyclic monophosphate levels in various tissue preparations. *Proc Natl Acad Sci U S A* **74**, 3203-3207.

Azouz R, Jensen MS & Yaari Y (1996). Ionic basis of spike after-depolarization and burst generation in adult rat hippocampal CA1 pyramidal cells. *J Physiol* **492 (Pt 1)**, 211-223.

Babu BR & Griffith OW (1998). N5-(1-Imino-3-butenyl)-L-ornithine. A neuronal isoform selective mechanism-based inactivator of nitric oxide synthase. *J Biol Chem* **273**, 8882-8889.

Bains JS & Ferguson AV (1997). Nitric oxide depolarizes type II paraventricular nucleus neurons in vitro. *Neuroscience* **79**, 149-159.

Bal T & McCormick DA (1997). Synchronized oscillations in the inferior olive are controlled by the hyperpolarization-activated cation current I(h). *J Neurophysiol* **77**, 3145-3156.

Banks MI & Smith PH (1992). Intracellular recordings from neurobiotin-labeled cells in brain slices of the rat medial nucleus of the trapezoid body. *J Neurosci* **12**, 2819-2837.

Banks MI, Pearce RA & Smith PH (1993). Hyperpolarization-activated cation current (Ih) in neurons of the medial nucleus of the trapezoid body: voltage-clamp analysis and enhancement by norepinephrine and cAMP suggest a modulatory mechanism in the auditory brain stem. *J Neurophysiol* **70**, 1420-1432.

Barbuti A, Gravante B, Riolfo M, Milanesi R, Terragni B & DiFrancesco D (2004). Localization of pacemaker channels in lipid rafts regulates channel kinetics. *Circ Res* **94**, 1325-1331.

Batini C, Compoint C, Buisseret-Delmas C, Daniel H & Guegan M (1992). Cerebellar nuclei and the nucleocortical projections in the rat: retrograde tracing coupled to GABA and glutamate immunohistochemistry. *J Comp Neurol* **315**, 74-84.

Beaumont V & Zucker RS (2000). Enhancement of synaptic transmission by cyclic AMP modulation of presynaptic Ih channels. *Nat Neurosci* **3**, 133-141.

Beavo JA (1995). Cyclic nucleotide phosphodiesterases: functional implications of multiple isoforms. *Physiol Rev* **75**, 725-748.

Beitz AJ & Chan-Palay V (1979). The medial cerebellar nucleus in the rat: nuclear volume, cell number, density and orientation. *Neuroscience* **4**, 31-45.

Bell DC, Yao H, Saenger RC, Riley JH & Siegelbaum SA (2004). Changes in local S4 environment provide a voltage-sensing mechanism for mammalian hyperpolarization-activated HCN channels. *J Gen Physiol* **123**, 5-19.

Bellamy TC, Wood J, Goodwin DA & Garthwaite J (2000). Rapid desensitization of the nitric oxide receptor, soluble guanylyl cyclase, underlies diversity of cellular cGMP responses. *Proc Natl Acad Sci U S A* **97**, 2928-2933.

Bellamy TC & Garthwaite J (2001a). "cAMP-specific" phosphodiesterase contributes to cGMP degradation in cerebellar cells exposed to nitric oxide. *Mol Pharmacol* **59**, 54-61.

Bellamy TC & Garthwaite J (2001b). Sub-second kinetics of the nitric oxide receptor, soluble guanylyl cyclase, in intact cerebellar cells. *J Biol Chem* **276**, 4287-4292.

Bellamy TC & Garthwaite J (2002a). The receptor-like properties of nitric oxide-activated soluble guanylyl cyclase in intact cells. *Mol Cell Biochem* **230**, 165-176.

Bellamy TC & Garthwaite J (2002b). Pharmacology of the nitric oxide receptor, soluble guanylyl cyclase, in cerebellar cells. *Br J Pharmacol* **136**, 95-103.

Bellamy TC, Griffiths C & Garthwaite J (2002). Differential sensitivity of guanylyl cyclase and mitochondrial respiration to nitric oxide measured using clamped concentrations. *J Biol Chem* **277**, 31801-31807.

Bender AT & Beavo JA (2004). Specific localized expression of cGMP PDEs in Purkinje neurons and macrophages. *Neurochemistry International* **45**, 853-857.

Bernstein HG, Krell D, Braunewell KH, Baumann B, Gundelfinger ED, Diekmann S, Danos P & Bogerts B (2001). Increased number of nitric oxide synthase immunoreactive Purkinje cells and dentate nucleus neurons in schizophrenia. *J Neurocytol* **30**, 661-670.

Biel M, Sautter A, Ludwig A, Hofmann F & Zong X (1998). Cyclic nucleotide-gated channels--mediators of NO:cGMP-regulated processes. *Naunyn Schmiedebergs Arch Pharmacol* **358**, 140-144.

Blatchley BJ, Cooper WA & Coleman JR (1987). Development of auditory brainstem response to tone pip stimuli in the rat. *Brain Res* **429**, 75-84.

Bliss TV & Collingridge GL (1993). A synaptic model of memory: long-term potentiation in the hippocampus. *Nature* **361**, 31-39.

Boer R, Ulrich WR, Klein T, Mirau B, Haas S & Baur I (2000). The inhibitory potency and selectivity of arginine substrate site nitric-oxide synthase inhibitors is solely determined by their affinity toward the different isoenzymes. *Mol Pharmacol* **58**, 1026-1034.

Bollmann JH, Helmchen F, Borst JG & Sakmann B (1998). Postsynaptic Ca2+ Influx Mediated by Three Different Pathways during Synaptic Transmission at a Calyx-Type Synapse. *J Neurosci* **18**, 10409-10419.

Bon CL & Garthwaite J (2001). Exogenous nitric oxide causes potentiation of hippocampal synaptic transmission during low-frequency stimulation via the endogenous nitric oxide-cGMP pathway. *Eur J Neurosci* **14**, 585-594.

Bon CL & Garthwaite J (2003). On the role of nitric oxide in hippocampal long-term potentiation. *J Neurosci* **23**, 1941-1948.

Bonigk W, Altenhofen W, Muller F, Dose A, Illing M, Molday RS & Kaupp UB (1993). Rod and cone photoreceptor cells express distinct genes for cGMP-gated channels. *Neuron* **10**, 865-877.

Boudreau JC & Tsuchitani C (1968). Binaural interaction in the cat superior olive S segment. *J Neurophysiol* **31**, 442-454.

Boulton CL, Southam E & Garthwaite J (1995). Nitric oxide-dependent long-term potentiation is blocked by a specific inhibitor of soluble guanylyl cyclase. *Neuroscience* **69**, 699-703.

Bredt DS & Snyder SH (1990). Isolation of nitric oxide synthetase, a calmodulin-requiring enzyme. *Proc Natl Acad Sci U S A* **87**, 682-685.

Bredt DS, Hwang PM & Snyder SH (1990). Localization of nitric oxide synthase indicating a neural role for nitric oxide. *Nature* **347**, 768-770.

Brenman JE & Bredt DS (1997). Synaptic signaling by nitric oxide. *Curr Opin Neurobiol* **7**, 374-378.

Brenman JE, Chao DS, Gee SH, McGee AW, Craven SE, Santillano DR, Wu Z, Huang F, Xia H, Peters MF, Froehner SC & Bredt DS (1996). Interaction of Nitric Oxide Synthase with the Postsynaptic Density Protein PSD-95 and [alpha]1-Syntrophin Mediated by PDZ Domains. *Cell* **84**, 757-767.

Brooks SP & Storey KB (1992). Bound and determined: a computer program for making buffers of defined ion concentrations. *Anal Biochem* **201**, 119-126.

Brown GC (2001). Regulation of mitochondrial respiration by nitric oxide inhibition of cytochrome c oxidase. *Biochim Biophys Acta* **1504**, 46-57.

Burette A, Zabel U, Weinberg RJ, Schmidt HH & Valtschanoff JG (2002). Synaptic localization of nitric oxide synthase and soluble guanylyl cyclase in the hippocampus. *J Neurosci* **22**, 8961-8970.

Cameron PL, Ruffin JW, Bollag R, Rasmussen H & Cameron RS (1997). Identification of caveolin and caveolin-related proteins in the brain. *J Neurosci* **17**, 9520-9535.

Casado M, Isope P & Ascher P (2002). Involvement of presynaptic N-methyl-D-aspartate receptors in cerebellar long-term depression. *Neuron* **33**, 123-130.

Castro-Alamancos MA, Rigas P & Tawara-Hirata Y (2007). Resonance (~10 Hz) of excitatory networks in motor cortex: effects of voltage-dependent ion channel blockers. *J Physiol (Lond)* **578**, 173-191.

Castro LR, Verde I, Cooper DM & Fischmeister R (2006). Cyclic guanosine monophosphate compartmentation in rat cardiac myocytes. *Circulation* **113**, 2221-2228.

Chang FJ, Lemme S, Sun Q, Sunahara RK, Beuve A (2005). Nitric oxide-dependent allosteric inhibitory role of a second nucleotide binding site in soluble guanylyl cyclase. *J Biol Chem* **280** (12), 11513-9.

Chen C & Regehr WG (1997). The Mechanism of cAMP-Mediated Enhancement at a Cerebellar Synapse. *J Neurosci* **17**, 8687-8694.

Chen S, Wang J & Siegelbaum SA (2001). Properties of hyperpolarization-activated pacemaker current defined by coassembly of HCN1 and HCN2 subunits and basal modulation by cyclic nucleotide. *J Gen Physiol* **117**, 491-504.

Chen X, Sirois JE, Lei Q, Talley EM, Lynch C, III & Bayliss DA (2005). HCN subunit-specific and cAMP-modulated effects of anesthetics on neuronal pacemaker currents. *J Neurosci* **25**, 5803-5814.

Chevaleyre V & Castillo PE (2002). Assessing the role of Ih channels in synaptic transmission and mossy fiber LTP. *Proc Natl Acad Sci U S A* **99**, 9538-9543.

Christopherson KS, Hillier BJ, Lim WA & Bredt DS (1999). PSD-95 Assembles a Ternary Complex with the N-Methyl-D-aspartic Acid Receptor and a Bivalent Neuronal NO Synthase PDZ Domain. *J Biol Chem* **274**, 27467-27473.

Clapham DE (1995). Calcium signaling. *Cell* **80**, 259-268.

Clapham DE (1998). Not So Funny Anymore: Pacing Channels Are Cloned. *Neuron* **21**, 5-7.

Cobb SR, Larkman PM, Bulters DO, Oliver L, Gill CH & Davies CH (2003). Activation of Ih is necessary for patterning of mGluR and mAChR induced network activity in the hippocampal CA3 region. *Neuropharmacology* **44**, 293-303.

Cocks TM & Angus JA (1983). Endothelium-dependent relaxation of coronary arteries by noradrenaline and serotonin. *Nature* **305**, 627-630.

Cooper CE (2002). Nitric oxide and cytochrome oxidase: substrate, inhibitor or effector? *Trends Biochem Sci* **27**, 33-39.

Corbin JD, Turko IV, Beasley A & Francis SH (2000). Phosphorylation of phosphodiesterase-5 by cyclic nucleotide-dependent protein kinase alters its catalytic and allosteric cGMP-binding activities. *Eur J Biochem* **267**, 2760-2767.

Craven KB & Zagotta WN (2004). Salt Bridges and Gating in the COOH-terminal Region of HCN2 and CNGA1 Channels. *J Gen Physiol* **124**, 663-677.

Craven KB & Zagotta WN (2005). CNG and HCN Channels: Two Peas, One Pod. *Annu Rev Physiol*.

Cudeiro J, Rivadulla C, Rodriguez R, Grieve KL, Martinez-Conde S & Acuna C (1997). Actions of compounds manipulating the nitric oxide system in the cat primary visual cortex. *J Physiol* **504 (Pt 2)**, 467-478.

Czubayko U, Sultan F, Thier P & Schwarz C (2001). Two types of neurons in the rat cerebellar nuclei as distinguished by membrane potentials and intracellular fillings. *J Neurophysiol* **85**, 2017-2029.

Daly JW, Padgett W & Seamon KB (1982). Activation of cyclic AMP-generating systems in brain membranes and slices by the diterpene forskolin: augmentation of receptor-mediated responses. *J Neurochem* **38**, 532-544.

Day M, Carr DB, Ulrich S, Ilijic E, Tkatch T & Surmeier DJ (2005). Dendritic excitability of mouse frontal cortex pyramidal neurons is shaped by the interaction among HCN, Kir2, and Kleak channels. *J Neurosci* **25**, 8776-8787.

Decher N, Bundis F, Vajna R & Steinmeyer K (2003). KCNE2 modulates current amplitudes and activation kinetics of HCN4: influence of KCNE family members on HCN4 currents. *Pflugers Arch* **446**, 633-640.

Degerman E, Belfrage P & Manganiello VC (1997). Structure, localization, and regulation of cGMP-inhibited phosphodiesterase (PDE3). *J Biol Chem* **272**, 6823-6826.

Detre JA, Nairn AC, Aswad DW & Greengard P (1984). Localization in mammalian brain of G-substrate, a specific substrate for guanosine 3',5'-cyclic monophosphate-dependent protein kinase. *J Neurosci* **4**, 2843-2849.

Dhallan RS, Yau KW, Schrader KA & Reed RR (1990). Primary structure and functional expression of a cyclic nucleotide-activated channel from olfactory neurons. *Nature* **347**, 184-187.

DiFrancesco D & Tortora P (1991). Direct activation of cardiac pacemaker channels by intracellular cyclic AMP. *Nature* **351**, 145-147.

DiFrancesco D (1999). Dual allosteric modulation of pacemaker (f) channels by cAMP and voltage in rabbit SA node. *J Physiol* **515 (Pt 2)**, 367-376.

Dimmeler S, Fleming I, Fisslthaler B, Hermann C, Busse R & Zeiher AM (1999). Activation of nitric oxide synthase in endothelial cells by Akt-dependent phosphorylation. *Nature* **399** , 601-605.

Ding JD, Burette A, Nedvetsky PI, Schmidt HH & Weinberg RJ (2004). Distribution of soluble guanylyl cyclase in the rat brain. *J Comp Neurol* **472**, 437-448.

El-Husseini AE, Williams J, Reiner PB, Pelech S & Vincent SR (1999). Localization of the cGMP-dependent protein kinases in relation to nitric oxide synthase in the brain. *Journal of Chemical Neuroanatomy* **17**, 45-55.

Endo S, Suzuki M, Sumi M, Nairn AC, Morita R, Yamakawa K, Greengard P & Ito M (1999). Molecular identification of human G-substrate, a possible downstream component of the cGMP-dependent protein kinase cascade in cerebellar Purkinje cells. *Proc Natl Acad Sci U S A* **96**, 2467-2472.

Erecinska M & Silver IA (2001). Tissue oxygen tension and brain sensitivity to hypoxia. *Respir Physiol* **128**, 263-276.

Fan Y, Fricker D, Brager DH, Chen X, Lu HC, Chitwood RA & Johnston D (2005). Activity-dependent decrease of excitability in rat hippocampal neurons through increases in I(h). *Nat Neurosci* **8**, 1542-1551.

Feelisch M (1998). The use of nitric oxide donors in pharmacological studies. *Naunyn Schmiedebergs Arch Pharmacol* **358**, 113-122.

Feelisch M, Kotsonis P, Siebe J, Clement B & Schmidt HH (1999). The soluble guanylyl cyclase inhibitor 1H-[1,2,4]oxadiazolo[4,3,-a] quinoxalin-1-one is a nonselective heme protein inhibitor of nitric oxide synthase and other cytochrome P-450 enzymes involved in nitric oxide donor bioactivation. *Mol Pharmacol* **56**, 243-253.

Feil R, Hartmann J, Luo C, Wolfsgruber W, Schilling K, Feil S, Barski JJ, Meyer M, Konnerth A, De Zeeuw CI & Hofmann F (2003). Impairment of LTD and cerebellar learning by Purkinje cell-specific ablation of cGMP-dependent protein kinase I. *J Cell Biol* **163**, 295-302.

Feil S, Zimmermann P, Knorn A, Brummer S, Schlossmann J, Hofmann F & Feil R (2005). Distribution of cGMP-dependent protein kinase type I and its isoforms in the mouse brain and retina. *Neuroscience* **135**, 863-868.

Fessenden JD, Altschuler RA, Seasholtz AF & Schacht J (1999). Nitric oxide/cyclic guanosine monophosphate pathway in the peripheral and central auditory system of the rat. *J Comp Neurol* **404**, 52-63.

Fujisawa S, Matsuki N & Ikegaya Y (2004). Chronometric readout from a memory trace: gamma-frequency field stimulation recruits timed recurrent activity in the rat CA3 network. *J Physiol* **561**, 123-131.

Furchgott RF & Zawadzki JV (1980). The obligatory role of endothelial cells in the relaxation of arterial smooth muscle by acetylcholine. *Nature* **288**, 373-376.

Gahwiler BH (1981). Organotypic monolayer cultures of nervous tissue. *J Neurosci Methods* **4**, 329-342.

Galione A, White A, Willmott N, Turner M, Potter BV & Watson SP (1993). cGMP mobilizes intracellular Ca2+ in sea urchin eggs by stimulating cyclic ADP-ribose synthesis. *Nature* **365**, 456-459.

Gamm DM, Francis SH, Angelotti TP, Corbin JD & Uhler MD (1995). The type II isoform of cGMP-dependent protein kinase is dimeric and possesses regulatory and catalytic properties distinct from the type I isoforms. *J Biol Chem* **270**, 27380-27388.

Garcia-Cardena G, Oh P, Liu J, Schnitzer JE & Sessa WC (1996). Targeting of nitric oxide synthase to endothelial cell caveolae via palmitoylation: implications for nitric oxide signaling. *Proc Natl Acad Sci U S A* **93**, 6448-6453.

Gardner-Medwin AR (1971). A supernormal period after an action potential in parallel fibres of the cerebellum. *J Physiol* **216**, 59P-60P.

Garthwaite G, Bartus K, Malcolm D, Goodwin D, Kollb-Sielecka M, Dooldeniya C & Garthwaite J (2006). Signaling from blood vessels to CNS axons through nitric oxide. *J Neurosci* **26**, 7730-7740.

Garthwaite J & Garthwaite G (1987). Cellular origins of cyclic GMP responses to excitatory amino acid receptor agonists in rat cerebellum in vitro. *J Neurochem* **48**, 29-39.

Garthwaite J, Charles SL & Chess-Williams R (1988). Endothelium-derived relaxing factor release on activation of NMDA receptors suggests role as intercellular messenger in the brain. *Nature* **336**, 385-388.

Garthwaite J, Garthwaite G, Palmer RM & Moncada S (1989). NMDA receptor activation induces nitric oxide synthesis from arginine in rat brain slices. *Eur J Pharmacol* **172**, 413-416.

Garthwaite J, Southam E, Boulton CL, Nielsen EB, Schmidt K & Mayer B (1995). Potent and selective inhibition of nitric oxide-sensitive guanylyl cyclase by 1H-[1,2,4]oxadiazolo[4,3-a]quinoxalin-1-one. *Mol Pharmacol* **48**, 184-188.

Garthwaite J (2005). Dynamics of cellular NO-cGMP signaling. *Front Biosci* **10**, 1868-1880.

Gasparini S & DiFrancesco D (1997). Action of the hyperpolarization-activated current (Ih) blocker ZD 7288 in hippocampal CA1 neurons. *Pflugers Arch* **435**, 99-106.

Gauck V & Jaeger D (2003). The contribution of NMDA and AMPA conductances to the control of spiking in neurons of the deep cerebellar nuclei. *J Neurosci* **23**, 8109-8118.

Gauss R, Seifert R & Kaupp UB (1998). Molecular identification of a hyperpolarization-activated channel in sea urchin sperm. *Nature* **393**, 583-587.

Geiger JRP & Jonas P (2000). Dynamic Control of Presynaptic Ca2+ Inflow by Fast-Inactivating K+ Channels in Hippocampal Mossy Fiber Boutons. *Neuron* **28**, 927-939.

Geiselhoringer A, Werner M, Sigl K, Smital P, Worner R, Acheo L, Stieber J, Weinmeister P, Feil R, Feil S, Wegener J, Hofmann F & Schlossmann J (2004). IRAG is essential for relaxation of receptor-triggered smooth muscle contraction by cGMP kinase. *EMBO J* **23** , 4222-4231.

Gibb BJ & Garthwaite J (2001). Subunits of the nitric oxide receptor, soluble guanylyl cyclase, expressed in rat brain. *Eur J Neurosci* **13**, 539-544.

Gibb BJ, Wykes V & Garthwaite J (2003). Properties of NO-activated guanylyl cyclases expressed in cells. *Br J Pharmacol* **139**, 1032-1040.

Glendenning KK, Hutson KA, Nudo RJ & Masterton RB (1985). Acoustic chiasm II: Anatomical basis of binaurality in lateral superior olive of cat. *J Comp Neurol* **232**, 261-285.

Gotoh H, Kajikawa M, Kato H & Suto K (1999). Intracellular Mg2+ surge follows Ca2+ increase during depolarization in cultured neurons. *Brain Research* **828**, 163-168.

Gotti S, Sica M, Viglietti-Panzica C & Panzica G (2005). Distribution of nitric oxide synthase immunoreactivity in the mouse brain. *Microsc Res Tech* **68**, 13-35.

Grafe P, Quasthoff S, Grosskreutz J & Alzheimer C (1997). Function of the hyperpolarization-activated inward rectification in nonmyelinated peripheral rat and human axons. *J Neurophysiol* **77**, 421-426.

Gravante B, Barbuti A, Milanesi R, Zappi I, Viscomi C & DiFrancesco D (2004). Interaction of the pacemaker channel HCN1 with filamin A. *J Biol Chem* **279**, 43847-43853.

Green LC, Tannenbaum SR & Goldman P (1981). Nitrate synthesis in the germfree and conventional rat. *Science* **212**, 56-58.

Gribble FM, Loussouarn G, Tucker SJ, Zhao C, Nichols CG & Ashcroft FM (2000). A Novel Method for Measurement of Submembrane ATP Concentration. *J Biol Chem* **275**, 30046-30049.

Griffiths C & Garthwaite J (2001). The shaping of nitric oxide signals by a cellular sink. *J Physiol* **536**, 855-862.

Griffiths C, Wykes V, Bellamy TC & Garthwaite J (2003). A new and simple method for delivering clamped nitric oxide concentrations in the physiological range: application to activation of guanylyl cyclase-coupled nitric oxide receptors. *Mol Pharmacol* **64**, 1349-1356.

Grubbs RD (2002). Intracellular magnesium and magnesium buffering. *Biometals* **15**, 251-259.

Gu N, Vervaeke K, Hu H & Storm JF (2005a). Kv7/KCNQ/M and HCN/h, but not KCa2/SK channels, contribute to the somatic medium after-hyperpolarization and excitability control in CA1 hippocampal pyramidal cells. *J Physiol* **566**, 689-715.

Gu Y, Wang L, Xiao C, Guo F & Ruan DY (2005b). Effects of lead on voltage-gated sodium channels in rat hippocampal CA1 neurons. *Neuroscience* **133**, 679-690.

Gupta G, Azam M, Yang L & Danziger RS (1997). The beta2 subunit inhibits stimulation of the alpha1/beta1 form of soluble guanylyl cyclase by nitric oxide. Potential relevance to regulation of blood pressure. *J Clin Invest* **100**, 1488-1492.

Hall CN & Garthwaite J (2006). Inactivation of nitric oxide by rat cerebellar slices. *J Physiol* **577**, 549-567.

Hall KU, Collins SP, Gamm DM, Massa E, Paoli-Roach AA & Uhler MD (1999). Phosphorylation-dependent inhibition of protein phosphatase-1 by G-substrate. A Purkinje cell substrate of the cyclic GMP-dependent protein kinase. *J Biol Chem* **274**, 3485-3495.

Han NL, Ye JS, Yu AC & Sheu FS (2006). Differential mechanisms underlying the modulation of delayed-rectifier K+ channel in mouse neocortical neurons by nitric oxide. *J Neurophysiol* **95**, 2167-2178.

Harris NC & Constanti A (1995). Mechanism of block by ZD 7288 of the hyperpolarization-activated inward rectifying current in guinea pig substantia nigra neurons in vitro. *J Neurophysiol* **74**, 2366-2378.

Herring N, Rigg L, Terrar DA & Paterson DJ (2001). NO-cGMP pathway increases the hyperpolarisation-activated current, I(f), and heart rate during adrenergic stimulation. *Cardiovasc Res* **52**, 446-453.

Hibbs JB, Jr., Vavrin Z & Taintor RR (1987). L-arginine is required for expression of the activated macrophage effector mechanism causing selective metabolic inhibition in target cells. *J Immunol* **138**, 550-565.

Hibbs JB, Jr., Taintor RR, Vavrin Z & Rachlin EM (1988). Nitric oxide: a cytotoxic activated macrophage effector molecule. *Biochem Biophys Res Commun* **157**, 87-94.

Hofmann F, Ammendola A & Schlossmann J (2000). Rising behind NO: cGMP-dependent protein kinases. *J Cell Sci* **113 (Pt 10)**, 1671-1676.

Hogg N (2002). The biochemistry and physiology of S-nitrosothiols. *Annu Rev Pharmacol Toxicol* **42**, 585-600.

Hopper R, Lancaster B & Garthwaite J (2004). On the regulation of NMDA receptors by nitric oxide. *Eur J Neurosci* **19**, 1675-1682.

Hopper RA & Garthwaite J (2006). Tonic and phasic nitric oxide signals in hippocampal long-term potentiation. *J Neurosci* **26**, 11513-11521.

Horie M & Irisawa H (1989). Dual effects of intracellular magnesium on muscarinic potassium channel current in single guinea-pig atrial cells. *J Physiol* **408**, 313-332.

Horn JP & McAfee DA (1977). Modulation of cyclic nucleotide levels in peripheral nerve without effect on resting or compound action potentials. *J Physiol* **269**, 753-766.

Huang CC, Chan SH & Hsu KS (2003). cGMP/protein kinase G-dependent potentiation of glutamatergic transmission induced by nitric oxide in immature rat rostral ventrolateral medulla neurons in vitro. *Mol Pharmacol* **64**, 521-532.

Huang CC & Hsu KS (2003). Reexamination of the role of hyperpolarization-activated cation channels in short- and long-term plasticity at hippocampal mossy fiber synapses. *Neuropharmacology* **44**, 968-981.

Ingram SL & Williams JT (1996). Modulation of the hyperpolarization-activated current (Ih) by cyclic nucleotides in guinea-pig primary afferent neurons. *J Physiol* **492 (Pt 1)**, 97-106.

Ishii TM, Takano M, Xie LH, Noma A & Ohmori H (1999). Molecular characterization of the hyperpolarization-activated cation channel in rabbit heart sinoatrial node. *J Biol Chem* **274**, 12835-12839.

Ishii TM, Nakashima N & Ohmori H (2006). Tryptophan scanning mutagenesis in the S1 domain of mammalian HCN channel reveals residues critical for voltage-gated activation. *J Physiol*.

Iwase K, Iyama K, Akagi K, Yano S, Fukunaga K, Miyamoto E, Mori M & Takiguchi M (1998). Precise distribution of neuronal nitric oxide synthase mRNA in the rat brain revealed by non-radioisotopic in situ hybridization. *Brain Res Mol Brain Res* **53**, 1-12.

Jahnsen H (1986a). Electrophysiological characteristics of neurones in the guinea-pig deep cerebellar nuclei in vitro. *J Physiol* **372**, 129-147.

Jahnsen H (1986b). Extracellular activation and membrane conductances of neurones in the guinea-pig deep cerebellar nuclei in vitro. *J Physiol* **372**, 149-168.

Johnston, D. & Amaral, D. G. (2004). Hippocampus. In *The Synaptic Organization of the Brain*, ed. Shepherd, G. M., pp. 455-498. Oxford University Press.

Joshi I & Wang LY (2002). Developmental profiles of glutamate receptors and synaptic transmission at a single synapse in the mouse auditory brainstem. *J Physiol* **540**, 861-873.

Jung HY, Staff NP & Spruston N (2001). Action potential bursting in subicular pyramidal neurons is driven by a calcium tail current. *J Neurosci* **21**, 3312-3321.

Katsuki S, Arnold W, Mittal C & Murad F (1977). Stimulation of guanylate cyclase by sodium nitroprusside, nitroglycerin and nitric oxide in various tissue preparations and comparison to the effects of sodium azide and hydroxylamine. *J Cyclic Nucleotide Res* **3** , 23-35.

Kaupp UB, Niidome T, Tanabe T, Terada S, Bonigk W, Stuhmer W, Cook NJ, Kangawa K, Matsuo H, Hirose T, Miyata T & NUMA S. (1989). Primary structure and functional

expression from complementary DNA of the rod photoreceptor cyclic GMP-gated channel. *Nature* **342**, 762-766.

Kaupp UB & Seifert R (2002). Cyclic nucleotide-gated ion channels. *Physiol Rev* **82**, 769-824.

Kazerounian S, Pitari GM, Ruiz-Stewart I, Schulz S & Waldman SA (2002). Nitric oxide activation of soluble guanylyl cyclase reveals high and low affinity sites that mediate allosteric inhibition by calcium. *Biochemistry* **41**, 3396-3404.

Keefer LK, Nims RW, Davies KM & Wink DA (1996). "NONOates" (1-substituted diazen-1-ium-1,2-diolates) as nitric oxide donors: convenient nitric oxide dosage forms. *Methods Enzymol* **268**, 281-293.

Keynes RG, Griffiths C & Garthwaite J (2003). Superoxide-dependent consumption of nitric oxide in biological media may confound in vitro experiments. *Biochem J* **369**, 399-406.

Keynes RG, Griffiths CH, Hall C & Garthwaite J (2005). Nitric oxide consumption through lipid peroxidation in brain cell suspensions and homogenates. *Biochem J* **387**, 685-694.

Kharitonov VG, Russwurm M, Magde D, Sharma VS & Koesling D (1997). Dissociation of nitric oxide from soluble guanylate cyclase. *Biochem Biophys Res Commun* **239**, 284-286.

Kim HY, Kim SJ, Kim J, Oh SB, Cho H & Jung SJ (2005). Effect of nitric oxide on hyperpolarization-activated current in substantia gelatinosa neurons of rats. *Biochem Biophys Res Commun* **338**, 1648-1653.

Kimura H, Mittal CK & Murad F (1975). Increases in cyclic GMP levels in brain and liver with sodium azide an activator of guanylate cyclase. *Nature* **257**, 700-702

Kimura H, Mittal CK & Murad F (1976). Appearance of magnesium guanylate cyclase activity in rat liver with sodium azide activation. *J Biol Chem* **251**, 7769-7773.

Kingston PA, Zufall F & Barnstable CJ (1996). Rat hippocampal neurons express genes for both rod retinal and olfactory cyclic nucleotide-gated channels: novel targets for cAMP/cGMP function. *Proc Natl Acad Sci U S A* **93**, 10440-10445.

Kingston PA, Zufall F & Barnstable CJ (1999). Widespread expression of olfactory cyclic nucleotide-gated channel genes in rat brain: implications for neuronal signalling. *Synapse* **32**, 1-12.

Kleppisch T, Wolfsgruber W, Feil S, Allmann R, Wotjak CT, Goebbels S, Nave KA, Hofmann F & Feil R (2003). Hippocampal cGMP-dependent protein kinase I supports an age- and protein synthesis-dependent component of long-term potentiation but is not essential for spatial reference and contextual memory. *J Neurosci* **23**, 6005-6012.

Kobayashi J, Ohta M & Terada Y (1997). Evidence for the involvement of Na+-K+ pump and K+ conductance in the post-tetanic hyperpolarization of the tetrodotoxin-resistant C-fibers in the isolated bullfrog sciatic nerve. *Neurosci Lett* **236**, 171-174.

Koch U, Braun M, Kapfer C & Grothe B (2004). Distribution of HCN1 and HCN2 in rat auditory brainstem nuclei. *Eur J Neurosci* **20**, 79-91.

Kocsis JD, Malenka RC & Waxman SG (1983). Effects of extracellular potassium concentration on the excitability of the parallel fibres of the rat cerebellum. *J Physiol* **334**, 225-244.

Koppenol WH (2002). NO nomenclature? *Nitric Oxide* **6**, 96-98.

Kornau HC, Schenker LT, Kennedy MB & Seeburg PH (1995). Domain interaction between NMDA receptor subunits and the postsynaptic density protein PSD-95. *Science* **269**, 1737-1740.

Korneev SA, Straub V, Kemenes I, Korneeva EI, Ott SR, Benjamin PR & O'Shea M (2005). Timed and targeted differential regulation of nitric oxide synthase (NOS) and anti-NOS genes by reward conditioning leading to long-term memory formation. *J Neurosci* **25**, 1188-1192.

Kumoi K, Saito N, Kuno T & Tanaka C (1988). Immunohistochemical localization of gamma-aminobutyric acid- and aspartate-containing neurons in the rat deep cerebellar nuclei. *Brain Res* **439**, 302-310.

Kuo CC & Lu L (1997). Characterization of lamotrigine inhibition of Na+ channels in rat hippocampal neurones. *Br J Pharmacol* **121**, 1231-1238.

Laerum H & Storm JF (1994). Hippocampal long-term potentiation is not accompanied by presynaptic spike broadening, unlike synaptic potentiation by K+ channel blockers. *Brain Research* **637**, 349-355.

Launey T, Endo S, Sakai R, Harano J & Ito M (2004). Protein phosphatase 2A inhibition induces cerebellar long-term depression and declustering of synaptic AMPA receptor. *Proc Natl Acad Sci U S A* **101**, 676-681.

Leao KE, Leao RN, Sun H, Fyffe REW & Walmsley B (2006a). Hyperpolarization-activated currents are differentially expressed in mice brainstem auditory nuclei. *J Physiol (Lond)* **576**, 849-864.

Leao RN, Svahn K, Berntson A & Walmsley B (2005). Hyperpolarization-activated (I) currents in auditory brainstem neurons of normal and congenitally deaf mice. *Eur J Neurosci* **22**, 147-157.

Leao RN, Sun H, Svahn K, Berntson A, Youssoufian M, Paolini AG, Fyffe RE & Walmsley B (2006b). Topographic organization in the auditory brainstem of juvenile mice is disrupted in congenital deafness. *J Physiol* **571**, 563-578.

Lipton SA, Choi YB, Takahashi H, Zhang D, Li W, Godzik A & Bankston LA (2002). Cysteine regulation of protein function--as exemplified by NMDA-receptor modulation. *Trends Neurosci* **25**, 474-480.

Liu H, Xiong Z & Sperelakis N (1997). Cyclic nucleotides regulate the activity of L-type calcium channels in smooth muscle cells from rat portal vein. *J Mol Cell Cardiol* **29**, 1411-1421.

Liu X, Miller MJ, Joshi MS, Sadowska-Krowicka H, Clark DA & Lancaster JR, Jr. (1998). Diffusion-limited reaction of free nitric oxide with erythrocytes. *J Biol Chem* **273**, 18709-18713.

Liu X & Stan Leung L (2004). Sodium-activated potassium conductance participates in the depolarizing afterpotential following a single action potential in rat hippocampal CA1 pyramidal cells. *Brain Research* **1023**, 185-192.

Llinas R & Muhlethaler M (1988). Electrophysiology of guinea-pig cerebellar nuclear cells in the in vitro brain stem-cerebellar preparation. *J Physiol* **404**, 241-258.

Lohmann SM, Walter U, Miller PE, Greengard P & De CP (1981). Immunohistochemical localization of cyclic GMP-dependent protein kinase in mammalian brain. *Proc Natl Acad Sci U S A* **78**, 653-657.

Lu YF, Kandel ER & Hawkins RD (1999). Nitric oxide signaling contributes to late-phase LTP and CREB phosphorylation in the hippocampus. *J Neurosci* **19**, 10250-10261.

Ludwig A, Zong X, Jeglitsch M, Hofmann F & Biel M (1998). A family of hyperpolarization-activated mammalian cation channels. *Nature* **393**, 587-591.

Maccaferri G, Janigro D, Lazzari A & DiFrancesco D (1994). Cesium prevents maintenance of long-term depression in rat hippocampal CA1 neurons. *Neuroreport* **5**, 1813-1816.

Maffei A, Prestori F, Shibuki K, Rossi P, Taglietti V & D'Angelo E (2003). NO enhances presynaptic currents during cerebellar mossy fiber-granule cell LTP. *J Neurophysiol* **90**, 2478-2483.

Magee JC (1998). Dendritic hyperpolarization-activated currents modify the integrative properties of hippocampal CA1 pyramidal neurons. *J Neurosci* **18**, 7613-7624.

Magee JC (1999). Dendritic Ih normalizes temporal summation in hippocampal CA1 neurons. *Nat Neurosci* **2**, 508-514.

Makara JK, Katona I, Nyíri G, Németh B, Ledent C, Watanabe M, de Vente J, Freund TF, Hájos N (2007). Involvement of nitric oxide in depolarization-induced suppression of inhibition in hippocampal pyramidal cells during activation of cholinergic receptors. *J Neurosci.* 27(**38**):10211-22

Malenka RC & Bear MF (2004). LTP and LTD: an embarrassment of riches. *Neuron* **44**, 5-21.

Mannikko R, Elinder F & Larsson HP (2002). Voltage-sensing mechanism is conserved among ion channels gated by opposite voltages. *Nature* **419**, 837-841.

Martin E, Berka V, Bogatenkova E, Murad F & Tsai AL (2006). Ligand selectivity of soluble guanylyl cyclase: effect of the hydrogen-bonding tyrosine in the distal heme pocket on binding of oxygen, nitric oxide, and carbon monoxide. *J Biol Chem* **281**, 27836-27845.

Martin W, Villani GM, Jothianandan D & Furchgott RF (1985). Selective blockade of endothelium-dependent and glyceryl trinitrate-induced relaxation by hemoglobin and by methylene blue in the rabbit aorta. *J Pharmacol Exp Ther* **232**, 708-716.

Martin W, Villani GM, Jothianandan D & Furchgott RF (1985). Blockade of endothelium-dependent and glyceryl trinitrate-induced relaxation of rabbit aorta by certain ferrous hemoproteins. *J Pharmacol Exp Ther* **233**, 679-685.

Martinez SE, Wu AY, Glavas NA, Tang XB, Turley S, Hol WG & Beavo JA (2002). The two GAF domains in phosphodiesterase 2A have distinct roles in dimerization and in cGMP binding. *Proc Natl Acad Sci U S A* **99**, 13260-13265.

Martins TJ, Mumby MC & Beavo JA (1982). Purification and characterization of a cyclic GMP-stimulated cyclic nucleotide phosphodiesterase from bovine tissues. *J Biol Chem* **257**, 1973-1979.

Matsuoka I, Giuili G, Poyard M, Stengel D, Parma J, Guellaen G & Hanoune J (1992). Localization of adenylyl and guanylyl cyclase in rat brain by in situ hybridization: comparison with calmodulin mRNA distribution. *J Neurosci* **12**, 3350-3360.

Matulef K & Zagotta WN (2003). Cyclic nucleotide-gated ion channels. *Annu Rev Cell Dev Biol* **19**, 23-44.

McCormick DA & Pape HC (1990a). Properties of a hyperpolarization-activated cation current and its role in rhythmic oscillation in thalamic relay neurones. *J Physiol* **431**, 291-318.

McNaughton BL, Shen J, Rao G, Foster TC & Barnes CA (1994). Persistent increase of hippocampal presynaptic axon excitability after repetitive electrical stimulation: dependence on N-methyl-D-aspartate receptor activity, nitric-oxide synthase, and temperature. *Proc Natl Acad Sci U S A* **91**, 4830-4834.

Meeks JP, Jiang X & Mennerick S (2005). Action potential fidelity during normal and epileptiform activity in paired soma-axon recordings from rat hippocampus. *J Physiol* **566**, 425-441.

Mellor J, Nicoll RA & Schmitz D (2002). Mediation of hippocampal mossy fiber long-term potentiation by presynaptic Ih channels. *Science* **295**, 143-147.

Menzel R & Muller U (1996). Learning and memory in honeybees: from behavior to neural substrates. *Annu Rev Neurosci* **19**, 379-404.

Mistrik P, Mader R, Michalakis S, Weidinger M, Pfeifer A & Biel M (2005). The murine HCN3 gene encodes a hyperpolarization-activated cation channel with slow kinetics and unique response to cyclic nucleotides. *J Biol Chem* **280**, 27056-27061.

Mo E, Amin H, Bianco IH & Garthwaite J (2004). Kinetics of a cellular nitric oxide/cGMP/phosphodiesterase-5 pathway. *J Biol Chem* **279**, 26149-26158.

Moncada S & Erusalimsky JD (2002). Does nitric oxide modulate mitochondrial energy generation and apoptosis? *Nat Rev Mol Cell Biol* **3**, 214-220.

Mons N, Harry A, Dubourg P, Premont RT, Iyengar R & Cooper DM (1995). Immunohistochemical localization of adenylyl cyclase in rat brain indicates a highly selective concentration at synapses. *Proc Natl Acad Sci U S A* **92**, 8473-8477.

Monteggia LM, Eisch AJ, Tang MD, Kaczmarek LK & Nestler EJ (2000). Cloning and localization of the hyperpolarization-activated cyclic nucleotide-gated channel family in rat brain. *Brain Res Mol Brain Res* **81**, 129-139.

Moore PK, al-Swayeh OA, Chong NW, Evans RA & Gibson A (1990). L-NG-nitro arginine (L-NOARG), a novel, L-arginine-reversible inhibitor of endothelium-dependent vasodilatation in vitro. *Br J Pharmacol* **99**, 408-412.

Moosmang S, Stieber J, Zong X, Biel M, Hofmann F & Ludwig A (2001). Cellular expression and functional characterization of four hyperpolarization-activated pacemaker channels in cardiac and neuronal tissues. *Eur J Biochem* **268**, 1646-1652.

Moosmann B & Behl C (2002). Antioxidants as treatment for neurodegenerative disorders. *Expert Opin Investig Drugs* **11**, 1407-1435.

Morgan SL & Teyler TJ (2001). Electrical stimuli patterned after the theta-rhythm induce multiple forms of LTP. *J Neurophysiol* **86**, 1289-1296.

Morley JE & Flood JF (1992). Competitive antagonism of nitric oxide synthetase causes weight loss in mice. *Life Sci* **51**, 1285-1289.

Moroz LL, Meech RW, Sweedler JV & Mackie GO (2004). Nitric oxide regulates swimming in the jellyfish Aglantha digitale. *J Comp Neurol* **471**, 26-36.

Mullershausen F, Friebe A, Feil R, Thompson WJ, Hofmann F & Koesling D (2003). Direct activation of PDE5 by cGMP: long-term effects within NO/cGMP signaling. *J Cell Biol* **160**, 719-727.

Munoz-Cuevas J, Vara H & Colino A (2004). Characterization of release-independent short-term depression in the juvenile rat hippocampus. *J Physiol* **558**, 527-548.

Munoz-Cuevas J, Vara H & Colino A (2006). Augmentation of excitability in the hippocampus of juvenile rat. *Neuroscience* **143**, 39-50.

Murthy KS (2004). Modulation of soluble guanylate cyclase activity by phosphorylation. *Neurochem Int* **45**, 845-851.

Musleh WY, Shahi K & Baudry M (1993). Further studies concerning the role of nitric oxide in LTP induction and maintenance. *Synapse* **13**, 370-375.

Namiki S, Kakizawa S, Hirose K & Iino M (2005). NO signalling decodes frequency of neuronal activity and generates synapse-specific plasticity in mouse cerebellum. *J Physiol* **566**, 849-863.

Notomi T & Shigemoto R (2004). Immunohistochemical localization of Ih channel subunits, HCN1-4, in the rat brain. *J Comp Neurol* **471**, 241-276.

Oster H, Werner C, Magnone MC, Mayser H, Feil R, Seeliger MW, Hofmann F & Albrecht U (2003). cGMP-dependent protein kinase II modulates mPer1 and mPer2 gene induction and influences phase shifts of the circadian clock. *Curr Biol* **13**, 725-733.

Palmer RM, Ferrige AG & Moncada S (1987). Nitric oxide release accounts for the biological activity of endothelium-derived relaxing factor. *Nature* **327**, 524-526.

Pape HC & Mager R (1992). Nitric oxide controls oscillatory activity in thalamocortical neurons. *Neuron* **9**, 441-448.

Paton JF, Kasparov S & Paterson DJ (2002). Nitric oxide and autonomic control of heart rate: a question of specificity. *Trends Neurosci* **25**, 626-631.

Pawlik G, Rackl A & Bing RJ (1981). Quantitative capillary topography and blood flow in the cerebral cortex of cats: an in vivo microscopic study. *Brain Res* **208**, 35-58.

Pedarzani P & Storm JF (1995). Protein kinase A-independent modulation of ion channels in the brain by cyclic AMP. *Proc Natl Acad Sci U S A* **92**, 11716-11720.

Pehl U & Schmid HA (1997). Electrophysiological responses of neurons in the rat spinal cord to nitric oxide. *Neuroscience* **77**, 563-573.

Peng C, Rich ED & Varnum MD (2004). Subunit configuration of heteromeric cone cyclic nucleotide-gated channels. *Neuron* **42**, 401-410.

Pian P, Bucchi A, Robinson RB & Siegelbaum SA (2006). Regulation of Gating and Rundown of HCN Hyperpolarization-activated Channels by Exogenous and Endogenous PIP2. *J Gen Physiol* **128**, 593-604.

Pifarre P, Garcia A & Mengod G (2007). Species differences in the localization of soluble guanylyl cyclase subunits in monkey and rat brain. *J Comp Neurol* **500**, 942-957.

Pineda VV, Athos JI, Wang H, Celver J, Ippolito D, Boulay G, Birnbaumer L & Storm DR (2004). Removal of G(ialpha1) constraints on adenylyl cyclase in the hippocampus enhances LTP and impairs memory formation. *Neuron* **41**, 153-163.

Pockett S, Slack JR & Peacock S (1993). Cyclic AMP and long-term potentiation in the CA1 region of rat hippocampus. *Neuroscience* **52**, 229-236.

Podda MV, Marcocci ME, Oggiano L, D'Ascenzo M, Tolu E, Palamara AT, Azzena GB & Grassi C (2004). Nitric oxide increases the spontaneous firing rate of rat medial vestibular nucleus neurons in vitro via a cyclic GMP-mediated PKG-independent mechanism. *Eur J Neurosci* **20**, 2124-2132.

Poolos NP, Migliore M & Johnston D (2002). Pharmacological upregulation of h-channels reduces the excitability of pyramidal neuron dendrites. *Nat Neurosci* **5**, 767-774.

Poolos NP, Bullis JB & Roth MK (2006). Modulation of h-channels in hippocampal pyramidal neurons by p38 mitogen-activated protein kinase. *J Neurosci* **26**, 7995-8003.

Pose I, Sampogna S, Chase MH & Morales FR (2003). Mesencephalic trigeminal neurons are innervated by nitric oxide synthase-containing fibers and respond to nitric oxide. *Brain Res* **960**, 81-89.

Proenza C, Angoli D, Agranovich E, Macri V & Accili EA (2002). Pacemaker channels produce an instantaneous current. *J Biol Chem* **277**, 5101-5109.

Proenza C & Yellen G (2006). Distinct Populations of HCN Pacemaker Channels Produce Voltage-dependent and Voltage-independent Currents. *J Gen Physiol* **127**, 183-190.

Qiu DI & Knopfel T (2007). An NMDA Receptor/Nitric Oxide Cascade in Presynaptic Parallel Fiber-Purkinje Neuron Long-Term Potentiation. *J Neurosci* **27**, 3408-3415.

Qu J, Altomare C, Bucchi A, DiFrancesco D & Robinson RB (2002). Functional comparison of HCN isoforms expressed in ventricular and HEK 293 cells. *Pflugers Arch* **444**, 597-601.

Qu J, Kryukova Y, Potapova IA, Doronin SV, Larsen M, Krishnamurthy G, Cohen IS & Robinson RB (2004). MiRP1 modulates HCN2 channel expression and gating in cardiac myocytes. *J Biol Chem* **279**, 43497-43502.

Quignard JF, Frapier JM, Harricane MC, Albat B, Nargeot J & Richard S (1997). Voltage-gated calcium channel currents in human coronary myocytes. Regulation by cyclic GMP and nitric oxide. *J Clin Invest* **99**, 185-193.

Raman IM, Gustafson AE & Padgett D (2000). Ionic Currents and Spontaneous Firing in Neurons Isolated from the Cerebellar Nuclei. *J Neurosci* **20**, 9004-9016.

Rapoport RM & Murad F (1983). Agonist-induced endothelium-dependent relaxation in rat thoracic aorta may be mediated through cGMP. *Circ Res* **52**, 352-357.

Rapoport RM, Draznin MB & Murad F (1983). Endothelium-dependent relaxation in rat aorta may be mediated through cyclic GMP-dependent protein phosphorylation. *Nature* **306**, 174-176.

Robinson RB & Siegelbaum SA (2003). Hyperpolarization-activated cation currents: from molecules to physiological function. *Annu Rev Physiol* **65**, 453-480.

Rodrigo J, Springall DR, Uttenthal O, Bentura ML, badia-Molina F, Riveros-Moreno V, Martinez-Murillo R, Polak JM & Moncada S (1994). Localization of nitric oxide synthase in the adult rat brain. *Philos Trans R Soc Lond B Biol Sci* **345**, 175-221.

Rosenbaum T & Gordon SE (2004). Quickening the Pace; Looking into the Heart of HCN Channels. *Neuron* **42**, 193-196.

Ruiz-Stewart I, Tiyyagura SR, Lin JE, Kazerounian S, Pitari GM, Schulz S, Martin E, Murad F & Waldman SA (2004). Guanylyl cyclase is an ATP sensor coupling nitric oxide signaling to cell metabolism. *Proc Natl Acad Sci U S A* **101**, 37-42.

Russwurm M, Wittau N & Koesling D (2001). Guanylyl cyclase/PSD-95 interaction: targeting of the nitric oxide-sensitive alpha2beta1 guanylyl cyclase to synaptic membranes. *J Biol Chem* **276**, 44647-44652.

Sakmann B & Neher E (1984). Patch clamp techniques for studying ionic channels in excitable membranes. *Annu Rev Physiol* **46**, 455-472.

Santoro B, Grant SG, Bartsch D & Kandel ER (1997). Interactive cloning with the SH3 domain of N-src identifies a new brain specific ion channel protein, with homology to eag and cyclic nucleotide-gated channels. *Proc Natl Acad Sci U S A* **94**, 14815-14820.

Santoro B, Liu DT, Yao H, Bartsch D, Kandel ER, Siegelbaum SA & Tibbs GR (1998). Identification of a gene encoding a hyperpolarization-activated pacemaker channel of brain. *Cell* **93**, 717-729.

Santoro B, Chen S, Luthi A, Pavlidis P, Shumyatsky GP, Tibbs GR & Siegelbaum SA (2000). Molecular and functional heterogeneity of hyperpolarization-activated pacemaker channels in the mouse CNS. *J Neurosci* **20**, 5264-5275.

Santoro B, Wainger BJ & Siegelbaum SA (2004). Regulation of HCN channel surface expression by a novel C-terminal protein-protein interaction. *J Neurosci* **24**, 10750-10762.

Sato K, Nakagawa H, Kuriyama H & Altschuler RA (1999). Differential distribution of N-methyl-D-aspartate receptor-2 subunit messenger RNA in the rat superior olivary complex. *Neuroscience* **89**, 839-853.

Sattler R, Xiong Z, Lu WY, Hafner M, MacDonald JF & Tymianski M (1999). Specific coupling of NMDA receptor activation to nitric oxide neurotoxicity by PSD-95 protein. *Science* **284**, 1845-1848.

Satzler K, Sohl LF, Bollmann JH, Borst JG, Frotscher M, Sakmann B & Lubke JH (2002). Three-dimensional reconstruction of a calyx of Held and its postsynaptic principal neuron in the medial nucleus of the trapezoid body. *J Neurosci* **22**, 10567-10579.

Savchenko A, Barnes S & Kramer RH (1997). Cyclic-nucleotide-gated channels mediate synaptic feedback by nitric oxide. *Nature* **390**, 694-698.

Schaeffer DF, Reuss MH, Riemann R & Reuss S (2003). A nitrergic projection from the superior olivary complex to the inferior colliculus of the rat. *Hear Res* **183**, 67-72.

Schlossmann J, Feil R & Hofmann F (2005). Insights into cGMP signalling derived from cGMP kinase knockout mice. *Front Biosci* **10**, 1279-1289.

Schmid HA & Pehl U (1996). Regional specific effects of nitric oxide donors and cGMP on the electrical activity of neurons in the rat spinal cord. *J Chem Neuroanat* **10**, 197-201.

Schmidt K, Desch W, Klatt P, Kukovetz WR & Mayer B (1997). Release of nitric oxide from donors with known half-life: a mathematical model for calculating nitric oxide concentrations in aerobic solutions. *Naunyn Schmiedebergs Arch Pharmacol* **355**, 457-462.

Schrammel A, Behrends S, Schmidt K, Koesling D & Mayer B (1996). Characterization of 1H-[1,2,4]oxadiazolo[4,3-a]quinoxalin-1-one as a heme-site inhibitor of nitric oxide-sensitive guanylyl cyclase. *Mol Pharmacol* **50**, 1-5.

Sesti F, Rajan S, Gonzalez-Colaso R, Nikolaeva N & Goldstein SA (2003). Hyperpolarization moves S4 sensors inward to open MVP, a methanococcal voltage-gated potassium channel. *Nat Neurosci* **6**, 353-361.

Shaikh AG & Finlayson PG (2003). Hyperpolarization-activated (I(h)) conductances affect brainstem auditory neuron excitability. *Hear Res* **183**, 126-136.

Shaikh AG & Finlayson PG (2005). Excitability of auditory brainstem neurons, in vivo, is increased by cyclic-AMP. *Hear Res* **201**, 70-80.

Shaw PJ, Charles SL & Salt TE (1999). Actions of 8-bromo-cyclic-GMP on neurones in the rat thalamus in vivo and in vitro. *Brain Res* **833**, 272-277.

Shepherd GM & Harris KM (1998). Three-dimensional structure and composition of CA3-->CA1 axons in rat hippocampal slices: implications for presynaptic connectivity and compartmentalization. *J Neurosci* **18**, 8300-8310.

Shibuki K & Kimura S (1997). Dynamic properties of nitric oxide release from parallel fibres in rat cerebellar slices. *J Physiol (Lond)* **498**, 443-452.

Shin JH & Linden DJ (2005). An NMDA receptor/nitric oxide cascade is involved in cerebellar LTD but is not localized to the parallel fiber terminal. *J Neurophysiol* **94**, 4281-4289.

Simeone TA, Rho JM & Baram TZ (2005). Single channel properties of hyperpolarization-activated cation currents in acutely dissociated rat hippocampal neurones. *J Physiol* **568**, 371-380.

Smith PH, Joris PX, Carney LH & Yin TC (1991). Projections of physiologically characterized globular bushy cell axons from the cochlear nucleus of the cat. *J Comp Neurol* **304**, 387-407.

Soderling SH & Beavo JA (2000). Regulation of cAMP and cGMP signaling: new phosphodiesterases and new functions. *Curr Opin Cell Biol* **12**, 174-179.

Soleng AF, Chiu K & Raastad M (2003). Unmyelinated axons in the rat hippocampus hyperpolarize and activate an H current when spike frequency exceeds 1 Hz. *J Physiol* **552**, 459-470.

Soleng AF, Baginskas A, Andersen P & Raastad M (2004). Activity-dependent excitability changes in hippocampal CA3 cell Schaffer axons. *J Physiol* **560**, 491-503.

Southam E & Garthwaite J (1993). The nitric oxide-cyclic GMP signalling pathway in rat brain. *Neuropharmacology* **32**, 1267-1277.

Sprigge JS (2002). Sir Humphry Davy; his researches in respiratory physiology and his debt to Antoine Lavoisier. *Anaesthesia* **57**, 357-364.

Stamler JS, Lamas S & Fang FC (2001). Nitrosylation: The Prototypic Redox-Based Signaling Mechanism. *Cell* **106**, 675-683.

Stanton PK, Winterer J, Bailey CP, Kyrozis A, Raginov I, Laube G, Veh RW, Nguyen CQ & Muller W (2003). Long-term depression of presynaptic release from the readily releasable vesicle pool induced by NMDA receptor-dependent retrograde nitric oxide. *J Neurosci* **23**, 5936-5944.

Strijbos PJ, Pratt GD, Khan S, Charles IG & Garthwaite J (1999). Molecular characterization and in situ localization of a full-length cyclic nucleotide-gated channel in rat brain. *Eur J Neurosci* **11**, 4463-4467.

Stuehr DJ & Marletta MA (1985). Mammalian nitrate biosynthesis: mouse macrophages produce nitrite and nitrate in response to Escherichia coli lipopolysaccharide. *Proc Natl Acad Sci U S A* **82**, 7738-7742.

Swensen AM & Bean BP (2003). Ionic mechanisms of burst firing in dissociated Purkinje neurons. *J Neurosci* **23**, 9650-9663.

Takahashi H, Shin Y, Cho SJ, Zago WM, Nakamura T, Gu Z, Ma Y, Furukawa H, Liddington R & Zhang D (2007). Hypoxia Enhances S-Nitrosylation-Mediated NMDA Receptor Inhibition via a Thiol Oxygen Sensor Motif. *Neuron* **53**, 53-64.

Traub RD, Spruston N, Soltesz I, Konnerth A, Whittington MA & Jefferys GR (1998). Gamma-frequency oscillations: a neuronal population phenomenon, regulated by synaptic and intrinsic cellular processes, and inducing synaptic plasticity. *Prog Neurobiol* **55**, 563-575.

Traut TW (1994). Physiological concentrations of purines and pyrimidines. *Mol Cell Biochem* **140**, 1-22.

Tsou K, Snyder GL & Greengard P (1993). Nitric oxide/cGMP pathway stimulates phosphorylation of DARPP-32, a dopamine- and cAMP-regulated phosphoprotein, in the substantia nigra. *Proc Natl Acad Sci U S A* **90**, 3462-3465.

Turko IV, Francis SH & Corbin JD (1998). Binding of cGMP to both allosteric sites of cGMP-binding cGMP-specific phosphodiesterase (PDE5) is required for its phosphorylation. *Biochem J* **329 (Pt 3)**, 505-510.

Ulens C & Tytgat J (2001). Functional heteromerization of HCN1 and HCN2 pacemaker channels. *J Biol Chem* **276**, 6069-6072.

Uusisaari M, Obata K & Knopfel T (2007). Morphological and Electrophysiological Properties of GABAergic and Non-GABAergic Cells in the Deep Cerebellar Nuclei. *J Neurophysiol* **97**, 901-911.

Vaandrager AB, Ehlert EM, Jarchau T, Lohmann SM & de Jonge HR (1996). N-terminal myristoylation is required for membrane localization of cGMP-dependent protein kinase type II. *J Biol Chem* **271**, 7025-7029.

van Staveren WC, Glick J, Markerink-van IM, Shimizu M, Beavo JA, Steinbusch HW & de Vente J (2002). Cloning and localization of the cGMP-specific phosphodiesterase type 9 in the rat brain. *J Neurocytol* **31**, 729-741.

van Staveren WC, Steinbusch HW, Markerink-van IM, Repaske DR, Goy MF, Kotera J, Omori K, Beavo JA & de VJ (2003). mRNA expression patterns of the cGMP-hydrolyzing phosphodiesterases types 2, 5, and 9 during development of the rat brain. *J Comp Neurol* **467**, 566-580.

van Staveren WC, Steinbusch HW, Markerink-van IM, Behrends S & de VJ (2004). Species differences in the localization of cGMP-producing and NO-responsive elements in the mouse and rat hippocampus using cGMP immunocytochemistry. *Eur J Neurosci* **19**, 2155-2168.

van Welie I, Remme MWH, van Hooft JA & Wadman WJ (2006). Different levels of Ih determine distinct temporal integration in bursting and regular-spiking neurons in rat subiculum. *J Physiol (Lond)* **576**, 203-214.

van Welie I, van Hooft JA & Wadman WJ (2004). Homeostatic scaling of neuronal excitability by synaptic modulation of somatic hyperpolarization-activated Ih channels. *Proc Natl Acad Sci U S A* **101**, 5123-5128.

Vargas G & Lucero MT (2002). Modulation by PKA of the hyperpolarization-activated current (Ih) in cultured rat olfactory receptor neurons. *J Membr Biol* **188**, 115-125.

Vasilyev DV & Barish ME (2004). Regulation of the hyperpolarization-activated cationic current Ih in mouse hippocampal pyramidal neurons by vitronectin, a component of extracellular matrix. *J Physiol*.

de Vente J, Asan E, Gambaryan S, Markerink-van IM, Axer H, Gallatz K, Lohmann SM & Palkovits M (2001). Localization of cGMP-dependent protein kinase type II in rat brain. *Neuroscience* **108**, 27-49.

Vervaeke K, Gu N, Agdestein C, Hu H & Storm JF (2006). Kv7/KCNQ/M-channels in rat glutamatergic hippocampal axons and their role in regulation of excitability and transmitter release. *J Physiol (Lond)* **576**, 235-256.

Vincent SR & Kimura H (1992). Histochemical mapping of nitric oxide synthase in the rat brain. *Neuroscience* **46**, 755-784.

Wagner DA, Young VR & Tannenbaum SR (1983). Mammalian nitrate biosynthesis: incorporation of 15NH3 into nitrate is enhanced by endotoxin treatment. *Proc Natl Acad Sci U S A* **80**, 4518-4521.

Wainger BJ, DeGennaro M, Santoro B, Siegelbaum SA & Tibbs GR (2001). Molecular mechanism of cAMP modulation of HCN pacemaker channels. *Nature* **411**, 805-810.

Wang J, Chen S & Siegelbaum SA (2001). Regulation of hyperpolarization-activated HCN channel gating and cAMP modulation due to interactions of COOH terminus and core transmembrane regions. *J Gen Physiol* **118**, 237-250.

Wang S, Teschemacher AG, Paton JF & Kasparov S (2006a). Mechanism of nitric oxide action on inhibitory GABAergic signaling within the nucleus tractus solitarii. *FASEB J* **20**, 1537-1539.

Wang S, Paton J & Kasparov S (2006b). Autonomic Neuroscience: Differential sensitivity of excitatory and inhibitory synaptic transmission to modulation by nitric oxide in rat nucleus tractus solitarii. *Exp Physiol* **92**, 371-382.

Wedel B, Humbert P, Harteneck C, Foerster J, Malkewitz J, Bohme E, Schultz G & Koesling D (1994). Mutation of His-105 in the beta 1 subunit yields a nitric oxide-insensitive form of soluble guanylyl cyclase. *Proc Natl Acad Sci U S A* **91**, 2592-2596.

Wei JY, Cohen ED, Genieser HG & Barnstable CJ (1998). Substituted cGMP analogs can act as selective agonists of the rod photoreceptor cGMP-gated cation channel. *J Mol Neurosci* **10** , 53-64.

Weitz D, Ficek N, Kremmer E, Bauer PJ & Kaupp UB (2002). Subunit stoichiometry of the CNG channel of rod photoreceptors. *Neuron* **36**, 881-889.

Wenthold RJ, Huie D, Altschuler RA & Reeks KA (1987). Glycine immunoreactivity localized in the cochlear nucleus and superior olivary complex. *Neuroscience* **22**, 897-912.

Wigstrom H & Gustafsson B (1981). Increased excitability of hippocampal unmyelinated fibres following conditioning stimulation. *Brain Res* **229**, 507-513.

Wong RK & Prince DA (1981). Afterpotential generation in hippocampal pyramidal cells. *J Neurophysiol* **45**, 86-97.

Wong ST, Athos J, Figueroa XA, Pineda VV, Schaefer ML, Chavkin CC, Muglia LJ & Storm DR (1999). Calcium-stimulated adenylyl cyclase activity is critical for hippocampus-dependent long-term memory and late phase LTP. *Neuron* **23**, 787-798.

Wood J & Garthwaite J (1994). Models of the diffusional spread of nitric oxide: implications for neural nitric oxide signalling and its pharmacological properties. *Neuropharmacology* **33**, 1235-1244.

Wu J & Hablitz JJ (2005). Cooperative Activation of D1 and D2 Dopamine Receptors Enhances a Hyperpolarization-Activated Inward Current in Layer I Interneurons. *J Neurosci* **25**, 6322-6328.

Wu SH & Kelly JB (1993). Response of neurons in the lateral superior olive and medial nucleus of the trapezoid body to repetitive stimulation: intracellular and extracellular recordings from mouse brain slice. *Hear Res* **68**, 189-201.

Wykes V, Bellamy TC & Garthwaite J (2002). Kinetics of nitric oxide-cyclic GMP signalling in CNS cells and its possible regulation by cyclic GMP. *J Neurochem* **83**, 37-47.

Wykes V & Garthwaite J (2004). Membrane-association and the sensitivity of guanylyl cyclase-coupled receptors to nitric oxide. *Br J Pharmacol* **141**, 1087-1090.

Yamada J, Sugimoto Y, Yoshikawa T & Horisaka K (1997). Involvement of nitric oxide in 2-deoxy-D-glucose-induced hyperphagia in rats. *Neuroreport* **8**, 2097-2100.

Ying SW, Abbas SY, Harrison NL & Goldstein PA (2006). Propofol block of Ih contributes to the suppression of neuronal excitability and rhythmic burst firing in thalamocortical neurons. *European Journal of Neuroscience* **23**, 465-480.

Yu H, Wu J, Potapova I, Wymore RT, Holmes B, Zuckerman J, Pan Z, Wang H, Shi W, Robinson RB, El-Maghrabi MR, Benjamin W, Dixon J, McKinnon D, Cohen IS & Wymore R (2001). MinK-related peptide 1: A beta subunit for the HCN ion channel subunit family enhances expression and speeds activation. *Circ Res* **88**, E84-E87.

Yu X, Duan KL, Shang CF, Yu HG & Zhou Z (2004). Calcium influx through hyperpolarization-activated cation channels (Ih channels) contributes to activity-evoked neuronal secretion. *Proc Natl Acad Sci U S A* **101**, 1051-1056.

Zabel U, Kleinschnitz C, Oh P, Nedvetsky P, Smolenski A, Muller H, Kronich P, Kugler P, Walter U, Schnitzer JE & Schmidt HH (2002). Calcium-dependent membrane association sensitizes soluble guanylyl cyclase to nitric oxide. *Nat Cell Biol* **4**, 307-311.

Zagotta WN, Olivier NB, Black KD, Young EC, Olson R & Gouaux E (2003). Structural basis for modulation and agonist specificity of HCN pacemaker channels. *Nature* **425**, 200-205.

Zalutsky RA & Nicoll RA (1990). Comparison of two forms of long-term potentiation in single hippocampal neurons. *Science* **248**, 1619-1624.

De Zeeuw CI & Berrebi AS (1995). Postsynaptic targets of Purkinje cell terminals in the cerebellar and vestibular nuclei of the rat. *Eur J Neurosci* **7**, 2322-2333.

Zeng X, Keyser B, Li M & Sikka SC (2005). T-type (alpha1G) low voltage-activated calcium channel interactions with nitric oxide-cyclic guanosine monophosphate pathway and regulation of calcium homeostasis in human cavernosal cells. *J Sex Med* **2**, 620-630.

Zhang N, Beuve A & Townes-Anderson E (2005). The nitric oxide-cGMP signaling pathway differentially regulates presynaptic structural plasticity in cone and rod cells. *J Neurosci* **25**, 2761-2770.

Zhao Y, Brandish PE, Ballou DP & Marletta MA (1999). A molecular basis for nitric oxide sensing by soluble guanylate cyclase. *Proc Natl Acad Sci U S A* **96**, 14753-14758.

Zheng J & Zagotta WN (2004). Stoichiometry and assembly of olfactory cyclic nucleotide-gated channels. *Neuron* **42**, 411-421.

Zhong N & Zucker RS (2004). Roles of Ca2+, hyperpolarization and cyclic nucleotide-activated channel activation, and actin in temporal synaptic tagging. *J Neurosci* **24**, 4205-4212.

Zhou L, Olivier NB, Yao H, Young EC & Siegelbaum SA (2004). A Conserved Tripeptide in CNG and HCN Channels Regulates Ligand Gating by Controlling C-Terminal Oligomerization. *Neuron* **44**, 823-834.

Zhuo M, Hu Y, Schultz C, Kandel ER & Hawkins RD (1994). Role of guanylyl cyclase and cGMP-dependent protein kinase in long-term potentiation. *Nature* **368**, 635-639.

Zolles G, Klocker N, Wenzel D, Weisser-Thomas J, Fleischmann BK, Roeper J & Fakler B (2006). Pacemaking by HCN channels requires interaction with phosphoinositides. *Neuron* **52**, 1027-1036.

Zong X, Eckert C, Yuan H, Wahl-Schott C, Abicht H, Fang L, Li R, Mistrik P, Gerstner A, Much B, Baumann L, Michalakis S, Zeng R, Chen Z & Biel M (2005). A novel mechanism of modulation of hyperpolarization-activated cyclic nucleotide-gated channels by SRC kinase. *J Biol Chem* **280(40)**, 34224-32